Rock and age relationships of the Talkeetna forearc subduction complex in the Nelchina area, southern Alaska

John Barefoot, Elisabeth Nadin, and Rainer Newberry
University of Alaska Fairbanks

Subduction-zone processes are still poorly understood due to the paucity of good exposures and the complexity of rock relationships within the accretionary prism. A remarkably well-preserved exposure of subduction-related rocks is located at the foot of Nelchina glacier in south-central Alaska. Here, the crystalline basement of the Talkeetna volcanic arc contacts the mélange of its related accretionary complex along the Border Ranges fault. Mapping and sampling of the mélange exposures of the complex revealed relatively undeformed argillite, metavolcanic rocks, and chert, as well as a roughly 100-m-diameter block of pillow basalt. Preliminary x-ray fluorescence data show that this pillow basalt formed in an intra-plate setting, suggesting it is unrelated to Talkeetna arc volcanism. Detailed compositional data from a transect across this basalt will show effects of progressive hydrothermal alteration from core to rim of the block. A zircon U-Pb age of a gabbro from the Talkeetna arc basement is 188.9 ± 2.2 Ma, which coincides with Talkeetna arc volcanism. A zircon U-Pb age of a felsic dike that cross-cuts the mélange is 53.0 ± 0.9 Ma, which is consistent with a period of near-trench plutonism across southern Alaska, and sets a minimum age for mélange deformation. Ages and compositions from rocks of the arc basement and juxtaposed accretionary prism, together with detailed petrographic descriptions, will expand the understanding of forearc accretionary complexes and how hydrothermal fluids interact with rocks within that complex.

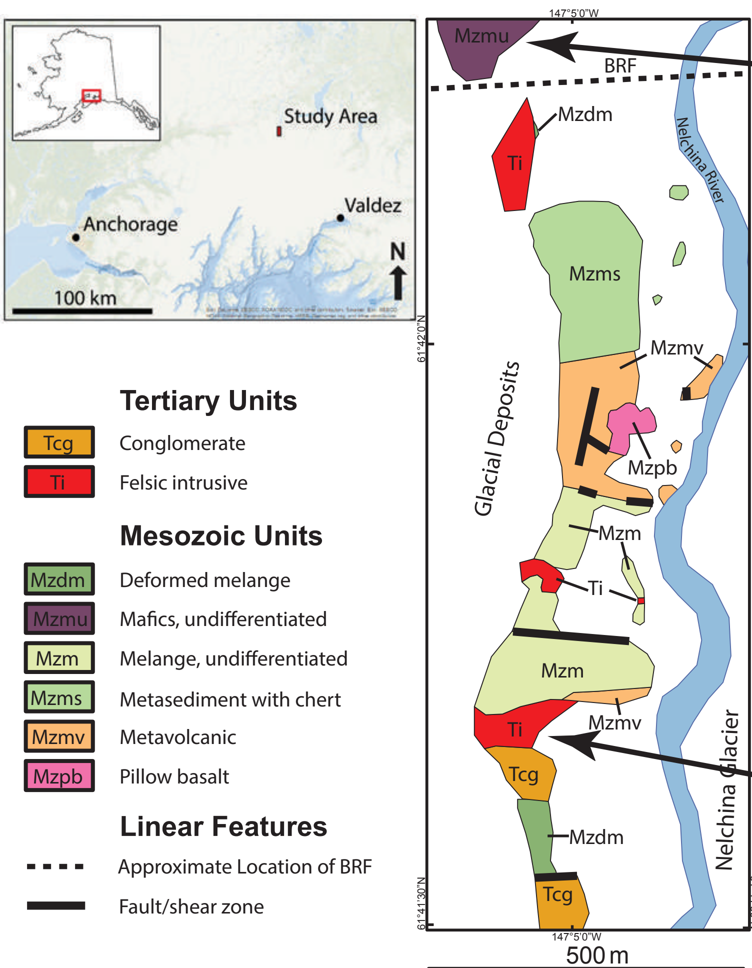

Figure 1: Area of the Talkeetna accretionary complex mapped in the summer of 2016. Border Ranges fault location approximated as the contact between the crystalline basement of the Talkeetna arc and its associated accretionary complex. Ages of units from Pessel et al. (1981).

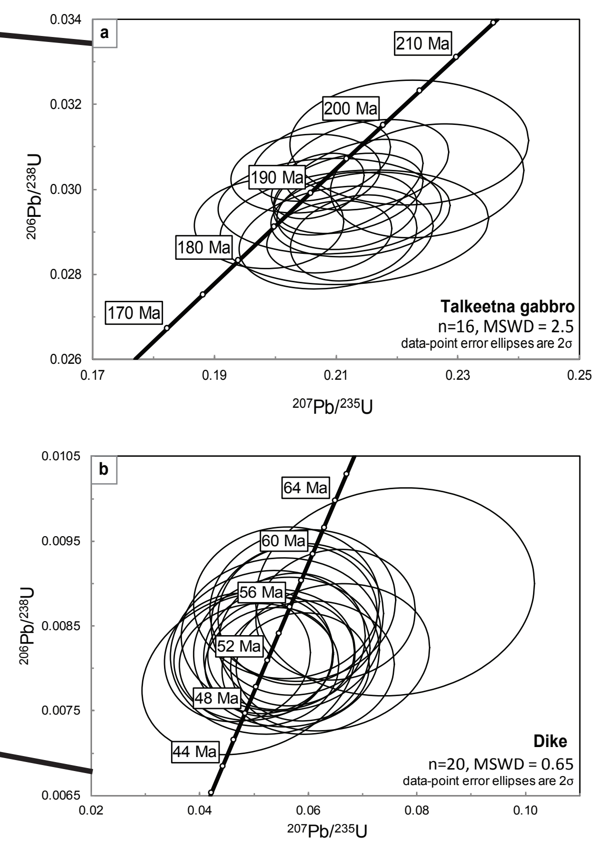

Figure 2: Zircon U-Pb concordia plots for two rocks from the Nelchina area: a) a gabbro from the crystalline basement of the Talkeetna arc is 189 ± 2.2 Ma; b) a cross-cutting felsic dike is 53.04 ± 0.93 Ma. Plots generated using ISOPLOT software of Ludwig (2003).

Title: 3D model of the subducting plate interface between Kodiak Island and Shumagin Islands offshore the Alaska Peninsula

Authors: Harold Kuehn[1], Mladen Nedimović[1], Donna Shillington[2], Anne Bécel[2], Jiyao Li[2], Matthias Delescluse[3], Spahr Webb[2], Keith Louden[1]

[1]Dalhousie University, [2]Lamont-Doherty Earth Observatory of Columbia University, [3]École Normale Supérieure de Paris

We present a 3D model of the interplate interface along the NE part of the Alaska-Aleutian subduction zone, from the SW edge of the Kodiak Island to just W of the Shumagin Islands. The model spans from the locked and stress accumulating Semidi Segment and Kodiak Asperity in the NE, both of which have recently ruptured in great megathrust events, to the weakly coupled Shumagin Gap in the SW. Our 3D model is based on interpretation of ~3700 km of long-streamer (8 km) and large source (6600 cu. in.) multichannel seismic (MCS) profiles and velocity tomography results derived from ocean bottom seismometer (OBS) data acquired during the ALEUT cruise in 2011. The reflection sections are remarkable for the continuity of the interplate interface reflection image and for the depth to which it is imaged (Figure 1), which at places exceeds 60 km, allowing for the construction of a globally unique regional 3D model of the interplate interface geometry. This model and the corresponding seismic velocity cube provide new insight into the subduction zone processes offshore Alaska Peninsula. For example, at a regional scale, our model shows that the plate interface systematically steepens from NE to SW. Additionally, the constructed 3D model of the interplate interface geometry represents a valuable tool for studying seismicity and tsunamis in this region, as well as development of plate dislocation models, because no such information currently exists.

Figure 1. Reflection profile of the ALEUT Line 3 superimposed over the corresponding velocity model derived from MCS data for the sediments, OBS data for the upper crust, and existing velocity information from the literature for the lower crust and uppermost mantle. Line 3 crosses the middle of the Semidi segment. The blue dotted line represents the interpreted interplate interface. In the shallower parts of the image, this line closely follows the single or the narrow set of reflections arising from the interplate interface. In deeper sections of the image, the interplate interface is characterized by multiple reflections and the blue dotted line follows the middle of this reflection band.

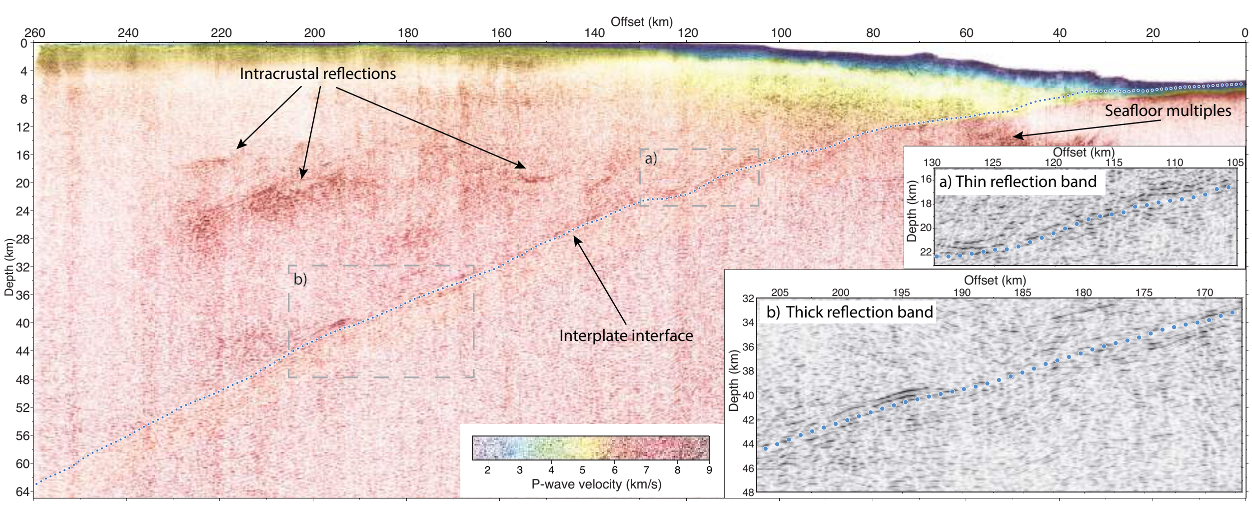

Seismic and Infrasonic Observations of Mount Cleveland, Alaska: An Open Vent Volcano in the Central Aleutian Arc

John Lyons[1], Diana C. Roman[2], John Power[1], Mathew M. Haney[1]

[1]U.S. Geological Survey, Alaska Volcano Observatory, Anchorage, AK
[2]Carnegie Institution for Science, Washington, DC.

Mount Cleveland is a frequently active stratovolcano in the central-Aleutian arc that has had 44 recorded explosions and produced 11 small lava domes since December 2011. We operated a six-station broadband seismic network on Cleveland between August 2015 and July 2016 that complemented two permanent seismoacoustic stations operated by the Alaska Volcano Observatory (AVO) since 2014. This network captured three explosive eruptions that occurred on April 16, May 6, and May 15, 2016 and swarms of VT earthquakes in August 2015 and April-May 2016. Preliminary analysis suggests that hypocenters of VT earthquakes concentrate beneath the NE flank of the volcano and range in depth between 2 and 10 km below sea level. Calculated duration magnitudes range from 0.0 to 1.6. The explosive events have low seismic-to-acoustic energy ratios and high absolute infrasound pressures suggesting a very shallow source. Ambient noise coda wave interferometry between a pair of stations crossing the NE flank shows a subtle increase in velocity starting in August/September 2015 followed by a decrease in velocity coincident with the explosions in April and May 2016.

The VT earthquake swarm observed at Cleveland is unique for frequently active volcanoes in the Aleutian arc. Other frequently active volcanoes such as Pavlof and Shishaldin, which have been monitored by permanent seismic networks operated by AVO since 1996 and 1997 respectively, have not hosted VT swarms. This suggests that magma ascent at Cleveland may involve greater stress perturbations and is perhaps more episodic than at other Aleutian arc volcanoes that are often characterized as open vent.

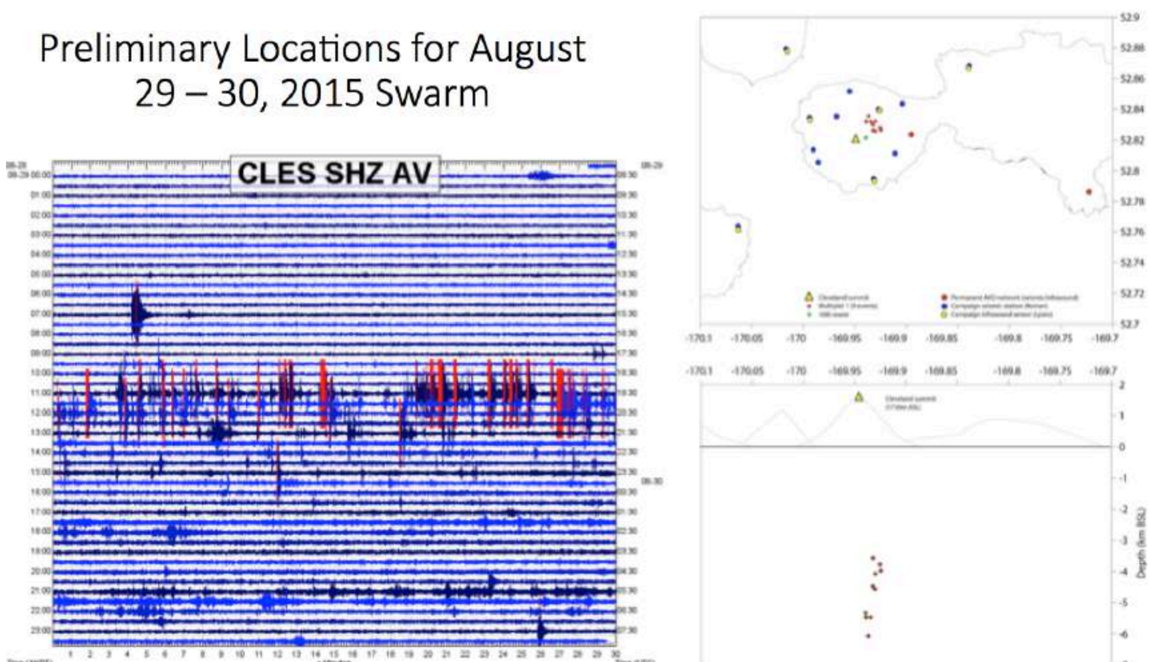

Segment boundary and upper plate characteristics
for the Kodiak region of the Alaska megathrust

Marlon D. Ramos and Lee M. Liberty

The Kodiak Islands segment of the Alaska-Aleutian megathrust ruptured with the Prince William and Kenai segments during the M9.2 1964 Great Alaska Earthquake. This devastating earthquake generated coseismic uplift and subsidence that initiated tectonic tsunamis across the Gulf of Alaska. Upper plate characteristics of the Kodiak segment differs from adjacent segments, as evinced through differences in plate coupling, island deformation, seismicity, and incoming plate morphology. The nature of earthquake segmentation for the Kodiak region has been largely addressed through paleoseismological studies and has not received a comprehensive comparison between upper and lower plate processes.

We analyze multiple geophysical datasets for the Kodiak region (e.g. seismic reflection, earthquake, potential fields data) to understand the spatial relationships between subduction, accretion, lower and upper plate structure including megathrust splay faults, and interseismic deformation.

Gravity and magnetic data show a clear geophysical expression of the boundaries with the Semidi and Kenai subduction zone segments. These boundaries represent changing Pacific plate structure and coincide with earthquake rupture limits. Furthermore, observed interseismic deformation from geodetic GPS, focal mechanism, and earthquake datasets point to changing forearc and splay fault geometries. An updated segmentation model is presented for the Kodiak region and physical drivers for upper plate deformation are derived from incoming plate characteristics.

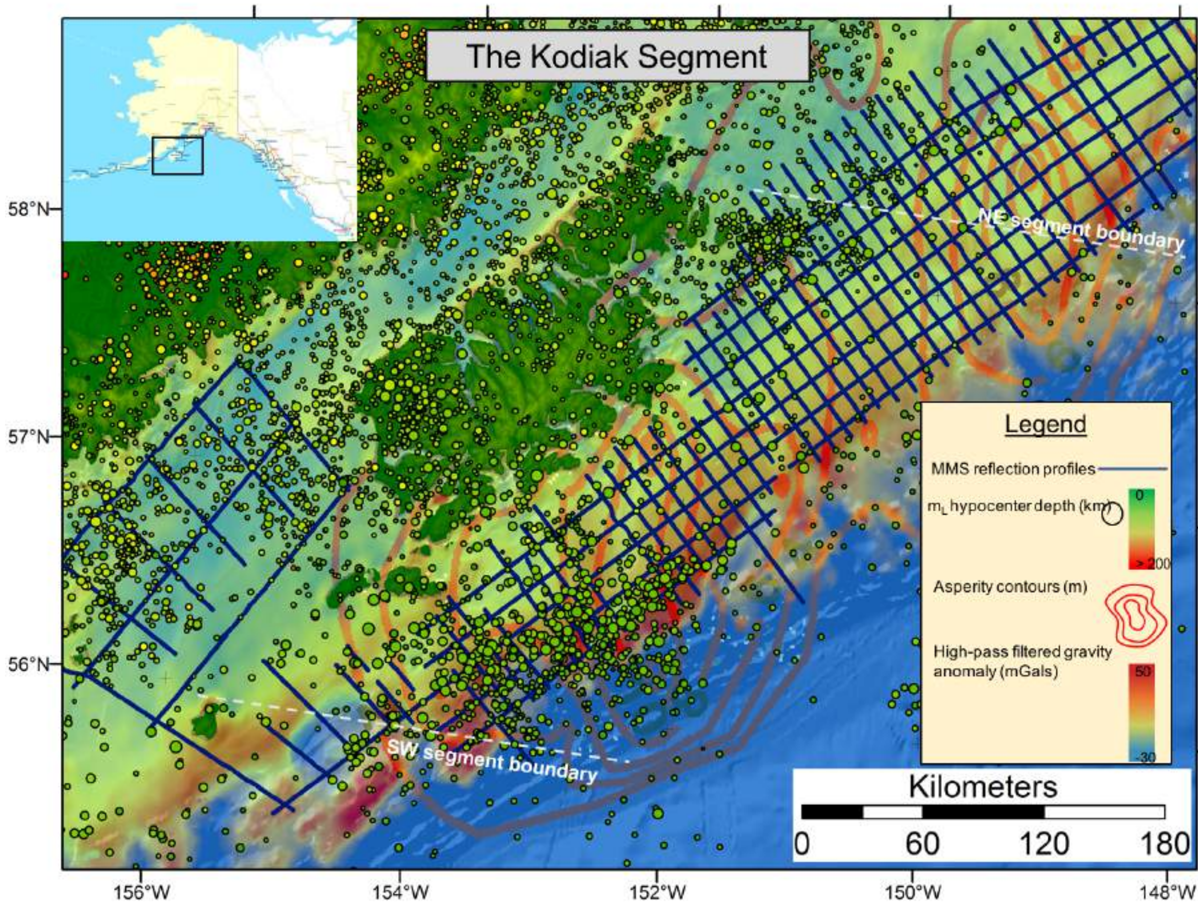

The Kodiak Segment
NE segment boundary
SW segment boundary
Legend
MMS reflection profiles
m_L hypocenter depth (km)
0
> 200
Asperity contours (m)
High-pass filtered gravity anomaly (mGals)
50
-30
Kilometers
0
60
120
180
58°N
57°N
56°N
156°W
154°W
152°W
150°W
148°W

Aleutian array of arrays (A-cubed) detects continuous tremor and low frequency earthquake activities

Bo Li, bli017@ucr.edu
Abhijit Ghosh, aghosh@ucr.edu
Department of Earth Sciences, University of California-Riverside

Compared to other subduction zones, tremor and low frequency earthquakes (LFEs) in the Alaska-Aleutian subduction zone, one of the most seismically and volcanically active plate boundaries, are relatively poorly studied due to the limited data availability, difficult logistics, and rugged terrain. Since the summer of 2014, we started to deploy an array of arrays, which consists of three well-designed mini seismic arrays, in the Unalaska Island to study the slow earthquakes (Figure 1). Using the beam back-projection method [Ghosh et al., 2009, 2012], we detect continuous tremor activities for over a year. Tremors are located south of the Unalaska and Akutan Islands. They are clustered in several patches, with a gap between the two major clusters (Figure 2). We also find multiple tremor migration patterns with propagation in both along- strike and dip directions and a wide range of velocities. In addition to tremor activities, we identify some LFE families and use them as templates to search for repeating LFE events with a template matching method. We detect thousands of LFEs for each family and their activities are spatiotemporally consistent with tremor activities. The details of tremor and LFE using the array techniques is helping us to better recognize the physical properties of the transition zone, providing new insights into the slow earthquake activity in this area, and exploring their potential relation with the local and teleseismic earthquakes.

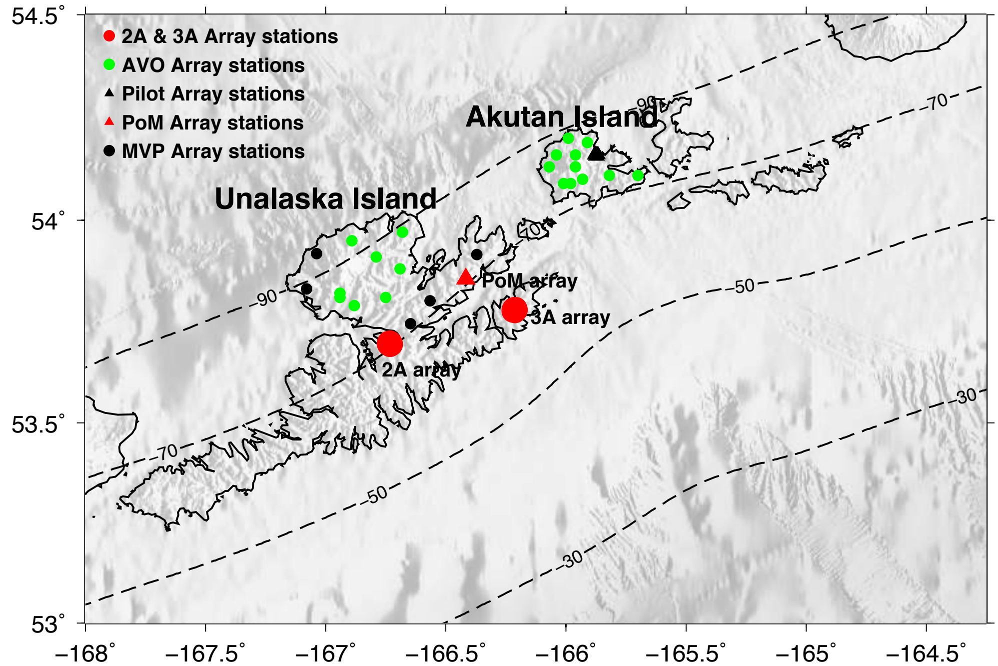

Figure 1. Array distributions. The red triangle and circles represent three mini arrays. The PoM array consists of 18 stations, and the 2A and 3A array each has 15 stations.

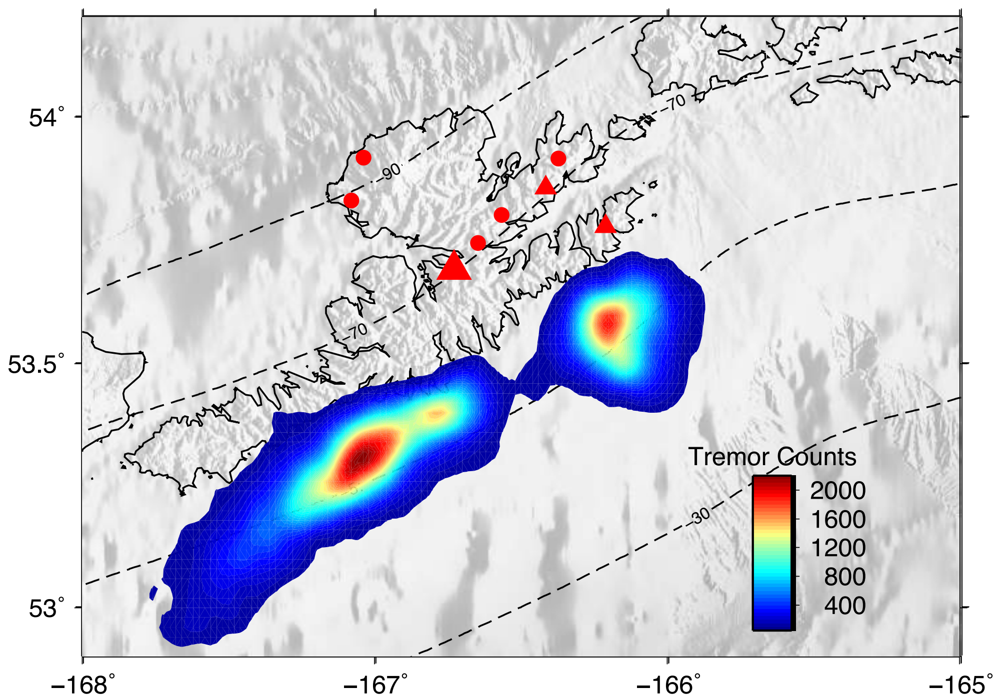

Figure 2. Tremor density distribution of the 2A array detections.

Mantle Structure of the Cascadia Subduction Zone and Juan de Fuca Plate System from Onshore/Offshore Teleseismic P-wave Tomography

Miles Bodmer, Doug Toomey, Emilie Hooft, Brandon Schmandt, Joe Byrnes, Max Bezada

We present tomographic images of the onshore and offshore mantle structure of the Cascadia subduction zone that reveal significant heterogeneities beneath the incoming plate system and provide new constraints on the morphology of the down-going slab. Our analysis utilizes P-wave delay times of teleseismic events from the existing onshore dataset of Schmandt and Humphreys (2010) and additional delay time measurements from the amphibious Cascadia Initiative community experiment. The tomographic method implements delay time corrections for shallow structure, iterative 3D raytracing, and frequency dependent sensitivity kernels. We observe N-S variations in the upper ~200 km offshore beneath the Gorda deformation zone and Juan de Fuca plate. Prominent low-velocity anomalies exist beneath the slab near its southern edge and toward the north below the Olympic mountains where the strike and dip of the subducting plate change. The Juan de Fuca Ridge is resolved as a slight decrease in velocity with an asymmetrical structure located outboard of the ridge north of Axial seamount and bending towards the Blanco transform to the south. Generally, peak-to-peak variations offshore are low compared to the onshore anomalies and recent S-wave images [Byrnes et al., submitted]. After non-linear inversion we image a more compact slab anomaly at depth and begin to image the shallow dipping portion of the slab at several latitudes. At depths near the transition zone we observe high-velocity anomalies in the central section of Cascadia and below a proposed slab gap. Offshore, our results are consistent with dynamic upwelling associated with the ridge-transform system and suggest that reorganization of upper mantle flow beneath the deforming Gorda plate dominates mantle dynamics in southern Cascadia. We compare our results to existing tomographic studies and discuss them in the context of heterogeneous anisotropic structure observed throughout the subduction zone.

Jonathan R. Delph, Alan Levander, Fenglin Niu
Department of Earth Science, Rice University
Houston, Texas

Title:
The effects of subduction on the seismic structure of the crust and upper mantle in the Pacific Northwest

Abstract:
The characteristics of subduction beneath the Pacific Northwest are variable along strike, showing marked differences in seismic properties such as tremor, seismicity, and volcanism. To understand what controls these variations, we are constructing seismic images of the subducting oceanic lithosphere and overriding North American lithosphere along the Cascadia margin using different seismic techniques.

In this study, a total of 30 permanent and temporary networks, including the Earthscope Transportable Array and FlexArrays, were combined to image fine-scale variations in crustal and uppermost mantle (<80 km) structure of the Pacific Northwest. Using Rayleigh and Love wave ambient noise cross-correlations paired with CCP-derived receiver functions, we can obtain information about the shear wave velocity and discontinuity structure in the region. With this model, we can investigate variations in the seismic structure of the downgoing oceanic lithosphere and overlying mantle wedge, the character of the crust-mantle transition beneath the volcanic arc, and local to regional variations in crustal structure. From these results, we can infer the presence, distribution, and pathways of fluids released from the subducting slab, and how they affect the seismic structure of the overriding lithosphere.

Weak Moho extends along the entire Cascadia forearc

Matthew M. Haney[1], Victor C. Tsai[2], Kevin M. Ward[3]
[1]*Alaska Volcano Observatory, U.S. Geological Survey, Anchorage, AK, USA*
[2]*California Institute of Technology, Seismological Laboratory, Pasadena, CA, USA*
[3]*University of Utah, Department of Geology and Geophysics, Salt Lake City, UT, USA*

The absence of a significant continental Moho in the Cascadia forearc has been imaged at several locations in Washington and Oregon (Bostock et al., 2002; Hansen et al., 2016). From measured Rayleigh-wave dispersion on the Earthscope Transportable Array (Ekström, 2014), we show a weak Moho extends along the entire Cascadia forearc. We have processed Rayleigh-wave phase-velocity maps over the contiguous US at periods between 12 and 40 s with a new surface wave inversion method developed by Haney and Tsai (2015). The method maps out the dominant surface waveguide interface and this is normally the Moho in the period range from 12 to 40 s (Fig. 1). However, as shown in the zoomed-in plot in Fig. 1, the dominant surface waveguide interface deepens to the west of the Cascades volcanic chain, shown as red triangles. Furthermore, this feature abruptly terminates at the southern extent of the subduction zone. We interpret this not as the deepening of the Moho but as the dominant waveguide interface transitioning to the slab west of the volcanic chain owing to the continental Moho becoming weak in the Cascadia forearc. The Moho is weak due to serpentinization of the mantle wedge and, as a result, the dominant waveguide interface in the forearc is the slab. This indicates a weak Moho is not an unusual characteristic of any particular location in Cascadia, but is in fact a general property of the subduction zone. The dominant waveguide interface we obtain in the forearc therefore represents a new constraint on the depth of the Juan de Fuca slab. We also show preliminary results of mapping Moho in Alaska, including areas of weak Moho, from Rayleigh wave dispersion measurements.

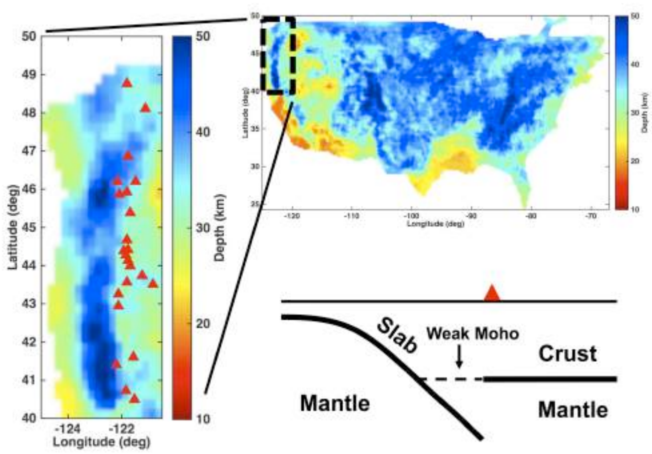

Fig. 1: Depth of the dominant surface waveguide interface across the contiguous US, and zoomed-in area of the Cascadia Subduction Zone (CSZ). Volcanoes above the CSZ are shown as red triangles in the zoomed-in panel. The depth of the interface corresponds to the Moho across most of the US, but transitions to the slab west of the Cascades volcanic chain due to the presence of a weak Moho.

REFERENCES

Bostock, M. G., Hyndman, R. D., Rondenay, S., and Peacock, S. M., 2002, An inverted continental Moho and serpentinization of the forearc mantle: Nature, 417, 536-538.

Ekström, G., 2014, Love and Rayleigh phase-velocity maps, 5-40 s, of the western and central USA from USArray data: Earth and Planetary Science Letters, 402, 42-49.

Haney, M. M. and Tsai, V. C., 2015, Nonperturbational surface wave inversion: A Dix-type relation for surface waves: Geophysics, 80, EN167-EN177.

Hansen, S. M., Schmandt, B., Levander, A., Kiser, E., Vidale, J. E., Abers, G. A., and Creager, K. C., 2016, Seismic evidence for a cold serpentinized mantle wedge beneath Mount St Helens: Nature Communications, 7, 13242.

Title: Crustal-scale seismic structure from trench to forearc in the Cascadia subduction zone

Authors; Sampath Rathnayaka[1], Haiying Gao[1] (1.University of Massachusetts, Amherst)
srathnayakam@geo.umass.edu
haiyinggao@geo.umass.edu

The (de)hydration process and the amount of hydrated sediment carried by the downgoing oceanic plate play a key role in the subduction dynamics. A high-resolution shear velocity model from the crust down to the uppermost mantle, extending from trench to forearc, is constructed in the northern Cascadia subduction zone to investigate seismic characteristics related to slab deformation and (de)hydration at the plate boundary. A total of 220 seismic stations are used, including the Cascadia Initiative Amphibious Array and inland broadband and short-period stations. The empirical Green's functions extracted from continuous ambient noise data from 2006-2014 provide high-quality Rayleigh-wave signals at periods of 4-50 s. We simulate wave propagation using finite-difference method to generate station Strain Green's Tensors and synthetic waveforms. The phase delays of Rayleigh waves between the observed and synthetic data are measured at multiple period ranges. We then invert for the velocity perturbations from the reference model and progressively improve the model resolution. Our tomographic imaging shows many regional- and local-scale low-velocity features, which are possibly related to slab (de)hydration from the oceanic plate to the overriding plate. Specifically, we observe (1) NW-SE oriented linear low-velocity features across the trench, indicating hydration of the oceanic plate induced by bending-related faultings; (2) W-E oriented fingerlike low-velocity structures off the continental margins due to dehydration of the Juan de Fuca plate; and (3) Seismic lows atop the plate interface beneath the Washington forearc, indicating fluid-rich sediments subducted and overthrusted at the accretionary wedge.

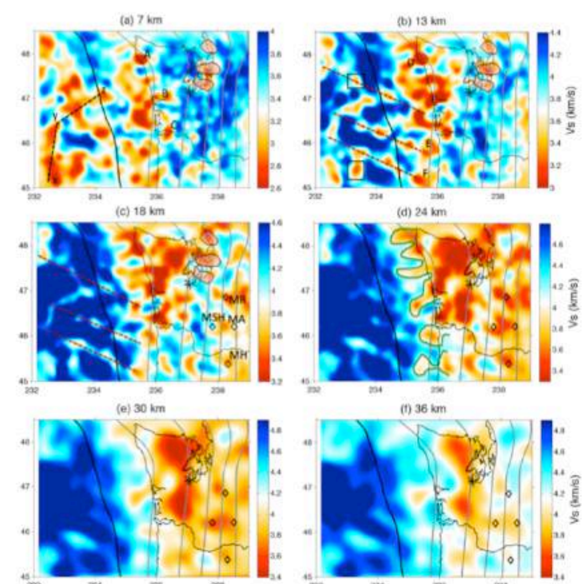

Figure caption. Shear wave velocity distribution at multiple depths. (a)-(c) Three shaded light red polygons with black outline from north to south represent the Everett, Seattle and Tacoma Basins, respectively. In (a), A - Ozette lake; B - Gray Harbor; C - Columbia estuary; Lines xy and yz mark the locations of the propagator wakes [Han et al. 2016]. (b) D, E, and F represent the low resistivity areas observed on the continental shelf using the magnetotelluric data by Bedrosian and Feucht [2014]. The black rectangles outline the locations of bending faults observed near the trench with active seismic data by Han et al. [2016]. Three maroon dash lines represent the linear alignment of the NW-SE oriented low velocity features across the trench. (c) MR - Mount Rainer; MSH – Mount St. Helens; MA– Mount Adams; MH – Mount Hood. (d) Green outlines represent the fingerlike structures. The depth contours of the plate interface from 20 - 100 km (gray lines) are from the model of McCrory et al. [2004].

GPS Imaging of vertical land motions in the Pacific Northwest

Justine Overacker[1], William C. Hammond[1], Meredith L. Kraner[1], Geoffrey Blewitt[1]
[1]Nevada Geodetic Laboratory, Nevada Bureau of Mines and Geology, University of Nevada, Reno, Reno, Nevada, USA

Abstract

We present a new image of the rate and patterns of vertical crustal motion in the Pacific Northwest region of the western United States based on GPS data. We use data from 455 GPS stations running continuously for a minimum of 4 years in networks including the EarthScope Plate Boundary Observatory and PANGA networks. Trends in the times series of vertical positions are obtained using the MIDAS robust trend estimator to estimate unbiased vertical rates that are robust and insensitive to the effects of outliers, seasonality and undocumented steps in the data [Blewitt et al., 2016]. We then apply the GPS Imaging algorithm that incorporates weighted median spatial filtering on a Delaunay triangulation of the network to obtain a vertical rate field with speckle noise removed [Hammond et al., 2016]. GPS Imaging enhances signals that are similar between stations, and hence may be attributable to spatially coherent movement of the solid Earth. The signals are interpolated to a grid using weighted median estimation to create a velocity field of vertical motions across the Pacific Northwest area. The result shows a 50-250 km wide swath of approximately 2 mm/yr of subsidence seemingly unrelated to topographic features of the region, but roughly corresponding to the Juan de Fuca plate subduction latitudes and longitude of the Cascade arc. This suggests that the signal is associated with ongoing deformation possibly related to plate-scale geodynamic forces arising from interseismic coupling, long term plate boundary tractions, volcanic loading and/or mantle flow. Our presentation will document the signals, uncertainties and hypotheses for the possible mechanisms behind this deformation.

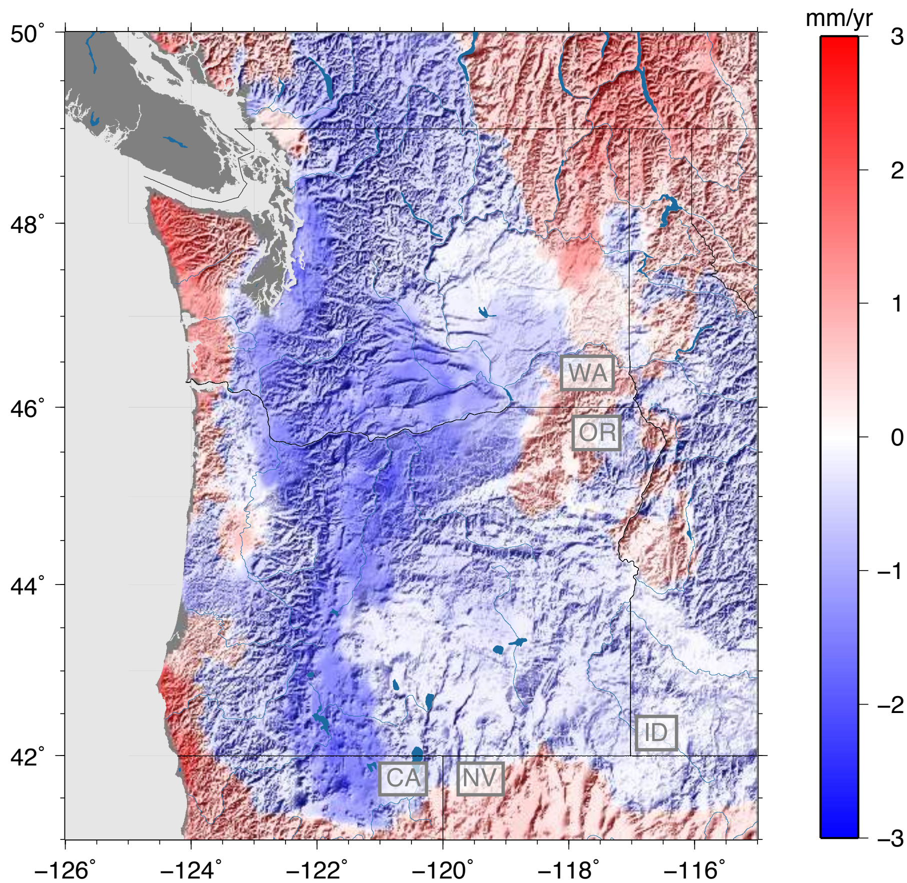

Figure 1: Pacific Northwest GPS Imaging result of vertical velocity field plotted over topographic relief map. Red indicates upward vertical motion, blue indicates downward vertical motion. Greatest amount of subsidence shown by GPS Imaging appear uncorrelated with topographic features.

References (Open Access)

Blewitt et. al. [2016], http://onlinelibrary.wiley.com/doi/10.1002/2015JB012552/full
Hammond et al. [2016], http://onlinelibrary.wiley.com/doi/10.1002/2016JB013458/full

Earthquake Science Center
U.S. Geological Survey
earthquake.usgs.gov

Orientations and relative shear-strain response coefficients for PBO Gladwin Tensor Strainmeters from teleseismic Love waves

Evelyn Roeloffs (evelynr@usgs.gov)
USGS Earthquake Science Center, Vancouver, WA

A Gladwin Tensor Strainmeter (GTSM) measures changes of areal and horizontal shear strain in the surrounding formation. The response coefficients to these strain components must be inferred from the GTSM's responses to well-characterized strain signals. In particular, teleseismic Love waves from great earthquakes can be used to determine the GTSM's orientation and to estimate the ratios between the shear strain response coefficients of the GTSM's four gauges. Applying this analysis to 14 PBO GTSMs confirms that orientations of some GTSMs differ significantly from those measured during installation, and indicates that the shear-strain response coefficients of a GTSM's four gauges can differ by more than 20%.

For example, orientations and relative shear-strain response coefficients were determined for five strainmeters in Oregon (see map) that have recorded strain accompanying episodic tremor and slow slip in the Cascadia subduction zone. Orientations for these strainmeters were previously estimated using earth tides by Roeloffs (2010) and Hodgkinson et al. (2012). Generally, the Love-wave derived orientations agree with those derived from earth tides to within 7° (figure at right).

For B027 and B028, tidal and Love wave analyses both yield orientations about 30° different from those measured at installation. The figure below shows shear strains at B027 and B028 during a period of tremor activity in February, 2016, and a model simulation of the strain. Model calculations assign each day's tremor epicenters to grid squares on the Cascadia subduction interface. Strain at the earth's surface was calculated using an elastic half space dislocation code, assuming each grid square slips the same amount on each day that it hosts at least one tremor epicenter. Net slip, and the ratio of right-lateral to thrust slip, were adjusted to match the offset at a coastal GPS station.

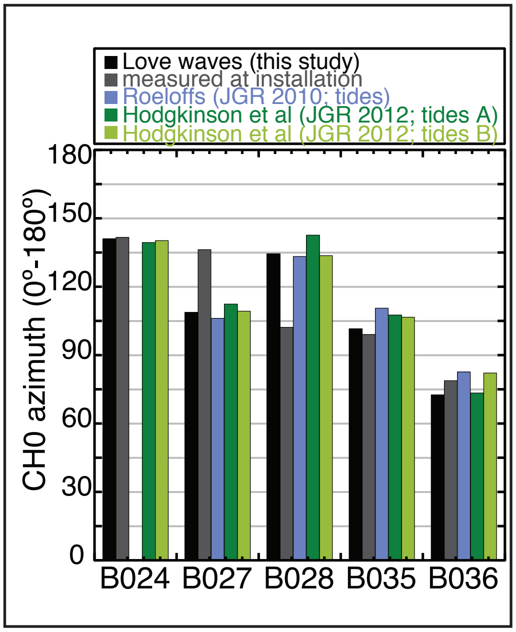

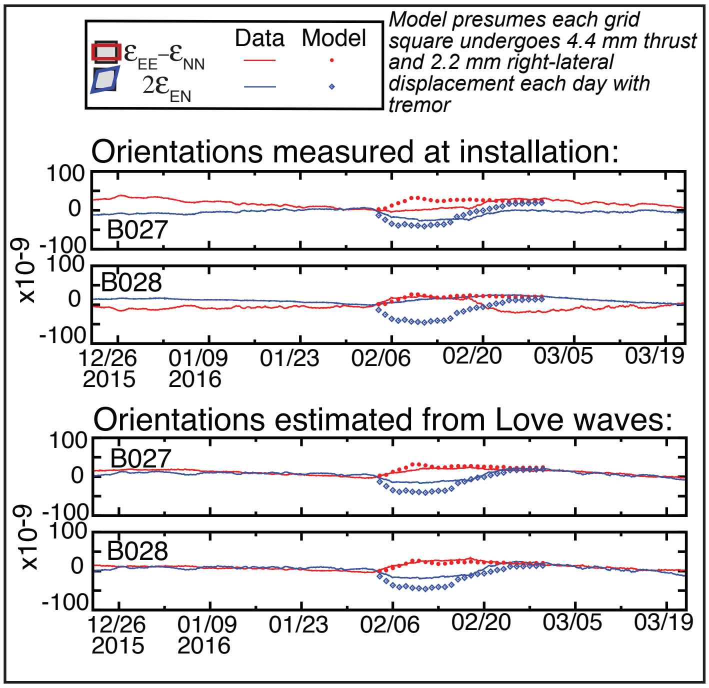

With the corrected orientations, the strains at co-located GTSMs B027 and B028 are in close agreement, and match the model calculations more closely.

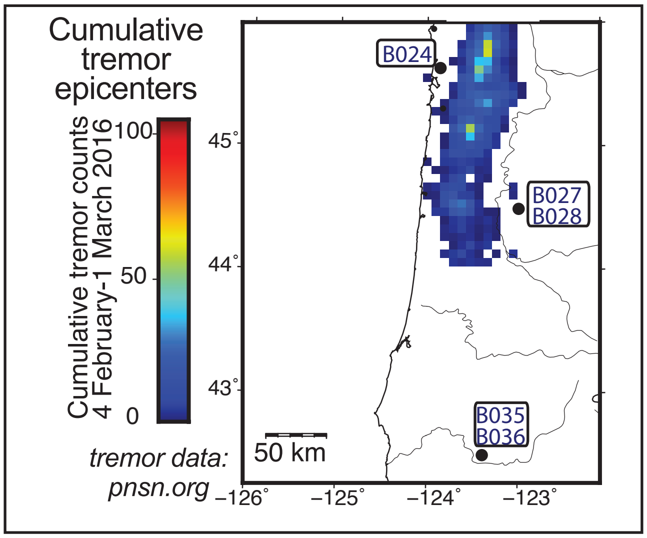

Acknowledgments: *The Gladwin Tensor strainmeters are part of the NSF-supported Earthscope Plate Boundary Observatory, operated by UNAVCO, Inc.*
Strain data were obtained from from ds.iris.edu/pbo/raw/bsm/ and processed by E. Roeloffs, USGS.

Origin of Yellowstone Volcanic Province due to Intruding Hot Mantle Driven by Ancient Farallon Slab

Quan Zhou*, Lijun Liu
University of Illinois at Urbana-Champaign

The origin of the Yellowstone Volcanic Province remains debated. Proposed mechanisms include a mantle plume, upwelling driven by lithosphere deformation or subducting slabs, and decompression melting due to small-scale convection. We reconstruct the mantle thermal states beneath the western U.S. during the past 20 million years using an inverse geodynamic model with data assimilation. The model simultaneously satisfies the past subduction process, present mantle tomographic image, and the volcanic history. We find that intra-plate volcanisms including the Columbia River flood basalt and subsequent Yellowstone-Newberry hotspot tracks all originate from eastward intruding hot oceanic asthenosphere through both a slab gap in Oregon and around the southern slab edge. These hot anomalies propagate eastward since mid-Miocene along the Snake River Plain, driven by mantle flow from the sinking Farallon slab below the eastern U.S. The shallow portion of the hot mantle starts to migrate northwestward toward Newberry during late Miocene, following the retreat of the Juan de Fuca slab. During this process, the role of a putative Yellowstone plume is minor. We conclude that subducted oceanic slabs could drive intra-plate volcanisms within the overriding continent throughout geological times.

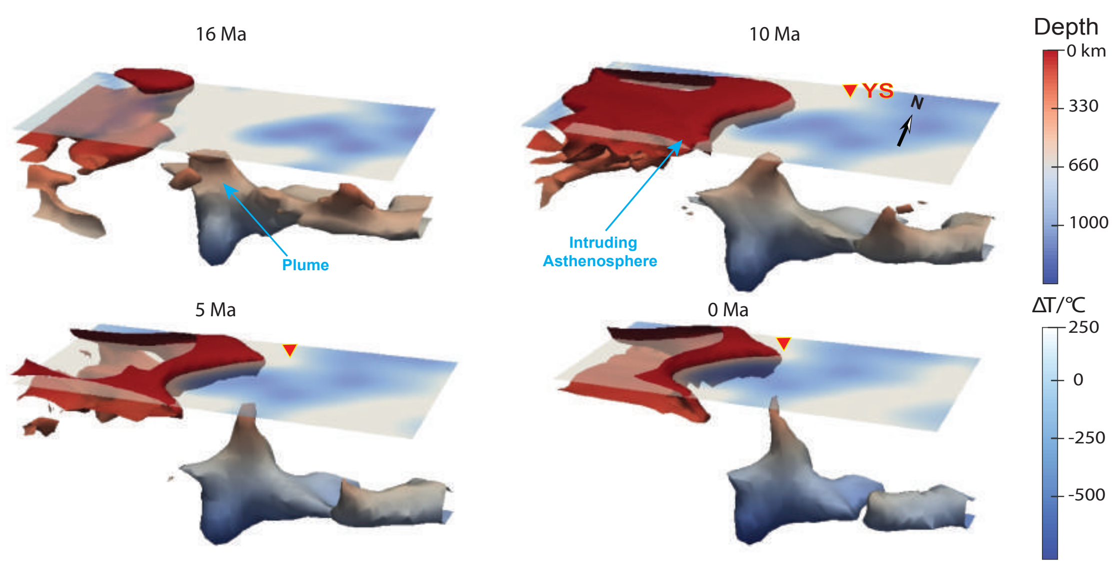

Template Matching Analysis of Swarms in Oaxaca, Mexico and Their Relationship to Slow Slip

S.L. Fasola, M.R. Brudzinski, S.G. Holtkamp, R.J. Skoumal, E. Cabral-Cano, A. Arciniega-Ceballos

The Mexico subduction zone is an ideal location for studying subduction processes due to the shallow subduction angle and short trench-to-coast distances that bring broad portions of the seismogenic and transitional zones of the plate interface inland. A recently generated seismicity catalog from a local seismic network in Oaxaca revealed about 20 earthquake swarms from 2006-2012 with less than 50 earthquakes in each cluster mostly occurring over a few days. Swarms were identified by inspecting every burst of seismicity for 3 empirical traits of swarm sequences: no clear triggering mainshock, many events the near the maximum size, and a relatively constant seismicity rate throughout the sequence. Swarms are of interest because previous work has suggested that slow slip is the driving mechanism for earthquake swarms. A prominent swarm in July 2006 was found to correspond to a shallow slow slip event (~20-35 km) suggesting the two may be related. A recent study by Colella et al. (2017) ran these events through template matching for data from 2010 through 2012 to identify other correlations with slow slip events. Results showed a swarm in July 2010 corresponding to a mid-2010 slow slip event, while the 2010/2011 and 2011/2012 slow slips showed no increase in seismicity rates. Instead, they were found to correspond to an increase in nonvolcanic tremor and aftershocks from the 2012 Ometepec earthquake, respectively, suggesting the shallower slow slip events are thought to drive earthquake generation while the deeper slow slip events are thought to drive nonvolcanic tremor. In order to better understand the spatiotemporal relationship of swarms and slow slip, we seek to employ template matching to a broader set of swarm earthquakes to improve our understanding of spatiotemporal relationships with slow slip events.

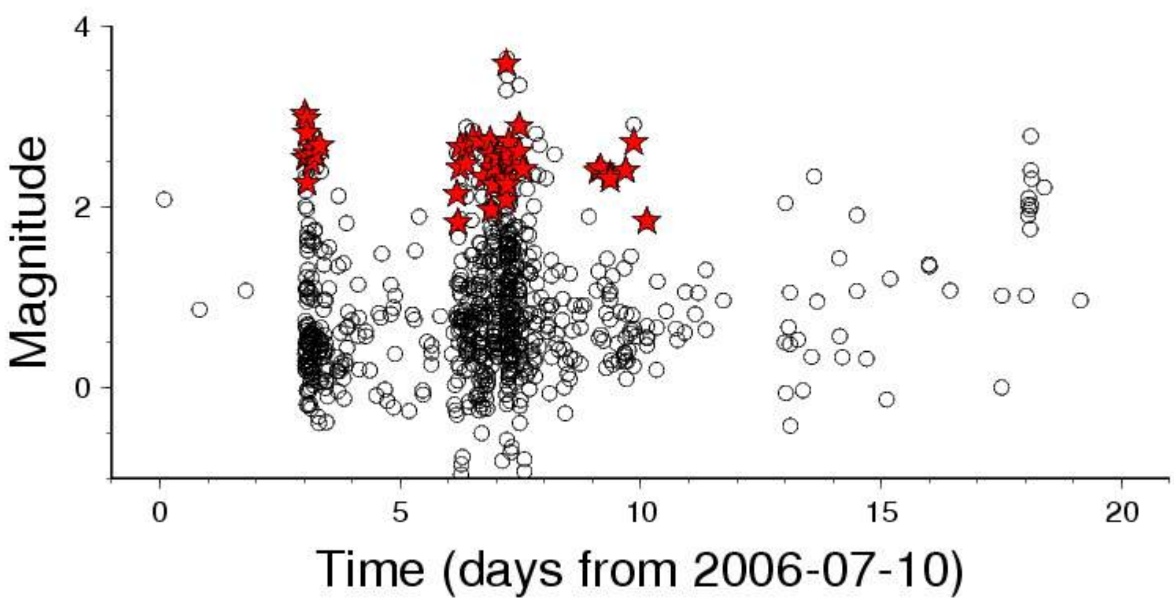

Figure 1. Magnitude-Time distribution for the July 2006 earthquake swarm. Red stars represent the 47 original swarm events and open black circles show the 725 template matching events.

High resolution, self-consistent and realistic subduction zone simulations

Xiaolin Mao[1] (xlmao@gps.caltech.edu), Micheal Gurnis[1], Dave May[2]

[1] Caltech, USA; [2] ETH Zürich, Switzerland

Several recently initiated subduction zones (SZs) show very high slab dip angles, e.g., New Hebrides SZ, New Britain SZ, Puysegur-Fiordland SZ. Some of them experienced slab detachment which usually happens during subduction cessation. These observations provide a good opportunity to reevaluate slab strength and to study force balances during subduction initiation. We use a recently developed software pTatin3D to study these young subduction zones. Free surface and surface process are included to track the long term topography evolution. Elasto-visco-plastic rheology, phase changes and fluid migration are implemented consistently to describe the complex evolutions of viscosity and density. Tracers are used to record chemical compositions and historical quantities. The resolution is around 1km x 1km near subduction zone.

In our model, density jump results from basalt to eclogite transition bends slab to higher dip angle, and water released from subducting lithosphere plays an important role in initiating the back-arc spreading. Without the effects of water weakening to the overriding plate, back-arc spreading is very hard develop. A yield stress of 150 MPa with a reference plastic strain of 0.4 is able to generate high dip angle and slab detachment at early subduction stage for young subducting slab. Fore arc depth, trench depth and fore bulge height with this yield stress are within reasonable ranges, and larger yield stress leads to larger topography variations. By comparison between models with and without elasticity, we notice that it is easier to get normal faults when including elasticity.

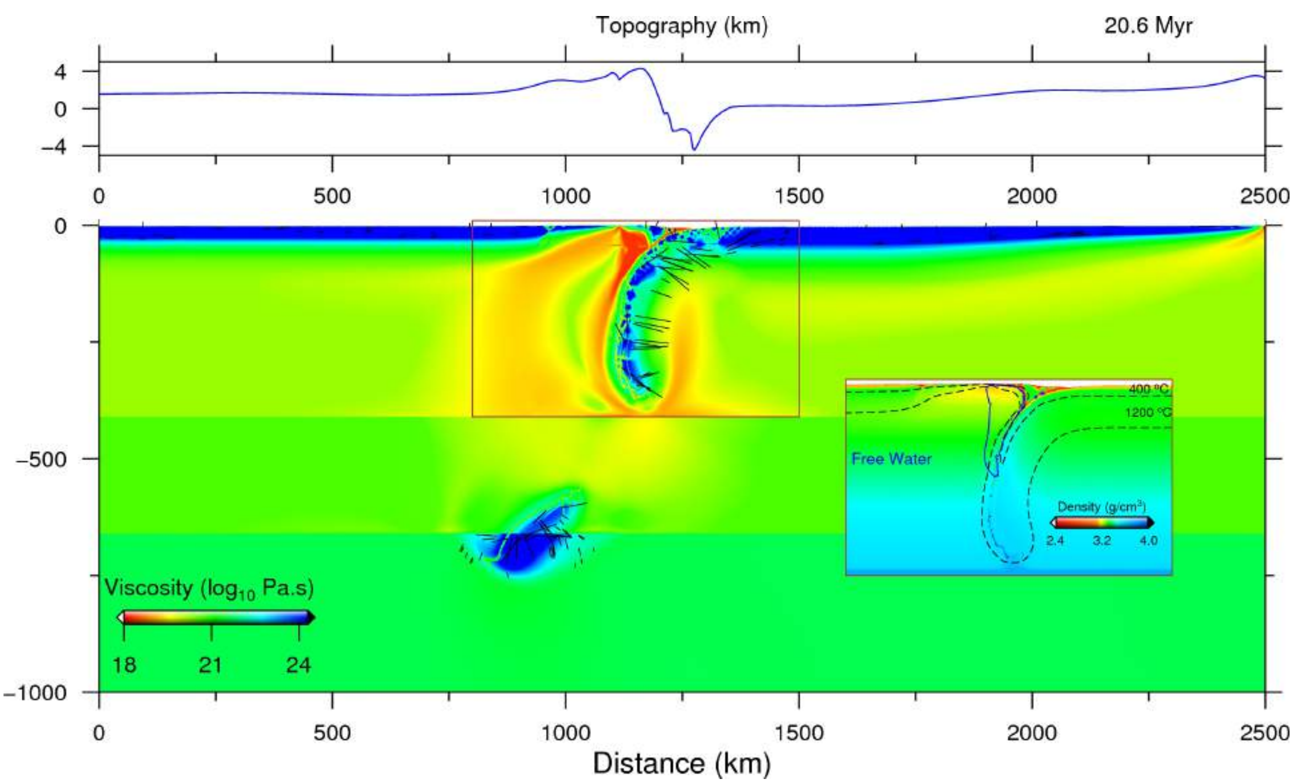

Figure 1: A subduction zone model with normal faults and back-arc spreading. Black lines show the direction and magnitude of σ_1, and the inset shows density variations and free water distribution.

“In the land of HOBITSS where the Slow Slip Events lie.”

Ryan Yohler[1], *Noel Bartlow*[1], *Laura Wallace*[2,3], *Charles Williams*[2]

1.University of Missouri, 2. GNS Science, 3. University of Texas Institute for Geophysics

Investigation of slow slip events (SSE) has become a useful tool for understanding plate boundary fault mechanics in subduction zones where the largest earthquakes occur. An area of specific importance is along the Hikurangi subduction zone in New Zealand, where the GeoNet cGPS network has been monitoring SSEs since 2002. During this time, known slow slip patches have been identified, and in some cases, directly linked to triggered earthquake swarms. Most models of offshore SSEs in New Zealand and elsewhere are based solely on land-based cGPS data. This has led to models with poor resolution out near the trench of the subduction zone, where tsunami hazards are greatest. However, a year-long deployment of seafloor pressure sensors and OBS took place from mid-2014 to mid-2015. The experiment, “Hikurangi Ocean Bottom Investigation of Tremor and Slow Slip” (HOBITSS) was deployed offshore of Gisborne, New Zealand and the northern Hikurangi subduction margin. In September 2014, a large slow slip event was recorded by HOBITSS ocean bottom pressure instruments which and onshore cGPS which allowed for better resolved offshore SSE slip distributions [Wallace et al., *Science*, 2016]. Here, we investigate the time-dependent slip propagation during the 2014 SSE by joint inversion of the HOBITSS ocean bottom pressure data and onshore cGPS data using the Network Inversion Filter (NIF). Future research will incorporate heterogeneous elastic properties into the model.

The results of this work will be used as a teaching and learning tool through New Zealand’s East Coast Life at the Boundary (East Coast LAB) initiative. This program is in place to teach the people of New Zealand, and specifically youth, about Hikurangi subduction zone science and raise awareness of the hazard it poses to the east coast.

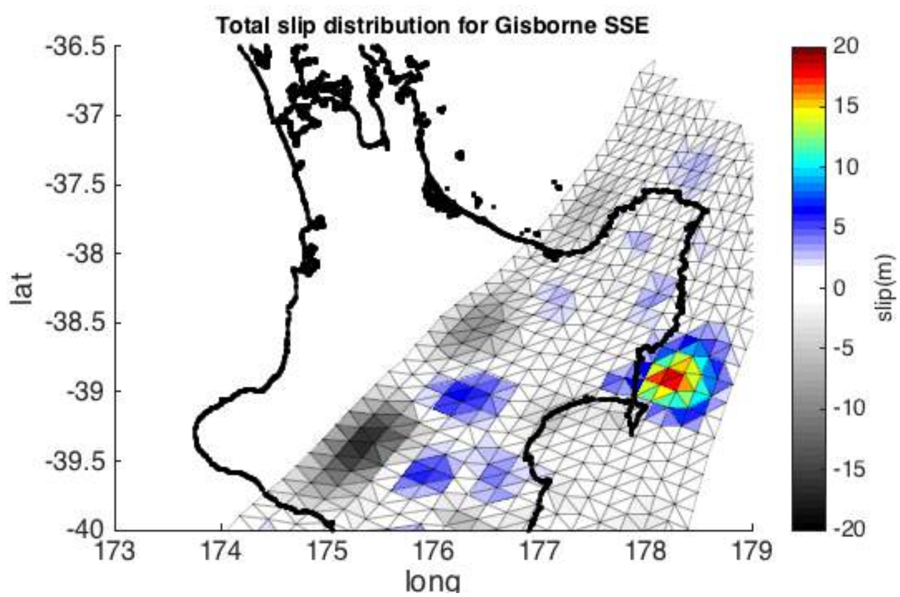

Figure 1: Slip distribution from a preliminary model of a joint inversion with cGPS and HORBITSS data

Imaging fluid accumulation and transportation in the Costa Rica subduction zone using elastic full waveform inversion

Liang Han, Adrien F. Arnulf, and Nathan L. Bangs
Institute for Geophysics, University of Texas at Austin, Austin, Texas, USA

The Cocos Plate subducts beneath the Caribbean Plate in NE direction at a rate of ~90 mm/yr in southern Costa Rica. In 2011, a 3D seismic reflection volume (11 x 55 km^2) was acquired across the Costa Rica margin NW of the Osa Peninsula to investigate the complex structure and the development of the seismogenic zone. Dense fluid seepage sites were also identified in this area from high resolution multibeam bathymetry, backscatter data and 3D seismic data. In this study, we selected one of the seismic lines that went through fluid seepage sites to investigate fluid accumulation and transportation in the upper crust.

The selected seismic line is ~65 km long in SE-NW direction, parallel to the Cocos Plate subduction. Over 1200 airgun shots as dense as 50 m were recorded on a 6-km long streamer with 468 channels in spacing of 12.5 m. We designed a synthetic ocean bottom experiment (SOBE) by utilizing downward continuation of the seismic streamer data to a datum close to the seafloor. Next 2D travel time tomography and elastic full waveform inversion (FWI) were performed. In total, 103,444 first arrival picks from 289 shots in spacing of 200 m were inverted to build a starting model for FWI. Preliminary results show that the resolution of the velocity model used by prestack depth migration has been significantly improved. Numerous faults are characterized by low velocity zones due to higher porosity and fluid contents. Low permeability sediment (< 3 km/s) is about 0.6 km thick in the subducting plate, and ~1-1.3 km thick on the slope and shelf. Basement (~5 km/s) is at ~0.7 km depth below the seafloor in the subducting plate, ~1.5 km on the slope, and ~2 km on the shelf. Apparently fluid seepage sites are located where slope sediment locally thins. Possibly a thinner low permeability sediment cover promotes the discharge of fluids. Although faults play a major role in transporting fluids from the plate interface, low permeability slope sediment might be a primary control on where fluids discharge.

Evidence from high frequency seismic waves for the basalt-eclogite transition under Japan

Wenbo Wu, Jessica C. E. Irving

Princeton University

The occurrence of intermediate-focus and deep earthquakes is not fully explained, although some physical models, such as dehydration and thermal runaway, have been proposed. Three intermediate-focus (140-160km) earthquake nests have been found beneath Japan and attributed to the stress changes associated with the basalt-eclogite transition in subducted oceanic crust (Nakajima et al., 2013). However, the specific depth of this phase transition depends on the pressure and temperature environment of subducted slab, which has large uncertainty. We investigated seismic waves at the Hi-net array in Japan from more than 450 earthquakes within and close to the nests. A pair of distinct P-wave signals with different arrival times are found in records of more than 100 earthquakes in the oceanic crust. Compared to the first P-wave signal, the delayed P-wave has a greater high frequency component (>15Hz). Considering the tectonic context of subduction, we attribute such multipathing to the difference in seismic properties between the mantle wedge and subducted crust. Specifically, the delayed P-wave signals travel in the low-attenuation oceanic crust and therefore contain more high frequency components. Relative to the onsets of the first P-waves, the delay times of the second P-wave signals first increase and then decrease with the depth of the earthquakes. This change indicates a positive seismic velocity change (relative to the mantle wedge) in the oceanic crust at a depth of around 140-155km. By incorporating mineral physics derived models into SPECFEM2D wave propagation simulations, we find a 4-9% P-wave velocity change associated with basalt-eclogite transition can replicate the observed pattern of changing delay times. Thus, the intermediate-focus earthquake nests beneath Japan might be associated with the gradually developing basalt-eclogite transition.

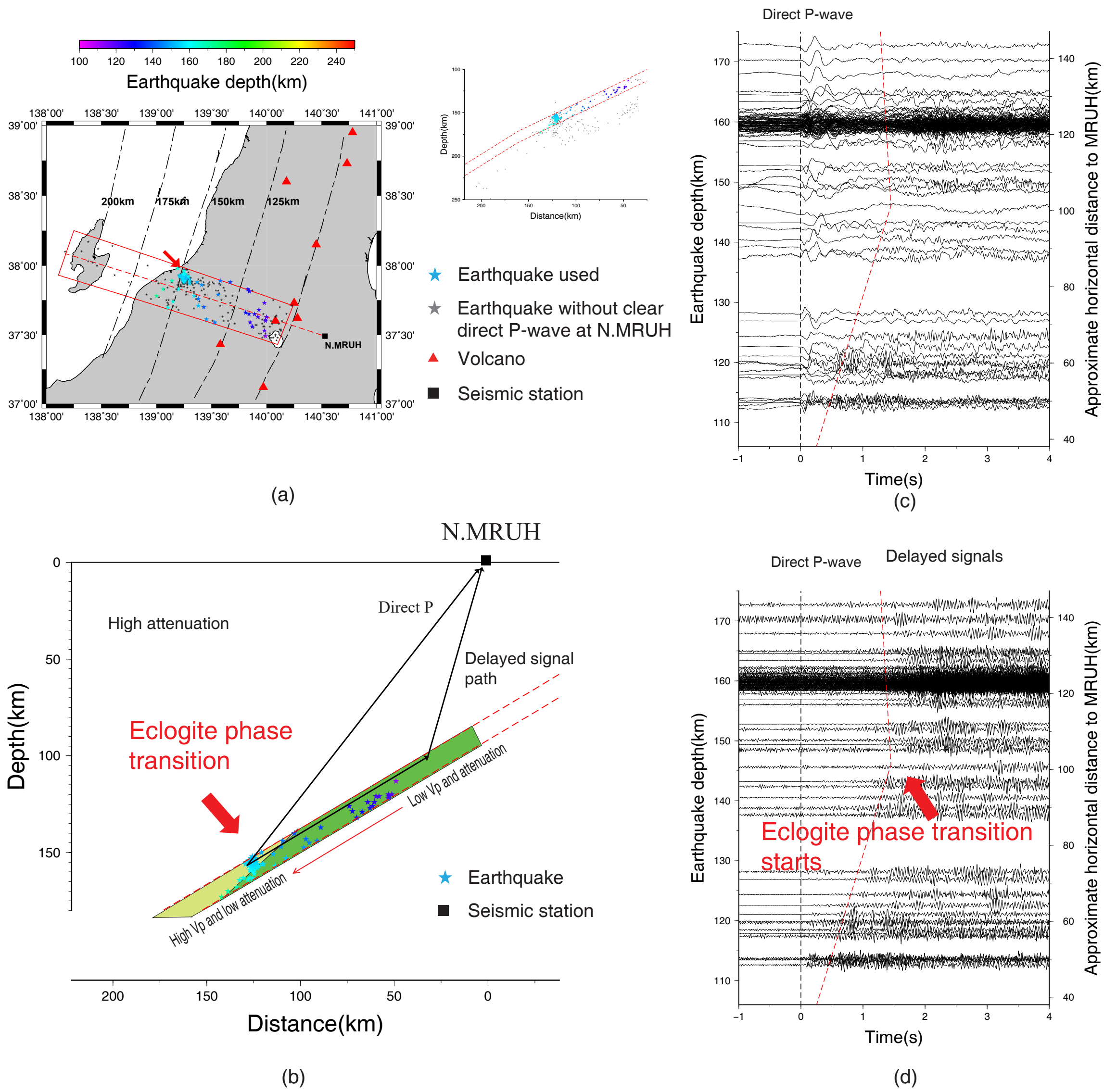

Figure 1. (a) Map of earthquakes. The red arrow points to the earthquake nest. Colored stars are earthquakes with clear seismograms at station N.MRUH. The inset figure is a vertical cross-section. The black dashed lines show the estimated geometry of the subducted Pacific plate. (b) Cartoon figure illustrating the ray paths of direct P-wave and the delayed signals. The delayed signals first travel in the oceanic crust then to the seismic station. (c) Distance profile of raw seismograms. (d) Distance profile of seismograms after high frequency filter (>20Hz).

Ophiolites: A new window probing deep subduction and recycling

Yang J.S. (1), Robinson P.T. (1), Dilek Y. (2, 1)

1. *CARMA, Institute of Geology, Chinese Academy of Geological Sciences, Beijing, China. Email: yangjsui@163.com;*
2. *Department of Geology & Env. Earth Science Miami University, Oxford, OH 45056, USA.*

Deeply subducted lithospheric slabs may reach to the mantle transition zone (MTZ, 410-660 km depth) or even to the core – mantle boundary (CMB) at depths of ~2900 km. Our knowledge of the fate of subducted surface material at the MTZ or near the CMB is poor and based mainly on the tomography data and laboratory experiments through indirect methods. Limited data come from the samples of deep mantle diamonds and their mineral inclusions obtained from kimberlites and associated rock assemblages in old cratons. We report in this presentation new data and observations from diamonds and other UHP minerals recovered from ophiolites that we consider as a new window into the life cycle of deeply subducted oceanic and continental crust.

Ophiolites are fragments of ancient oceanic lithosphere tectonically accreted into continental margins, and many contain significant podiform chromitites. Our research team has investigated over the last 10 years ultrahigh-pressure and super-reducing mineral groups discovered in peridotites and/or chromitites of ophiolites around the world, including the Luobusa (Tibet), Ray-Iz (Polar Urals-Russia), and 12 other ophiolites from 8 orogenic belts in 5 different countries (Albania, China, Myanmar, Russia, and Turkey). High-pressure minerals include diamond, coesite, pseudomorphic stishovite, qingsongite (BN) and Ca-Si perovskite, and the most important native and highly reduced minerals recovered to date include moissanite (SiC), Ni-Mn-Co alloys, Fe-Si and Fe-C phases. These mineral groups collectively confirm extremely high pressures (300 km to ≥660 km) and super-reducing conditions in their environment of formation in the mantle. All of the analyzed diamonds have unusually light carbon isotope compositions ($\delta^{13}C$ = -28.7 to -18.3‰) and variable trace element contents that distinguish them from most kimberlitic and UHP metamorphic varieties. The presence of exsolution lamellae of diopside and coesite in some chromite grains suggests chromite crystallization depths around >380 km, near the mantle transition zone.

The carbon isotopes and other features of the high-pressure and super-reduced mineral groups point to previously subducted surface material as their source of origin. Recycling of subducted crust in the deep mantle may proceed in three stages: *Stage 1* – Carbon-bearing fluids and melts may have been formed in the MTZ, in the lower mantle or even near the CMB. *Stage 2* – Fluids or melts may rise along with deep plumes through the lower mantle and reach the MTZ. Some minerals, such as diamond, stishovite, qingsongite and Ca-silicate perovskite can precipitate from these fluids or melts in the lower mantle during their ascent. Material transported to the MTZ would be mixed with highly reduced and UHP phases, presumably derived from zones with extremely low fO_2, as required for the formation of moissanite and other native elements. *Stage 3* – Continued ascent above the transition of peridotites containing chromite and ultrahigh-pressure minerals transports them to shallow mantle depths, where they participate in decompressional partial melting and oceanic lithosphere formation.

The widespread occurrence of ophiolite-hosted diamonds and associated UHP mineral groups suggests that they may be a common feature of *in-situ* oceanic mantle. Because mid-ocean ridge spreading environments are plate boundaries widely distributed around the globe, and because the magmatic accretion of oceanic plates occurs mainly along these ridges, the on-land remnants of ancient oceanic lithosphere produced at former mid-ocean ridges provide an important window into the Earth's recycling system and a great opportunity to probe the nature of deeply recycled crustal material residing in the deep mantle.

Hydrological Loading Deformation in Southern Alaska Measured by EarthScope's GPS Network

Yuning Fu[1], Jeff Freymueller[2]

1. Department of Geology, School of Earth, Environment and Society, Bowling Green State University, OH
2. Geophysical Institute, University of Alaska Fairbanks, AK

Mountainous and located at high latitude, southern Alaska has a long winter season for snow and ice accumulation and a warm summer season for melting, an ideal situation for strong seasonal hydrologic mass variation. The lithosphere of southern Alaska, behaved as an elastic body, deforms seasonally due to the strong seasonal hydrological mass variations. In this study, we will analyze the GPS time series in the southern Alaska, part of the Plate Boundary Observatory of the EarthScope project, to particularly investigate the seasonal hydrological loading deformation. We will compare GPS-measured, GRACE-modeled loading deformation and modeled results from other independent hydrology models. Additionally, we will also discuss how the modeled hydrological loading deformation can be used to remove non-tectonic deformation in Alaska so as to better reveal crustal deformation only due to tectonics. Our results indicate that long-term Slow Slip Events can be better identified if non-tectonic hydrological loading deformation is removed with GRACE-modeled results.

Slow Slip and Mixed Seismic/Aseismic Moment Release Episodes on the Alaskan-Aleutian Megathrust

The Alaska/Aleutian subduction zone has a well-documented history of great earthquakes across it's nearly 4000 km span. Over the past century, a majority of the plate interface has ruptured in five great earthquakes (1938, M8.3; 1946, M8.6; 1957, M8.6; 1964, M9.2; and 1965, M8.7) as well as several notable major earthquakes. Following the discovery of aseismic slip transients at subduction margins worldwide, researchers have been attempting to determine any potential relationship between slow slip events and earthquakes. Here, we focus on two new regions of aseismic fault slip in Alaska.

The first slow slip region is near Kodiak Island, where a coincident series of earthquake swarms and non-volcanic tremor in 2009 is associated with trenchward transients in geodetic data at four nearby GPS stations (Figure 1). We invert these GPS displacements for fault slip, finding that the total fault movement over several months with moment release equivalent to Mw=6.7. This region was identified by Brown et al. (2013) as a non-volcanic tremor (NVT) source region. Using low frequency earthquake (LFE) templates from this study, we identify four additional bursts of LFE's in late 2008 to early 2009. Two earthquake swarms, occurring in March and May of 2009, accompany this activity. Our interpretation is that the slow slip event triggered swarms up-dip of the slow slip source region, and NVT down-dip of the slow slip source region.

The second slow slip region is near Adak Island in the Aleutians, where a ~6 month long geodetic transient was accompanied by numerous earthquake swarms. In the Adak case, the beginning of the geodetic transient coincided with a M6.5 mainshock event. This region was also identified by Brown et al. (2013) as a non-volcanic tremor (NVT) source region, though we have not yet searched for NVT during this sequence of events. Following the initiating mainshock, three earthquake swarms occurred over a ~5 month period. These swarms were up-dip and to the west of the initiating mainshock. This sequence appears very similar to the sequence of events in northern Peru described in Villegas-Lanza et al. (2015). Our interpretation of the Adak sequence is similar to this study: that a slow slip event was triggered by an initiating mainshock, which propagated away from the mainshock region into a region of velocity strengthening or conditional stability.

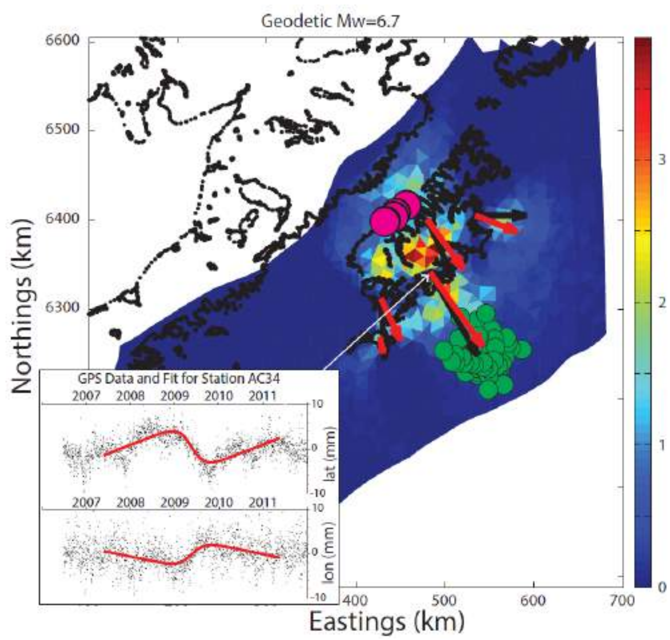

Figure 1: From late 2008 to mid-2009 there were Low Frequency Earthquakes (LFE's, purple dots), and megathrust earthquake swarms (green dots), near Kodiak Island. These are accompanied by transient displacements visible on 4 GPS stations (black arrows – fit to data; red arrows – modeled surface displacement). Our hypothesis is that slow slip is statically triggering LFE swarms on the down-dip end of slip, and megathrust earthquake swarms on the up-dip end. Unfortunately, any slip near the earthquake swarms is unconstrained due to being so far out of the GPS network. (inset) GPS data and static displacement estimation for station AC34, during this event.

Short-term Slow Slip Events at the Southcentral Alaska Subduction Zone

Jessica McGuire[1], Yuning Fu[1] and Jeff Freymueller[2]

1. Department of Geology, Bowling Green State University, Ohio
2. Geophysical Institute, University of Alaska Fairbanks, Alaska

Along the Aleutian Trench, the Pacific Plate is subducting beneath the North American Plate. This boundary is one of the most tectonically active regions on Earth and is home to some of the largest earthquakes on record including the 1964 M9.2 Prince William Sound Earthquake. The large amount of tectonic movement here makes it an ideal area for studying all processes associated with the earthquake cycle. At the Alaska subduction zone, long-term slow slip events have been identified in both upper Cook Inlet and lower Cook Inlet. The two long-term slow slip events that occurred in upper Cook Inlet each lasted between three and four years, 1998-2001 and 2010-2014. Though they have yet to be well studied, short-term slow slip events also appear to be present here due to the definitive change of motion evident in crustal deformation provided by EarthScope's continuous GPS measurements (Figure 1). This study analyzes these short-term slow slip events using GPS time series data from stations of the Plate Boundary Observatory (PBO) Network. Surface displacement was calculated for three short-term slow slip events, one at the beginning of 2006, the end of 2006, and at the end of 2007. These three short-term slow slip events are situated between the two long-term slow slip events which have been identified. Using an inversion modeling technique, this study determines the location of slip along the plate interface. This study will then compare the slip distribution of these short-term slow slip events to that of the long term slow slip events to analyze similarities and differences between the short-term and long-term slow slip events.

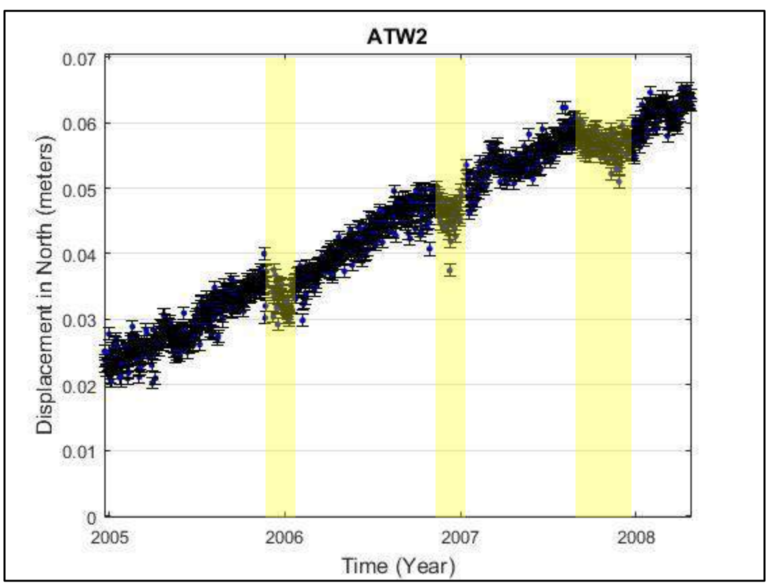

Figure 1. GPS Time series shows deformation in north direction for station ATW2. Several periods of short term SSEs can easily be identified because of the deviation from the linear trend representing the steady plate motion.

Short-term stresses, displacements and gravity change associated with cryospheric fluctuations in tectonically active south-central Alaska.

Jeanne Sauber, Jeffrey Freymueller, James Davis, Natalia Ruppert, Shin-Chan Han, Bryant Loomis, and Scott Luthcke

In southern Alaska a strong seasonal cycle of snow accumulation and melt is superimposed on a variable rate of glacier mass wastage. At the same time, southern Alaska is a tectonically active with frequent major earthquakes. Numerical modeling of the solid Earth response to cryosphere change on a variety of temporal and spatial scales plays a critical role in supporting the interpretation of continuous PBO GPS data and time-variable gravity in tectonically active southern Alaska. In this study, we calculated the surface displacements and stresses associated with variable spatial and temporal cryospheric loading and unloading in south-central coastal Alaska. Here we report calculated differences in the predicted surface displacements and stresses during the GRACE time period (2002 to present). Broad-scale, GRACE-derived estimates of cryospheric mass change, along with independent snow melt onset/refreeze timing, snow depth and annual glacier wastage estimates from a variety of methods, were used to approximate the magnitude and timing of cryospheric load changes. We used the CIG finite element code PyLith to enable input of spatially complex surface loads. An as example of our evaluation of the influence of variable short-term surface loads, we calculated and contrasted the predicted surface displacements and stresses for a cooler than average and higher precipitation water year (WY12, Figure 1) versus a warmer than average year (WY05). Our calculation of these comparative stresses is motivated by our earlier empirical evaluation of the influence of short-term cryospheric fluctuations on the background seismic rate between 1988-2006 (*Sauber and Ruppert,* 2008). During the warmer than average years between ~2002-2006 we found a stronger seasonal dependency in the frequency of small tectonic events in the Icy Bay region relative to cooler years. To date, we have focused our 3-D modeling on changes in the thickness of the primarily elastic layer and we also varied the Maxwell viscoelastic relaxation times for the lower crust and upper mantle. We anticipate exploring the influence alternate loading input and 3-D rheological structures.

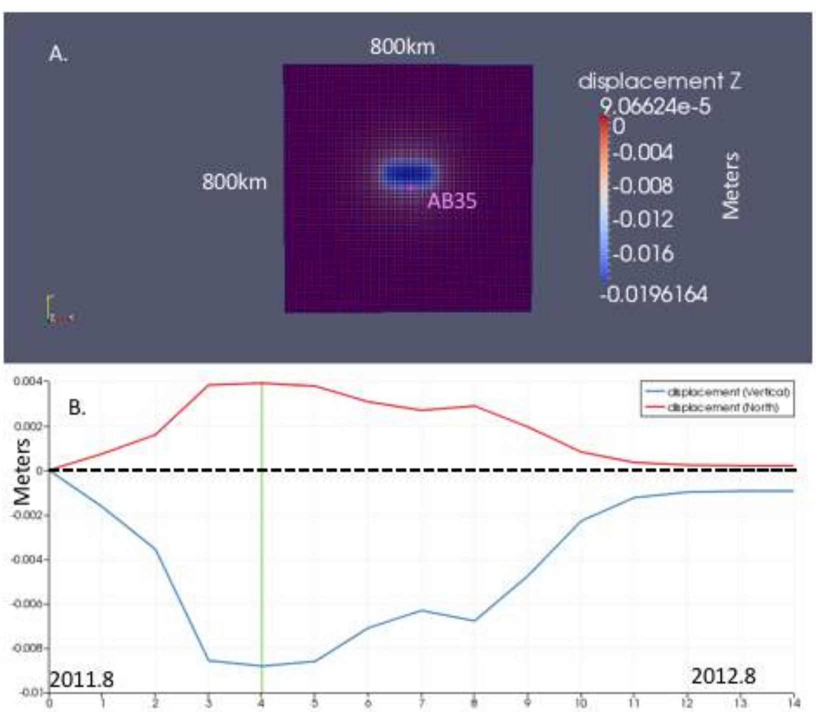

Figure 1**A**. Predicted vertical displacements near the PBO site AB35 due to seasonal loading and unloading associated with snow accumulation and wastage calculated using the CIG code PyLith (Aagaard et al., JGR, 2013). The 800 km X 800 km X 200 km finite element model (FEM) grid has 10 km spacing and a layered rheological model. For the example given here, we assumed a 40 km elastic layer over a 160 km Maxwell viscoelastic layer. The season load was input over a 160 km (East-West) by 80 km (North-South) region with no load over the ocean.

B. Predicted displacement of the PBO site AB35 over the time period of 2011.8-2012.8. The largest snow loading is primarily North of AB35 so during the late Fall and Winter months the station position moves northward and it subsides relative to its early Fall position.

Title: Remote explosive volcanic eruption detection, location, and characterization using the EarthScope Transportable Array in Alaska.

Authors: R.W. Sanderson[1], R.S. Matoza[1], D. Fee[2,3], M.M. Haney[3, 4], J.J. Lyons[3,4]
[1] UC, Santa Barbara (UCSB); [2] University of Alaska, Fairbanks (UAF); [3] Alaska Volcano Observatory (AVO); [4] USGS

The ongoing deployment of the EarthScope Transportable Array (TA) in Alaska affords an unprecedented opportunity to study explosive volcanic eruptions using a dense regional seismo-acoustic network. Active volcanism in the Aleutian Arc poses a risk to both regional and international aircraft. Infrasound monitoring has demonstrated utility for the detection of remote explosive volcanism, but previous studies have utilized relatively sparse networks of infrasound stations in comparison to the TA in Alaska. We are developing capabilities for the detection, location, and characterization of remote explosive volcanic eruptions in the seismic, infrasonic, and ground-coupled airwave regimes. Data used incorporate both that from the TA and additional regional networks such as those of the Alaska Volcano Observatory (AVO) and Alaska Earthquake Center (AEC). Here we implement a Reverse Time Migration (RTM) technique to locate explosive eruptions in Alaska, with a focus on the recent explosive activity at locally-unmonitored Bogoslof volcano (active since mid-December 2016). Numerous large eruptive events from Bogoslof provide a unique calibration dataset allowing experimentation and optimization of different RTM strategies. Tuning the RTM algorithm is key to its success, but many challenges exist such as varying signal durations and amplitudes, as well as the typical source-station distributions and most volcanic eruptions occurring outside the network. Our methods cater to both event detection using real-time data as well as scanning of data archives for detecting and discriminating volcanic and non-volcanic events. The TA's rich records of infrasound from volcanic eruptions allow comparison with plume heights derived from other instruments and may help constrain models on eruptive processes and improve future forecasts of ash dispersal. We plan to distribute event catalogs and additional data products for use by other researchers. We plan to produce multi-media products illustrating the RTM method and wavefields from volcanic eruptions in Alaska for use in public and undergraduate education and outreach.

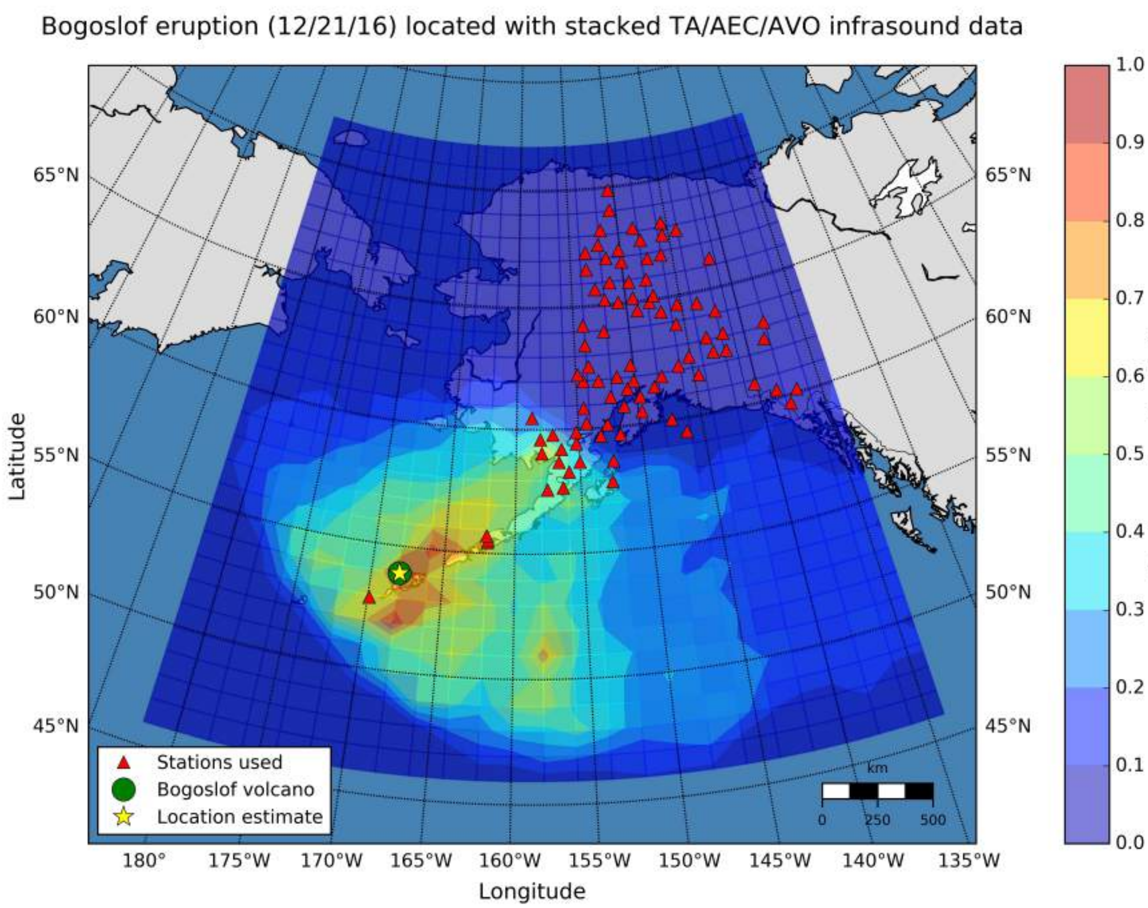

An unscented Kalman filter combining GPS and InSAR for time-dependent modeling of volcanic deformation at Okmok volcano, Alaska

Xueming Xue[1], **Jeffrey Freymueller**[1]

[1]Geophysical Institute, University of Alaska Fairbanks, Fairbanks, Alaska, USA

Corresponding author: Xueming Xue, `xxue@alaska.edu`

Abstract

The Kalman filter is an effective tool for time-dependent inversion of geodetic data. Based on a Mogi point source model, an unscented Kalman filter (UKF) was developed for volcanic source modeling using GPS observations. The UKF allows retrieval of the time-dependent history of both source strength and source location. We have expanded the UKF to be able to integrate Interferometric Synthetic Aperture Radar (InSAR) observations. Before applying the UKF, it is necessary to estimate the uncertainty of the InSAR data. We remove a time-independent Mogi source and phase ramp from every InSAR image and use the residual to obtain its variance-covariance information. The GPS and InSAR time series can then be combined using the UKF. Continuous GPS data indicates that Okmok volcano, Alaska, started inflating soon after the 2008 eruption. The inflation then slowed down, but suddenly sped up again in the middle of 2013. We apply this approach to the post-eruptive inflation of Okmok. We use GPS data from 4 continuous sites and 3 campaign sites and InSAR data from 4 different acquisition tracks of TerraSAR-X and Envisat satellites throughout the 2008-2014 time period.

EarthScope Transportable Array Posthole Sensor Emplacements in Alaska and Canada

K. Aderhold, R. W. Busby, A. Frassetto, M. Enders, J. Miner, R. M. Bierma, R. Woodward

From 2011 to 2016, IRIS has built or upgraded 139 broadband seismic stations in Alaska and western Canada as part of the EarthScope Transportable Array (TA) program. The TA will complete another 78 installations in 2017 and operate the full network of 270 real-time stations through at least 2019. The removal of some TA stations is tentatively planned for 2020, but upgrades to existing stations are permanent contributions to these networks. Nearly all use new posthole seismometers, emplaced at ~3 m depth in cased holes within fractured bedrock outcrops, permafrost, or soil.

The TA stations are a proof of concept for a new approach to emplacement of seismometers across a large network and will enable high-quality scientific research as well as advances in hazard monitoring. To evaluate the new and upgraded stations, we use probability density functions of hourly power spectral density computed by the IRIS DMC MUSTANG metric service. Our results show significant improvement of TA postholes in Alaska and Canada over the tank vaults of the lower-48 TA. With an ideal posthole drilled into bedrock or permafrost, noise levels can approach the quality of GSN stations particularly on the horizontal channels at long periods [>70 seconds]. Stations also display a strong but expected regional and seasonal variation.

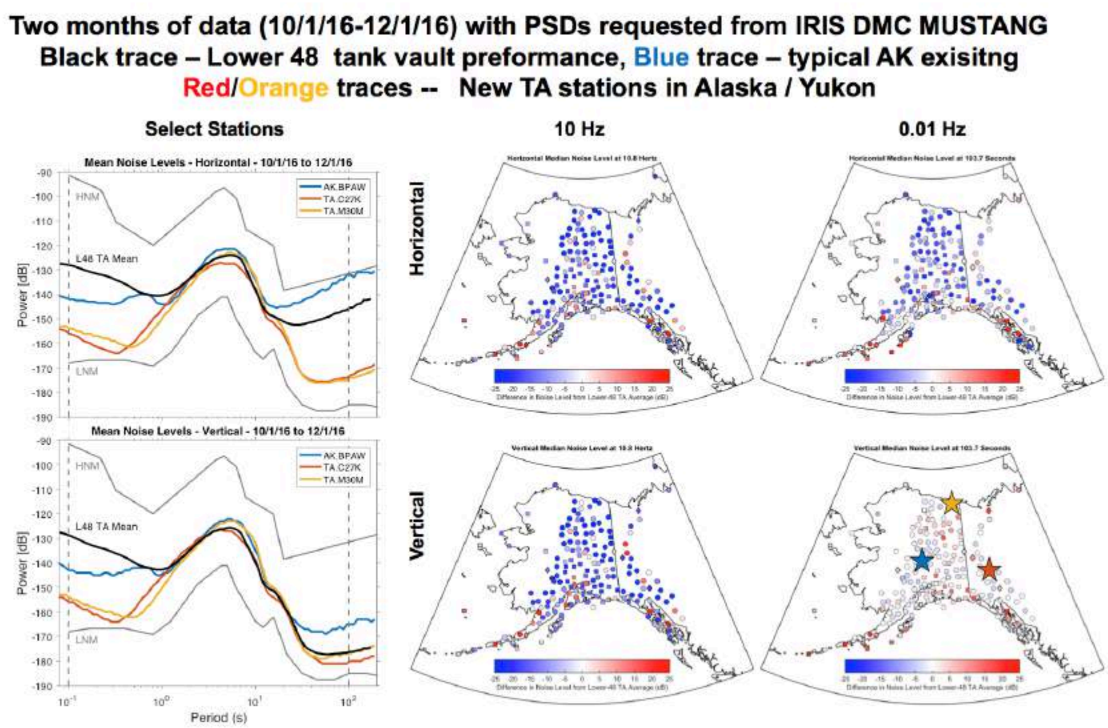

Full waveform time domain analysis of ionospheric current and magnetotelluric electromagnetic fields in Poker Flat, Alaska

Naoto Imamura (nimamura@ceoas.oregonstate.edu) [1], Adam Schultz[1], and Russell Cosgrove[2]
[1]Oregon State University, Corvallis, OR, USA, [2]SRI International, Menlo Park, CA, USA

While significant inroads are being made in jointly interpreting and even jointly inverting seismic and magnetotelluric (MT) data to reveal new details about Earth structure and dynamics, leveraging joint ionospheric physics and MT data in this way is very much a frontier activity, particularly at higher geomagnetic latitudes where the usual assumption of plane wave sources for MT data may break down in the presence of highly non-stationary, structurally complex auroral current systems. We report on efforts to image the electrical conductivity structure of the lithosphere and upper asthenosphere in the interior of Alaska where we allow for a non-stationary ionospheric source fields of arbitrary complexity above a 3-D Earth, and we set up an inversion of the MT time series waveform directly for Earth structure, given constraints on the ionospheric electric fields that are the source of the MT induction signal.

This goal would not be obtainable if one were to adopt the finite difference time-domain (FDTD) approach for the forward problem. This is particularly true for the case of magnetotelluric (MT) surveys, since an enormous number of degrees of freedom are required to represent the observed MT waveforms across the large frequency bandwidth. This means that for FDTD simulation, the smallest time steps should be finer than that required to represent the highest frequency, while the number of time steps should also cover the lowest frequency. We have implemented our code that addresses this situation through the use of a fictitious wave domain method and GPUs to speed up the computation time. We also substantially reduce the size of the time series by applying concepts from successive cascade decimation, through quasi-equivalent time domain decomposition. By combining these refinements, we have made good progress toward implementing the core of a full waveform joint source field/earth conductivity inverse modeling method.

Recent analysis of the Alaska data sets shows that EM fields measured at the Earth's surface are not orthogonal. This indicates underlying 3D Earth structure in this area. Furthermore, the assumption that is typically made for MT analyses, that the inducing field is plane-wave in form, does not hold in this region. We also see the magnetic field at the MT sensor is aligned with the ionospheric electric field, which drives a Hall current, as expected from the underlying physics. We report on initial inversion of this data set.

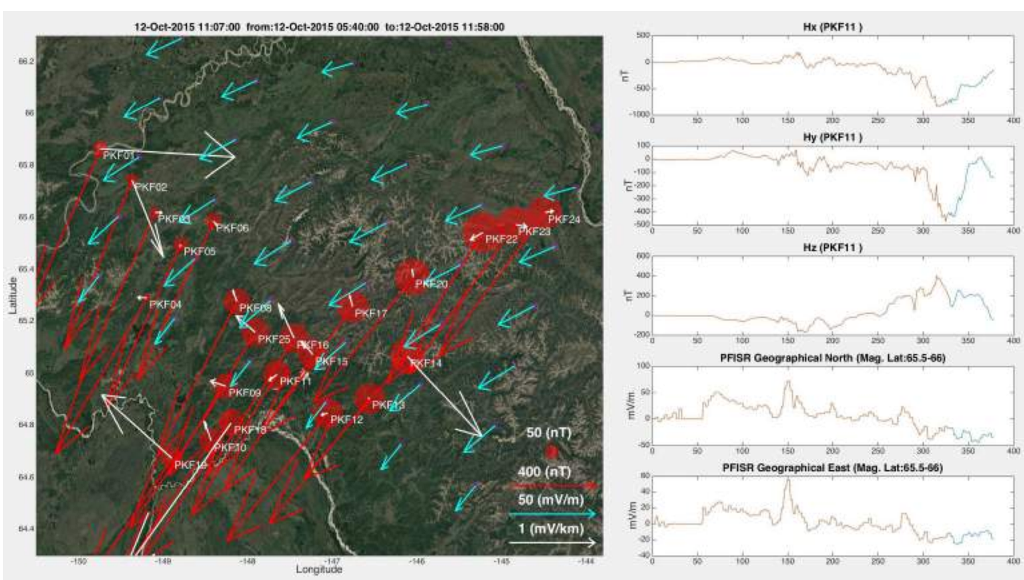

Figure 1. Field vectors measured at Earth's surface, and those inferred in the ionosphere, for a geomagnetically disturbed interval. Colored vectors indicate the ionospheric electric field (cyan), the horizontal electric (white) and magnetic (red) field measured by the MT systems, and the vertical magnetic field downward (red) or upward (blue) circles whose radius is proportional to the intensity of the vertical component. The ionospheric electric field drives a Hall current perpendicular to the electric field. The Hall current generates a magnetic field at MT systems. It means the magnetic field at the MT systems is aligned with the ionospheric electric field.

Investigating the Effect of Mantle Flow and Viscosity Structure on Surface Velocities in Alaska Using 3-D Geodynamic Models

Joseph McConeghy, Lucy Flesch, and Julie Elliott

The Pacific-North American plate boundary zone in Alaska and northwest Canada remains an important area of research due to its unique geologic features and enigmatic geodetic observations. Specifically, GPS velocity data from the Plate Boundary Observatory and other geodetic studies, display uncharacteristic surface motion inland of the plate boundary compared to other convergent and transform margins. Specifically, the velocity field in southern Alaska displays a rapid decrease in northwestward-directed velocity moving north from the plate boundary but deformation continues for several hundred kilometers. Additionally, southward motion directed towards the plate boundary is observed in northern and central Alaska, as well as southwestward motion in western Alaska. It has been proposed that mantle flow coupled to the North American lithosphere generates the anomalous surface motions here, yet a complete 3-D understanding of the forces generating these observations remains elusive. We present a 3-D geodynamic model of Alaska to better understand the variables involved in producing these surface velocities. We solve the force balance equations for stokes flow through finite element modeling using COMSOL multiphysics software (comsol.com). The spherical model geometry incorporates the observed topography of the area, the subducting oceanic and Yakutat slabs, and the boundaries of the crust and lithosphere. Model densities are taken from CRUST 1.0. Viscosity structure is varied laterally and vertically within the continental plate and is determined using the vertical averaged effective viscosity estimates of previous studies. We investigate possible combinations of force balance, inclusion of lithospheric faults, and viscosity structures to determine models that produce surface velocity solutions that provide a best fit to the GPS velocity observations, which include updated data sets correct for the effects of elastic strain accumulation, post-seismic motion, and glacial isostatic adjustment so as to represent the long-term velocity field. We test different mantle flow models by applying a velocity boundary condition to the base of the model and varying the asthenospheric viscosity to investigate the level of lithospheric mantle coupling in generating the observed surface motions.

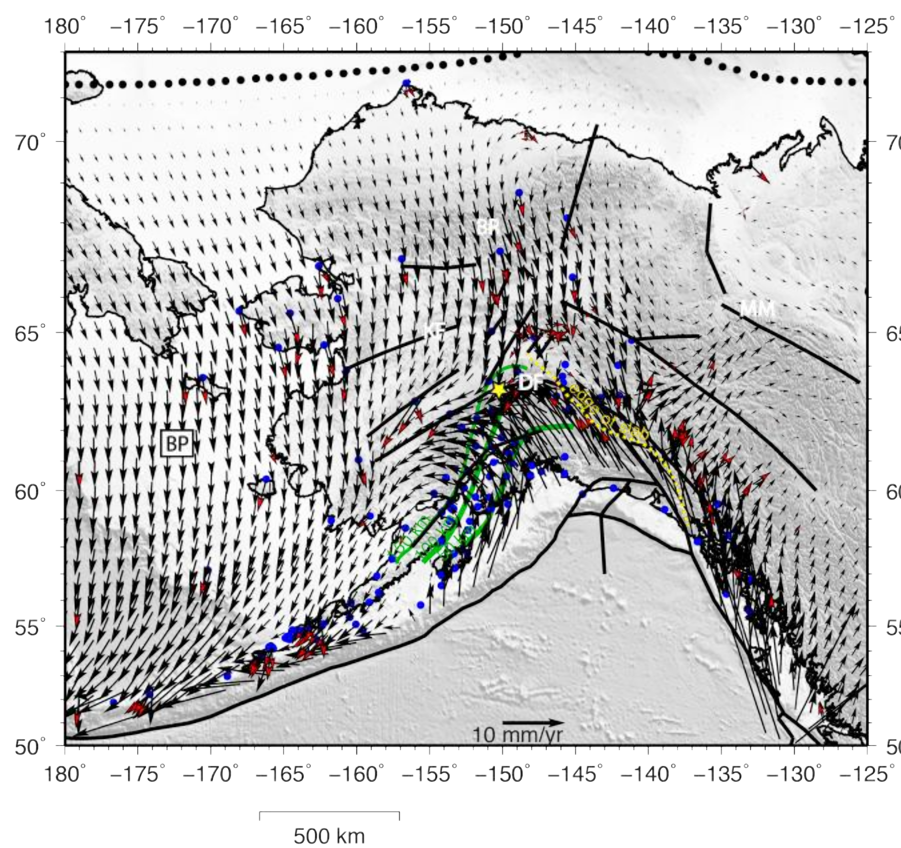

__Figure 1__. GPS data (red vectors) and kinematic model velocity field (black vectors, Finzel et al., 2015) plotted in a North American reference frame. Blue dots show locations of PBO sites. Green contours show position of the slab at 50 km intervals. Dashed yellow line represents the best estimate for the eastern edge of the slab (Eberhart-Philips et al., 2006; Jadamec and Billen, 2010). MM = Mackenzie Mountains; BR = Brooks Range; KF = Kaltag fault; BP = Bering Plate. Yellow star point where slip rates decrease on the Denali fault (Mériaux et al., 2009; Matmon et al., 2006). Black lines represent Quaternary fault traces from Finzel et al. (2011a).

Effects of Flat Slab Subduction on Shear Wave Splitting in Alaska

Amanda McPherson and Douglas Christensen
Geophysical Institute and Department of Geosciences, University of Alaska Fairbanks

Shear wave splitting studies have been used for decades to identify anisotropy and possible flow in the upper mantle. In this study we use approximately 2500 SKS wave splitting observations to study anisotropy over a broad region in Alaska, and in particular aim to understand mantle processes at plate margins. The recent expansion of broadband stations in Alaska through the EarthScope Temporary Array (TA) deployment, and several temporary PASSCAL/EarthScope experiments allow us to greatly expand the coverage from previous studies. Southern Alaska is dominated by young Pacific plate and the Yakutat block subducting under the North American plate, which yields flat slab subduction under south-central Alaska. New results confirm fast directions within the mantle wedge above the subducting Pacific slab parallel the strike of the subducting plate, and reveal that they change direction to follow the slab contours. The largest time delay observations are associated with these fast directions. In the region of flat slab subduction, oceanward of the mantle wedge, fast directions are parallel to Pacific plate motion (trench normal). There is evidence to suggest that this pattern changes to trench parallel to the west as flat slab subduction transitions into more typical subduction. Additionally, in southeast Alaska, fast directions follow the strike of the transform boundary between the Pacific and North American plates. This direction is also the direction of absolute motion for the Pacific plate.

SKS Splitting Observations

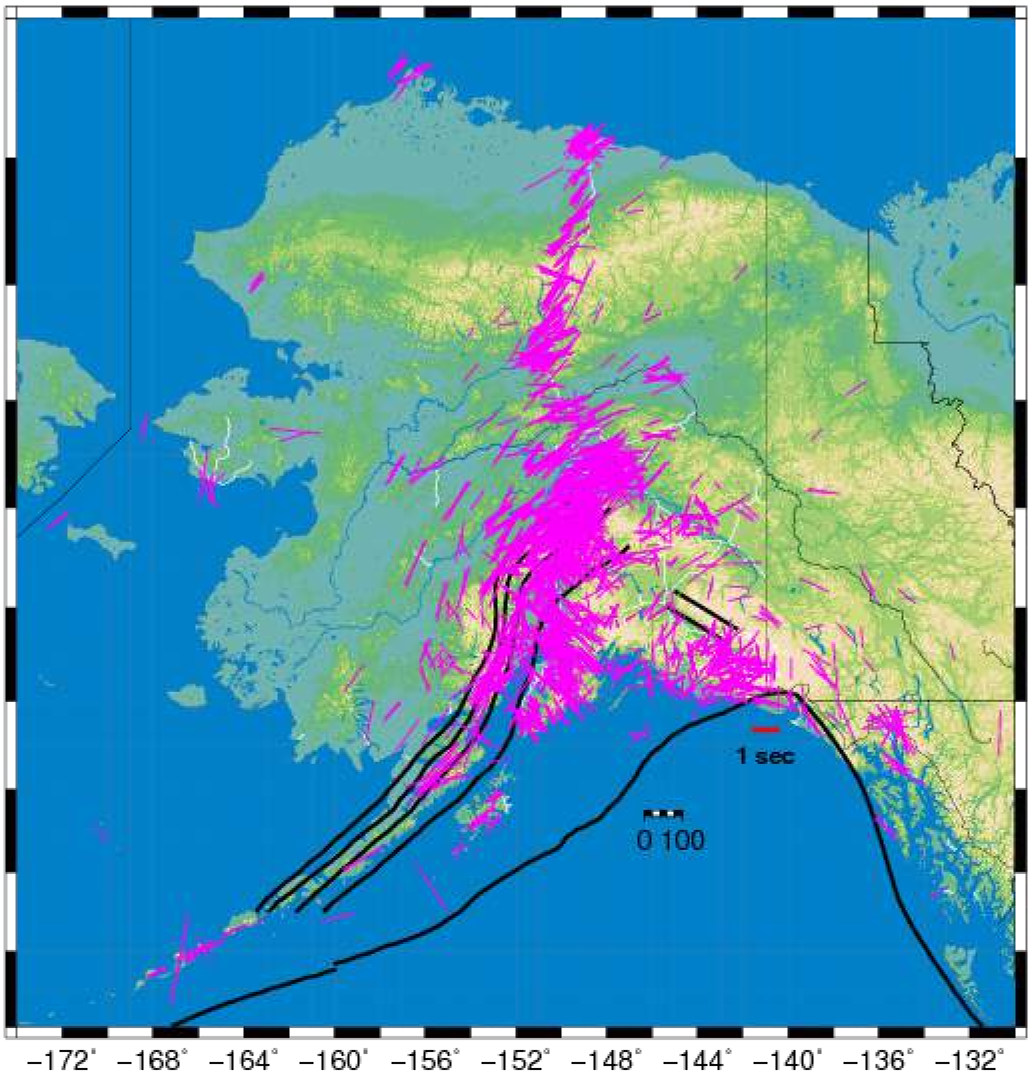

Sarah Robinson

Title: Assessing the role of water in Alaskan flat slab subduction

Authors: Sarah Robinson, Ryan Porter, Thomas D. Hoisch

Abstract:
Although plate tectonic theory is well established in the geosciences, the mechanisms and details of various plate-tectonics related phenomena are not always well understood. In some (~10%) convergent plate boundaries worldwide, subducting slabs do not sink into the mantle at a high angle as in the classic model of subduction zones. Rather, subduction of downgoing ocean plates is characterized by low angle to horizontal geometries and is termed "flat slab subduction". The mechanism(s) driving this form of subduction not well understood. My research will explore the role that water plays in these flat slab subduction settings. Understanding the role of water in subduction zones is important not only for providing a better understanding of flat slab subduction, but is also important for understanding volcanic hazards associated with both subduction and slab rollback (the process by which a subducting slab "rolls back" and sinks down into the mantle, often generating violent volcanism across a wide region). Using geophysical methods involving seismic data from seismometers deployed in the Alaska region, I will be assessing how slab hydration and dehydration play a role in creating the necessary buoyancy to maintain and end flat-slab subduction. This will be accomplished by producing shear velocity models for the Alaska region and comparing these results to forward models of seismic velocities using thermodynamic modeling software. These observations will provide constraints on the composition within these regions, as hydrated phases can be identified within these models due to higher Vp/Vs ratios, reduced shear velocities, and seismic anisotropy. My work will create models and quantify anisotropy within the crust and upper mantle.

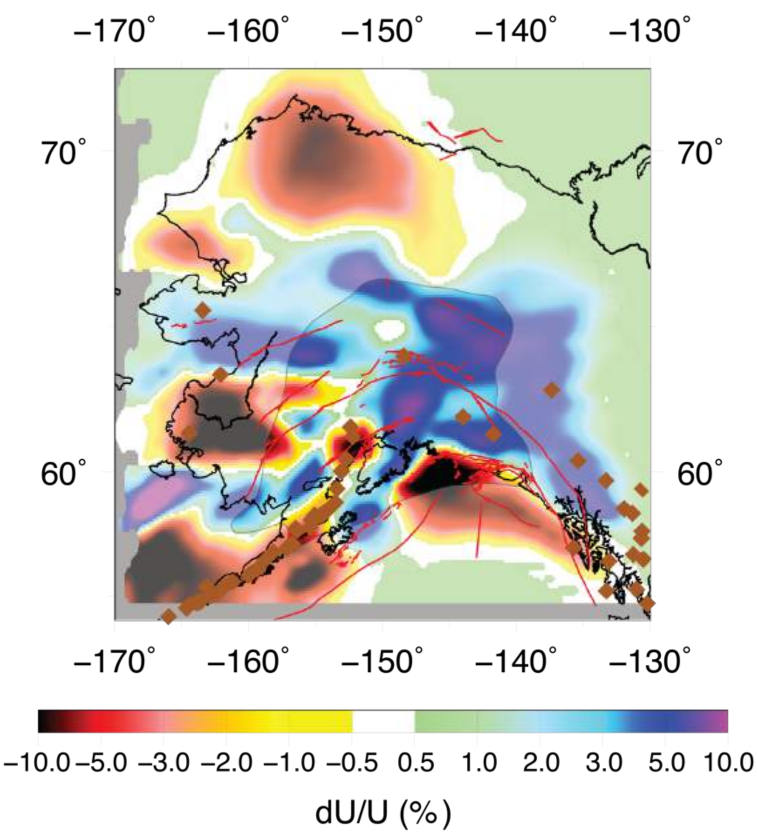

Figure shows Ambient Noise Tomography phase velocities at 10 seconds (~10 km depths) using data from 546 stations. Brown diamonds are Quaternary volcanoes and red lines are Quaternary faults.

Contributions of USArray to Earthquake Monitoring in Alaska

Natalia A. Ruppert and Michael West, University of Alaska Fairbanks

Alaska is the most seismically active state in the nation with earthquakes spanning tectonic regimes, including transform faulting in the southeast Alaska, collision in the St.Elias region, subduction in southern Alaska and along the Aleutian Island Arc, and complex crustal faulting extending north to the Beaufort Sea. As a result of this tectonic complexity, earthquake detection in Alaska is non-trivial. Automatic earthquake detection and review procedures have existed at the Alaska Earthquake Center for decades. The procedures have been calibrated to measure as much seismicity as feasible while minimizing errors and workload. In the last two years, the seismic station coverage in Alaska has grown significantly with the presence of the USArray TA. The TA stations have provided an unprecedented opportunity to expand earthquake reporting in areas of Alaska that have never been instrumented. The Alaska Earthquake Center has been incorporating all TA data into its routine earthquake analysis. Recent increases in the number of reported earthquakes (just under 38,000 in 2016) can be correlated with additional TA stations, especially those installed in the northeast Brooks Range, Bristol Bay region and interior Alaska. In recent months, phase picks from TA stations totaled about 20,000 per month (or about 25% of the total picks). In the northeastern Brooks Range, the number of stations went from a handful to a couple of dozen. As a result, the magnitude detection threshold has decreased by about an order of magnitude. We expect that installation of the remaining TA stations in western Alaska will yield similar results. This presentation will assess the quantitative changes in earthquake reporting that have occurred because of the inclusion of data from the TA stations.

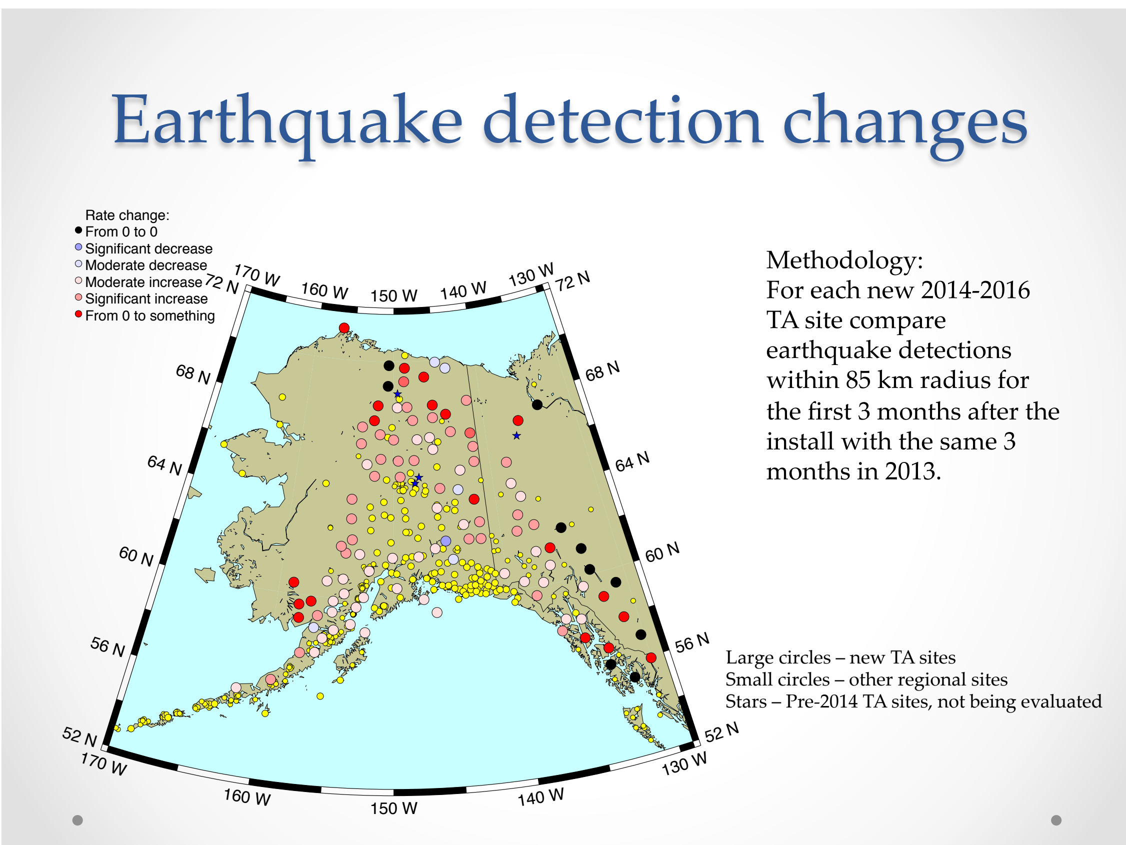

Amplification of seismic waves in Nenana basin, central Alaska

Kyle Smith, Carl Tape

Geophysical Institute
University of Alaska Fairbanks, USA
EarthScope Annual Meeting, May 2017
Anchorage, Alaska

We are interested in better understanding the interactions between the seismic wavefield and large-scale sedimentary basins. Our region of focus is Nenana basin in central Alaska. Nenana basin is a northeast-trending, several-km-thick, narrow sedimentary basin overlying the Minto Flats fault zone. Seismic stations, including the temporary FLATS network and EarthScope's Transportable Array, record regional earthquakes as well as continuous ambient noise. Seismic waves from earthquakes and from ambient noise are strongly amplified within the basin. We identified specific frequencies where amplification occurs by applying various filters to earthquake waveforms. Our approach considers amplification with the waveform metrics: duration, radiated energy, peak displacement, peak velocity, and peak acceleration. With two published maps of the depth-to-basement, we test the linearity between depth and our calculated metrics and explore differences between the two maps. We find good correlations between depth and the values of several metrics for periods near 1 second. We use amplitude spectra of recorded earthquakes from stations inside and outside the basin to quantify the influence of the basin, which is prominent at periods of about 1 second. We also use frequency-dependent variations in ambient noise to investigate the basin response. Amplitudes of ambient noise correlate with basin depth at periods greater than 1 second. Our results from earthquake metrics, spectral ratios, and ambient noise show that basin excitation occurs at periods of 0.5–2 seconds, consistent with observations from other large basins.

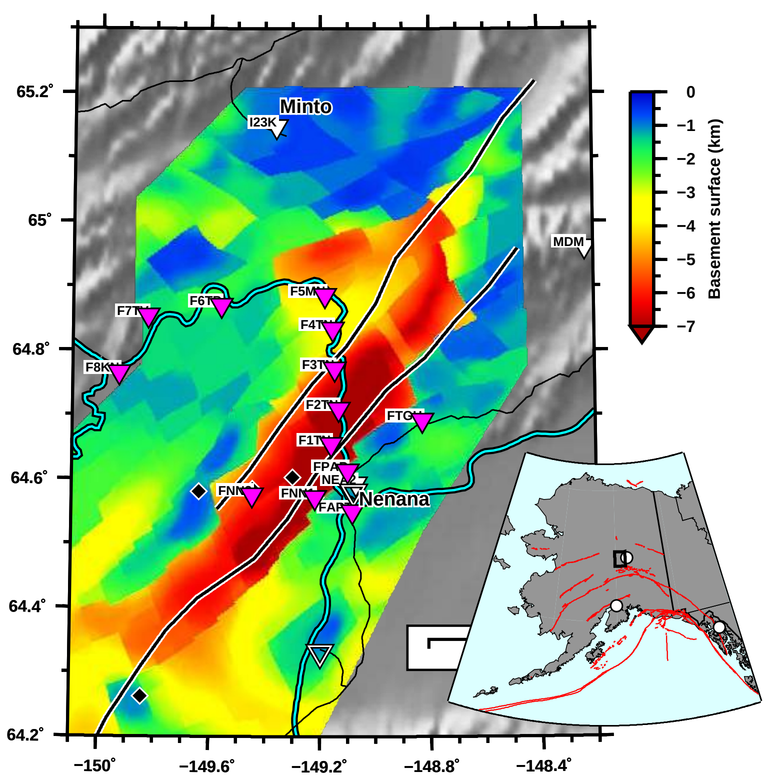

Figure 1: Basement surface (Doyon, Ltd.) for Nenana basin, central Alaska. Magenta triangles show the FLATS seismic stations, which cross the Minto Flats fault zone.

A seismic noise analysis to assess the influences of structure, site, and installation for the SALMON experiment in the Cook Inlet region, southern Alaska

Carl Tape[1], Justin Sweet, Kyle Smith, Douglas Christensen, Melissa M. Moore-Driskell

[1]Geophysical Institute
University of Alaska Fairbanks, USA
EarthScope Annual Meeting, May 2017
Anchorage, Alaska

The Southern Alaska Lithosphere and Mantle Observation Network (SALMON) is a deployment of 28 broadband, direct-burial posthole seismometers in the Cook Inlet region of the southern Alaska subduction zone. Here we describe the objectives of the project, the deployment strategy, and station design. We analyze time-dependent and frequency-dependent seismic noise for the first year of data at 18 SALMON stations, 11 of which are inside Cook Inlet basin, 7 of which are outside the basin. We compare noise at SALMON stations with four previous co-located seismic stations, two Transportable Array stations, and one Global Seismographic Network station. The type of site—notably surface bedrock versus sedimentary basin—has the strongest impact on seismic noise levels across all periods and especially on horizontal components at long periods (>20 s). Seismic noise and earthquakes recorded by SALMON stations reveal amplification of seismic waves in Cook Inlet basin. Aftershocks of a $M_{\mathrm{w}}\,7.1$ intraslab earthquake augment a catalog of local earthquakes to be used for source inversions and seismic imaging of the complex seismic structure in the Cook Inlet region.

An unwanted long-period step-response signal: examples from Alaska earthquakes

Carl Tape, Vipul Silwal, Stephen Holtkamp

Geophysical Institute
University of Alaska Fairbanks, USA
EarthScope Annual Meeting, May 2017
Anchorage, Alaska

We present waveform record sections of 8 earthquakes in the Minto Flats fault zone in central Alaska. These include the largest earthquakes to have occurred within the Minto Flats fault zone since the installation of the 13-station FLATS network in September 2015. The first four earthquakes exhibit a long-period "step-response signal," an unwanted signal that does not reflect regional ground motion. For background on the step-response signal and related signals, see *Zahradnik and Plešinger* (2005); *Boore and Bommer* (2005); *Delorey et al.* (2008); *Zahradnik and Plešinger* (2010); *Vackar et al.* (2015); *Sakai et al.* (2016); *Wilson et al.* (2017). A complementary report by *Holtkamp and Tape* (2016) used waveform template matching to examine the occurrences of the step-response signal on stations throughout Alaska, during earthquakes and during quiescence. We use the term "artificially high amplitudes" to refer to amplitudes within a certain bandpass that exceed the amplitude of earthquake ground motion (within the same bandpass). We attribute artificially high amplitudes to three possibilities: (1) step-response signal, (2) clipping, and (3) high noise (including before earthquake). We find widespread occurrences of the step-response signal for earthquakes in the Minto Flats fault zone. Additional laboratory testing and analysis of previously recorded data are needed to understand the conditions that promote the unwanted step-response signal, in hopes of mitigating its influence in future sensors and installations.

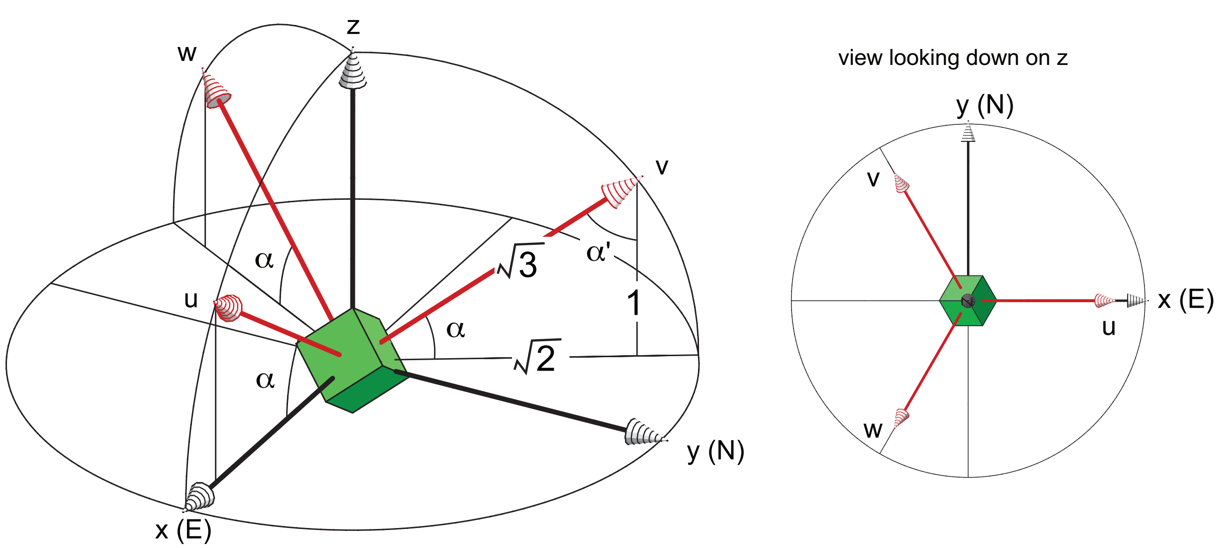

Figure 1: Relationship between xyz axes and uvw axes for the Nanometrics Trillium T120PH sensor. Each uvw axis makes an angle of $\alpha' = \cos^{-1}(1/\sqrt{3}) \approx 54.74°$ with the vertical direction. Rotating the coordinates for the recorded wavefield (from xyz to uvw) can help isolate the source of the step-response signal.

References

Boore, D. M., and J. J. Bommer (2005), Processing of strong-motion accelerograms: needs, options and consequences, *Soil Dynamics and Earthquake Engineering*, *25*, 93–115, doi:10.1016/j.soildyn.2004.10.007.

Delorey, A. A., J. Vidale, J. Steim, and P. Bodin (2008), Broadband sensor nonlinearity during moderate shaking, *Bull. Seismol. Soc. Am.*, *98*(3), 1595–1601, doi:10.1785/0120070225.

Holtkamp, S., and C. Tape (2016), Step-response signals recorded at seismic stations in Alaska, ScholarWorks@UA at `http://hdl.handle.net/11122/7019` (last accessed 2016-10-14).

Sakai, T., H. Kumagai, N. Pulido, J. Bonita, and M. Nakano (2016), Discriminating nonseismic longperiod pulses and noise to improve earthquake source inversion, *Earth Planets Space*, *68*(50), 1–14, doi:10.1186/s40623-016-0426-0.

Tape, C., and M. E. West (2014), Fault Locations and Alaska Tectonics from Seismicity, International Federation of Digital Seismograph Networks. Other/Seismic Network. `doi:10.7914/SN/ZE_2015`.

Vackar, J., J. Burjanek, and J. Zahradnik (2015), Automated detection of long-period disturbances in seismic records; MouseTrap code, *Seismol. Res. Lett.*, *86*(24), 442–450, doi:10.1785/0220140168.

Wilson, D., A. T. Ringler, and C. R. Hutt (2017), Detection and characterization of pulses in broadband seismometers, *Bull. Seismol. Soc. Am.* (in review).

Zahradnik, J., and A. Plešinger (2005), Long-period pulses in broadband records of near earthquakes, *Bull. Seismol. Soc. Am.*, *95*(5), 1928–1939, doi:10.1785/0120040210.

Zahradnik, J., and A. Plešinger (2010), Toward understanding subtle instrumentation effects associated with weak seismic events in the near field, *Bull. Seismol. Soc. Am.*, *100*(1), 59–73, doi:10.1785/0120090087.

Lithospheric Structure across the Alaskan Cordillera from Surface Wave Analysis

Kevin M. Ward[1] & Fan-Chi Lin[1]
[1]The University of Utah

The long awaited Transportable Array (TA) deployment in Alaska and western Canada is nearing its final deployment stage. With only one more deployment season, most of the TA station locations have been occupied and begun providing data. These TA stations combined with upgraded existing locations have provided enough high quality data to begin investigating the crustal and upper mantle structure across the entire Alaskan Cordillera. From a tectonic standpoint, many interesting questions remain unanswered. *For example, how does the transition from oceanic-oceanic subduction to continental-oceanic normal subduction to continental-oceanic "flat-slab" subduction to strike-slip conservative plate motion affect the deformation/uplift of the overriding plate and mantle geodynamic characteristics? How does the long and completed terrene accretion process partition stress/strain in the crust? On more local scales, are there any significant mid-crustal magmatic systems as observed in other sections of the American Cordillera, and if so, what is there role in uplift and crustal deformation?*

Our approach to investigating these questions is though surface wave imaging from ambient noise and earthquake generated sources along with Rayleigh wave ellipticity. Our preliminary tomography results agree with previous studies but expand the spatial coverage showing additional detail. Our ellipticity results show a heterogeneous but spatially consistent anisotropic shallow crust. Although the complete TA data set has not yet been collected, we have begun the initial steps required to combine our results with both body waves and receiver functions with the end goal of inverting for a 3-D shear-wave velocity model across the entre Alaskan Cordillera. This model will provide the basis for addressing many of the questions outlined above.

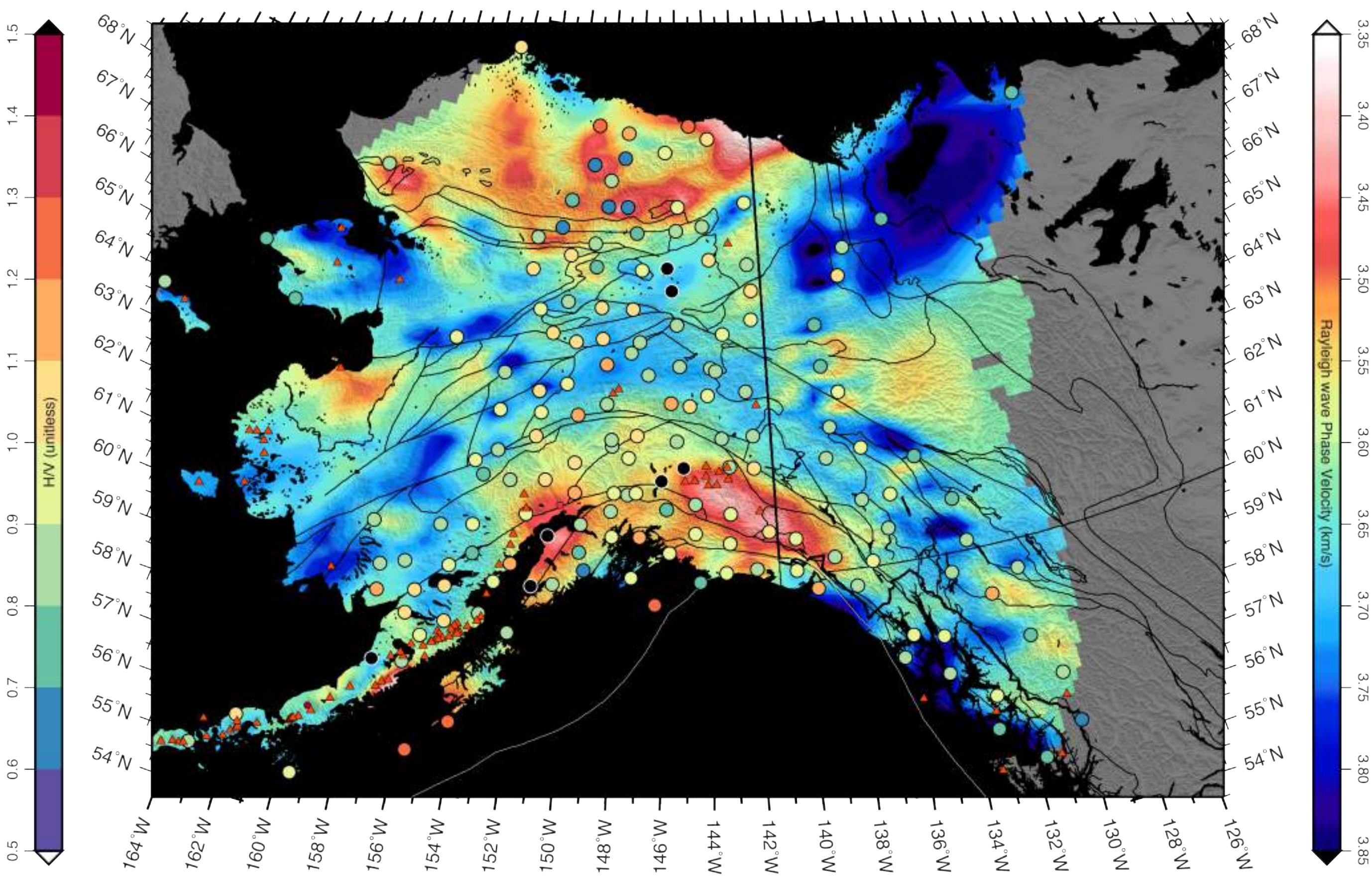

Figure 1. Rayleigh wave phase velocity map at 25 seconds period across the Alaskan Cordillera (more sensitive to crustal thickness variations). Rayleigh wave ellipticity (H/V) at 10 seconds period (more sensitive to top 5km) shown as colored small circles.

Shear Wave Splitting Underneath Northwest Canada and Eastern Alaska

Derek R. Witt[1], Derek L. Schutt[1], Richard C. Aster[1], Jeff T. Freymueller[2], and Joel Cubley[3]

[1]Department of Geosciences, Colorado State University, Fort Collins, CO, USA
[2]Department of Geology and Geophysics, University of Alaska – Fairbanks, Fairbanks, AK, USA
[3]Centre for Northern Innovation in Mining, Yukon College, Whitehorse, YT, CAN

Preliminary shear wave splitting results from the Northern Cordillera and surroundings will be presented. This complex tectonic setting contains a subduction zone responding to the Yakutat Indenter, an oceanic plateau fragment; a slab window under the Yukon Territory; and the actively uplifting Mackenzie Mountains. A particular goal of this project is to understand whether asthenospheric tractions play a significant role in Mackenzie Mountain uplift. Using a new method for calculating station averaged splitting parameters, we have analyzed stations that span a large part of the region (Figure 1) and therefore can see the variation in splitting parameters from the dynamic NA-PA subduction zone to the stable Slave Craton. Like other shear wave splitting studies in the Northern Cordillera, we find abrupt changes in fast axis direction along the continental margin, while the continental interior displays more coherent splitting parameters. This study is also the first to look at data from a recent site deployed at Macmillan Pass near the Yukon – Northwest Territories border in the center of the Mackenzie Mountains. At this station, we find an average fast axis direction that is very close to the absolute NA plate motion but our large deviations from event to event suggest that there is some crustal anisotropy and/or dipping structure present. This observation may support the idea of a lower crustal décollement that has been put forth by Mazzoti and Hyndman [2002]. These results serve as a broad regional overview of mantle anisotropy and may also shed light on frozen lithospheric deformation.

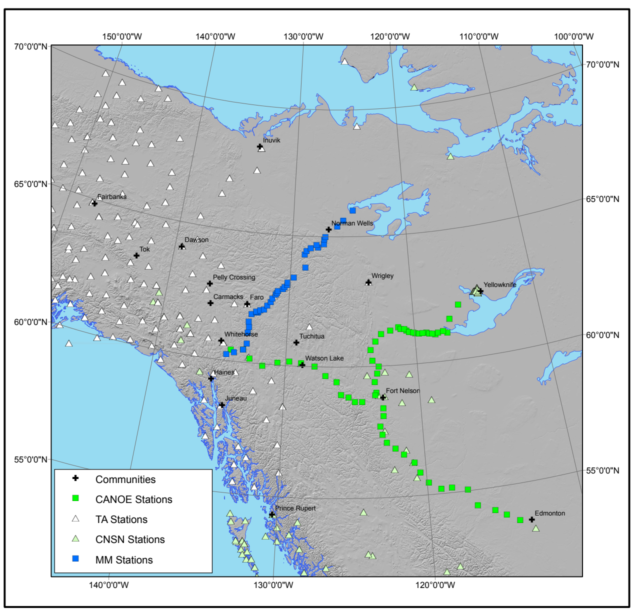

Figure 1. Regional map of present and past broadband seismic stations. The networks included in this map are Transportable Array (white triangles), Canadian National Seismographic Network (yellow triangles), Mackenzie Mountains transect (blue squares) and CANOE (green squares). Note that a subset of these were chosen for our study.

Mazzotti, S., and Hyndman, R. D., 2002, Yakutat collision and strain transfer across the northern Canadian Cordillera: Geology, v. 30, no. 6, p. 495-498.

A 10-Year Catalog (2007–2016) of Seismic Moment Tensors in Southern Alaska

Joshua Purba, Vipul Silwal, and Carl Tape

Geophysical Institute
University of Alaska Fairbanks, USA
EarthScope National Meeting, May 15-18, 2017
Anchorage, Alaska

We present a moment tensor catalog of 146 crustal and slab earthquakes in southern Alaska from August 2009 to April 2016 with $M_\mathrm{w} \geq 4.0$. Moment tensor solutions are estimated by fitting observed and synthetic waveforms for body and surface waves using different bandpass filters. The earthquakes are assumed to be double couple mechanisms, and the inversion parameters are strike, dip, rake, M_w, and source depth. For some events we also incorporate the first-motion polarities to help constrain the solution. The waveform fitting approach provides higher-quality solutions in comparison with existing catalogs made using first-motion polarities only. Time shifts between data and synthetics in the moment tensor inversions provide insight into the deviation of actual structure from the used 1D velocity model. These 146 events—together with 106 presented in presented in Silwal and Tape (2016)—form the major part of the sources to be used in and adjoint tomographic inversion for the structure of southern Alaska. The improved mechanisms will reduce errors in tomographic inversions, while also providing a framework for interpreting active tectonics in Alaska.

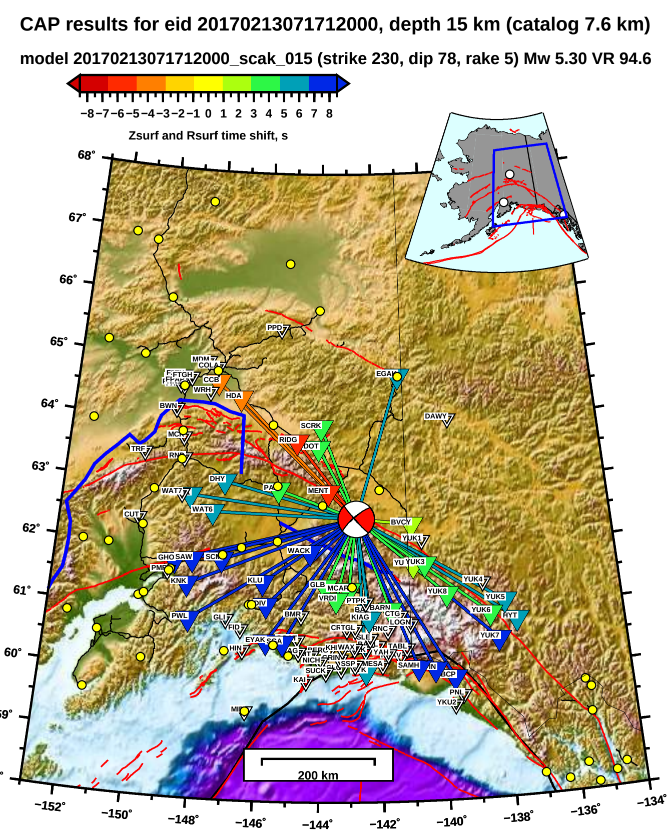

Figure 1: Rayleigh wave time-shifts for 2017–02–13 Totschunda earthquake. The triangles represent AEC broadband stations. The time-shift values are calculated by the waveform fitting approach. A negative time-shift means that the synthetic waveforms need to be shifted back in order to match with the observed seismogram, and vice versa.

Crustal earthquakes in the Cook Inlet and Susitna regions, southern Alaska

Vipul Silwal and Carl Tape

Geophysical Institute
University of Alaska Fairbanks, USA
EarthScope National Meeting, May 15-18, 2017
Anchorage, Alaska

Several large ($M > 6$) earthquakes have occurred in the vicinity of Anchorage within the past century. However, the presense of the underlying subducting Pacific slab makes it difficult to determine the origin of these older earthquakes as either crustal, slab, or the subduction plate interface. Here we focus on modern crustal seismicity to better understand the style of faulting and the location of active structures immediately west of Anchorage. We investigate regions of high crustal seismicity within three region: Beluga mountain, upper Cook Inlet, and Susitna. We perform double-couple moment tensor inversions using high frequency body waves (1–10 Hz) for small to moderate ($M > 2.5$) crustal earthquakes (dep <30 km) occurring from 2007 to 2016. Our misfit function combines both waveforms differences as well as first-motion polarities in order to obtain reliable moment tensor solutions. Results show that most crustal earthquakes in Cook Inlet have reverse faulting with strike aligned with the Cook Inlet anticlines. In Susitna most earthquakes have strike-slip or reverse faulting with strike aligned with the fault delineated from the seismicity rate. Hypocenter relocations using travel-time double-difference algorithm *Waldhauser and Ellsworth* (2000) reveal diffuse crustal deformation.

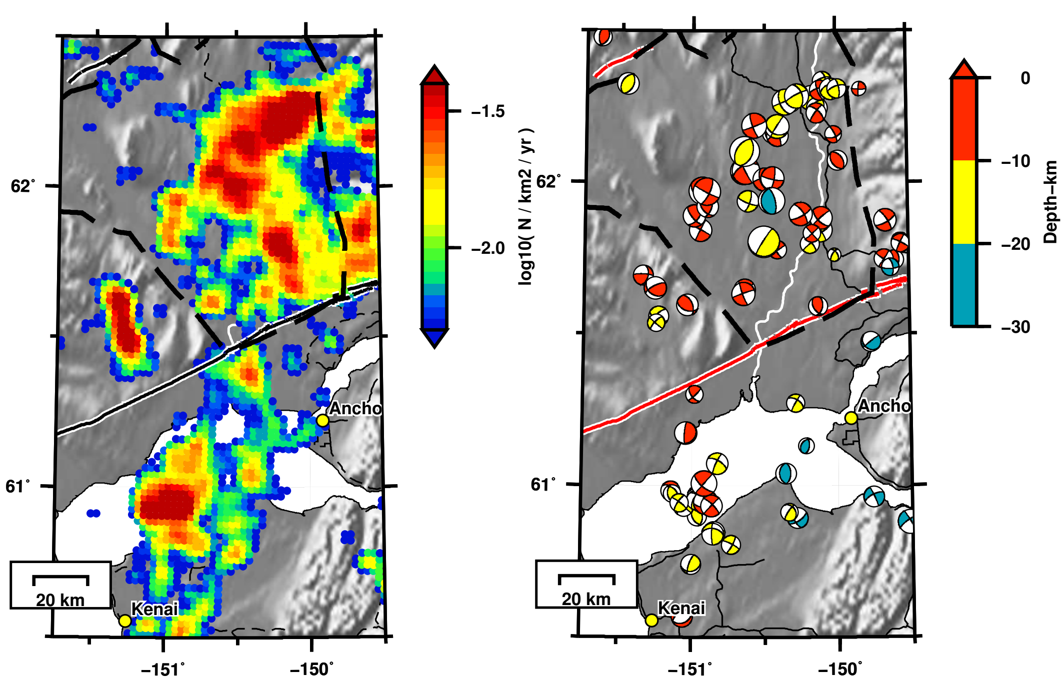

Figure 1: Crustal seismicity (depth $\leq$ 30 km) from 1990–2016 around Cook Inlet and Susitna regions, southern Alaska. **(left)** Smoothed logarithmic seismicity rate estimated using $M > 1.5$ earthquakes. Marked in pink are the boundaries for the regions of enhanced seismicity. **(right)** AEC fault-plane solutions for moderate ($M > 3.5$) crustal earthquakes. We also peform moment tensor inversion for some of these which occured after August 2007 (deployment of MOOS array; so that we can get decent station coverage). The beachballs in red and yellow are interpreted to be crustal events; and the blue beachballs (most certainly the ones to the south-east) to be slab events.

Examination of Network Matched Filtering MAD Thresholding Issues with application to interior Alaska Earthquake Swarms

The Minto Flats fault zone (MFFZ) in central Alaska is a left-lateral strike-slip fault system expressed as multiple, partially overlapping faults. We have documented earthquake swarms and Very Low Frequency Earthquakes in the MFFZ, some of which immediately precede larger mainshock (MS) events. We used the Alaska Earthquake Center catalog to systematically search through groups of earthquakes in interior Alaska to locate potential earthquakes swarms. We have found ~35 swarms occurring in the last two decades, including swarms possibly triggered by teleseismic events and five foreshock (FS) swarms that occurred directly before mainshock events. The FS swarms, as well as swarms on or near the main fault strands, tend to occur on the faults and at depths between 18- 24 km, while the swarms not associated with MS events or main fault strands occur throughout the entire seismic region at various depths.

We used these swarm events as templates in a network matched filtering process to build a catalog of swarm earthquakes in order to test dynamic triggering hypotheses and determine any relation to larger MS events. While utilizing network matched filtering, we found that the thresholding method used, median absolute deviation (MAD), allowed for more false positive detections than predicted, especially when the templates were of longer lengths. This disagreed with our hypothesis that longer templates would be more difficult to match, and therefore produce less detections. Using MAD requires a normal distribution of the correlation values around 0; however, we found that the set of peaks of the cross correlation values (i.e., the set of values which could pass through the filter) were not normally distributed and centered on a positive number. This shift in distribution caused the MAD designated threshold to allow for false detections of low correlation value. We will systematically test the parameters used in template creation to determine a more appropriate way to set a threshold that will optimize the matched filtering process and minimize the false detection rate. We suspect that every matched filter analysis which uses MAD thresholding is plagued by this improper assumption, though most have avoided the problem by using short template durations or very high thresholds.

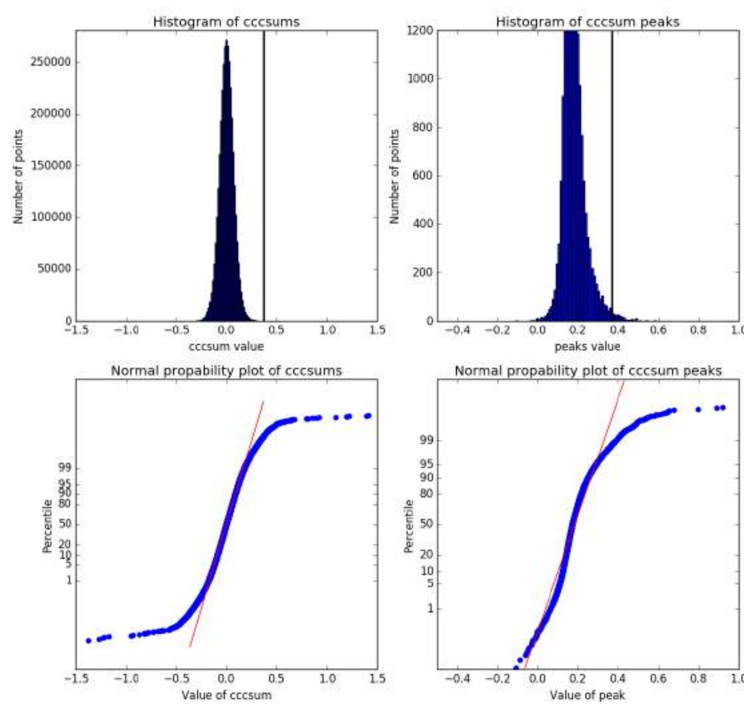

Figure: Distributions of cross-correlation sums (cccsum) calculated using matched filtering of one template over one day of data. Top: Histograms of cccsums (left) and cccsum peaks (right). Black line indicates value of MAD threshold. Bottom: Normal probability plots of cccsums and cccsum peaks. Red line indicates best fit line for a normal distribution. According to Shelly et. al (2007), using a threshold of 8*MAD we should expect ~0.17 false detections a day or 1 every six days. We had 319 detections pass over the 8*MAD threshold.

The M_s 7.3 earthquake of August 27, 1904 in central Alaska

Carl Tape[1], Anthony Lomax, Vipul Silwal, James D. Agnew, Brian Brettschneider

[1]Geophysical Institute
University of Alaska Fairbanks, USA
EarthScope Annual Meeting, May 2017
Anchorage, Alaska

On August 27, 1904, seismic stations from around the globe recorded a $M > 7$ earthquake originating from central Alaska. Very little was known about this earthquake. One felt report from Rampart, Alaska, had been attributed to the notes of Harry Fielding Reid, yet its original source was unknown. Here we present five felt reports for the 1904 earthquake that show evidence of felt shaking across most of central Alaska. Using the 1904 arrival time data, we estimate an epicentral location near Lake Minchumina at the northeastern extent of the Iditarod-Nixon fault. Our preferred fault for the 1904 earthquake is the right-lateral Iditarod-Nixon fault, which, though relatively seismically quiet, generated a M 6.2 earthquake in 1935. Paleoseismic investigations are needed to search for evidence for fault activity, including the 1904 earthquake rupture, in the tectonically complex region of the 1904 earthquake.

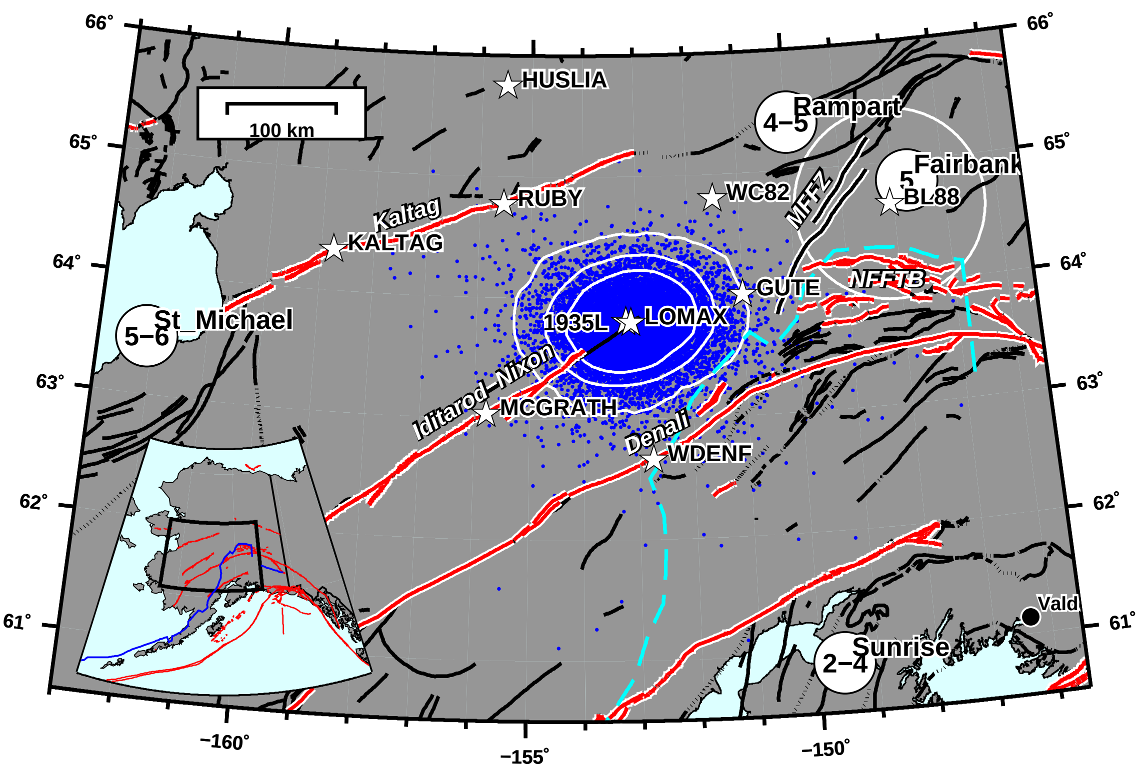

Figure 1: Epicenter and samples of the posterior probability distribution for the 1904 earthquakes. Plotted for reference are the active faults of *Koehler et al.* (2012), the faults of *Plafker et al.* (1994), the Minto Flats fault zone (MFFZ) of *Tape et al.* (2015), and the lateral extent of slab seismicity (dashed line). 1904-08-27 M_s 7.3 earthquake (LOMAX) plotted as posterior samples with confidence curves for 50%, 70%, and 90%. The epicenter LOMAX is 107 km west of Gutenberg's (GUTE) and 5 km from the epicenter of the 1935 earthquake (1935L). The expected rupture length for the M_s 7.3 earthquake is 120 km, which is approximately the scale bar at upper left. Also plotted as a white circle is the 75% confidence ellipse reported for BL88 *Boyd and Lerner-Lam* (1988).

References

Boyd, T. M., and A. L. Lerner-Lam (1988), Spatial distribution of turn-of-the-century seismicity along the Alaska-Aleutian Arc, *Bull. Seismol. Soc. Am.*, *78*(2), 636–650.

Koehler, R. D., R.-E. Farrell, P. A. C. Burns, and R. A. Combelick (2012), Quaternary faults and folds in Alaska: A digital database, Alaska Div. Geol. Geophys. Surv. Miscellaneous Publication 141, 31 p., 1 sheet, scale 1:3,700,000.

Plafker, G., L. M. Gilpin, and J. C. Lahr (1994), Neotectonic Map of Alaska, in *Geology of Alaska*, *The Geology of North America*, vol. G-1, edited by G. Plafker and H. C. Berg, Geol. Soc. Am., Boulder, Colo., USA, Plate 12.

Tape, C., V. Silwal, C. Ji, L. Keyson, M. E. West, and N. Ruppert (2015), Transtensional tectonics of the Minto Flats fault zone and Nenana basin, central Alaska, *Bull. Seis. Soc. Am.*, *105*(4), 2081–2100, doi:10.1785/0120150055.

Analysis of regional seismograms and 3D synthetic seismograms for the 2016-01-24 M_w 7.1 Iniskin earthquake in southern Alaska

Carl Tape

Geophysical Institute
University of Alaska Fairbanks, USA
EarthScope Annual Meeting, May 2017
Anchorage, Alaska

I perform two analyses to identify cases of seismogram clipping or other problems (e.g., data gaps) for the 2016-01-24 M_w 7.1 Iniskin, Alaska, earthquake. The first analysis is a comparison of synthetic and observed seismograms: three-component, displacement seismograms filtered between periods 4–80 s. The subset of 141 stations is limited to an oblique rectangular region that is 1200 km x 600 km and used in a seismic wavefield simulation with a three-dimensional seismic velocity model. I identify 60 out of 141 stations that are suspected of clipping or other problems. Of the 81 good stations, only 8 are within 250 km of the Iniskin epicenter, and all 8 stations are outside of Cook Inlet basin, which strongly amplifies ground motion (both in data and in synthetics). The second, much simpler, analysis is to identify clipping based on the maximum counts on the waveforms. The max-counts approach reveals general agreeement with the classification based on long-period data and synthetics. The analysis suggests that (1) some recorded waveforms that exceed clipping levels may still be usable for some modeling purposes, and (2) some recorded waveforms that appear to be suitable for modeling purposes should probably be discarded due to clipping at high frequencies. The identification of suspected stations, along with the waveform comparisons, may help network operators assess the possibility of unexpected performance during the M_w 7.1 slab earthquake. A key unanswered question is: What kinds of modeling (e.g., moment tensor inversions) can be done with "lightly" clipped seismograms?

References

Ekström, G., M. Nettles, and A. M. Dziewoński (2012), The global GCMT project 2004–2010: Centroid-moment tensors for 13,017 earthquakes, *Phys. Earth Planet. Inter.*, *200-201*, 1–9, doi: 10.1016/j.pepi.2012.04.002.

Shellenbaum, D. P., L. S. Gregersen, and P. R. Delaney (2010), Top Mesozoic unconformity depth map of the Cook Inlet Basin, Alaska, doi:10.14509/21961, Alaska Div. Geol. Geophys. Surv. Report of Investigation 2010-2, 1 sheet, scale 1:500,000, available at `http://www.dggs.alaska.gov/pubs/id/21961` (last accessed 2016-10-30).

Detecting and Characterizing Repeating Event Sequences at Alaskan Volcanoes

Gabrielle Tepp, Matt Haney, Aaron Wech
USGS Alaska Volcano Observatory

Repeating event sequences at volcanoes have the potential to improve our understanding of magma ascent and allow for short-term forecasting of possible eruptions. Bogoslof volcano produced over 30 repeating event sequences during 4 months of volcanic activity between December 2016 and April 2017. Around half of these sequences preceded explosive eruptions. Preliminary analysis suggests that the inverse moment rate, a measure of seismic energy release over time, progressed differently for the sequences ending in eruptions compared with those that ended without one. Throughout the eruptive period, several different families were observed as repeating events, indicating that a variety of processes or sources produced the sequences. The progression and evolution of sequences also varied. We constructed an automated repeating event detector to identify sequences in progress and send near real-time notifications. Adding in real-time inverse moment rate measurements could potentially further improve our ability to forecast eruptions.

We apply the detector to the 2016-2017 Bogoslof eruption and other Alaskan volcanoes that have produced repeating event sequences prior to eruptions. During the 2009 Redoubt eruption, sequences were observed in the months leading up to the eruptive activity beginning in March 2009 as well as immediately preceding 3 of the 19 explosive events. In contrast, Okmok gave little warning of its 2008 eruption – only 3-5 hours of precursory seismic activity, which included repeating events. The repeating event alarm provides the opportunity to catch precursory activity early enough to lead to effective eruption forecasts at some volcanoes.

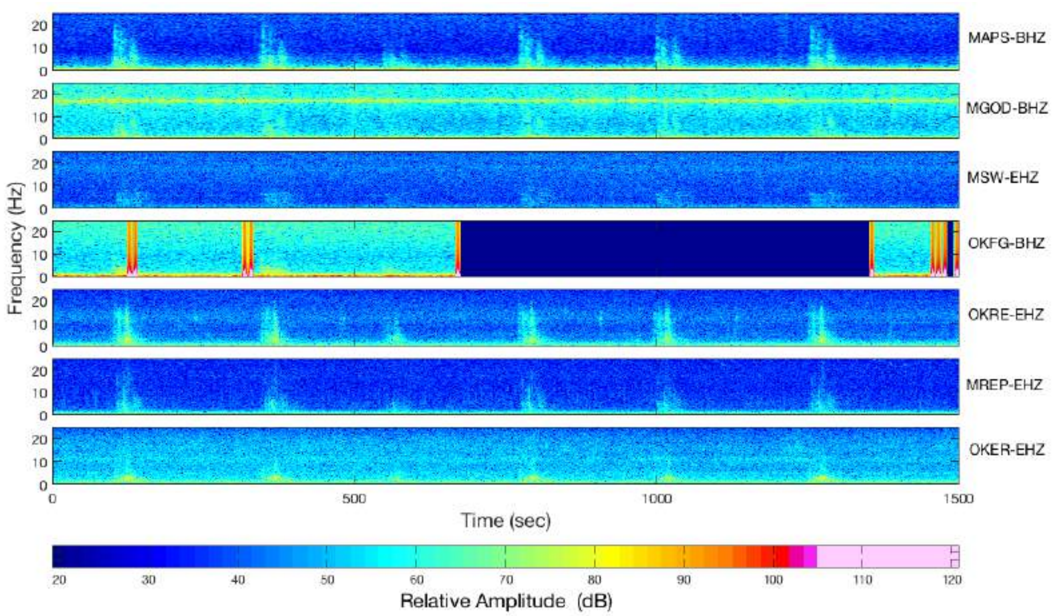

Event Sequence at level 2!

5 stations have at least one sequence at level 2! Time is 09-Jan-2017 05:32:30 UTC. Sequence parameters: min 5 events in 25 minutes.

Stations on level 2: MAPS, MGOD, MSW, OKRE, MREP

Figure: Example alert notification from the 9 January 2017 Bogoslof eruption.

3-D seismic imaging of Makushin Volcano, Alaska

F. Lanza, C. Thurber, E. Syracuse, A. Ghosh, and J. Power

Located in the eastern portion of the Alaska-Aleutian subduction zone, Makushin Volcano is among the most active volcanoes in the United States and has been classified as high threat based on eruptive history and proximity to the City of Unalaska and international air routes. Seismic imaging of its complex plumbing system has been previously attempted, but the unfavorable network geometry presented a great challenge. Here we expand on previous work in order to improve the resolution of the seismic structure beneath the volcano. We supplemented the one-sided station coverage provided by the Alaska Volcano Observatory (AVO) permanent seismic network with a set of five individual stations and three mini seismic arrays of 15 stations each. It provides us better azimuthal coverage with higher signal-to-noise ratio. Preliminary P-wave images obtained using data collected during the 2015-2016 deployment confirm the presence of high Vp features in the upper 5 km beneath the caldera, possibly delineating a remnant magma pathway or conduit. Low-Vp regions are found at approximately 7.5 km depth, which have been identified as a possible long-term source of magma based on geodetic models using InSAR data.

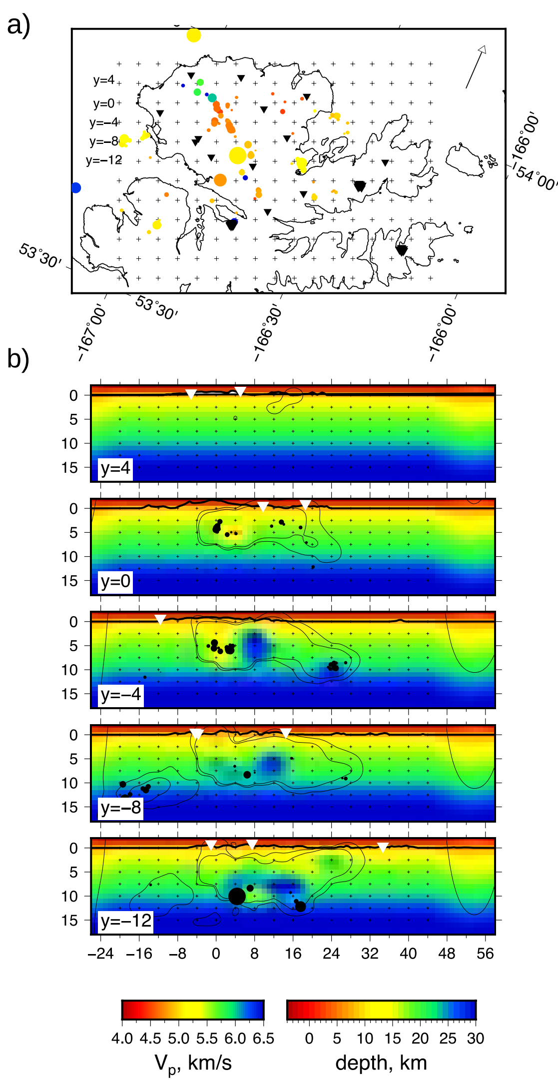

Figure. a) Relocations of 2015-2016 seismicity at Makushin volcano, with color indicating depth and symbol size indicating magnitude. b) Cross sections of the absolute Vp model and relocated seismicity. Black lines outline areas of the model with denser ray coverage, as defined by the 1% if the maximum body wave DWS value.

Relationships Between Gravity Waves Observed At The Surface
And In The Stratosphere Over The Continental United States

Michael A.H. Hedlin, Catherine D. de Groot-Hedlin,
M. Joan Alexander, Lars Hoffmann and Claudia Stephan

We examine propagating gravity waves detected at the Earth's surface and compare them to stratospheric gravity wave observations made with the AIRS satellite. Gravity waves are detected at the Earth's surface with sensors that comprise the USArray Transportable Array (TA), a network of approximately 400 seismo-acoustic stations deployed on a 70 km Cartesian grid covering an area of 2,000,000 km^2 in the continental United States. The network moves slowly eastward through station redeployments and from 2010 – 2012, was located in the Central US, near the Great Lakes. Using a novel technique to detect very long period pressure disturbances traversing the TA, we have found two distinct populations of gravity waves (GWs). Small amplitude waves have a diurnal pattern, which we believe is associated with the solar terminator. The larger amplitude waves that appear to be connected to convective cloud sources are the focus of this investigation. We have applied a 'rain mask' to these detections to ensure that we are examining gravity waves propagating away from the source regions, and not the movement of large-scale weather patterns. We report two lines of research with this new dataset. First, we study the long-term occurrence statistics of gravity waves and compare them to satellite observations of convective clouds and gravity waves in the stratosphere. We also study day-to-day occurrence of gravity waves on the ground and in the stratosphere in a smaller region to the west of the Great Lakes where activity peaks during the thunderstorm season in 2011.

In the recent past our research has been presented to the general public via televised lectures and seminars. This outreach will continue in the coming year.

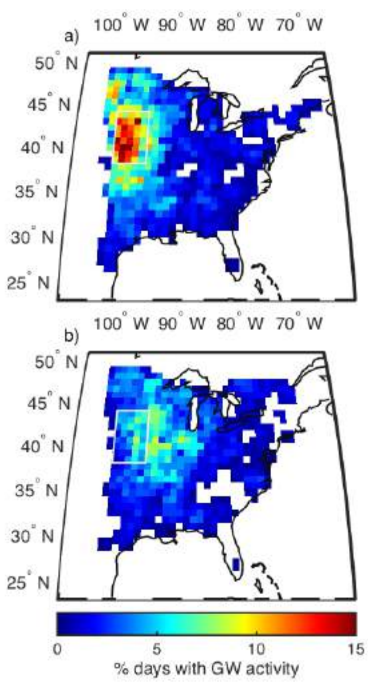

Occurrence rate of gravity waves in the 2-6 hr frequency band observed at the Earth's surface during thunderstorm season (May-Aug) during local night (03:30-09:30 UT) on top and during local day (15:30-21:30 UT) on bottom. Gravity waves in the central United States are much more common at night and are due to convective activity. These signals are highly correlated with gravity waves observed in the stratosphere by satellite.

Detection of Seismic and Infrasound Fields
at the USArray Transportable Array

Catherine D. de Groot-Hedlin and Michael A.H. Hedlin

Laboratory for Atmospheric Acoustics, U.C. San Diego

Many geophysical events, of natural or anthropogenic origin, are significant sources of both seismic and infrasound signals. Routine detection and accurate location of sources that generate both signal types is a significant processing challenge. We have recently developed a novel 'big data' method to detect and locate geophysical events using a dense sensor network. In this method, the stations are divided into a mesh of "triad" arrays, which each comprise three adjacent stations. Standard array processing methods are used at each triad to detect signals that are consistent with plane wave propagation. When a coherent signal is detected, its phase velocity and direction of propagation is computed using tau-p. Results from all triads with signal detections that are consistent with a common source are collectively used to automatically and rapidly provide an accurate estimate of the source's origin time and location. This method has proven highly effective at detecting weak sources of infrasound and seismic signals that were located within or near the 400-station USArray Transportable Array. Examination of contemporaneous seismic and infrasound event catalogs reveals a number of sources that generate both infrasound and seismic signals. Most of these are identified as anthropogenic, as they occur during regular working hours each week, however a few of the sources appear to have a natural origin.

In the recent past our research has been presented via scientific conferences, and to the general public via lectures and seminars. This outreach will continue in the coming year.

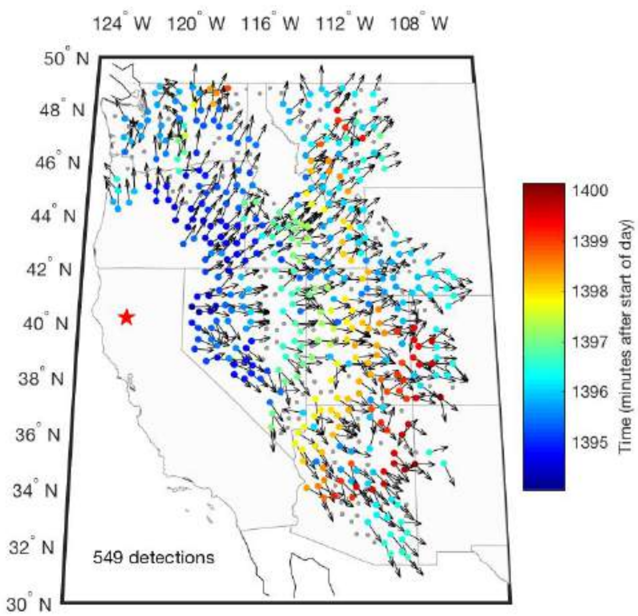

A seismic event that was located in northern California was detected by 549 triads in the USArray using vertical component seismic sensors. The arrows show the direction of wave propagation across each triad with color showing relative time of the detected signals.

Constraints on radial and azimuthal anisotropy in the central Pacific upper mantle from the NoMelt OBS array

Joshua B. Russell, James B. Gaherty, Peiying (Patty) Lin, Molly Zebker

Observations of seismic anisotropy in the ocean basins are important for constraining deformation and melting processes in the upper mantle. The NoMelt OBS array was deployed on relatively pristine, 70 Ma seafloor in the central Pacific with the aim of constraining upper mantle circulation and the evolution of the lithosphere-asthenosphere system. Azimuthal variations in Rayleigh-wave velocity suggest strong anisotropic fabric both in the lithosphere and deep in the asthenosphere, and we aim to evaluate whether radial anisotropy shows a similar pattern. High-frequency ambient noise (4-10 s) is used to estimate V_{SV} and V_{SH} in the uppermost mantle beneath the NoMelt array. Waveform fitting of the ambient-noise cross spectra provides phase-velocity estimates that are sensitive to the upper ~10 km of the mantle. Our best fitting models require radial anisotropy in the uppermost mantle with $V_{SH} > V_{SV}$ by $3 - 7\%$ and as much as 2% radial anisotropy in the crust. Additionally, we find strong 2θ and 4θ azimuthal signals for Rayleigh and Love waves, respectively, with Rayleigh fast direction (Love slow direction) parallel to the fossil spreading direction. Together, these observations of radial and azimuthal anisotropy are consistent with horizontal alignment of olivine with the a-axis parallel to fossil spreading and having an orthorhombic or hexagonal symmetry.

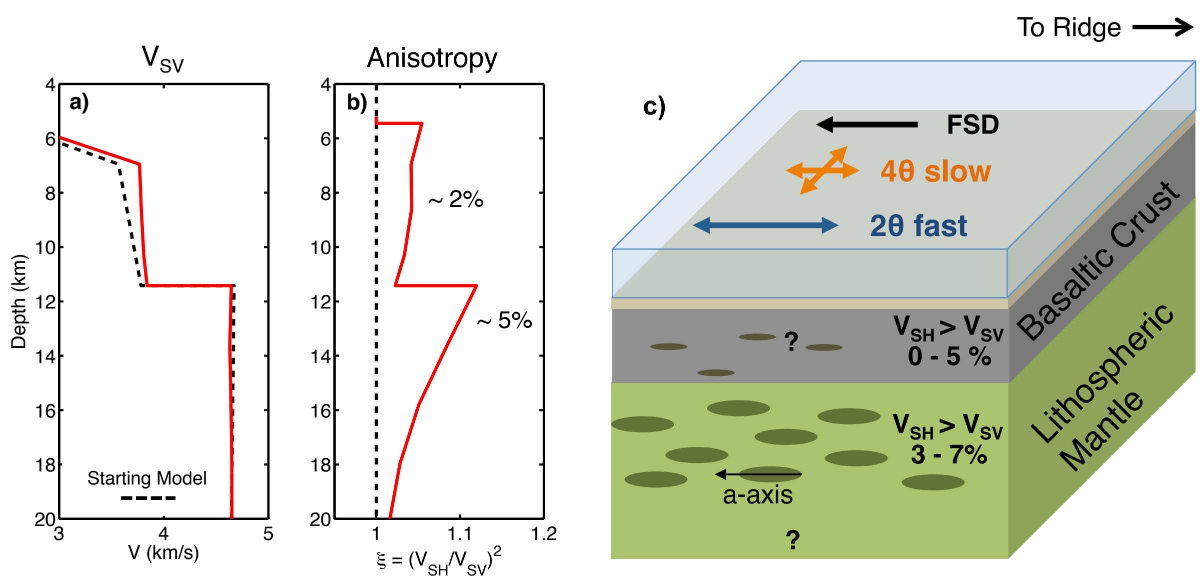

Figure. a) Vertical shear velocity V_{SV} and b) radial anisotropy ξ of the starting model in black and the inversion result in red. c) A schematic illustration of the crust and shallow mantle beneath the NoMelt array. Rayleigh 2θ fast and Love 4θ slow directions align parallel with the FSD. Additionally, strong radial anisotropy ($V_{SH} > V_{SV}$) in the mantle suggests horizontal orientation of the olivine a-axes associated with seafloor spreading.

The 2016 Central Italy sequence: comparing InSAR-constrained synthetic seismograms of surface waves with Transportable Array data from Alaska

Nader Shakibay Senobari, Gareth J. Funning, and Ana M. G. Ferreira

One of InSAR's main strengths, with respect to other methods of studying earthquakes, is finding the precise location of the best point source (or 'centroid') for an earthquake. Unfortunately the number of earthquakes for which we have InSAR data is low, compared with the number of earthquakes recorded seismically. Also, earthquake centroid moment tensor (CMT) inversion using InSAR data usually has a latency of days to months, due to the time taken in acquiring, processing and inverting the data. On the other hand, earthquake centroid inversion methods using long period seismic data (e.g. the Global CMT method) are fast but include errors caused by inaccuracies in both the Earth velocity model and in wave propagation assumptions (e.g. Hjörleifsdóttir and Ekström, 2010; Ferreira and Woodhouse, 2006). Here for the first time we use the EarthScope Transportable Array to investigate source-receiver phase corrections for three recent earthquakes in central Italy with locations constrained by InSAR.

Our method is based on the observation that synthetic seismograms produced from InSAR source models and locations match the data very well except for some phase shifts between the two waveforms likely corresponding to inaccuracies in Earth velocity models (Weston et al., 2014). Our previous work shows that adding such phase shifts to the Green's functions can improve the accuracy of long period seismic CMT inversions by reducing tradeoffs between the moment tensor components and centroid location (e.g. Shakibay Senobari et al., AGU Fall Meeting 2015).

A sequence of neighboring shallow Mw>6 events in central Italy occurred in 2016, during the current Transportable Array deployment in Alaska. This provides an opportunity to investigate our approach for correcting source-receiver travel times. Our previous work on several neighboring events (e.g. Landers–Hector Mine, the 2000 South Iceland earthquake sequences) strongly suggest it is possible to determine phase corrections for the source regions of these events. Specifically, the dense array of seismic stations in Alaska, distributed with a narrow azimuth with respect to the source regions of the Italy events, allow us to investigate the presence of any site effects within the receiver region.

Preliminary results from deep seismic profiling in North Qilian, Hexi Corridor and South Alxa terranes: evidence for the northward growth and uplifting of the Qinghai-Tibet Plateau

CHEN Xuanhua[1], GAO Rui[2], XIONG Xiaosong[2], ZHOU Qi[1], SHAO Zhaogan[1], DING Weicui[1], LI Bing[1], WANG Zengzhen[1], ZHANG Yiping[1], XU Shenglin[1]

1. SinoProbe Center, Chinese Academy of Geological Sciences, China Geological Survey

2. Institute of Geology, Chinese Academy of Geological Sciences, China Geological Survey

The North Qilian Shan, the Hexi Corrador, and the Alxa Terrane are the key areas for the understanding of the north growth and uplifting of the Qinghai-Tibet Plateau. In the year 2016, we have carried out about 200-km-length deep seismic reflection profiling, combined with wide-angle reflection and refraction profiling, across the North Qilian, through the Hexi Corridor, and go into the Alxa Terrane. Preliminary result of the integrated reflection and refraction profiling, reveals the northward subduction of the Qinghai-Tibet Plate (the North Qilian Ocean) underneath the lithosphere of the Alxa Terrane, and the change of the Moho depths from ~64 km (18s) in the North Qilian to ~50 km (15s) in the Alxa Terrane. The records of this subduction are the granitoid magmatism in the Heli Shan (Longshou Shan) and the Beida Shan (Daqing Shan) areas in Late Paleozoic, and the occurrence of ophiolite mélanges (the suture), and rarely outcropped eclogites in the areas, reflecting the closure of an ocean in the Paleo-Tethys Ocean and the collision of the North Qilian and the Alxa Terranes in Late Paleozoic. We suggest that this limited ocean between the North Qilian and the Alxa Terranes should be named as the Heli Ocean, and that this ocean could be the passageway linking the Central Asian Ocean and the Paleo-Tethys Ocean. After the subductional orogeny, there are widespread basic dyke swarms in Permian, indicating post-orogeny extension and rifting related to the Permian Tarim LIP (Large Igneous Province).

Additional to the geophysical survey, detailed geological and structural analyses in the field revealed several tectonic events since Middle Triassic. The deformation related to the Indosinian Movement in Early Mesozoic is recorded by the folded Middle Triassic growth strata, which are laying unconformity on the Ordovician basalt and limestone strata in the Baiquanmen Basin, North Qilian. The most significant pre-Indo-Asia Collision deformation in Late Mesozoic is the North-South compression in the early time of Early Cretaceous, and the formation of foreland basins such as the Pingshanhu Basin and thrust-fold system of the Lower Cretaceous. In the late time of Early Cretaceous, the widespread N-S extension resulted in the formation of graben and half-graben basins such as Qiuxi Basin controlled by normal faults. Then, planation is the leading role during Late Cretaceous and Paleogene. The northward growth of the northern margin of the Qinghai-Tibet Plateau began in Miocene, resulting in uplifting of the Yumushan and formation of the northern boundary blind thrust of the Plateau, the Xiaogengzi Fault, in Holocene (Late Quaternary).

This research is granted by the China Geological Survey through project “Deep geological survey of the Qilian Shan and the Tianshan mountains and surrounding basin-range junction zones” (No. DD20160083; 2016-2018).

Measuring ground deformations caused by 2015 Mw7.8 Nepal earthquake using high-rate GPS data

Yong Huang[1,2]

1. Key Laboratory of Earthquake Geodesy, Institute of Seismology, China Earthquake Administration, Wuhan, 430071, China

2. Geophysical Institute, University of Alaska Fairbanks, Fairbanks, Alaska, USA

Abstract: The April 25, 2015 Mw7.8 Nepal earthquake was successfully recorded by Crustal Movement Observation Network of China (CMONOC) and Nepal Geodetic Array (NGA). We processed the high-rate GPS data(1 Hz and 5 Hz) by using relative kinematic positioning and derived dynamic ground motions caused by this large earthquake. The dynamic displacements time series clearly indicated the displacement amplitude of each station was related to the rupture directivity. The stations which located in the direction of rupture propagation had larger displacement amplitudes than others. Also dynamic ground displacement exceeding 5 cm was detected by the GPS station that was 2000 km away from the epicenter. Permanent coseismic displacements were resolved from the near-field high-rate GPS stations with wavelet decomposition-reconstruction method and P-wave arrivals were also detected with S transform method. The results of this study can be used for earthquake rupture process and Earthquake Early Warning studies.

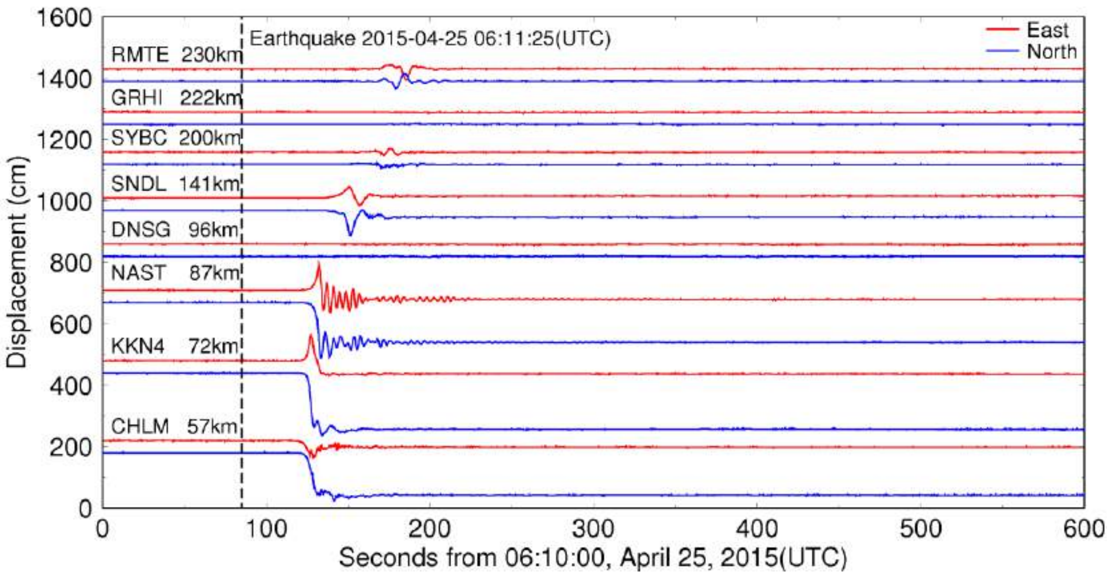

Fig.1 The 5 Hz dynamic displacements time series in east-west, north-south

components for NGA cGPS sites

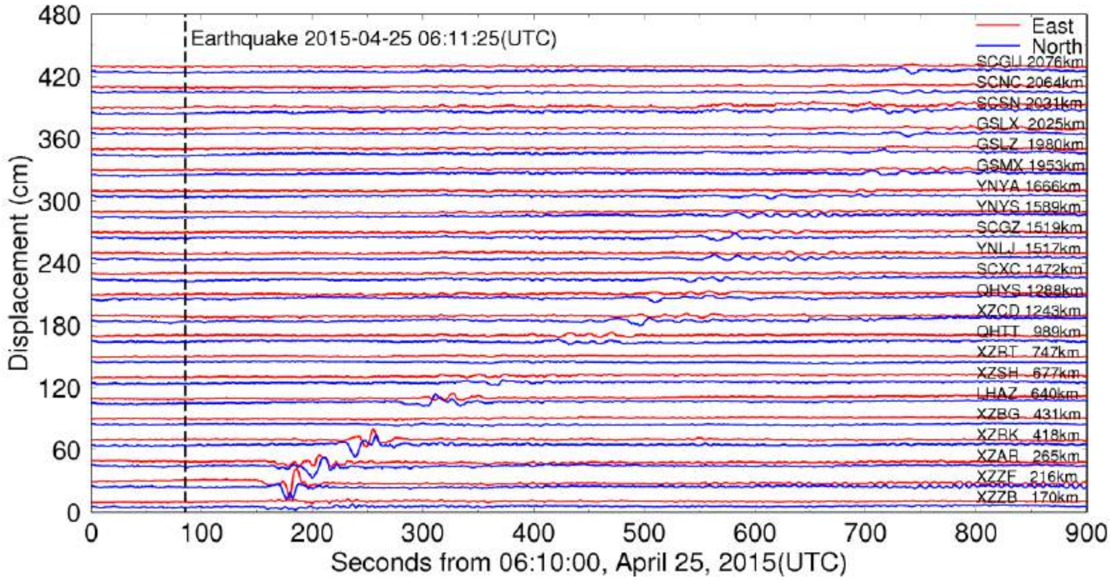

Fig.2 The 1 Hz dynamic displacements time series in east-west, north-south components for CMONOC cGPS sites

Large explosive shot gathers along the SinoProbe deep seismic reflection profile and Moho depth beneath IYS and BNS

Zhanwu Lu[1,2]*, Rui Gao[1,2], Wenhui Li[1,2], Hongqiang Li [1,2], Tairan Xu[1,2]

[1] Institute of Geology, Chinese Academy of Geological Sciences , Beijing,100037, China
[2] Key Laboratory of Earthprobe and Geodynamics, Ministry of Land and Resources of PRC, Beijing,100037, China

Owing to extreme topography, rapid velocity and thickness variation of near-surface layer and strong seismic attenuation through the thickest crust of the Earth, it is not easy to acquire reflective lower crust and Moho in Tibet. However, with help from the SinoProbe deep seismic reflection experiment, large explosive of 1000 kg seismic sources have been tentatively detonated beneath IYS and BNS. Compared with multifold data, the single-fold record from single shot gather can show clear Moho image. Beneath IYS, Moho reflection appears continuously at ~ 23 s TWT (~69km) without Moho offset. That means the IYS is not a super crustal structure. Beneath BNS, Moho reflection appears at ~ 24 s TWT (~ 75.1 km)in the northernmost Lhasa terrane and at about 21 ~ 20 s TWT (65.7 - 62.6 km) beneath the Qiangtang terrane. We speculate that Moho gets 9.4 km-12.5 km shallower from the Lhasa to the Qiangtang terrane rather than a 20 km offset.

Airborne gravity technique in the application of deep earth exploration

Guoqing Ma, Danian Huang, Lili Li
College of Geoexploration Science and Technology, Jilin University, Changchun, China
E-mail:maguoqing@ jlu.edu.cn

0- Introduction

In this paper, we will introduce development about gravity exploration instrument, and we can see that the new measurement way can delineate the feature of the source more correctly, and improve the horizontal resolution to source. In order to satisfy the requirement of deep earth exploration, we study new methods to enhance the anomaly of deeper source. We also introduce gravity gradient tensor data to improve the resolution to source. Seismic prospecting cannot obtain good results of deep layer, and we use the integrated inversion of gravity and seismic to obtain the correct distribution of deep layer.

1-Development about Airborne gravity technique

Airborne gravity technique has the advantages of deep depth, large area and high efficiency, which can obtain the distribution of structure, the location of geological body, and the layer change, and this technique also can help seismic data to obtain some subtle information. In order to obtain the feature of the source more correctly, gravity gradient tensor measurement is developed, which can provide different-direction information of the source. Full tensor measurement began in 1990, which is an effective tool in geophysical measurement, which can delineate the feature of the source more correctly, and is insensitive to noise.

2- New interpretation methods

We study many methods to improve the response of deep source, which use the ratio functions of horizontal derivatives to vertical derivative, and these methods also can distinguish the horizontal range of the source and the location of faults. The previous methods use the ratio of the same order derivatives, and we use the different order derivative to build ratio function, and new methods can obtain the information of the source more correctly and clearly. Full tensor measurement has six components, which is the derivative of the gravity anomaly, so the inversion results computed by matrix composed by them are more correct. However, When use the functions of vertical derivative to interpret the potential field data that exist positive and negative anomalies simultaneously, the inversion results will produce additional results (Figure1), but the matrix or function composed by the horizontal derivatives will not have additional results, and we also find that the results computed by the matrix composed by the horizontal derivatives are insensitive to noise.

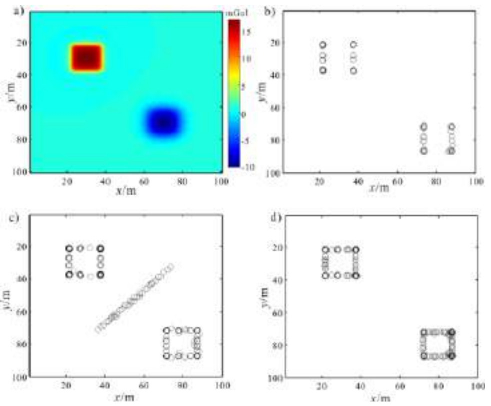

Figure1. (a) Synthetic gravity anomaly generated by two prisms, and their densities are +1 and -1 g/cm^3. (b) Estimated horizontal locations by x-direction derivative.(c) Estimated horizontal locations by horizontal and vertical derivatives. (d) Estimated horizontal locations computed by horizontal derivatives.

3- Integrated interpretation method to reveal the deep structure

Seismic exploration cannot obtain clear event to some deeper structures, and gravity exploration can obtain the response of deeper source, so we can use the integrated inversion of seismic and gravity data to obtain the deep layer.

4- Conclusion

Gravity prospecting can obtain more information about the source, which can obtain more accurate results as the development of interpretation methods, and it can be used widely in the exploration of deep earth because the advantages of deep depth, high resolution and high precision.

Reference

GuoqingMa, Danian Huang, Cai Liu. Step-Edge Detection Filters for the Interpretation of Potential Field Data, Pure and Applied Geophysics, 2016, 173(3), 795-803.

Tectonics studies based on potential field characteristics in Beikang area, South China Sea

Xiaohong Meng[1,2], Zhaoxi Chen[1,2], Guofeng Liu[1,2], Jun Wang[1,2]

1 Key Laboratory of Geo-detection, Ministry of Education, Beijing 100083, China.

2 School of Geophysics and Information Technology, China University of Geosciences, Beijing 100083, China

The South China Sea (SCS), located in the tropical-to-subtropical western North Pacific, is one of the largest marginal seas in the world. Even if the SCS is a well-studied Tertiary marginal sea, there are a number of unsolved questions concerning its formation. Here we focus on the local region in Beikang area and conduct a series of tectonics studies based on gravity and magnetic data as well as additional geological data and seismic profiles. The main workflow that have been utilized can be summarized as the following list.

1) Modelling along some major profiles have been accomplished based on potential field data and seismic interpretations.

2) Depth of sediment basement, magnetic basement, the Moho interface and the Curie interface in the study area have been acquired from the constrained interface inversion of potential field data.

3) Faults and sedimentary basins in the study area have been interpreted.

The methodologies in this study mainly include: anomaly Separation of gravity and magnetic data based on preferential continuation, inversion of physical interfaces (density and magnetic) in space and frequency domain, linear features enhancement on gravity and magnetic data.

After a series of analysis, processing and comprehensive interpretation, we conclude:

1) The depth of sedimentary basement is between 2km and 12km.This means the depression areas are generally correspond to the sedimentary basins.

2) The depth of magnetic basement is between 5km and 14km and is relatively flat compared with the sedimentary basement.

3) 26 sedimentary basins are deduced based on the features of the gravity anomaly of the basement.

This work was supported by the Sinoprobe-01-05 Project and 863project (2013AA063901).

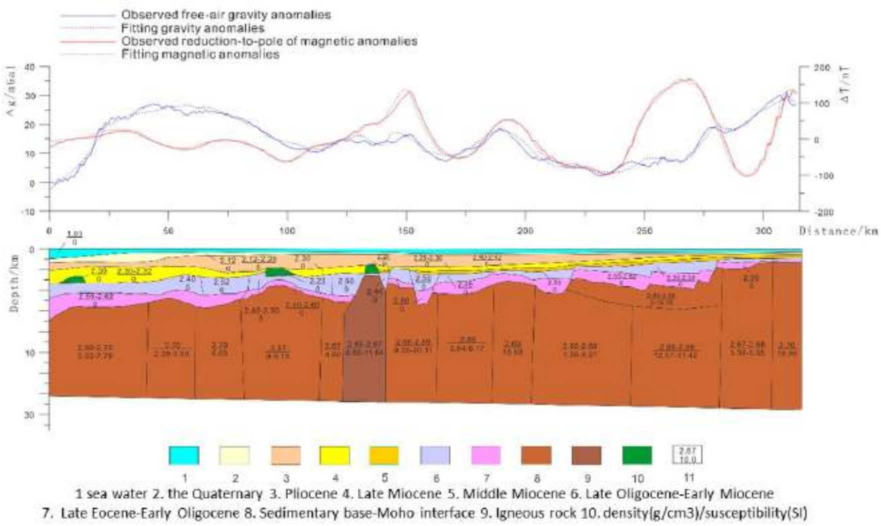

Figure 1 The model results of one of the selected profiles in Beikang area, SCS

Lithospheric Electrical Characteristics of Eastern Jiangnan Orogen, South China

QIU Gengen; FANG Hui; ZHONG Qing

(Institute of Geophysical and Geochemical Exploration， Langfang 065000， Hebei， China)

Summary

In south China there have enrichment of mineral resources, which have experienced complicated geological tectonic evolution history. We built 3 d lithospheric electrical structure model of eastern Jiangnan orogenic in this paper based on three dimensional OCCAM inversion calculation program. The 3 d lithospheric electrical structure model has a good corresponding relationship with the ground geology and regional magnetic anomalies, reflecting rich underground informations. From the perspective of three-dimensional electrical structure model in combination with regional geology and regional magnetic materials, we divided the eastern Jiangnan orogenic belts and its adjacent area into four first-order tectonic units and 16 secondary tectonic units. The four first-order tectonic units are: low resistance belts of southern north China, high resistance band of Dabie mountain, interval abnormal belts of low resistance and high resistance in Yangtze, high resistance band of the north of south China. Three-dimensional electrical structure model also shows contact relationship between the different tectonic units clearly: U-shap high resistance characteristics under Dabie mountain deep depth means that the south side of Yangtze massif and the north side of the north China massif subduct under Dabie mountains, showing strong compressive tectonic environment; Yangtze massif overall performance for low resistance and high resistance ribbon resistivity anomalies. HuaiYu block located in the east of Yangtze shows low resistance characteristics, implying collage tectonic framework apparently. There exists obvious assaulting low resistance anomalous below along the collage tectonic belt, and the low resistance anomalous may be related to the distribution for the formation of a large number of metals above. The low resistance anomalous whose tendency for south east along Jiangshao fault zone suggest that south China massif obduction onto Yangtze massif. Building 3 d lithospheric electrical structure model of eastern Jiangnan orogenic, to reveal the relationship between different tectonic units and analyzes the formation and evolution of south China continent and direct the next step mineral prospecting breakthrough and forecast, may have important reference value.

Introduction

The study area is located in the eastern of Jiangnan orogenic, containing the middle and lower reaches of the Yangtze river metallogenic belt and Qin - Hangzhou metallogenic belt. The middle and lower reaches of the Yangtze river metallogenic belt is eastern part of China's famous Mesozoic endogenous metal metallogenic belt with characteristics of magma contact confessed "skarn type copper mine" and volcanic rock "porphyrite iron ore", and it is the base China's Yangtze river industrial corridor mineral (Dong,2011). Qin - Hangzhou metallogenic belt is relatively "young" metallogenic belt, which was introduced in the 1980 s. From analysis of the location of tectonic metallogenic belt and magmatic activity and regional strata, Qin - Hangzhou metallogenic belt has many similarities with the middle and lower reaches of the Yangtze river metallogenic, and it's even more superior in some respects. Along with the middle and lower reaches of the Yangtze river metallogenic belt and Qin - Hangzhou metallogenic belt there have many large and super large mineral resources. The reason for the formation of so many mineral resources in the metallogenic belt has to been the focus problem in geologists.

Magnetotelluric sounding method is a using natural electromagnetic field explored method proposed by A.N.T ikhonov and L.C agnird in the early 1950 s. Because of its advantages of deep detecting, light equipment, stationing flexibly, low-cost, it was widely used in resource exploration field. At present, data processing and interpretation techniques of magnetotelluric sounding method has been mature basically. This paper introduces building 3 d lithospheric electrical structure model using 3 d inversion calculation program based on OCCAM calculation method in eastern Jiangnan orogenic belts. In combination with regional geology and regional magnetic materials we divided the tectonic units of eastern Jiangnan orogenic belts and its adjacent regions into several parts. We also analyzed basic electrical characteristics and the contact structure relationship between various adjacent tectonic units, it can provide important reference basis for analysis of the formation and evolution of south China continent and the next step mineral prospecting breakthrough and prediction.

REBOCC 3D inversion theory

Data-space method is proposed by professor Weerachai Siripunvaraporn on the improvement of Occam inversion algorithm(Siripunvaraporn W,2004). It is base on the sensitivity function that is derived from the original model of space form (M * M) computing and storage format into a data space form (N * N) computing and storage. As flexible as possible in order to make model, and to suppress the geoelectric structure irrationality, it can be solved by defining the model roughness. In OCCAM inversion, by solving the unqualified equation $U(m,\lambda)$ can achieve the goal:

$$U(m,\lambda)=(m-m_0)^{\mathrm{T}}C_m^{-1}(m-m_0)+\lambda^{-1}\{(d-F[m])^{\mathrm{T}}C_d^{-1}(d-F[m])-X_*^2\} \tag{1}$$

In order to get the solution required, usually do not directly solution equation, but by solving the penalty function as follows, Because of when λ fixed, $\partial\mathbf{U}/\partial\mathbf{m}=\partial\mathbf{W}/\partial\mathbf{m}$， $U(m,\lambda)$ and $W_\lambda(m)$ have the same value.

$$W_\lambda(m) = (m-m_0)^{\mathrm{T}} C_m^{-1}(m-m_0) + \lambda^{-1}\{(d-F[m])^{\mathrm{T}} C_d^{-1}(d-F[m])\} \tag{2}$$

λ^{-1} as the Lagrange multiplier, is used to control the smoothness of model fitting.

In general, the MT data is smooth and redundant, so in the data space, do not need to use all sensitivity matrix as the base functions. The minimization of equation (2) in number k iteration can be expressed as a linear combination line of smooth sensitivity matrix $C_m J_k^{\mathrm{T}}$:

$$m_{k+1} - m_0 = C_m J_k^{\mathrm{T}} \beta_{k+1} \tag{3}$$

β_{k+1} is unknown coefficient vector of basis functions $[C_m J_k^{\mathrm{T}}]_j$, (j=1， …， N). put (3) into (2) type, it can be obtained:

$$W = \beta_{k+1}^{\mathrm{T}} \Gamma_k^n \beta_{k+1} + \lambda^{-1}\{(d_k - \Gamma_k^n \beta_{k+1})^{\mathrm{T}} C_d^{-1}(d_k - \Gamma_k^n \beta_{k+1})\} \tag{4}$$

$\Gamma_k^n = J_k C_m J_k^{\mathrm{T}}$ is N * N order "data subspace cross-product" matrix. Beta differential of equation (4), make the result is zero, and rearranging, unknown expansion coefficient can be written as:

$$\boldsymbol{\beta}_{k+1} = (\boldsymbol{\lambda C_d} + \boldsymbol{\Gamma_k^n})^{-1} \boldsymbol{d_k} \tag{5}$$

By solving (5) over and over again, search model according to the method similar to the model space can obtain the optimization of the inversion results.

Model building of eastern Jiangnan orogeny

500 MT stations are layout in the study area. Affected by the large number of survey stations and huge memory are needed for caculation, the whole work area is divided into six sub block to take part in three-dimensional inversion separately, retaining a certain overlap between adjacent two child block for sub block mosaics work next. Figure 1 for distribution of survey stations in work area and six sub block partition map. Each station choose total 21 frequency evenly from 320hz - 3000s frequency band. We subdivided the model by 10 km block grid within the stations region, while outside by 1.5 times of 10 km block grid until the boundaries far enough. On the vertical depth, 50 m thickness for the first layer, and then downward by 1.1 times of upper layer, until the depth of model deep enough. We choose 100 Ω • m uniform half space as the initial inversion model, using undiagonal line impedance tensor for three dimensional inversion calculation. After each sub block finished 3 d inversion calculation on the workstation in turn, finally we can get fusion electrical structure model of whole work area using each sub block 3 d inversion result (figure 2).

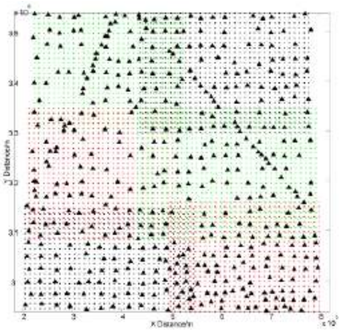

Fig.1 Distribution of MT stations in research area and sub model

block diagram

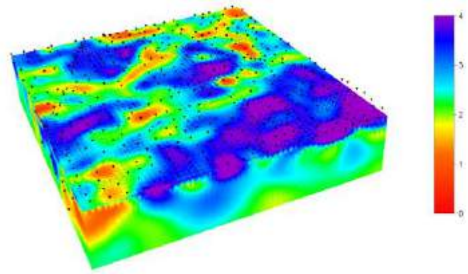

Fig.6 Three-dimensional lithosphere electrical structure model(Figure values for the logarithmic values)

Division of geotectonic units

Longitudinal conductance value is calculated by the layer thickness and corresponding resistivity values, its value represents local rock conduction ability of a certain thickness, usually use symbol S, S = H/rho. Tectonic characteristics of south China is complex, and has experienced complicated geological tectonic evolution history. Different exploration methods has different theoretical basis, so tectonic units designed by different methods are offten different. Longitudinal conductance plane map for underground 50 km depth is calculated using three-dimensional electrical structure model in the study area(FIG. 3 a). The study area is divided into 4 first-order tectonic units and 16 secondary tectonic units while referencing resistivity characteristics plane map at the depth of 10 km (FIG. 3 b) and the ground geology (FIG. 3 c) and magnetic anomalies (FIG. 3 d) at the same time. Four first-order tectonic units are: low resistance belts of southern north China, high resistance band of Dabie mountain, abnormal belts of low resistance and high resistance interval in Yangtze, high resistance band of the north of south China. As can be seen from the figure 3, there have good relationship among the electrical characteristics of different tectonic units and the surface geology, magnetic anomalies in corresponding space.

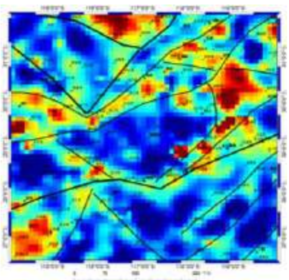

(a)

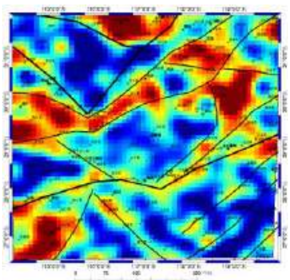

(b)

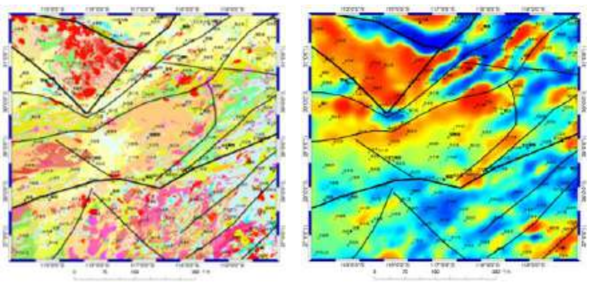

(c) (d)

Fig.3 Division of tectonic units in the study area(a for longitudinal conductance within 50 km depth; b for electrical resistivity characteristics plane at 10 km depth; c for regional geological map; d for regional magnetic anomaly)

Three-dimensional electrical characteristics of the east section of the Jiangnan orogenic

Can be seen from the longitudinal conductance plane map, south of north China massif shows high conductivity characteristics, Qinling - dabie orogenic belt shows high resistance characteristics, Yangtze massif shows high resistance characteristics in central space with high conductivity around, while the north of south China block performance for high resistance characteristics.

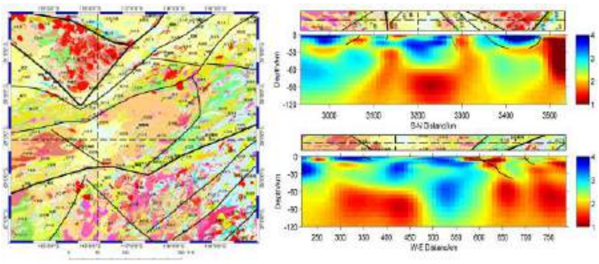

Fig.4 Two electrical section profile across the study area(Figure values for the logarithmic values)

In order to study contact relationship between different tectonic units, 2 electrical section profile was choosed from research zone (figure 4). Can be seen from electrical profile LINE1: Dabie mountain overall performance for high resistance with a U-shaped structure, the deepest place can reach about 100 km depth, which is located in the front orogenic belt, showing obvious high resistance "root" characteristics. There exist a high conductivity layer in depth about 30 km in the crust under the high resistance Dabie mountain. The fracture located on both sides of Dabie mountain is steep, and enclosed to the high conductivity layer underground in the deep depth. Yangtze massif performs high resistance of electrical characteristics in the central part with high conductivity in the north and the south edge. Under the high resistance body there exist a huge low resistance anomalous. Jiangnan fault located in the north of Yangtze massif rim shows obvious high conductivity characteristics. The low resistivity zone is linked to low resistance anomalous in deep mantle. Jiangshao fault located in the southern margin of the Yangtze massif shows a small low resistance characteristics. The low resistance anomalous apart with a low resistance upwarding abnormal body relatively by a via high resistance layer below. Can be seen from the electrical profile LINE2: the central space in Yangtze massif performance for a large high resistance anomalous, it may be an old structure formed in S ancient. The scope of high resistance anomalous is larger than Dabie mountain, while there is also exist a large low resistance of abnormal body under the high resistance anomalous. HuaiYu massif located in the east of Yangtze massif shows high conductivity characteristics. The shallow low-resistance anomalous connected with low resistance fluid in deep mantle through a narrow passage. Low resistivity anomalous with tendency for south east direction, and in the depth of about 5 km there exist a continuous high conductivity layer. The above two electrical profile shows the electrical characteristics of each tectonic unit and the contact relationship between each other clearly. It is has important significance for the formation and evolution of the south China mainland and controlling factors research of the deep structure to the ground mineral resources distribution.

Geological significance revealed by the three dimensional electrical model

Dabie mountain with the U-shaped structural resistance characteristics represent the north China massif dive under northern margin of Dabie mountain and the Yangtze massif in south also dive under Dabie mountain. This situation shows Dabie mountain is obvious in squeezing uplift tectonic framework. When southern China during stretching period, the squeezing tectonic environment is also stretching, it formed a low resistance layer of decollement under the 30 km depth position at the bottom of the Dabie mountains, which was formed possibly in permian-triassic era. Jiangnan fault located in front-end Dabie orogenic belt shows obvious high conductivity characteristics. The low resistivity anomalous are linked to deep mantle low resistance body, forming the deep channel of soft fluid migration. The low resistance channel may have relationship with the formation of a large number of metal mineral resources distribution along the shallow surface fracture. HuaiYu massif located in the east of Yangtze in overall performance for high conductivity characteristics, showing obvious collage tectonic framework clearly. There exists double high conductivity layer in the earth's crust. Double crust structure has formed its unique form of mineral resources system. Jiangshao fault zone is characterized by a small high conductivity anomaly zone, with its tendency to south east direction, cracking events happened span from neoproterozoic - early Paleozoic may be associated with the deep low resistance of soft upward fluid. When south China in period of pyrolysis stage, it has formed a wide range of shell conductive layer in crust meanwhile.

Lithospheric Electrical Characteristics of Eastern Jiangnan Orogen, South China

Conclusions

1. Magnetotelluric sounding method is an effective exploration methods to obtain deep electrical structure characteristics. For large number magnetotelluric sounding data, USES sub model block 3 d inversion technology can be relatively build a wide range of construct three-dimensional electrical structure model effectivly.
2. It is the first time to build 3 d electrical structure model of the Jiangnan orogenic belt. In combination with regional geology, regional magnetic materials we divide the study area including eastern Jiangnan orogenic belts and its adjacent area into four first-order tectonic units and 16 secondary tectonic units.
3. Dabie mountain with the U-shaped structural resistance characteristics represent the north China massif dive under northern margin of Dabie mountain and the Yangtze massif in south also dive under Dabie mountain. This situation shows Dabie mountain is obvious in squeezing uplift tectonic framework; Yangtze massif performs high resistance of electrical characteristics in the central part with high conductivity in the north and the south edge. HuaiYu massif located in the east of Yangtze in overall performance for high conductivity characteristics, showing obvious collage tectonic framework clearly. The low resistance whose tendency for south east along Jiangshao fault zone suggest that south China massif obduction onto Yangtze massif. There exits soft fluid channel below connected to the deep mantle under the Yangtze river fault zone and the northeastern Jiangxi fault, and the soft fluid channel may be related to the formation of a large number of metals along the above fault zone.

Acknowledgments

Thanks for the fund of the national key research and development plan " Three-dimensional Electrical Detection Research of the Northern Section of South China Crustal Structure "（2016YFC0600201-4）、National natural science fund project "Study of Three-dimensional Electrical Lithosphere Structure in Eastern Jiangnan Orogenic Belts " (41574068)、Large geological survey project " Deep Geological Investigation in Qin-hangzhou belt and its neighboring area" (121201108000160913) and " Magnetotelluric Sounding Prospect in Wuyishan metallogenic belt area" (12120114005801).

References

Dong S W, Ma licheng. 2011, On Dynamics of the Metallogenic Belt of Middle-LowerReaches of Yangtze River, Eastern China [J]. Journal of geology, 12:612-625.

Siripunvaraporn W, Uyeshima M, Egbert G. 2004. Three-dimensional inversion for Network-Magnetotelluric data. Earth Planets and Space, 56(9): 893-902.

Siripunvaraporn W, Egbert G, Lenbury Y, et al. 2005. Three-dimensional magnetotelluric inversion: data-space method. Physics of the Earth and Planetary Interiors, 150(1): 3-14.

Siripunvaraporn W, Egbert G. 2009. WSINV3DMT: Vertical magnetic field transfer function inversion and parallel implementation. Physics of the Earth and Planetary Interiors, 173(3): 317-329.

Continental lithosphere extending, the preliminary results of broadband array in southeast China

Qiusheng Li[1, 2], Hongshuang Zhang[1, 2], Zhuo Ye[1, 2], Xiaoran Wang[1, 2], Chen Gong[1, 2]

1. Institute of geology, CAGS, Beijing, Beijing, China.

2. key Laboratory of Earthprobe and Geodynamics, CAGS, Beijing, China.

The southeastern China, located at the southeastern margin of the Eurasia plate and the northwestern coast of Pacific, is one of ideal area to study interaction of Ocean-continent. In the last decades geometry of gradual thinning toward sea was presented by the regional and local scale seismic studies and a model of lithosphere extending was proposed. But the model has not convinced for absences of lithosphere thickness data.

Southeast China Array (SCA) is a subsequent regional scale observatory designed to provide a foundation for integrated studies of continental lithosphere and deep Earth structure post Sinoprobe. In the program 200 portable broadband instruments were deployed over several provinces in Southeastern China in a space of around 40 km and operated continually form October of 2014 to summer of 2016. Data from this site was collected on a regular schedule and in a sampling rate of 100 per second.

Here we present preliminary results of receiver function analysis and body wave finite-frequency tomography.

The crust thickness thinning slowly to coast, there are ±2km differences on the background of the 32 km in the Jiangnan orogenic belt and Cathaysia Block. Vp/Vs ratio changes more obviously in the East-West direction.

LAB varies on the background of 80 km on average. There are two local uplifts by 10~20 km appear in the Jiangnan orogenic belt.

There are significant low velocity anomalies in southeastern Southern China and a high velocity anomaly under Dabie orogenic belt down southward the upper mantle transition zone that is more obvious in the image of S wave tomography.

We believe that the observation is related to regional lithospheric extension Since Mesozoic. Further analysis is in progress.

Numerical Simulations in SinoProbe

Yaolin SHI, Huai ZHANG, Yuanze ZHOU, Huihong CHENG
(Laboratory of Computational Geodynamics, University of Chinese Academy of Sciences)

The SinoProbe Program is a Chinese earth science program with the overall aim of exploring the composition, structure, material property and the evolution and dynamics of the continental lithosphere beneath China, in order to better understand the processes causing earthquakes, geo-hazards and natural resources. Numerical simulation is an indispensable component in SinoProbe We have used seismic data as constraints to calculate 3D thermal structure of China （Figure 1） by finite element method, outlined 3D rheological structure of China （Figure 2） based on seismic and laboratory data. SinoProbe revealed valuable data on structures of the Chinese lithosphere, these provide better foundation for numerical simulation; while numerical simulation provide better physical interpretation of mechanism of phenomena SinoProbe observed. We will describe some of our findings, such as: mechanism of the northeastern growth of the Tibetan plateau （Figure 3）, the occurrence of Wenchuan earthquake, relation between impoundment of Zipingpu reservoir and Wenchuan earthquake series （Figure 4）, co-seismic deformation in a heterogeneous ellipsoid earth and changes of Coulomb stresses changes on subsequent seismicity, etc.

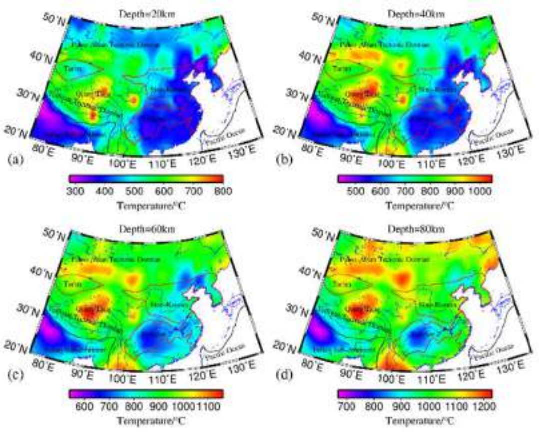

Figure 1

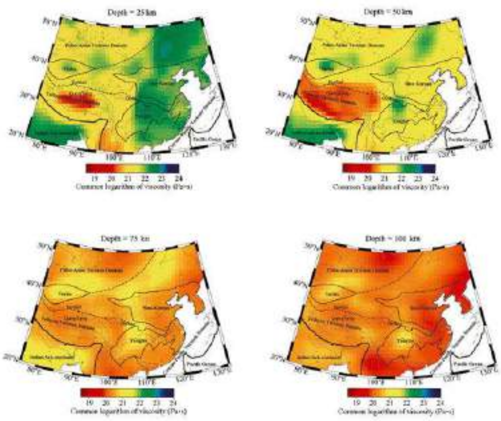

Figure 2

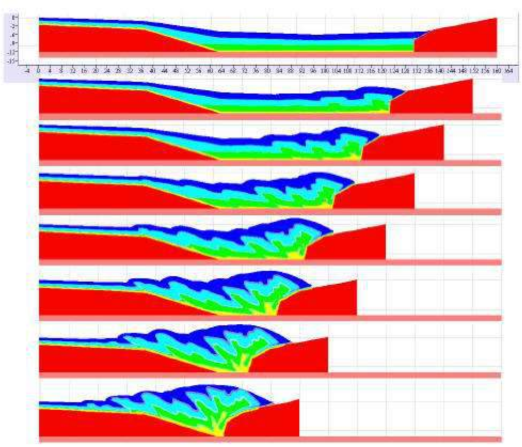

Figure 3

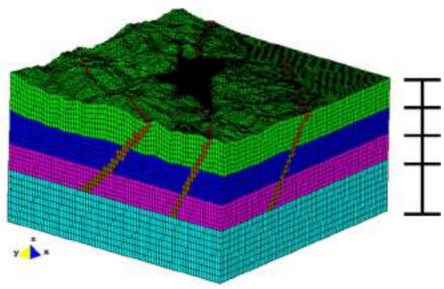

Figure 4

Crustal structure and crust-mantle deformation in NE Tibet and adjacent regions

Xu Wang[1,2], Ling Chen[1,2,3], Yinshuang Ai[2,4], Yifan Gao[1,2]

1. State Key Laboratory of Lithospheric Evolution, Institute of Geology and Geophysics, Chinese Academy of Sciences, Beijing 100029, China
2. University of Chinese Academy of Sciences, Beijing 100049, China
3. CAS Center for Excellence in Tibetan Plateau Earth Sciences, Beijing 100101, China
4. Key Laboratory of the Earth's Deep Interior, Institute of Geology and Geophysics, Chinese Academy of Sciences, Beijing 100029, China

Lithospheric deformation beneath northeastern (NE) Tibet records the far field effects of the continental collision between the Indian and Eurasian plates. More detailed studies of the crust-mantle structure beneath NE Tibet can improve our understanding of the crust-mantle deformation and the plateau growth mechanisms. A NW-SE-trending linear array including 64 broadband seismic stations was conducted across the Longmenshan Fault Belt (LFB) and the Kunlun Fault (KF). The crustal structure and the anisotropy beneath NE Tibet and the western Sichuan Basin are obtained by using the P-wave receiver functions and the shear wave splitting methods, respectively. The Moho is the shallowest (~43km) beneath western Sichuan Basin (ScB) and the Longmenshan Fault Belt and deepens to the northwest with the maximum depth of ~55 km under the northern Kunlun Block (KLB), roughly mirroring the surface topography. Obvious Moho offsets and differences in the intracrustal structures appear right beneath the boundary zones between different blocks (the Longmenshan Fault Belt, the Kunlun Fault and the South Qilian Suture (SQS)). The negative polarity discontinuities are detected in the mid-lower crust beneath the Songpan-Ganzi Block (SGB) and the southern Kunlun Block with a higher Vp/Vs ratio (~1.771) than the northern Kunlun Block (~1.714), which reveals a crustal channel flow maybe exist under NE Tibet and may cross through the Kunlun Fault, and is consistent with the double-layer anisotropy under the Kunlun Block and the southeastern Songpan-Ganzi Block deduced from the shear wave splitting. The anisotropy of the lower layer under the southeastern SGB is similar to that under the northwestern SGB, implying that the anisotropy of the upper layer under the southeastern SGB may localize in crust and can be explained by the mid-lower crustal flow. The double-layer anisotropy and the anti-correlation between the average crustal thickness and Vp/Vs ratio under NE Tibet illustrate the inconsistent lithospheric deformation in vertical and horizontal and the significance of the mid-lower crustal LVZs in the complex deformation.

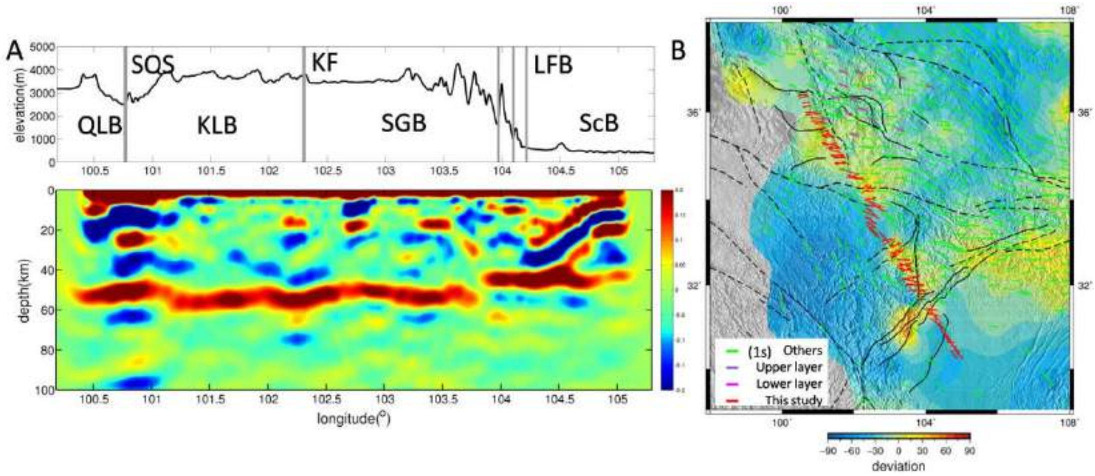

Fig. A: Topographic map and the migrated image for Ps; B: Shear wave splitting results.

A Study on petrophysical features and it's geological significance in west Liaoning, China

Xuechun Xu[1], Zhaohai Meng[2], Bo Lin[1]
[1] College of Earth Sciences, Jilin University, Changchun, Jilin 130061, China.
[2] Tianjin Navigation Instrument Research Institute, Tianjin 300131,China

Petrophysical properties are important physical parameters of rocks. However, this study is not got enough attention. In the current rock study, the petrogeochemical research is the main study point. It can be used to determine rock properties, to give answers to the geological problems, such as the origins of rocks and petrogenesis. Compared with the petrogeochemical distribution of the elements, petrophysical properties are more intuitive and easier to understand. Combining with the geophysical prospecting, the physical parameters of rocks can easily study the characteristics of rocks in the deep earth comparing with the geochemical elements of rocks. According with the study on the correlation between physical properties and geochemical elements of surface rocks, using the deep sub-surface rock properties can solve the corresponding study of the rock evolution. This poster focuses on using the correlation characteristics between petrophysical properties and petrogeochemical distribution of the elements to determine rock properties and to study the origin of the rocks. It has important theoretical and practical value. Petrophysical property is the key to merge the three major branches of earth science, i.e., geology, geophysics and geochemistry. In petrography which studies rocks using the correlation characteristics of the petrophysical parameters, different types of rocks correspond to different petrophysical parameters. The locations where petrophysical parameters change drastically usually correspond to major rock boundaries and locations with tectonic changes. Research on petrophysical parameters greatly enriched the geological information, increase the depth and accuracy of geological research. Geophysical methods are widely used in solving geological problems by combining petrophysics and petrography to establish theoretical and empirical formulae, and by determining rock types using petrophysical parameters. The research on petrogeochemical distribution of the elements is an important means to study petrogenesis and tectonic evolution. But it is both costly and time consuming.

Under laboratory conditions, we obtained a large amount of data of petrophysical properties and petrogeochemical distribution of the elements, and determined the types of rock specimen basing on the observations on hand specimen and microscopic observation of rock thin sections. Then, basing on the principles of mathematical statistics, we established the relationships between various types of petrophysical parameters and geochemical element content, and thus research and solve related geological problems of petrogenesis and regional tectonic evolution history. The study on petrophysical properties is an important means of interpreting the distribution of rocks and geological structure in deep earth. Using the rock samples from the formations of different ages, and by building statistical correlation characteristics between petrophysical properties and petrogeochemical distribution of the elements measured in the lab, a geoscience system of petrography, petrophysics and petrogeochemistry is formed. Currently, petrophysical properties are rarely used in geophysical and geological prospecting. Geophysicists use the petrophysical properties only as a constraint in geophysical prospecting rather than as an independent research means to solving geoscience problems. Researches on the correlation characteristics between petrophysical properties and petrogeochemical distribution of the elements are rare. Through a number of recent studies, it is found that these correlation characteristics can help us solve some difficult geological problems, especially in important geological problems such as geological structures and rock distributions in deep earth.

Xingcheng, Liaoning Province and its neighboring areas are chosen for this study and inside which, the geological corridor chosen by “the Instrumentation Development and Field Experimentation” subproject of the “Deep Exploration in China” project and its surrounding regions are selected as the key research area. This area has clear geological structure, is of clear scientific significance, and is representative. The lithology, depth, physical properties, thermal state and geophysical interface of the target layer is clear. The layer contains stratigraphic sequences of most geological eras, is of good representative significance in Earth science, and can be used to investigate such geological problems as petrogenesis, change in sedimentary environments, and history of tectonic evolution in each era. Using the characteristics of the changes in the physical parameters and geochemical composition of rock samples in the geological corridor in western Liaoning, we obtained the correlation characteristics between petrophysical properties and petrogeochemical distribution of the elements of the study area. This can provide comparison and verification standard for the study of basic geological science, and to interpret and to establish the fundamental model of Earth sciences in this region.

Over 1000 rock samples with typical features are collected in the western Liaoning Geological Corridor as the basis for this study. They are identified both as hand sample and as thin sections under a microscope to be classified, and will be used as the basis of the petrographic studies. Due to the limited number of metamorphic rock samples, it is difficult to study them statistically. So, the main targets in the study area are igneous and sedimentary rocks. Physical parameters such as density, magnetic susceptibility, resistivity, elastic wave velocity were measured. Statistical study of rock physical properties was conducted by drawing petrophysical frequency distribution histogram. The characteristics of physical parameters of various types of rocks and the corresponding geological tectonic background and rock genesis were investigated. The “SinoProbe 09-06: Experimental Study on the Technique of In Situ Stress Measurements and Monitoring “ subproject conducted prospecting using various geophysical methods in western Liaoning Geological Corridor, including seismic, magnetotelluric sounding, gravity and magnetic, remote sensing interpretation and aeromagnetic exploration, to complete a comprehensive geological and geophysical sectional study of nearly 100km. Using the petrophysical statistical results in a variety of comprehensive geological - geophysical interpretations makes the inversion results of geophysical data and the interpretation of which more accurate and more in line with the actual geological conditions. The petrophysical distribution map of western Liaoning Geological corridor with its surroundings was drawn, and was then compared with the geological mapping results. The locations with significant petrophysical property changes correspond to the primary locations of geological tectonic movement, and also correspond to the positions of rock type change. This is an effective complement to geological mapping, and can solve the geological problems such as the geological structure and facies division more effectively.

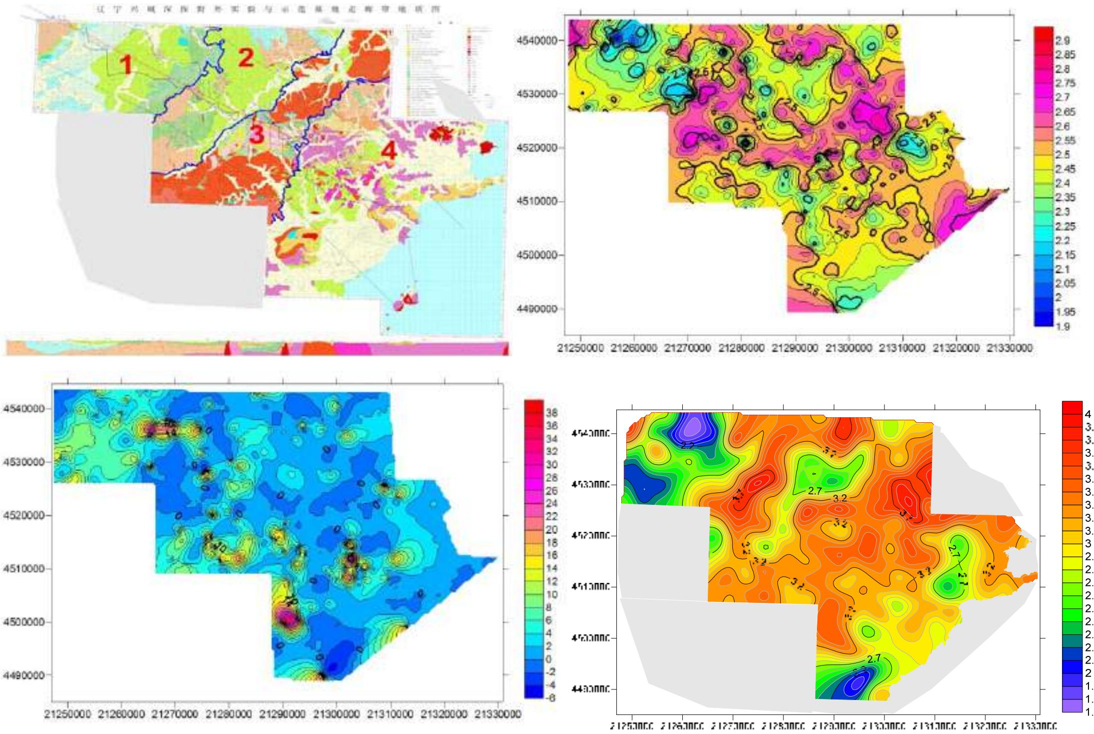

Fig.1 Comparative analysis of rock property and rock lithology

a: Geological map of study area; b: map plotting with density of rocks; c: map plotting with magnetic susceptibility of rocks; d: map plotting with resistivity of rocks

Table 1 Correlation coefficient between density and geochemical elements of rocks

	Major elements	Correlation coefficient R^2	Trace element	Correlation coefficient R^2	Rare earth elements	Correlation coefficient R^2
Plutonic rock DEN and geochemical correlation coefficient	SiO_2**	0.295	Cu	0.0611	La	0.0586
	Al_2O_3**	0.3025	Pb	0.0349	Ce	0.0768
	Fe_2O_3	0.176	Zn	0.1189	Pr	0.1152
	FeO	0.2452	Cr	0.0196	Nd	0.1446
	TFeO	0.2271	Ni	0.0786	Sm	0.1506
	CaO	0.1266	Co	0.2651	Eu	0.2497
	MgO**	0.3725	Rb	0.1312	Gd	0.1331
	K_2O	0.2054	Sr	0.024	Tb	0.1012
	Na_2O	0.1274	Ba	0.0744	Dy	0.0636
	TiO_2	0.203	V	0.2528	Ho	0.0411
	P_2O_5	0.2213	Sc	0.1702	Er	0.0251
	MnO	0.0054	Nb	0.2192	Tm	0.0048
			Ta**	0.3142	Yb	0.001
			Zr	0.0373	Lu	1.52E-04
			Hf	2.73E-04	Y	0.0388
			Ga	0.2685		
			U	0.2204		
			Th**	0.3541		

** The correlation coefficient is above 0.01

*** The correlation coefficient is above 0.001 and represents strong correlation

Three-hundred and ninety-eight rock samples were chosen to conduct geochemical composition measurements, to draw scatter map of petrophysical properties and petrogeochemical distribution of the elements, and to find the correlation characteristics between them. These characteristics can be used to solve the geological problems such as the origin of the plutonic magma, petrogenesis and tectonic evolution history of western Liaoning Geological Corridor. Meanwhile, the correlation characteristics can be applied to solve the geological problems such as the change of sedimentary environments of sedimentary rocks and the ancient climate change. The conclusions made from these correlation characteristics are consistent with previous findings, indicating the validity and accuracy of solving geological problems using correlation characteristics between petrophysical properties and petrogeochemical distribution of the elements. The following tables can clearly show the relationship between petrophysical properties and geochemical elements. Using these tables, we can use the geophysical prospecting to study the sub-surface rock properties. And then the change regulation rock geochemical elements can be obtained. According to these characteristics, the sub-surface geological structures can be studied clearly.

Table 2 Correlation coefficient between magnetic susceptibility and geochemical elements of rocks

	Major elements	Correlation coefficient R^2	Trace element	Correlation coefficient R^2	Rare earth elements	Correlation coefficient R^2
Plutonic rock SUS and geochemical correlation coefficient	SiO_2***	0.5324	Cu	0.0372	La***	0.4269
	Al_2O_3	0.1304	Pb	0.0054	Ce***	0.5536
	Fe_2O_3***	0.688	Zn	0.1189	Pr***	0.6021
	FeO***	0.6909	Cr	0.131	Nd***	0.6519
	TFeO***	0.7485	Ni	0.1676	Sm***	0.6818
	CaO***	0.6788	Co***	0.5163	Eu***	0.6925
	MgO***	0.617	Rb	0.1655	Gd***	0.6597
	K_2O	0.2166	Sr**	0.3253	Tb***	0.6276
	Na_2O	0.1467	Ba	0.0577	Dy***	0.5448
	TiO_2***	0.5338	V***	0.6268	Ho***	0.475
	P_2O_5***	0.6345	Sc	0.1989	Er**	0.3987
	MnO	0.1573	Nb	0.0568	Tm**	0.2987
			Ta	0.1905	Yb	0.2541
			Zr	0.1642	Lu	0.2502
			Hf	0.0502	Y***	0.5092
			Ga***	0.6299		
			U	0.1177		
			Th	0.155		

** The correlation coefficient is above 0.01

*** The correlation coefficient is above 0.001 and represents strong correlation

The measurements of petrophysical and geochemical element parameters in the western Liaoning Geological corridor not only provided basic rock properties to the study of this area, but also helped the statistical study in the correlation characteristics between petrophysical properties and petrogeochemical distribution of the elements. This is universally significant in Earth science in solving geological problems such as petrogenesis and tectonic evolution, and provides new ideas and research directions to solving future geological problems.

Table 3 Correlation coefficient between resistivity and geochemical elements of rocks

	Major elements	Correlation coefficient R^2	Trace element	Correlation coefficient R^2	Rare earth elements	Correlation coefficient R^2
Plutonic rock RESIS and geochemical correlation coefficient	SiO_2**	0.481	Cu	0.0073	La	0.3319
	Al_2O_3	0.3036	Pb	0.2311	Ce	0.3489
	Fe_2O_3	0.2054	Zn	0.1202	Pr	0.3233
	FeO	0.4078	Cr	0.0613	Nd	0.3215
	TFeO	0.3428	Ni	0.1281	Sm	0.2954
	CaO***	0.7568	Co	0.2896	Eu	0.4262
	MgO	0.3421	Rb	0.0692	Gd	0.2977
	K_2O	0.4552	Sr	0.2111	Tb	0.2423
	Na_2O	0.2624	Ba	0.0335	Dy	0.1918
	TiO_2	0.2823	V	0.3529	Ho	0.1488
	P_2O_5	0.3198	Sc	0.1404	Er	0.1221
	MnO	0.0154	Nb	0.1131	Tm	0.0698
			Ta	0.2657	Yb	0.0506
			Zr	0.0063	Lu	0.0514
			Hf	0.0368	Y	0.186
			Ga	0.4271		
			U	0.416		
			Th**	0.4731		

** The correlation coefficient is above 0.01

*** The correlation coefficient is above 0.001 and represents strong correlation

A goal-oriented adaptive finite-element method for 3D MT anisotropic modeling with topography

YIN Chang-Chun*, CAO Xiao-Yue, ZHANG Bo, Huang Xin, LIU Yun-He, CAI Jing

College of Geo-exploration Sciences and Technology, Jilin University, Changchun 130026, China

Abstract Traditional 3D MT data interpretations are based on an isotropic model that is sometimes inappropriate, because it has been well established that electrical anisotropy is widely present in the deep earth. The MT anisotropic modelling is generally worked on by structured meshes that has a limited accuracy but cannot model complex geology. We present a goal-oriented adaptive unstructured finite-element method for accurately and efficiently simulating 3D anisotropic MT responses. This is largely different from the traditional 3D MT modelling methods of finite-difference or integral equation that use artificially refined grids. The accuracy of the latter methods are severely influenced by the mesh quality, especially for complex geology and topography.

We use Galerkin method to discretize the electric filed vector wave equation for obtaining the finite-element equation. Once the electric field is solved, the magnetic field is calculated via Faraday's law. By solving two polarization modes with source parallel to the *x*- and *y*-axes, respectively, we get the impedance tensor. For the adaptive strategy, we use the continuity of normal current to evaluate the posterior error, where the weighting coefficient of the posterior error is obtained by solving a dual problem of the forward problem. Besides, we use a convergence rule to determine which receiver will be used in the next refinement iteration.

We check the accuracy of our algorithm against the analytical solutions for a layered anisotropic earth. Further, we study the anisotropic effect on the adaptive meshes and MT responses by models with anisotropic bodies embedded in a half-space. At last, we study the MT responses for an anisotropic body located under a trapezoid hill. The numerical experiments show that our algorithm is an effective tool for modelling 3D anisotropic MT soundings with topography. The numerical results demonstrate that: 1) Anisotropy influences the adaptive meshes differently based on the resistivity contrasts in different directions; 2) The influences of topography on MT responses depends on the polarization mode, while the anisotropy influences the MT responses depending on the direction of anisotropic principal axes and polarization; 3) Anisotropy is resolvable from the distribution of the apparent resistivities by polar plots. Our study aims to provide foundations for the interpretation of 3D MT data on the conditions of topography and anisotropy for purposes of deep earth study.

Research on key technology of "Crust 1" 10K ultra-deep scientific drilling rig

Ping Yu, Youhong Sun, Yongbai Sha, Qingyan Wang, Ke Gao, Yan zhao

College of Mechanical Science and Engineering, Jilin University

Scientific drilling is the only and most direct technical means to explore the mysteries of the earth's interior and to develop underground resources. In order to meet the significant needs of the deep earth exploration project in China, funded by the Ministry of land and resources, the Ministry of Finance and the China Geological survey, we have successfully developed China's "crust 1" 10K ultra-deep Continental Scientific Drilling equipment after more than 4 years of technological research, solved the technical problems of small capability and low automation degree of scientific drilling equipment. The main results obtained are as follows:

1. Hydraulic Top-drive Technology.

We have invented the Hydraulic Top-Drive System to unravel the problems of oversized system. The difficulties on controlling the system and heat dissipation on the hydraulic system have also been handled. This has achieved coring drilling of large diameter long - stroke hydraulic drive.

2. Hydraulic Pipe Handle

Using Bionics theory of similarity, simulating Artificial Motivation, we have developed pipe automatic transferring on second working platform of the rig; handled the complex rotary motion, extension and retraction motion, and clapping motion of large-weight drill string horizontally and on the range of ±90º; accomplished the automation of Drill pipe between the rig and racking board area.

3. high - Precision auto-drilling technology

Utilizing Intelligence Controller and winch, we have designed high-precision automatic drilling device and solved the problem of high-precision drilling process control under heavy load.

4.Automatic transmission drilling technology

We have invented hydraulic catwalk, achieved the automatic transmission and reverse transmission between the working platform and the ground for various types of drilling device, which has greatly imporved the efficiency of drilling and reduced labor intensity.

An algorithm for computing synthetic body waves due to underside conversion on an undulating interface and application to the 410 km discontinuity

Han Zhang[1,2], Sidao Ni[1*], Risheng Chu[1], Brandon Schmandt[2]

[1] *State Key Laboratory of Geodesy and Earth's Dynamics, Institute of Geodesy and Geophysics, Wuhan, 400077, China.*

[2] *Department of Earth and Planetary Science, University of New Mexico, Albuquerque, NM 87131, USA.*

Abstract

The topography of the 410 km discontinuity provides helpful constraints on both petrologic and geodynamic models of the mantle transition zone. Previous studies involving differential times between scattered phases ($S_{410}S$, $p_{410}P$, $s_{410}P$, etc.) and reference phases (SS, P, pP, sP, etc.) have revealed large scale topography on the 410 km discontinuity. In contrast, amplitude variations of converted phases are more sensitive to smaller scale topography. We develop an algorithm to calculate synthetic S to P conversions at the 410 km discontinuity above deep earthquakes using ray theory and the representation theorem. After benchmarking our method with geometrical ray theory, we perform tests on elevated and depressed topography with dome or ridge shapes. We find that focusing/defocusing due to discontinuity topography substantially alters the amplitudes of converted phases (60% - 300% based on our examples). We then use the new algorithm to model amplitude variations of the $s_{410}P$ waves from a deep earthquake beneath western Brazil. A grid search over potential values for the width and height of a ridge-like elevation of the 410 km discontinuity found that the observed amplitude pattern can be explained by a ridge with a height of 12 km and width of 180 km near the expected location of a subducted slab. The new method demonstrated here can be easily adapted to model downgoing $S_{410}P$ or $S_{660}P$ waves, but the representation theorem needs to be combined with numerical solvers to tackle complex 3-D structures near mantle discontinuities.

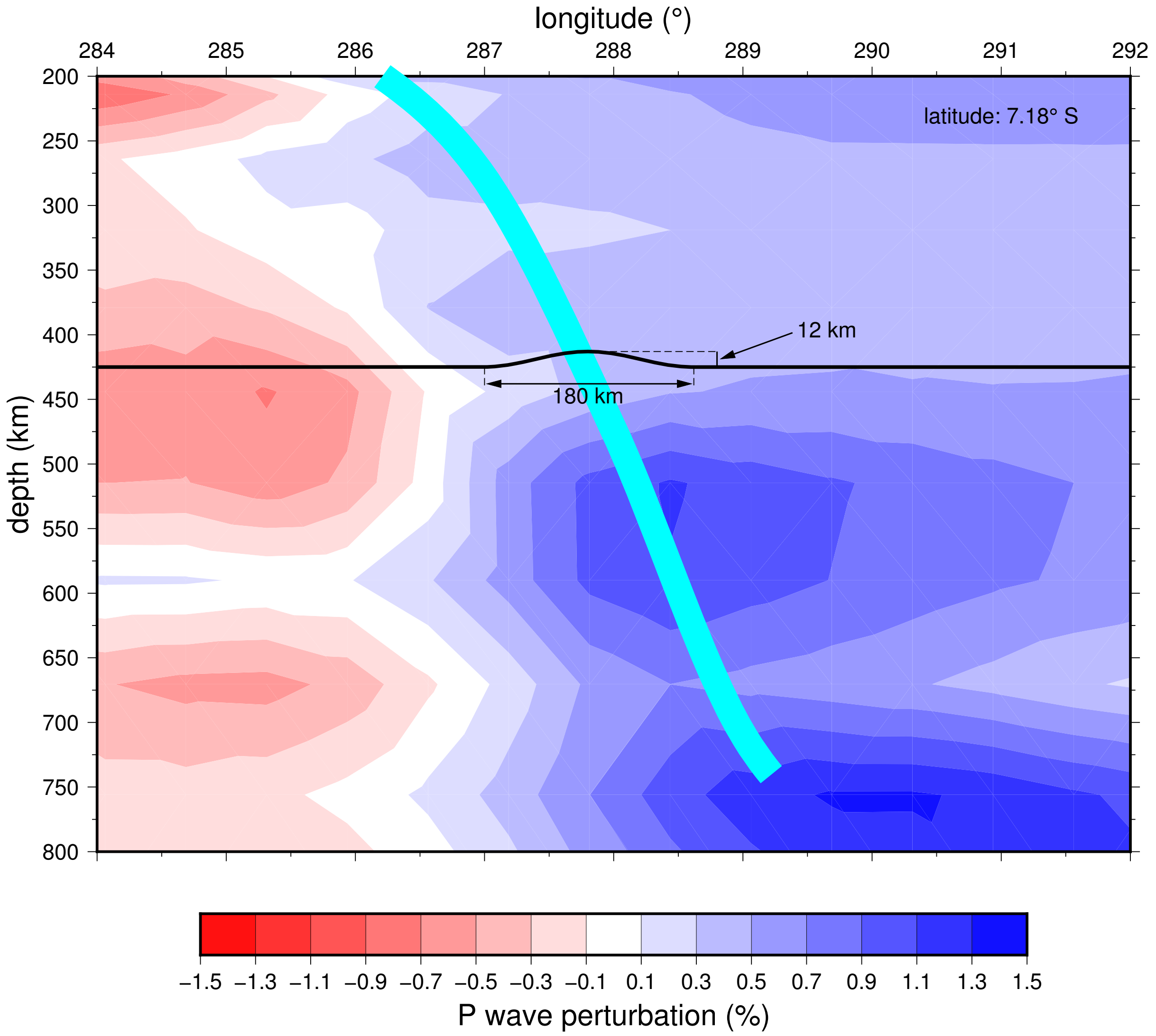

Figure 1. Topography model of a deeper 410 km discontinuity (actual depth of 425 km, solid line) overlaid over a tomography model. Tomographic model from GAP_P4 (Obayashi et al. 2013; Fukao and Obayashi 2013) and slab position from Slab 1.0 (Hayes et al. 2012) are also plotted for reference.

Scientific drilling - to construct the telescopes that inserting to the earth interior

Zhang Xiaoxi[1], Zhang Hui[1], Hu Yule[1]

[1] CUG（China University of Geosciences）, No.388 Lumo Road, Wuhan city, Hubei province, China.

E-mail: zxxcug@cug.edu.cn zxxcug@126.com

Mankind has live in the earth for countless years，but until now; people do not really understand the connotation of the Earth. We know that the earth composition including the lithosphere, the asthenosphere, mantle and core. Of course, the lithosphere supports all the life on Earth. For a long time, geoscientists trying to use all kind of methods such as geological, geophysical and geochemical methods to detect and study the earth, but the knowledge about earth are mostly indirect. Through the direct observation to the lithosphere, people can understand and recognize the plate movement of ocean and the mainland, crustal stress, earthquakes, volcanic processes, deep resources, the origins of life , global climate change and biodiversity. They are all the basis of a series of geosciences problems [1].

Geological specimens, especially the true samples from deep of the Earth, are the most directly study subjects for geologists. But the only way to access the true samples from deep of the earth is drilling. The most directly relevant evidence always originated from the deep of the earth, such as core, cuttings, fluid samples and other physical samples.

Continental scientific drilling has been demonstrated which is an efficient technique for directly obtaining information from the Earth’s surface to the deep crust, and is acknowledged as “to build a telescope inserting to the interior of the Earth”, as well as “a key for opening the door of the Earth”. Over the last four decades, continental scientific drilling has achieved great success in enhancing our knowledge of the Earth, and in providing information on mineral resources, large engineering projects and global change. SinoProbe-05 is a new scientific drilling venture, which builds on the success of the Chinese Continental Scientific Drilling Project (CCSD), and is similar to the current major scientific drilling project on the Wenchuan earthquake fault. SinoProbe-05 will focus on 6 critical tectonic and mineral resource regions, including the Jinchuan Cu-Ni sulphide deposits in Gansu, the Luobusa chromite deposits in Tibet, the Tengchong volcano-thermal tectonic zone in Yunnan, the Yudu-Ganxian polymetallic deposits in South China, the Tongling polymetallic deposit and the Luzong volcanic basin and mineral deposit district in Anhui. As of the end of 2013, all of these pilot holes have been completed, all of them have achieved the desired scientific objectives.

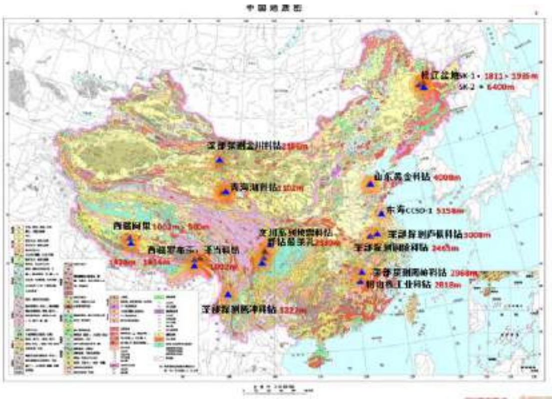

Fig.1 Part of the scientific drilling projects distribution map finished within recent 15 years in china

The construction of another ICDP project, Songke No.2 well, has come to an end. Current well depth is 5929m. Drilling throughout the Cretaceous strata is just around the corner (The design well depth is 6400m.). This will be the first complete Cretaceous stratigraphic profile in the world.

The deep exploration project which will be stared soon will build a large number of different depths of scientific drilling holes. The deepest hole depth will reach to 13000m. We believe that the construction of these scientific coring drilling holes will provide geologists with a lot of real core samples. These cores can meet the needs for different geoscience research areas. No doubt, the research results based on these cores will promote China's geological science research to a new height, of course; will also contribute to the progress of the world's earth science. This is also a good opportunity to promote China's drilling technology.

So we know that no advanced drilling technology, no enough high quality samples from the deep of the Earth, the in-depth studies for geosciences will be restricted of course[2].

References:

[1] Su D et al. (2010) ACTA GEOLOGICA SINICA. Vol.84 No.6:873-886

[2] Zhang X et al. (2013) GEOLOGY IN CHINA. Vol. 40 No.3:681-693

zxxcug@cug.edu.cn

Velocity structures of the mantle transition zone beneath the southeastern and western margins of Tibetan Plateau

Yuanze Zhou[1,2], Yajian Gao[1,2], Guohui Li[3]

1 Laboratory of Computational Geodynamics, University of Chinese Academy of Sciences

2 College of Earth Science, University of Chinese Academy of Sciences

3 Institute of Tibetan Plateau Research, Chinese Academy of Sciences

P-wave triplications related to the 410 km discontinuity (the 410) are clearly observed from the vertical component seismograms recorded by the Chinese Digital Seismic Network (CDSN). By matching the observed P wave triplications with synthetics through grid search, we find that there is a ubiquitous low-velocity layer (LVL) atop the mantle transition zone (MTZ) beneath the southeastern margin of the Tibetan Plateau (TP). The LVL is 25 to 40 km thick with a P-wave velocity decrement of up to -5.3%~-3.6% related to the standard Earth model IASP91. The abrupt transition in the velocity decrement of the LVL means that the mantle structure beneath the southeastern margin of the TP is primarily controlled by the southeast extrusion of the TP to the north, combined with the eastward subduction of the Indian Plate to the south, but not affected by the Emeishan mantle plume. A high-velocity anomaly of up to 1.0%~1.5% is also detected at a depth of 542-600 km, providing additional evidence for the remnants of the subducted Pacific plate within the MTZ.

Seismic velocity and the detailed topography of the 410 km discontinuity beneath the Central Tianshan-Tarim basin are also detected. Beneath the Tarim basin, the 410 depressed about 10 km, above which there exists a 70 km-thick low velocity zone and the decrease of the P-wave velocity is -3%. The LVL is attributed to the dehydration of the upwelling material from the mantle transition zone, which was caused by the detachment of the lithosphere beneath Central Tianshan. Beneath the Central Tianshan, 410 km discontinuity depressed about 10 km, above which there exists a 70 km-thick low velocity zone as well, and the decrease of the P-wave velocity is -1%. This may relate to the expansion from Tarim basin.

Damage Zone Structure of a Supershear Earthquake: Dense Temporary Array Analysis of Fault Zone Trapped Waves and Ambient Noise

A. A. Allam, C. Tape, F.-C. Lin

Abstract

In 2002, a 341km long section of the Denali fault ruptured in a Mw 7.8 earthquake which potentially reached supershear rupture velocities near the Richardson highway. In April-May 2016, we deployed nearly 200 three-component geophones in a dense 2D array in the rupture zone with 75m average station spacing. After deployment and retrieval under grueling conditions, we recorded 22 days of continuous data including six teleseismic events with M>6.0 and 37 local events with M>2.0. The local events produce clear fault zone trapped waves, which are a resonant phase that record the low velocity signature of the near-fault damage zone structure. From the distributions of trapped wave amplitude and duration, we are able to constrain the width and average velocity reduction of the damage zone in two dimensions. Using the continuous data, we reconstruct coherent Rayleigh wave signals by stacking five-minute cross-correlations for the entire deployment duration. We interpret variations in the teleseismic waveforms, including delay times, as the result of local fault zone interfaces. The combined dataset is completely unique for the Denali fault and is the first of its kind in a supershear rupture zone.

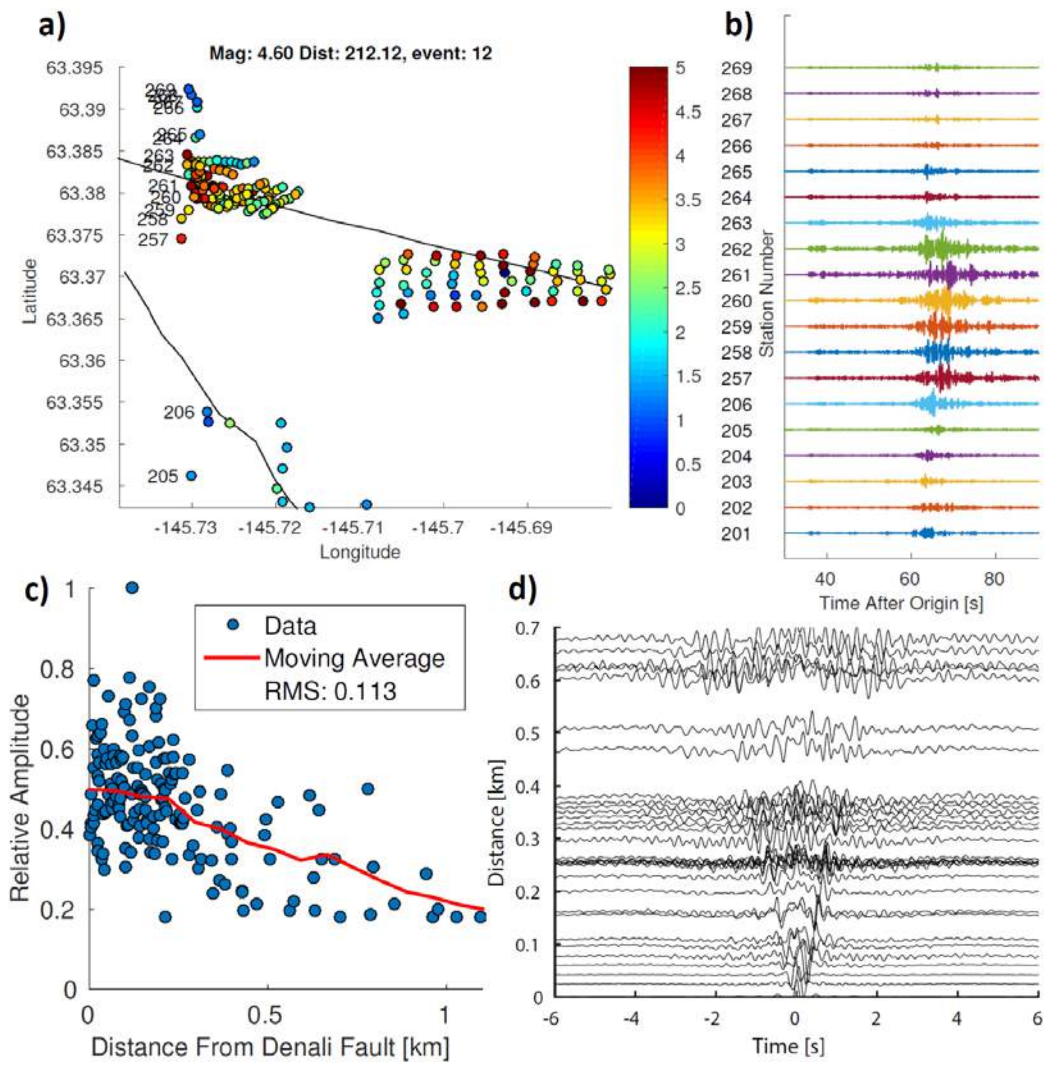

Miocene-Pliocene Strike-slip Basin Development Along the Denali Fault System in the Eastern Alaska Range: Chronostratigraphy and Provenance of the McCallum Formation and Implications for Displacement

Authors: Wai K. Allen, Kenneth D. Ridgway, Jeff Benowitz, Trevor Waldien, Sarah Roeske

Analysis of sedimentary and volcanic strata of the Miocene-Pliocene McCallum Formation provides new insight into Neogene transpressional foreland basin development and strike-slip displacement along the Denali Fault system in the eastern Alaska Range. The McCallum basin is located within the regional footwall of a series of dextral-oblique reverse faults that parallel the south side of the eastern Denali fault. The McCallum Formation is defined by a two-part stratigraphy that represents the progradation of alluvial-fan deposystems of an upper member over mainly lacustrine strata of a lower member. This upward-coarsening, progradational package has a minimum thickness of 564 m based on our measured stratigraphic sections. Our dataset consists of measured stratigraphic sections, paleocurrent data, clast composition data from conglomerate, U-Pb detrital zircon geochronology from sandstone, and Ar-Ar geochronology of volcanic glass.

New ages from $^{40}Ar/^{39}Ar$ geochronology of tephras show that the lower member ranges in age from 6.17 to 5.07 Ma and that the upper member ranges from 5.03 to 3.80 Ma. Our preliminary detrital zircon analysis of sandstone from the lowest stratigraphic units of the McCallum basin document a unique 123-124 Ma detrital age signature. These samples are located between two of our dated volcanic ashes that range in age from 6.1 to 5.8 Ma. The only known potential source rocks with this age are located across the Denali fault in the eastern Alaska Range and are referred to as the Klein Creek Pluton of the White Mountain granitoid suite. The Klein Creek pluton is located 230 km southeast of the current position of the McCallum basin (Figure 1). Another unique detrital signature in our dataset is 26 Ma. The potential source rocks with this age are the Sonya Creek and Rocker Creek volcanic fields located southeast of the White Mountain granitoid suite (Figure 1). If the Klein Creek Pluton and Sonya Creek and Rocker Creek volcanic fields directly sourced the McCallum basin, this would require 230 km of strike-slip displacement since 6.1 Ma. This would also require much higher slip rates than the current slip rates along the fault system (~13 mm/yr) based on geodetic data (Mériaux et al., 2006, and Matmon et al., 2009). The potential fault path of this displacement is consistent with the 7.9 M Denali Earthquake in 2002.

We are interested in discussions regarding:

- Geophysical linkages between the Denali and Totschunda fault systems
- Seismicity and earthquake hazards of the Totschunda and Denali fault systems
- Subsurface geometry and configuration of the Denali fault system

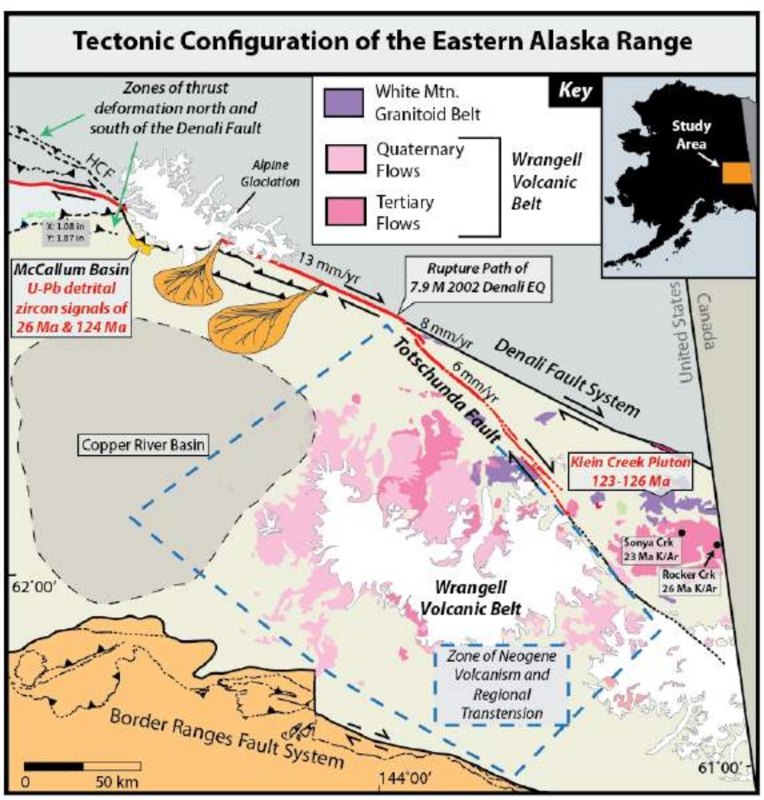

Figure 1. Tectonic configuration and simplified geology of the eastern Alaska Range. Key features include the location of the McCallum basin and its potential offset of 230 km from the Klein Creek Pluton north of the Totschunda fault. Red line shows Denali Earthquake rupture path derived from Crone et al. 2004. Geologic units are derived from Wilson et al. 2016.

Proximity of Precambrian basement affects the likelihood of induced seismicity in the Appalachian, Illinois, and Williston Basins

M.R. Brudzinski (1), R.J. Skoumal (2), and B.S. Currie (1)

(1) Miami University, Oxford, OH; (2) USGS, Menlo Park, CA

A dramatic seismicity rate increase in the Central and Eastern United States (CEUS) over the past decade has been largely associated with the increase in enhanced oil and gas recovery operations and change in industry practices. However, certain areas of the CEUS that have experienced large increases in oil and gas operations, such as the Bakken and Marcellus shale plays, have very little (if any) induced seismicity. No prior study has adequately explained the occurrence or absence of induced seismicity on a regional, basin-to-basin scale in the CEUS. In this study, we improve the basement depth characterization and induced seismicity detection for the Appalachian, Illinois, and Williston basins to determine whether the proximity of wastewater disposal and/or hydraulic fracturing to the crystalline basement increases the likelihood of induced seismicity. We also investigate the lithologic characteristics of sedimentary strata situated between injection intervals and the crystalline basement to evaluate the role they may play in diminishing the transmission of pore pressure during well stimulations. We find that wastewater disposal in basal sediments or hydraulic fracturing operations < 1 km from the Precambrian basement raise the likelihood of induced seismicity, an observation that is consistent with the apparent absence of induced seismicity related to production from the Bakken and Marcellus shale plays.

Considering the national debate over hydraulic fracturing, we have sought to disseminate our induced seismicity research to a wide range of stakeholders, including public outreach through the traditional popular press and new media such as a Reddit and Twitter. We have also met individually with industry and regulators to share findings and discuss operation strategies for mitigating hazard. This has led us to contribute to the StatesFirst Induced Seismicity Working Group primer document that is helping to shape regulations across the US.

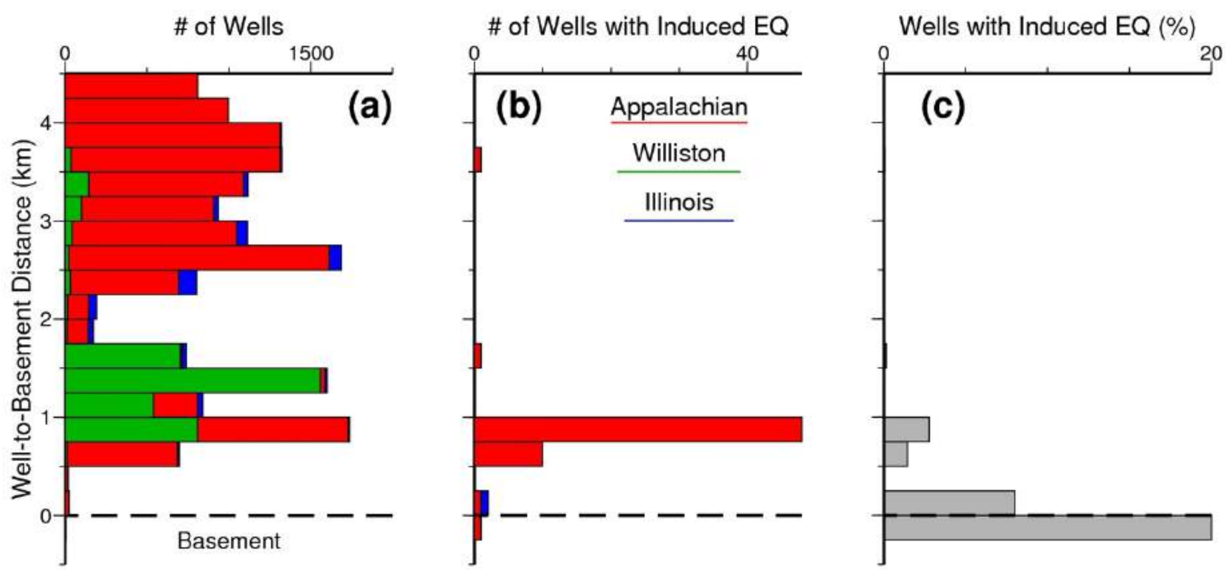

Figure 1. Histogram summary of our results for all basins in this study. (a) Number of wells (wastewater disposal and hydraulic fracturing) in each 0.25 km histogram bin of depth between well target and basement. Bars are colored for each basin in this study. (b) Number of wells in each histogram bin that have been associated with induced seismicity (M > 1). (c) Percentage of wells in each histogram bin that have been associated with induced seismicity.

A Neogene shortening budget for the eastern Alaska Range: implications for strain transfer in the lithosphere

Oblique convergence in the Denali fault system may absorb up to ~20% of Yakutat-North America relative plate motion inboard of the plate boundary faults. While dextral strike-slip motion on the master Denali fault is well established in the neotectonic record, the history of Neogene-Quaternary shortening across the Denali fault system is considerably less well known. The Broxson Gulch fault is often cited as a locus of Neogene shortening south of the Denali fault in the eastern Alaska Range. However, the magnitude and rate of shortening accommodated by the Broxson Gulch fault and subsidiary structures remain unresolved, leading to uncertainties in the Neogene shortening budget across the Alaska Range and, as a result, the amount of plate boundary strain absorbed by the Denali fault system.

We present new geologic mapping, low temperature thermochronometry, and fault kinematic analysis from the Broxson Gulch fault and related structures defining the southern margin of the eastern Alaska Range. Our new data indicate a minimum of 20 km of post-30 Ma shortening accommodated by thrust faults south of the Denali fault. The shortening direction on these thrusts is oriented nearly perpendicular to the Denali fault, indicative of highly partitioned oblique convergence in this region. On the basis of cooling ages, metamorphic rock fabrics, and fault-bounded Neogene strata, we posit that the most recent phase of convergence south of the Denali fault in the eastern Alaska Range initiated at, or shortly after, 30 Ma. Since inception, the Broxson Gulch thrust system has propagated southward and along strike as a series of imbricated thrusts and folds. Faults in the lowest structural position define the range front and have experienced Quaternary slip.

Our dataset, combined with other researchers' results, contains apparently contradictory predictions regarding the mechanics of vertical and horizontal strain transfer in the crust and addresses the potential for hypothesized plate-scale sub-horizontal detachments transferring convergence across continental transform faults in the Cordillera. Cooling ages and rock fabric analysis show that metamorphic rocks from the structurally highest portion of the Broxson Gulch thrust system, nearest to the Denali fault, have been exhumed from below the brittle-ductile transition since ~30 Ma. Shortening structures at this location appear to be reactivating an inherited crustal boundary. Across the Denali fault to the north, exhumation from similar depths began at ~25 Ma, but was accommodated primarily by oblique shear in a narrow zone adjacent to the fault rather than splay thrusts. Although the two locales are now on opposite sides of the Denali fault, they were separated by up to 250 km when exhumation initiated. Thus the mid-crustal rock fabrics north and south of the Denali fault appear to be truncated by, or merge with, the sub-vertical master strike-slip fault zone. Focused exhumation of these mid-crustal rocks adjacent to both sides of the Denali fault is likely controlled by horizontal rheologic contrasts within the crust rather than increased convergence related to the curvature of the Denali fault.

In contrast, aftershocks from the 2002 Denali earthquake and balanced cross-sections of the Pliocene-Recent thrust systems north and south of the Denali fault show the splay thrust systems linking to the Denali fault at ~8-10 km depth. Combined with published results from north of the Denali fault, our data reveal non-uniform Quaternary shortening rates across the eastern Alaska Range. These neotectonic observations predict effective 'decapitation' of the Denali fault via slip along a sub-horizontal fault in the upper crust, while the longer-term evolution of the thrust system appears to favor discrete structures penetrating through at least the middle crust. With the present data, we suggest that detachment horizons in the middle-upper crust may be relatively ephemeral features spatially restricted to regions actively experiencing heterogeneous strain.

Integrating our new structural analysis and geochronology into the tectonic evolution of southern Alaska reveals that shortening in the eastern Alaska Range is broadly synchronous with initiation of the Wrangell volcanic arc, regional exhumation, and drainage reorganization. Collectively, these processes record widespread modification to the upper plate of the southern Alaskan margin, likely in response to a plate boundary reorganization at ~30-25 Ma.

Neogene slip distribution in the Alaska Range

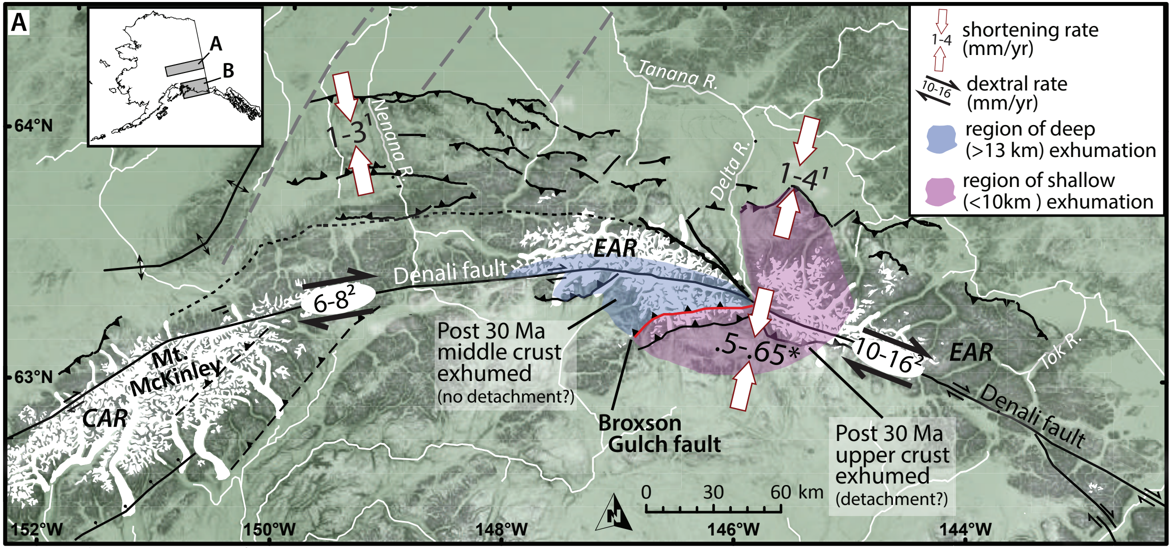

[1] Bemis et al. (2015), [2] Mériaux et al. (2009), * This study

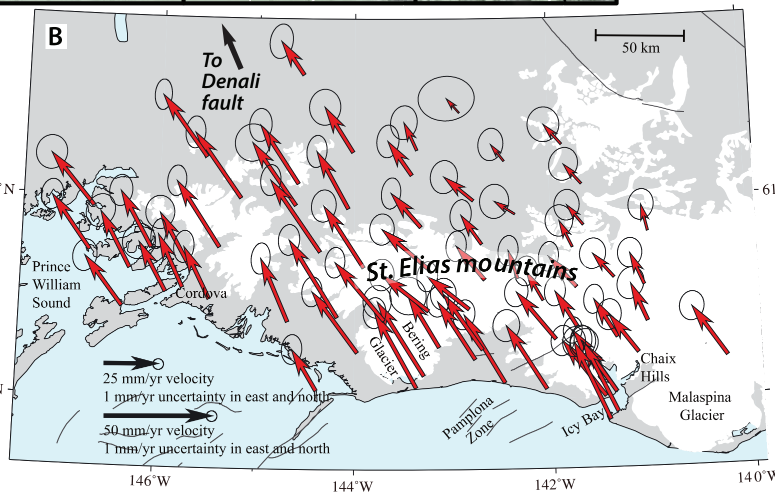

A) Shaded relief map of the eastern and central Alaska Range (EAR and CAR) overlain by the structures of the Denali fault system. The Broxson Gulch fault and related thrusts south of the Denali fault in the eastern Alaska Range are the focus of this study. Known shortening and dextral slip rates are shown in mm/yr. Exhumation depth is only indicated for regions where we have data. The timing and depth of exhumation north of the Denali fault are from Benowitz et al. (2014). White areas represent perennial ice cover. Modified from Bemis et al. (2015). **B)** Map of the St. Elias region (white ice covered area) with GPS vectors showing shortening across the St. Elias orogen. Residual northwest-directed block motion, indicated by vectors north of the St. Elias Mountains, is absorbed by the Denali fault system as oblique convergence. Modified from Elliott et al. (2013).

Surface wave investigation of crustal seismic anisotropy at the Ruby Mountains Core Complex

Justin T. Wilgus, Brandon Schmandt
University of New Mexico

Within the highly extended Basin and Range (BR) lie several distinctive uplifts called metamorphic core complexes consisting of rocks exhumed from middle to lower crustal depths adjacent to mylonitic shear zones. The Ruby Mountain Core Complex (RMCC), located in northeast Nevada, records exhumation depths up to 30 km indicating an anomalously high degree of extension relative to the BR average. Recent regional western US lithospheric seismic anisotropy studies have concluded that the distribution of strain in the lower crust is diffuse throughout the BR and that deformation in the crust and mantle are largely uncoupled. However, the relative importance of potential controls on crustal seismic anisotropy such as deformational fabrics in specific crustal minerals and the contemporary state of stress remain enigmatic. The geologic setting of the RMCC and the availability of dense broadband data enable a local scale investigation of crustal anisotropy with surface wave data from the TA and the Ruby Mountain Seismic Experiment (RMSE), part of EarthScope's Flexible Array. These data will be used to evaluate the degree to which anisotropy of the RMCC deviates from regional scale properties of the BR. Preliminary azimuthal anisotropy results using Rayleigh waves reveal clear anisotropic signals at periods between ~5-40 s, and demonstrate significant rotations of fast orientations relative to prior regional scale results. Moving forward we will focus on quantification of depth-dependent radial anisotropy from inversion of Rayleigh and Love waves. These results will be relevant to identification of the deep crustal distribution of strain associated with RMCC formation and may aid interpretation of controls on crustal anisotropy in other regions.

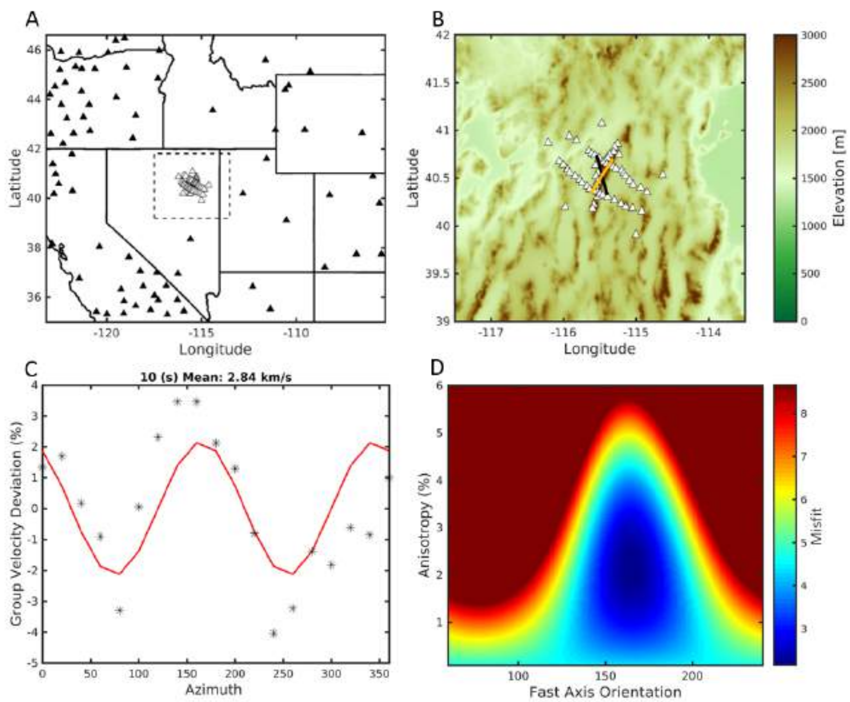

Figure 1. Area maps and projection and measurement of azimuthal anisotropy. A) Map of locality and seismic stations used for ambient noise correlations. White triangles are RMSE stations and Black triangles are external stations. Dashed box delineates area projected in B. B) Topographic map. Bold lines show azimuthal anisotropy fast axis orientation. Black line is the fast axis measured in C and D. Orange line shows azimuthal anisotropy fast axis orientation at a 12 s period over the RMCC from Lin et al., (2010) for comparison. Note the ~40° rotation discrepancy. C) Mean Rayleigh wave group velocity (Expressed as percent deviation from mean) from ambient noise cross correlations between external stations and the RMSE for 10 s period as a function of azimuth. Asterisks represent averaged (Binned every 20°) group velocities. Red line is the best fit 2θ L2 sinusoidal curve. D) Misfit surface from measurements in C showing magnitude and fast axis azimuth of anisotropy. The minimum misfit in C gives a magnitude of ~2% and an anisotropic fast axis of 165°.

Field Study of the Border Ranges Fault System in Southwestern Alaska

Veselina Yakimova and Elisabeth Nadin

The Border Ranges fault (BRF) system of southern Alaska is a major fault zone long associated with accretion of the Talkeetna volcanic arc and the growth of the North American margin. Previous studies of the BRF reveal a history of repeated reactivation, but fabrics of the initial subduction thrust have not been well documented. We plan to map the BRF region in detail and measure rock fabrics and fractures of key localities along the fault that may preserve remains of the original subduction-related boundary. Samples will be further examined by electron back-scatter diffraction (EBSD) to determine orientations of preferred fabrics. The fault is a terrane boundary, expressed as the contact between arc basement and adjacent accretionary wedge deposits. There are additional faults in the vicinity of the main BRF strand, and we will determine if they are members of the BRF zone associated with early thrusting, part of the subsequent phase of dextral motion, or can be classified as unassociated with BRF activity. Our three mapping targets are: (1) near the Nelchina glacier, where ice retreat has revealed a hundreds-meter-wide zone of ductile through brittle deformation, including pseudotachylite, near a gabbronorite–mélange contact; (2) the Kenai peninsula; and (3) Kodiak island. The BRF at the latter two sites places lower-arc rocks against accretionary complex schists. While the eastern segment of the BRF has been shown to be heavily overprinted by subsequent dextral deformation, the sites listed here are the most likely to preserve early thrust fabrics. Even if the western portion is likewise overprinted by transpressional motion, the detailed mapping, fracture survey and supporting rock-fabric studies will give insight into the timing and nature of change in conditions during the ductile to brittle transition of BRF activity. In addition, structural, geochemical and petrologic analyses of a sulfide vein network in the Nelchina map area will give insight into the fluid budget of hydrothermal alteration that is likely related to either dewatering during ca. 200 Ma subduction accretion or much later during ca. 50 Ma ridge migration along the southern Alaska margin. This will help determine the extent and nature of fluid mobilization and will also result in a better understanding of the role of fluids in major fault zones.

Figure on next page...

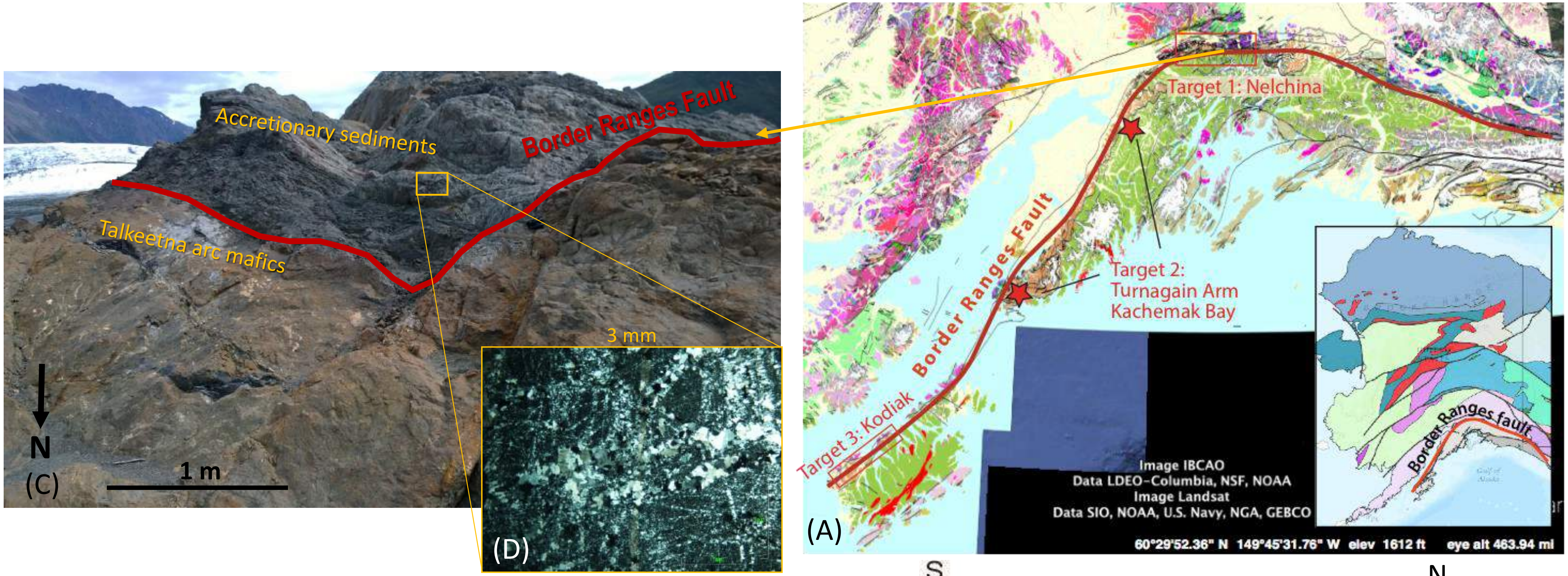

The Border Ranges fault (BRF) system of southern Alaska is a major fault zone long associated with accretion of the Talkeetna ocean island arc and growth of the North American margin. Previous studies of the BRF reveal a history of repeated reactivation, and no fabrics of the initial subduction thrust have been documented. I propose that such fabrics would be best preserved at contacts between the arc basement and metamorphosed sediments of the accretionary prism. **(A)** shows the location of my three targets along the western part of the BRF (USGS Scientific Investigations Map 3340). **(B)** is a schematic cross section of the BRF zone in southwestern Alaska, where Jurassic mafic–ultramafic arc rocks (basement) are juxtaposed with Jurassic blueschist–greenschist facies accretionary prism rocks (modified from Clift et al. 2005). **(C)** is a field photo from the Nelchina target mapping area, showing this contact. In order to understand the timing and change in conditions during the fault evolution, I plan on pursuing detailed structural mapping and supporting rock fabric studies. Including, petrographic **(D;** thin section image showing a complex network of monomineralic quartz veins in a fine matrix**)** for fabrics description, and EBSD for their quantitative analysis.

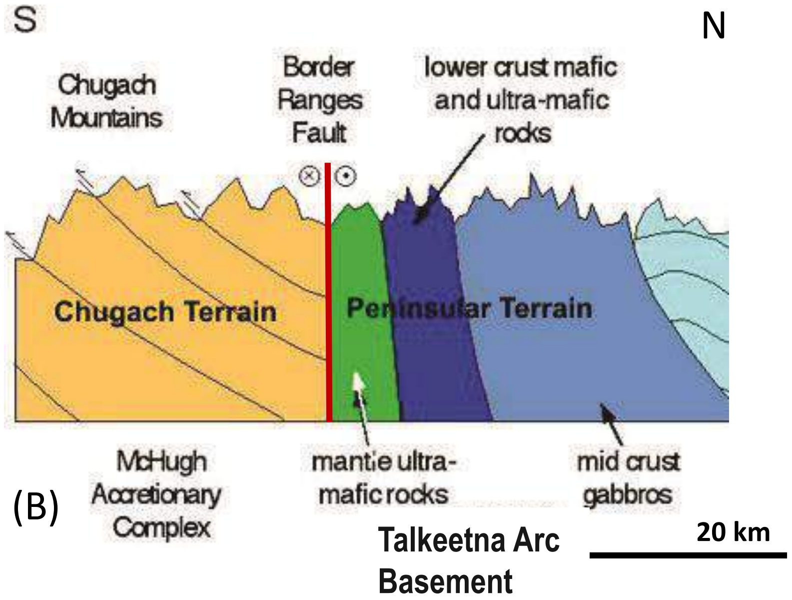

A GEOPHYSICAL STUDY OF THE CASTLE MOUNTAIN FAULT SYSTEM AND MATANUSKA-SUSITNA VALLEY NEAR ANCHORAGE, ALASKA

F. D. Ziwu[1], S. M. Shinagel[2], D.I. Doser[3] and L.F. Serpa[1], [1,2,3,4]Department of Geological Sciences, University of Texas at El Paso, El Paso, Texas, 79968

Abstract: The Castle Mountain Fault (CMF) is the closest (~50 km) active fault to Anchorage, Alaska. Located within the Matanuska and Susitna (Matsu) Valleys, the CMF shows repeated, unmistakable evidence for Holocene motion. Recent geologic studies estimate that this fault is capable of producing earthquakes of magnitude 7.0-7.1. Several mapping and trenching studies have been conducted along the CMF with limited geophysical studies. There is little information on the subsurface structure of the fault and how it may control the fault segmentation and depth of seismicity. The interaction between the CMF with adjacent, seismically active, reverse faults and folds is also poorly understood. A vital first step in predicting strong ground motion caused by events along the fault zone is to better understand the structure of the CMF. Using over 700 recently collected (between 2010 – 2011), closely spaced gravity observations, in addition to existing regional gravity, aeromagnetic, seismic reflection, well log data, and geologic information, we developed new 2D models of the deeper structure of the CMF system.

Our integrated models show a thick basin full of Tertiary and Mesozoic sediments in a Peninsula terrane basement at varying depths within the area. We modeled several granitic intrusions that may have some effect on the mechanical behavior of the CMF where sediments are pinched out and/or serpentinization is occurring.

The 2D model shows the CMF shallowing from west to east CMF (~25km to 10km deep). The CMF cuts through the Late Mesozoic at depth.

Opportunities and Efforts for Education and Public Outreach

I am currently looking to showcase this work at research meetings as well as other organized symposia to educate the public on my findings and solicit expert ideas on key things to consider to modify the research. I have also presented this research in 2017 Colloquium organized by University of Texas at El Paso Geological Science Department and received helpful feedback. My main objective is to finally get a publication that will add to the research knowledge of the tectonics of the CMF and the possible hazards associated with this fault.

.

Figures

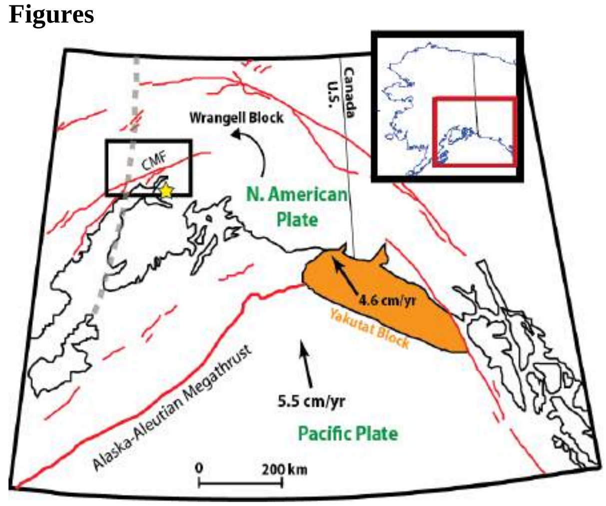

Figure 1: Tectonic setting of southern Alaska showing collision of the Pacific plate and Yakutat block with North American Plate. Black rectangle is the area of research and yellow star is Anchorage (modified from Haeussler et al., 2000)

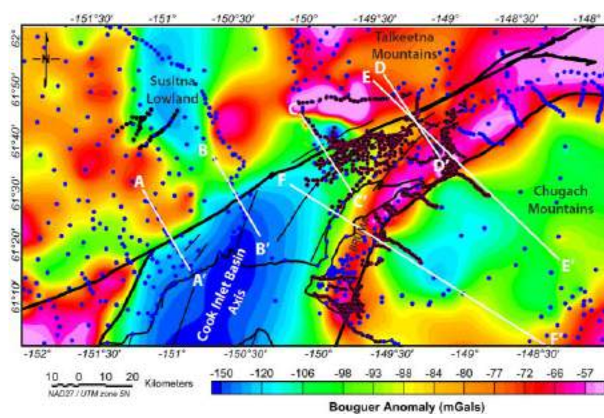

Figure 2: A 1000 m grid Bouguer anomaly map. White lines A-A’, B-B’, C-C’, and D-D’ are locations for 2D models developed in this study. Line F-F’ and E-E’ are initial models from Mankhemthong et al., (2012). BRUMA= Border Range Ultramafic and Mafic Assemblages.

High-resolution spatial variation of stress drops illuminates shallow fault zone behavior in the 2008 Mogul earthquake swarm (Nevada)

Christine J. Ruhl[1,3], Rachel E. Abercrombie[2,3], Kenneth D. Smith[3]
1. Univ. of California, Berkeley, Berkeley, CA; 2. Boston University, Boston, MA; 3. Univ. of Nevada, Reno, Reno, NV

After approximately 2 months of swarm-like earthquakes in the Mogul neighborhood of west Reno, NV, seismicity rates and event magnitudes increased over several days culminating in an M_w 4.9 (M_L 5.1) dextral strike-slip earthquake on 26 April 2008. Rapid temporary instrument deployment directly above the sequence provides high-resolution coverage of microseismicity, enabling a detailed analysis of swarm behavior and faulting geometry. Double-difference waveform-based relocations reveal an internally clustered sequence in which foreshocks evolved on multiple structures surrounding the eventual main shock rupture [Ruhl et al., 2016, JGR]. Seismicity also defines a fault-fracture mesh and detailed fault structure from approximately 2–6 km depth on the previously unknown Mogul fault that may be an evolving incipient strike-slip fault zone in a zone of distributed deformation (the Walker Lane). The seismicity volume expands before the main shock, consistent with pore pressure diffusion related to fluids [Ruhl et al., 2016, JGR]. We estimate well-constrained, independent P and S wave corner frequencies and stress drop for 148 earthquakes ($2.2 \geq M_L \leq 5.1$) using EGF-derived spectral ratios. Resulting stress drops vary over two orders of magnitude and enable investigation of stress drop variation within a well-recorded sequence. Along the mainshock fault plane, high stress drop foreshocks cluster around an absence of seismicity which is only ruptured by low stress drop foreshocks and is not re-ruptured in the aftershock period. The area of the "seismicity void" is approximately equal to the expected rupture dimension for the mainshock earthquake, which also has a relatively high stress drop. These observations are best explained by a difference in rheology along the fault plane where a velocity-weakening region of the fault (i.e., an asperity) is surrounded by velocity-strengthening (e.g., creeping) regions [Chen and Lapusta, 2009, JGR]. As stress accumulates in the seismic cycle, aseismic slip occurs in the transitional areas on the periphery of the asperity causing numerous high-stress drop foreshocks just prior to the high-stress drop rupture of the asperity (i.e., the mainshock). The unprecedented detail achieved for these shallow, moderate magnitude earthquakes confirms that stress drop, when measured precisely, is a valuable observation of physically-meaningful fault zone properties and earthquake behavior.

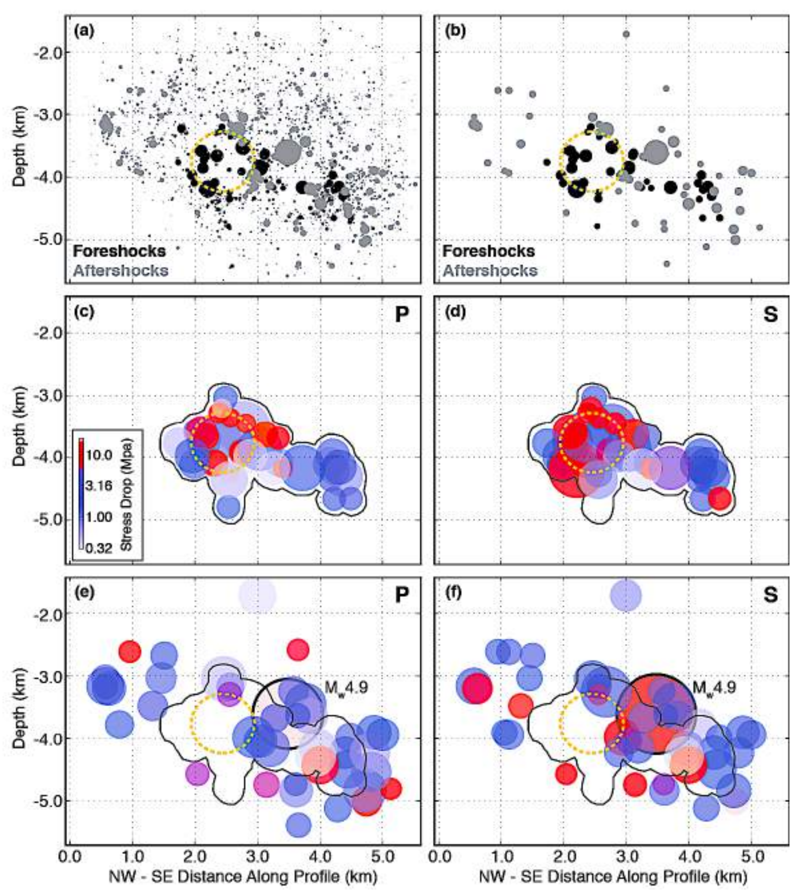

cGPS and Borehole Strainmeter Measurements of the September 2013 Episodic Tremor and Slip Event

Nicholas Benz[1], Noel Bartlow[1], Evelyn Roeloffs[2]
[1] University of Missouri, [2] USGS Cascades Volcano Observatory

The addition of borehole strainmeter (BSM) to cGPS time series inversions has the potential to yield more precise slip distributions at the subduction interface during episodic tremor and slip (ETS) events in the Cascadia subduction zone. Traditionally very noisy BSM data has not been easy to interpret until recently; developments in processing noise, re-orientation of strain components, removal of tidal, hydrologic, and atmospheric signals have made this additional source of data viable. The major advantage with BSMs are their sensitivity to spatial derivatives in slip compared to cGPS data, which is valuable for investigating the ETS nucleation process and stress changes on the plate interface due to ETS. Here we simultaneously invert PBO GPS time series data together with processed BSM data with the Network Inversion Filter (NIF) for slip and slip rate as a function of time during the October 2013 northern Cascadia ETS. This event was selected for its proximity to a set of four BSMs located along a downdip transect lying along the northern coastline of the Olympic Peninsula. The 2013 ETS is also a particularly complex event, with multiple nucleation sites. We also calculate stress changes on the plate interface during this ETS event, and compare inversion results with and without including BSM data to highlight the role of BSM data in constraining slip and stress.

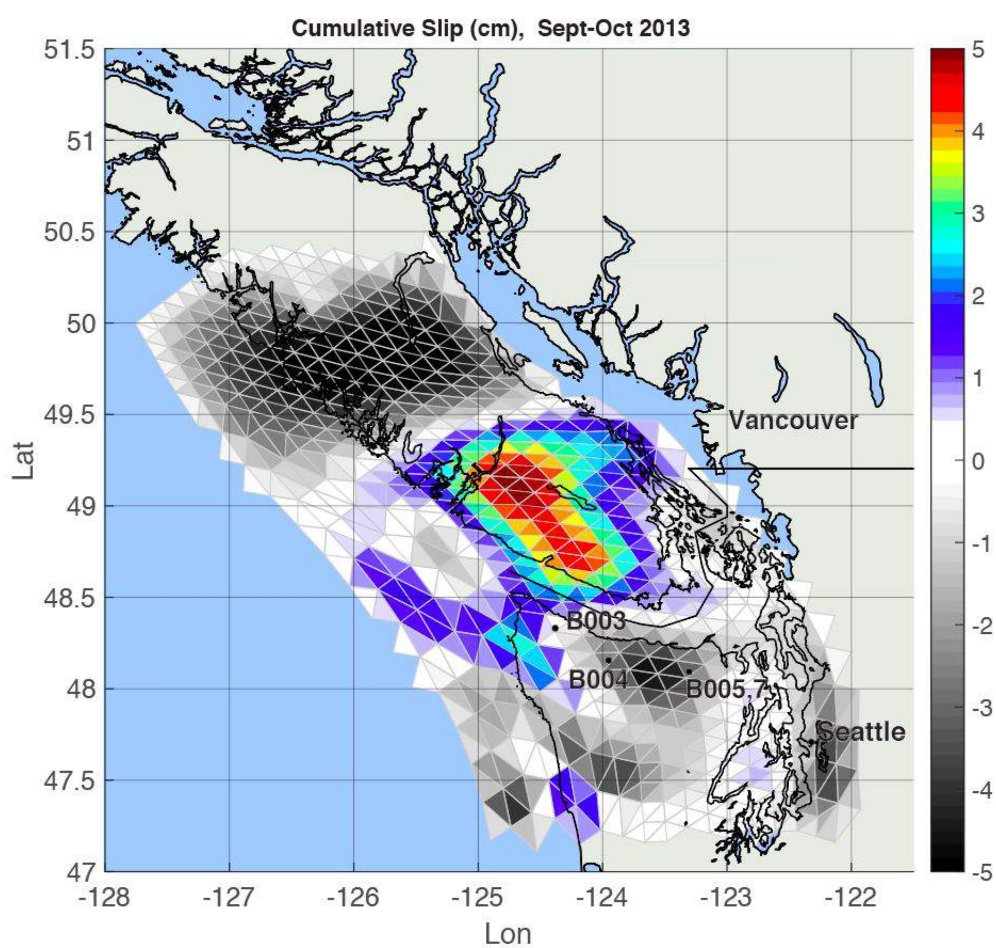

Uncertainty in structural boundaries and scale from transdimensional tomography with USArray

Scott Burdick, Vedran Lekic, and Tolulope Olugboji
University of Maryland, College Park

The assembly of the North America continent left behind a lithosphere characterized by distinct terranes with hidden boundaries at depth. In the mantle beneath the continent, the remnants of the seafloor that was subducted as the terranes came together give evidence of the timing and geometry of assembly. Thanks to the USArray Transportable Array (TA), it is now possible to investigate the seismic properties of these structures with ever greater clarity. The reliable, high-quality data from the TA have enabled robust measurements of traveltimes and ambient noise-derived Green's functions for use in tomographic inversions. Taking advantage of the broad baseline and uniform density, transdimensional tomography with data from the TA allows us to decouple the effects of irregular data coverage from estimates of structural scale and to investigate sharp boundaries in seismic properties.

Transdimensional tomography based on Bayesian inference searches the model space with a reversible-jump Markov chain Monte Carlo algorithm in order to create an ensemble of velocity models that explain the data. Within the search, the number, shape, and location of the parameters defining the model is allowed to vary in addition to their velocity value. We choose to parametrize our models with Voronoi cells because of they can define arbitrarily small volumes and preserve sharp boundaries. From the ensemble, we can derive standard statistics of the seismic properties, including the mean velocity and model covariance, but it is also possible to recover information about the boundaries and scale of structure. Careful interrogation of the ensemble can reveal the uncertainty in the location of the boundaries between parameters and determine the probability that a point in space belongs in one domain or another.

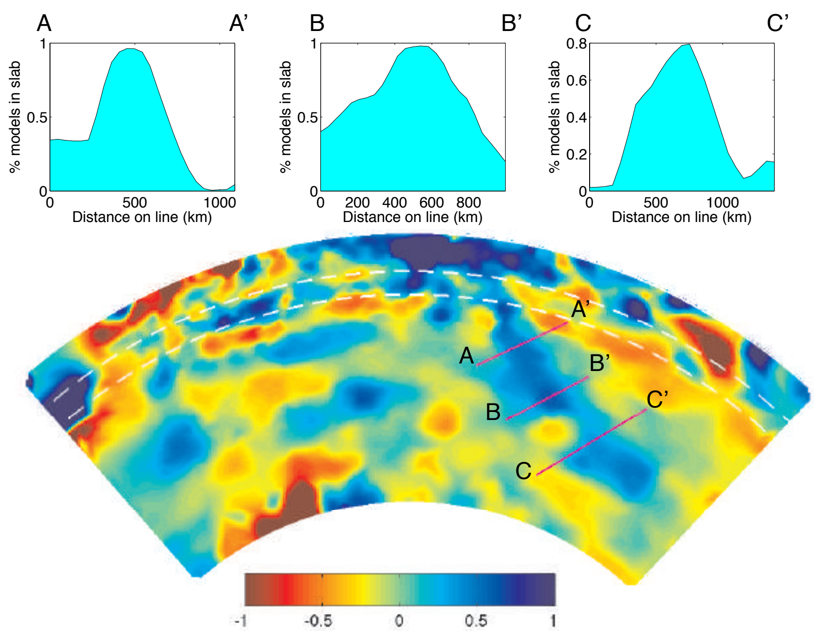

We present transdimensional body and surface-wave tomography using TA data, and interpret the resulting ensembles for the scale and geometry of structure in the crust and mantle and their uncertainty. Surface wave tomography (*Olugboji et al. submitted*) with ambient noise crosscorrelations reveals the structure of the continental lithosphere and the tectonic boundaries therein. Body wave traveltime tomography using TA and global data (*Burdick & Lekic, 2017*) is analyzed to determine the difference in the scale of heterogeneity between the tectonically active western margin and the stable eastern part of the continent, and to provide estimates of uncertainty in volume and geometry of the slabs beneath North America.

Using Receiver Function Analysis to Place Constraints on Depth Dependent Seismic Anisotropy within the Basin and Range Province

By: Heather A. Ford and Em Schnorr

Shear wave splitting analysis, combined with the uniform and relatively dense station spacing of Earthscope, has illuminated a number of tectonic and/or dynamic features that go beyond the notion of deformation related to either plate motion oriented shear or simple asthenospheric flow. One such region where this is true is within the Basin and Range, where a "swirl", characterized using shear wave splitting, has been long observed, and more fully characterized during the passage of Transportable Array. While dynamic arguments related to subduction-related flow (Zandt and Humphreys, 2008) and/or dripping lithosphere (West et al., 2009) have been made, evidence from ambient noise tomography (Lin et al., 2011) indicates that multiple layers of anisotropy within the crust and upper mantle are present and may explain shear wave splitting observations. With these earlier observations in mind, we have targeted the Basin and Range for a more careful analysis of depth dependent anisotropy using receiver function analysis.

In our study we utilize information on both the radial and transverse components from six long-running stations- BMN, ELK, NEE, MNV, TPNV and WVOR, in order to place constraints on the location of anisotropic boundaries. Our initial results indicate a coherent positive phase, interpreted to be the Moho, at 3.7-4.2 seconds for stations NEE, BMN, ELK, MNV, and WVOR. At TPNV, the Moho exhibits laterally complex behavior with a phase arrival at 4.3 to 5.4 seconds. Our results also indicate the presence of significant energy on the transverse component at delay times of 2.8-5.2 seconds at stations WVOR, TPNV, and MNV. Within this time window, a polarity flip on the transverse component, indicative of dipping structure and/or anisotropy, occurs at approximately 90° back azimuth at each of the three stations. We have completed preliminary forward modeling at stations WVOR and MNV and are able to rule out dipping isotropic structure as a possible explanation for the observed features. Instead, our preliminary models are best fit by two layers of anisotropy (4 km and 8 km thick, respectively) in the lower crust, just above the Moho. The presence of anisotropy in the lower crust, coupled with other lines of evidence, suggests the presence of lower crustal flow. Future work will focus on better constraining the origin and geometry of anisotropy in order to place the results in context of our current understanding of the deformation history of the Basin and Range.

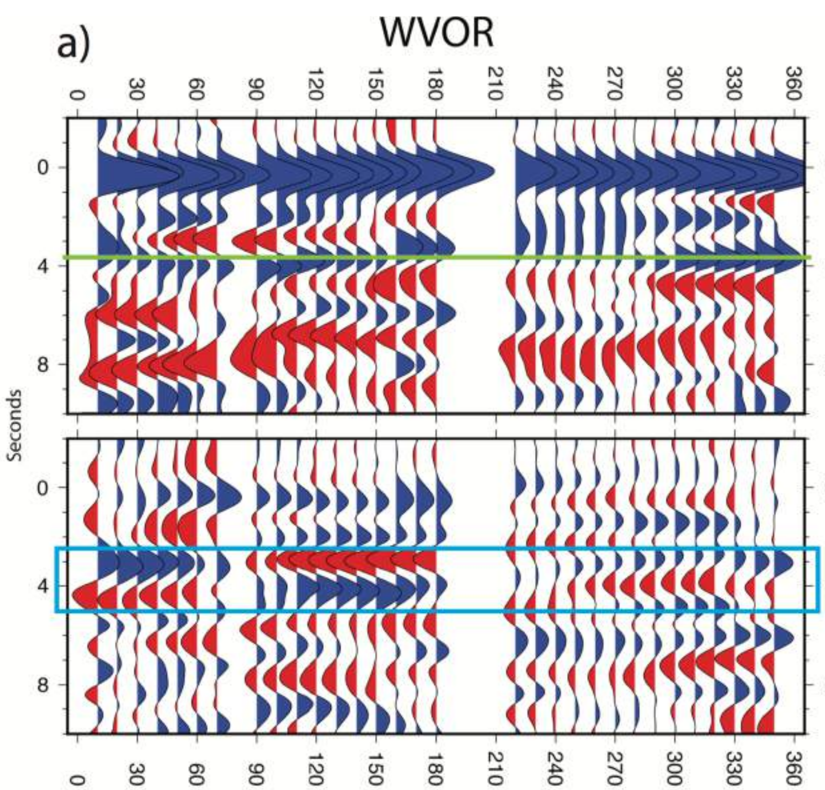

Radial (**top**) and transverse (**bottom**) component receiver functions for station WVOR. Green line on radial component indicates Moho arrival, picked from single station stack. Blue box on transverse component highlights polarity flip at 3.0 and 4.5 seconds.

Tracking the Onset of Induced Seismicity in Northeastern Pennsylvania

Martone, P., Nikulin, A., Pietras, J.

The link between induced seismicity and injection of hydraulic fracturing wastewater has largely been accepted and corroborated through case studies in Colorado, Arkansas, Texas, and Oklahoma. Increasing pore pressure and decreasing effective normal stress causes the shear stress to surpass the critical point inducing fault failure and releasing seismic energy. To date, induced seismicity has largely impacted hydrocarbon-producing regions in the Central United States, while the seismic response in Eastern states, like Pennsylvania, has been relatively muted. In recent years, Pennsylvania exponentially increased hydrocarbon production from the Marcellus and Utica Shales and our preliminary results indicate that this activity has triggered an onset of induced seismicity in areas of the state where no previous seismic activity was reported. While the seismicity in Western Pennsylvania has been attributed to wastewater injection, three recent earthquakes in Northeastern Pennsylvania directly correlate to hydraulic fracturing activity. We present signal analysis results of recorded waveforms of the three identified events and results of a high-precision relocation effort aimed at constraining the horizontal and vertical error in hypocenter position. We show that at least one event is positioned directly along the wellbore track of an active well and correlate its timing to the hydraulic fracturing schedule. Our preliminary results show that in the absence of wastewater disposal in this area, it is possible to confidently make the connection between the hydraulic fracturing process and induced seismicity. Future work entails additional waveform analysis, improving the regional velocity model, and correlating hydraulic fracturing parameters to earthquake hypocenter location, rupture duration, and magnitude.

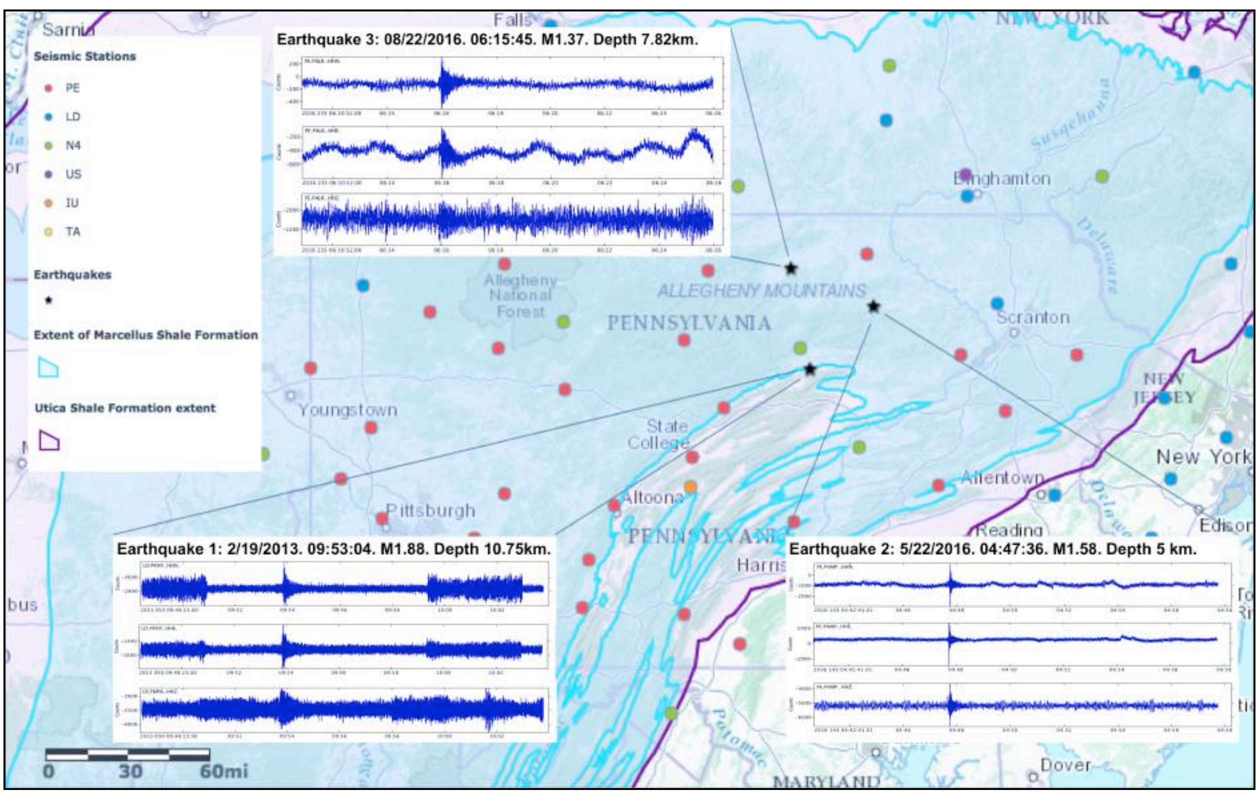

Figure 1: Map of Pennsylvania and neighboring states with stars indicating locations of the three seismic events of interest. Circles represent seismic stations, color-coded by the seismic network they are associated with. Shaded regions reflect extents of Marcellus and Utica Shale Formations. Insets are waveforms from three component seismic stations that recorded each event.

Measuring Aseismic Slip through Characteristically Repeating Earthquakes at the Mendocino Triple Junction

Kathryn Materna, Taka'aki Taira, Roland Bürgmann

The Mendocino Triple Junction (MTJ) lies at the transition point between the San Andreas fault system, the Mendocino Transform Fault, and the Cascadia Subduction Zone. Most of the active faults of the triple junction are located offshore, making it especially difficult to characterize aseismic creep. In this work, we study aseismic creep rates near the MTJ using characteristically repeating earthquakes (CREs) as indicators of creep rate. Using seismic data from 2008-2017, we identify CREs as recorded by an array of eight 100-Hz borehole seismometers deployed in the Cape Mendocino area. We apply a repeating earthquake detection criterion to the waveforms, and identify several dozen sequences of repeating earthquakes. The CRE data implies a creep rate of ~3 cm/yr on the downgoing extension of the Mendocino Transform Fault, consistent with estimates of coupling on other oceanic transform faults. We also find repeating earthquakes on the southern margin of the North American accretionary wedge. This project is an example of gains made through the Earthscope Plate Boundary Observatory program, which provided the seismic data required to characterize offshore aseismic creep.

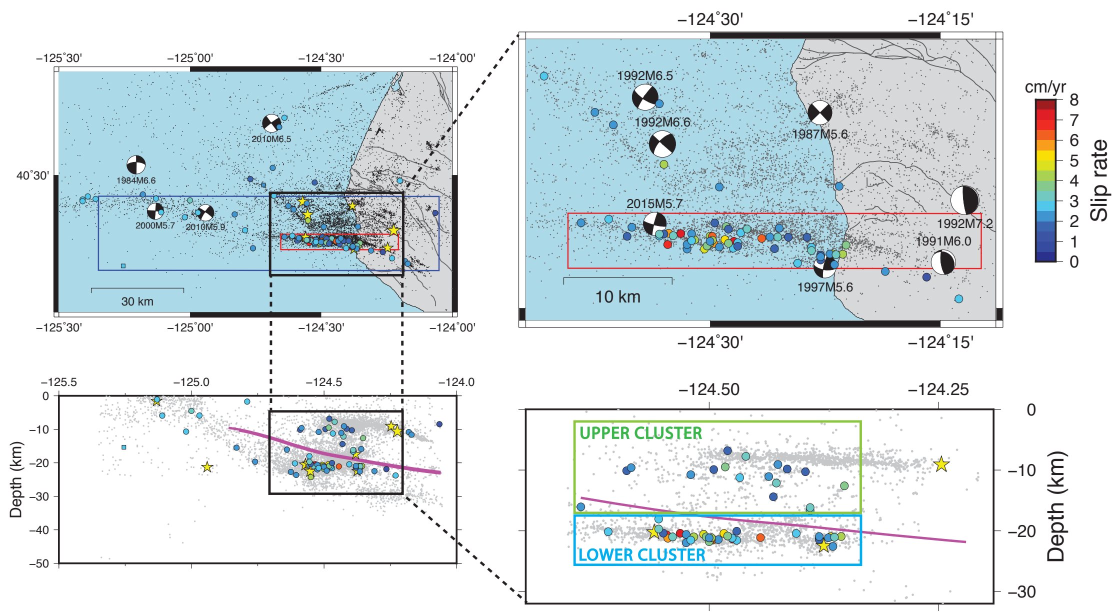

Joint Inversion of Continuous GPS and InSAR Data to Constrain the Spatiotemporal Evolution of Strain Release from the 2016 Kumamoto Earthquake Sequence: Implications for the Shallow Slip Deficit and the Role of Aseismic Slip

Milliner, C; Burgmann, R.; Teng, W.; Inbal, A.; Liang, C.; Fielding, E.

Estimates of coseismic slip at depth from finite-fault inversions provide important information about faulting mechanics, and empirical constraints for dynamic rupture simulations. However, due to the lack of spatially dense and temporally continuous geodetic data it has been difficult to assess reliably i) whether large ruptures typically exhibit a deficit of shallow slip (where lack of near-field surface data in finite-fault inversions has been shown to bias and significantly underestimate shallow slip, Xu et al. (2016), and ii) whether shallow slip primarily occurs co- or post-seismically as rapid afterslip. Here we investigate the spatiotemporal evolution of strain release during the 2016 Kumamoto sequence, Japan, that was composed of a prolonged foreshock sequence followed by a M_w 7.0 mainshock. We jointly invert for fault slip using Sentinel 1 and ALOS-2 InSAR timeseries and pixel-tracking, 170 continuous GPS stations that provide dense spatial and temporal coverage of surface motion, and optical image correlation results which capture details of the near-field surface deformation pattern. We filter the GPS data using principal component analysis which allows for detection of subtle ground motion, revealing a significant aseismic slip transient that preceded the mainshock. We find this spatiotemporal filtering approach helps significantly improve constraints on the magnitude and spatial distribution of slip at depth and gives better insight into the contribution of aseismic slip to the overall slip budget. We also present preliminary results using relocated seismicity and the network inversion filter of Bekaert et al. (2016 JGR) inverting GPS and InSAR, to further constrain the migrating pattern of aseismic strain release. Understanding whether ruptures exhibit a shallow slip deficit holds significance for how strain is released through the seismic cycle, and allows for generating realistic synthetic rupture simulations important for hazard analysis.

The power of higher-order cross-correlations (C^3) to image the Earth from the crust to the core

Zack Spica

Stanford University

The ambient noise correlation technique allows retrieving the Green's function between pairs of synchronous seismic sensors by correlating long time series of seismic noise (C^1). While the method is widely used to map the seismic velocity in the crust and upper mantle with surface waves, recent works highlighted the possibility to retrieve teleseismic body waves, offering a better sampling geometries to image the Earth's core. However, the method relies on the availability of synchronous networks, which considerably limits the ray-paths coverage and therefore the resolution of the resulting tomographic images.

My point is to show that performing higher-order correlations (C^3) makes it possible to bridge all the seismic networks in time and space, and therefore significantly enhance the resolving power of the ambient noise tomographies. I will discuss the feasibility and the potential of the method for Rayleigh waves retrieval, and present its first application to obtain a high-resolution tomographic image of Mexico and south US. In addition, I will show that the method can also be extended to retrieve teleseismic body waves such as reflections on the core mantle boundary. I will present a spatial analysis of the differential travel time of the ScS phase along the Meso America Subduction Experiment (MASE) array and discuss the strong influence of the shallow surface on such measurements.

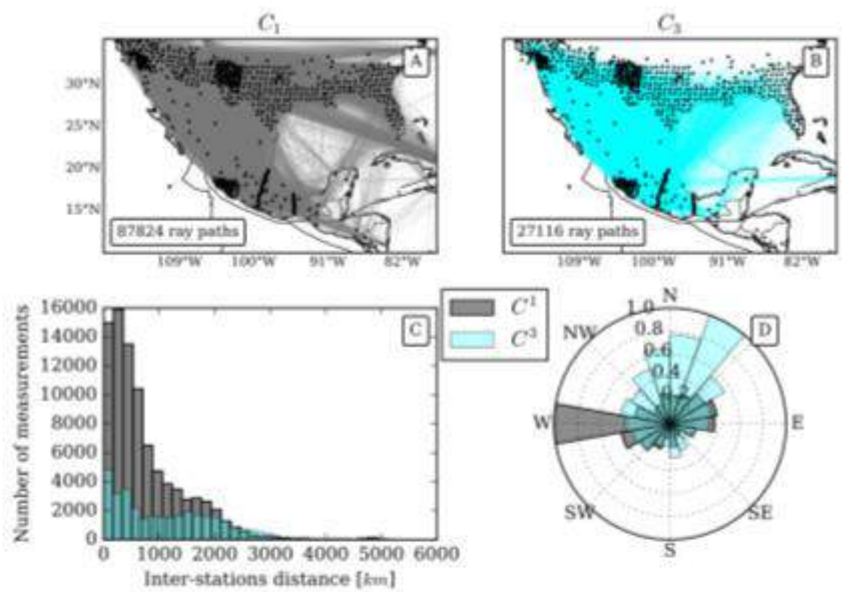

Earthquake Slip Distribution Inversion Using Tsunami Waves, Crustal Deformation Data and Tsunami Deposits with Ensemble Kalman Filter

Hui Tang, Department of Geosciences, Virginia Polytechnic Institute and State University

Population living close to coastlines is increasing, which creates higher risks due to coastal hazards, such as the tsunami. Earthquake-induced tsunami is one of the most dangerous hazards in the coastal zone worldwide. The generation of a tsunami by a megathrust earthquake is not fully understood yet. Tsunami wavefield is valuable for inferring the tsunamigenic earthquake slip distribution. Tsunami deposits are one of the concrete evidence in the geological record which we can apply for estimating paleo-earthquake displacement. Meanwhile, crustal deformation due to the earthquake can be observed by the GPS GEONET. Here we present a new inverse approach using the ensemble Kalman filter method (EnKF) to estimate slip distribution based on tsunami wave, the spatial distribution of tsunami deposits and seafloor crustal deformation data. While more computationally expensive, the EnKF approach potentially provides more accurate reconstructions for earthquake displacement. The method is tested on a 1D tsunami model derived from simulations of the 2011 Tohoku earthquake. The results from the EnKF method will be compared to the results from Gusman et al. 2012.

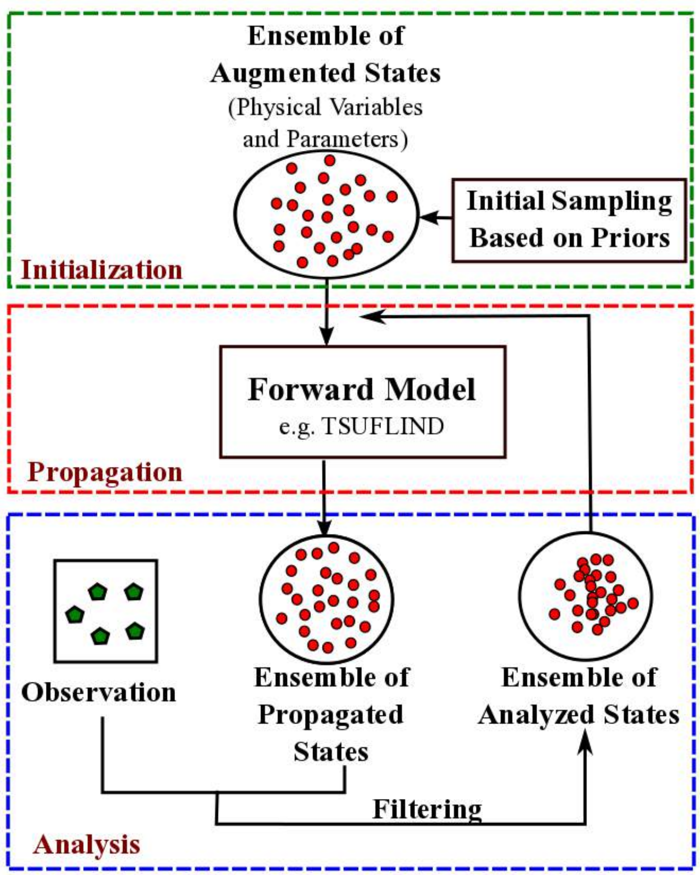

Reactivation of Taconic Thrust Faults in the Late Devonian Acadian Orogenic Front

Laura Webb[1], Keith Klepeis[1], Jonathan Kim[2], and Patrick Sullivan[1]
[1]Department of Geology, University of Vermont, Burlington, Vermont, USA
[2]Vermont Geological Survey, Montpelier, Vermont, USA

The northeastern Appalachians were affected by four major Paleozoic orogenies (Taconian, Salinian, Acadian, and Alleghenian). The reactivation of pre-existing structural features is a natural consequence of superposed deformations. The Acadian Orogeny is a major Late Silurian–Devonian orogenic event that affected much of eastern North America. While there is still debate regarding tectonic drivers (e.g. collision of Avalonia and/or the Meguma terrane with Laurentia vs. Andean-type flat-slab subduction), there is general agreement regarding growth of the orogen in New England in association with a NW-migrating orogenic front that eventually overrode the Taconic-modified Laurentian margin. The Acadian orogeny in Vermont is largely associated with metamorphism, folding, and syntectonic magmatism in the Connecticut Valley Trough. While previous workers have proposed multiple slip events on Taconic thrust faults, including probable Acadian slip, radiometric data elucidating the timing of reactivation have been elusive. This study presents integrated $^{40}Ar/^{39}Ar$ geochronologic, field and (micro)structural data that provide new insight into the distribution and timing of Acadian deformation in NW Vermont (Fig. 1). Results from the Arrowhead and Hinesburg thrust fault zones, including a newly discovered pseudotachylyte locality, support Late Devonian reactivation of Taconic (Ordovician) thrust faults. These data demonstrate that deformation in the mapped western-most limit of the Acadian orogenic front in New England included seismogenic faulting on pre-existing low-angle thrust faults. The study areas include popular destinations for university and professional field trips with foci ranging from structural geology and tectonic processes to the role of bedrock geology in water resources. The new findings present additional thematic opportunities for the discussion of tectonic inheritance in orogenesis, the ability to discern and date reactivation events, and the formation and preservation of pseudotachylyte.

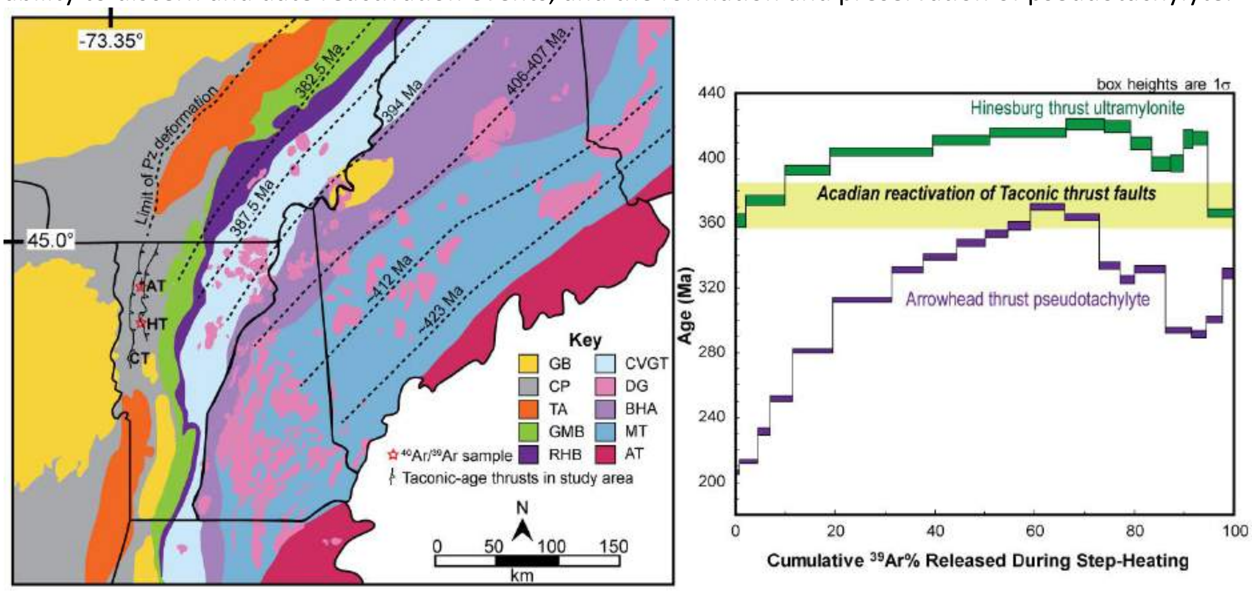

Figure 1. Study area shown in context of regional geologic provinces and $^{40}Ar/^{39}Ar$ apparent age spectra from noted samples. GB-Grenvillian Basement; CP-Carbonate Platform; TA-Taconic Allochthon; GMB-Green Mountain Belt; RHB-Rowe-Hawley Belt; CVGT-Connecticut Valley Gaspé Trough; BHA-Bronson Hill Anticlinorium; MT-Merrimack Trough; AT-Avalon Terrane; CT-Champlain thrust; AT-Arrowhead thrust; HT-Hinesburg thrust. DG-Devonian-aged granitic plutons. Dashed lines are timing and position of the Acadian orogenic front are from Bradley et al. (2000).

Reference: Bradley, D. C., Tucker, R. D., Lux, D. R., Harris, A. G., & McGregor, D. C. (2000). Migration of the Acadian Orogen and foreland basin across the Northern Appalachians of Maine and adjacent areas (No. 1624, pp. 0-55). US Geological Survey.

Identifying Moho depths and velocity anomalies in the uppermost mantle of the Mississippi Embayment from Pn tomography study

Urbi Basu (ubasu@memphis.edu) , University of Memphis, TN, USA
Christine Powell, University of Memphis, TN, USA

I will discuss the results of Pn tomography study using the NELE (Northern Embayment Lithosphere Experiment) and TA (Transportable Array) station data to obtain the depth and lateral variations of the Mohorovicic discontinuity and the location, shape of the P and S wave velocity anomalies at uppermost mantle depths. The New Madrid Seismic Zone (NMSZ), part of the Mississippi Embayment, lies in the NE-SW trending Reelfoot rift and is one of the most studied intraplate earthquake zones in the world. It poses the highest seismic hazard risk in the central United Sates. The main objective of this research is to determine the depth and orientation of seismic anomalies in the crust and uppermost part of the mantle under NMSZ in the northern Mississippi Embayment. Prior studies indicate the presence of velocity anomalies beneath the NMSZ that may contribute to the active seismicity. The cause and origin of these velocity anomalies is still under debate. Also, the NMSZ is unique from other mid-continent rifts with the presence of a prominent, SW dipping low P- and S-wave velocity upper mantle anomaly.

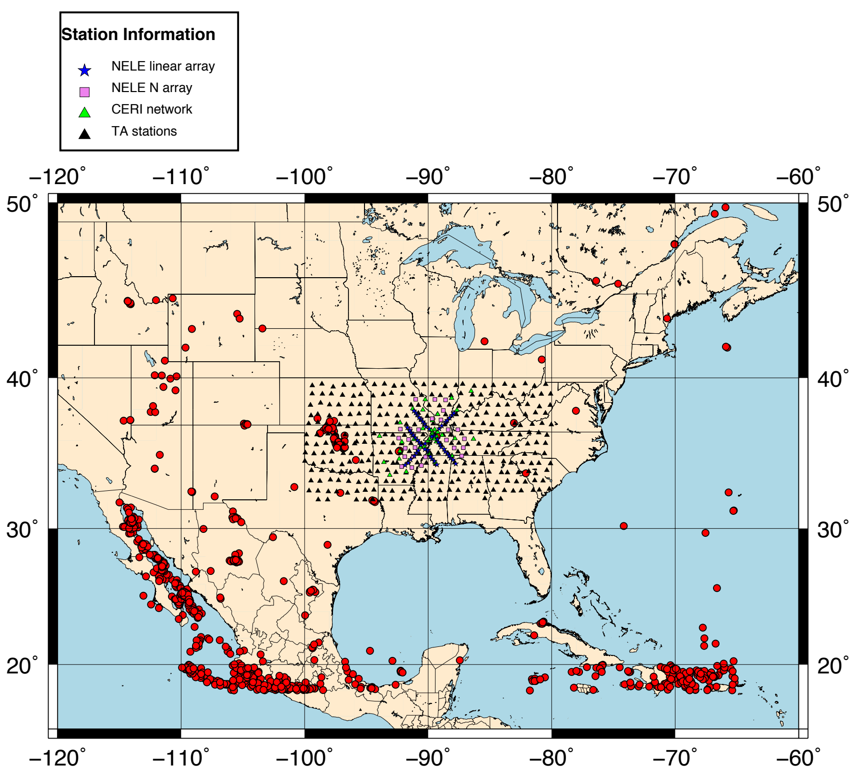

Fig 1.: Earthquake distribution (red circles) and recording stations in the study area

Characterizing seismic anisotropy in the Chester gneiss dome, Vermont: Moving from red and blue to rock type and mineralogy

Sarah J. Brownlee[1], Brittany Watling[1], and Jasneel Mahal[1]
1. Wayne State University, Department of Geology, Detroit, MI 48201

The continental crust is the window through which we view the deep Earth. The different expressions of continental crust in seismic data are thus critical to our understanding of the crust, and the deep Earth as well. Seismic anisotropy in the crust is complex, and has multiple causes, making its interpretation difficult. A basic requirement for interpretation of crustal anisotropy is that the elasticity of crustal rocks is well characterized, including the full anisotropic elastic tensor.

This study is focused on characterizing the elasticity of rocks from the Chester gneiss dome in southeastern Vermont, USA. Chester dome is composed of gneisses and schists deformed at moderate pressure and temperature conditions corresponding to depths in the mid- to lower crust. We have collected ~75 oriented samples from throughout Chester dome covering a wide range in composition and deformation texture from dominantly quartzofeldspathic gneiss with weak lineation to amphibolite with very strong lineation. The goal is to develop a framework relating rock type and mineralogy to particular properties of the intrinsic elastic tensor, including magnitude of anisotropy and the tensor symmetry components, in order to improve the inverse path from seismic observations to rock type and composition. We use electron backscatter diffraction (EBSD) to measure the crystallographic preferred orientation (CPO) of the constituent minerals in oriented thin sections, and then calculate an aggregate elastic tensor for each sample. Results from 20 samples thus far indicate trends in magnitude and symmetry of anisotropy that correlate with mineralogy and rock type, with gneisses showing lower anisotropy and higher orthorhombic symmetry components than schists. Mica content correlates with both magnitude of anisotropy and the hexagonal symmetry component, and hornblende correlates with the orthorhombic symmetry component when significant hornblende is present. In addition to characterizing the elastic tensors of our samples, we model how these rocks should appear in seismic data, with particular attention to receiver functions and the common tensor parameter, eta.

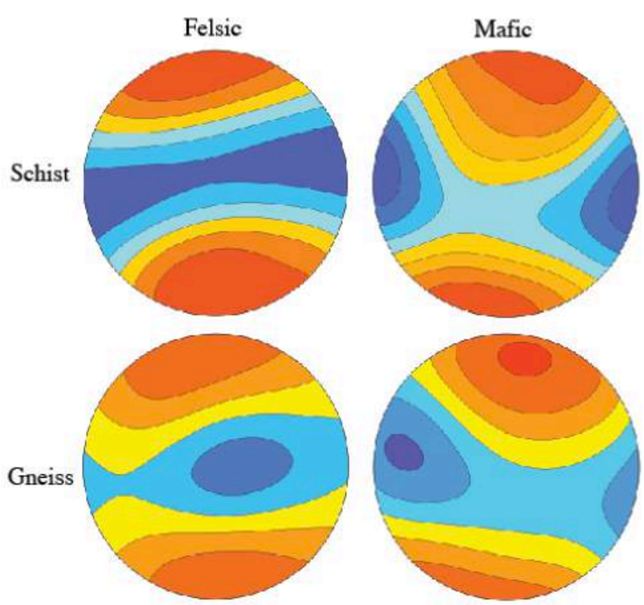

Figure 1. Schists and gneisses from Chester dome contain different symmetry components that are related to the rock type and mineralogy. In general, schists are more anisotropic and more hexagonal, and gneisses are more orthorhombic. More mafic compositions tend to be more orthorhombic, and their hexagonal component tensor is closer to elliptical than the felsic compositions, which become more non-elliptical with increasing anisotropy.

Lithospheric discontinuities beneath the US Midcontinent – signatures of Proterozoic terrane accretion and a failed rift

Chen Chen[1], Hersh Gilbert[1†], Karen M. Fischer[2], Christopher L. Andronicos[1], Gary L. Pavlis[3], Michael W. Hamburger[3], Stephen Marshak[4], Timothy Larson[5], Xiaotao Yang[6]

1. Department of Earth, Atmospheric, and Planetary Sciences, Purdue University, West Lafayette, IN 47907
2. Department of Geological Sciences, Brown University, Providence, RI 02912
3. Department of Geological Sciences, Indiana University, Bloomington, IN 47405
4. School of Earth, Society, and Environment, University of Illinois at Urbana-Champaign, Urbana, IL 61801
5. Illinois State Geological Survey, Champaign, IL 61820
6. Department of Geosciences, University of Massachusetts, Amherst, MA 01003

† Current address: Department of Geoscience, University of Calgary, Alberta, T2N 1N4, Canada

Seismic discontinuities in the upper mantle between the Moho and the inferred lithosphere-asthenosphere boundary (LAB) are referred to as mid-lithospheric discontinuities (MLD) and have been ascribed to a variety of phenomena that are critical to understanding lithospheric growth and evolution. In this study, we used S-to-P converted waves recorded by the USArray Transportable Array and the OIINK (Ozarks-Illinois-Indiana-Kentucky) Flexible Array in the central US to investigate lithospheric structure. This area, a portion of North America's cratonic platform, represents an ideal region to explore the record of terrane accretion on continental formation and the influence of subsequent rifting on lithospheric structure. The 3D common conversion point (CCP) volume produced by stacking of back projected Sp receiver functions reveals a general absence of negative Sp phases at the depths of the LAB across much of the central US, which suggests a gradual velocity decrease between the lithosphere and asthenosphere. Within the lithosphere, the CCP stacks display a negative arrival at depths between 65 km and 125 km that we interpret to result from the top of layer containing crystallized melts or otherwise chemically modified lithosphere that is enriched in water and/or hydrous minerals. The depth and amplitude of negative MLD phases vary a great deal both within and between the physiographic provinces of the central US. Double, or overlapping, MLDs can be seen along the isotopically defined Nd-line. We hypothesize these multiple arrivals to be a manifestation of stacked or imbricated lithospheric blocks that formed during convergence and accretion of lithosphere less than 1.55 Ga onto lithosphere older than 1.55 Ga. A prominent negative Sp phase at 80 km depth can be clearly identified within the Reelfoot Rift. Based on the coincidence of this negative arrival with the top of a zone of low shear-wave velocities, we interpret this arrival to mark the seismic LAB at unusually shallow depth; it corresponds to the top of a region of mechanically and chemically rejuvenated mantle that likely formed during late Precambrian and early-Cambrian rifting and/or the passage of a Cretaceous mantle plume.

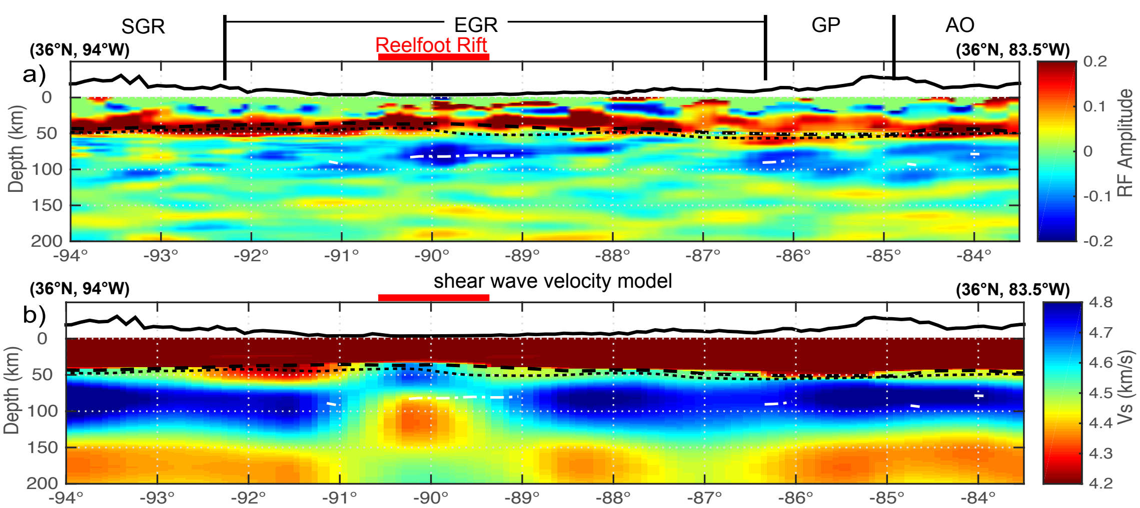

a) Cross-section through mean of bootstrapped CCP stack. SGR: Southern Granite Rhyolite Province; EGR: Eastern Granite Rhyolite Province;GP: Grenville Province; AO: Apalachian Orogen. b) Shear wave velocity model for comparison. Thick black line marks topography, with 50x vertical exaggeration. Dashed and dotted black lines mark Moho from two Ps receiver function studies. White dashed line highlights auto picked negative phase that has strength greater than 10% of the parent phase.

Detailed Study of Seismic Anisotropy in the Upper Mantle of Eastern North America

Xiaoran Chen, Yiran Li, Vadim Levin
Rutgers University, New Brunswick

We collected observations of core refracted shear waves on a 1300 km long array crossing the eastern part of the North American continent from James Bay to the Fundy Basin with an instrumental spacing of around 50 km. The combined array forms a linear transect across main tectonic units of eastern North America: Archean Superior Province, Proterozoic Grenville Province and Paleozoic Appalachian Orogen and it crosses two major collisional tectonic boundaries (Appalachian Front and Grenville Front) and a major shear zone (Norumbega Fault Zone) in northeastern Maine. We combined data from 62 stations, including sites of the Earthscope Transportable Array, Canadian and US permanent observatories, and Earthscope FlexArray QMIII. For this project, we chose observations from 13 earthquakes with magnitudes over 6.8 from 2013 to 2015 that were observed over the entire length of our array.

We measured splitting of SKS and/or SKKS phases using SplitLab software. We made 569 measurements in total, obtaining 7 measurements per station on average. 164 measurements were designated as NULL (no observable splitting). By analyzing the non-NULL results obtained, we found evidence for shear wave splitting at all stations. Fast polarizations are predominantly NE-SW, which is consistent with numerous past studies in the same region (as shown in Figure 1). Within individual event, fast polarizations along the array are consistent, however they vary from event to event.

We find that splitting delay times for individual events increase systematically from around 0.3 s in the Superior Province to over 1.5 s in the Appalachians. This implies that smaller delays are observed over thicker older lithosphere. Furthermore, we found that in observations from the NE the change in delays is abrupt, and takes place near the Appalachian Front. In observations from the NW the change is more gradual, with a possible shift in delay values close to the eastern edge of faster cratonic lithosphere at depth.

Thus, in the eastern part of the North American continent, fast polarization of split core-refracted shear waves varies depending on the direction of wave propagation (as shown in Figure 2), while the delay varies laterally, and appears to reflect the age of the lithosphere.

Directional dependence of fast polarization cannot be explained by a single layer of anisotropy in the upper mantle, and are consistent with the previously proposed notion of layered anisotropy in the upper mantle of the North American continent.

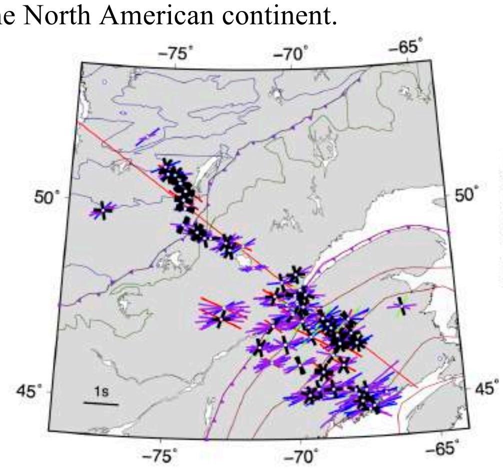

Figure 1

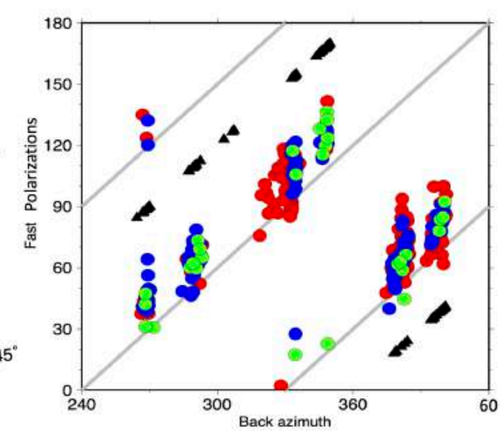

Figure 2

Figure 1 shows splitting results from all 13 earthquakes plotted at the locations of the stations we used. Blue, red, green, purple sticks stand for splitting results from earthquakes with back azimuths 0 ~ 90°, 90° ~ 180°, 180° ~ 270°, 270° ~ 360°. Directions of the sticks represent fast polarizations. Lengths are proportional to delay times. Black sticks stand for NULL measurements and are aligned along the azimuth of corresponding event and lengths are defined to be 0.5 s. Figure 2 shows the fast polarizations of all the splitting results along the back azimuths.

Long-period Rayleigh wave phase velocity tomography using USArray

Jordyn Cloud and Colleen Dalton, Brown University, Providence, RI 02906

Over its ten-year deployment across the continental U.S., the EarthScope USArray recorded the most robust seismic data set to date for North America. In this study, Rayleigh wave amplitudes and travel times have been measured in the period range 20-200 s for nearly 1000 global events over the time period 2009-2016. The measurements were obtained by cross-correlation of waveforms at nearby stations. The Helmholtz tomography method of Lin et al. (2011) is then applied to the measurements to determine high-resolution Rayleigh wave phase-velocity maps. Preliminary results show consistency at shorter periods with the results of previous studies. The new long-period maps represent an opportunity to resolve mantle structure at greater depths. Future work will be focused on using both surface-wave and body-wave amplitude measurements to image seismic attenuation beneath USArray. This study ultimately seeks to answer questions about how melt is distributed in the mantle, particularly in the tectonically active parts of the western U.S., including the Colorado Plateau and the Basin and Range area, and how the processes governing melt evolve across North America.

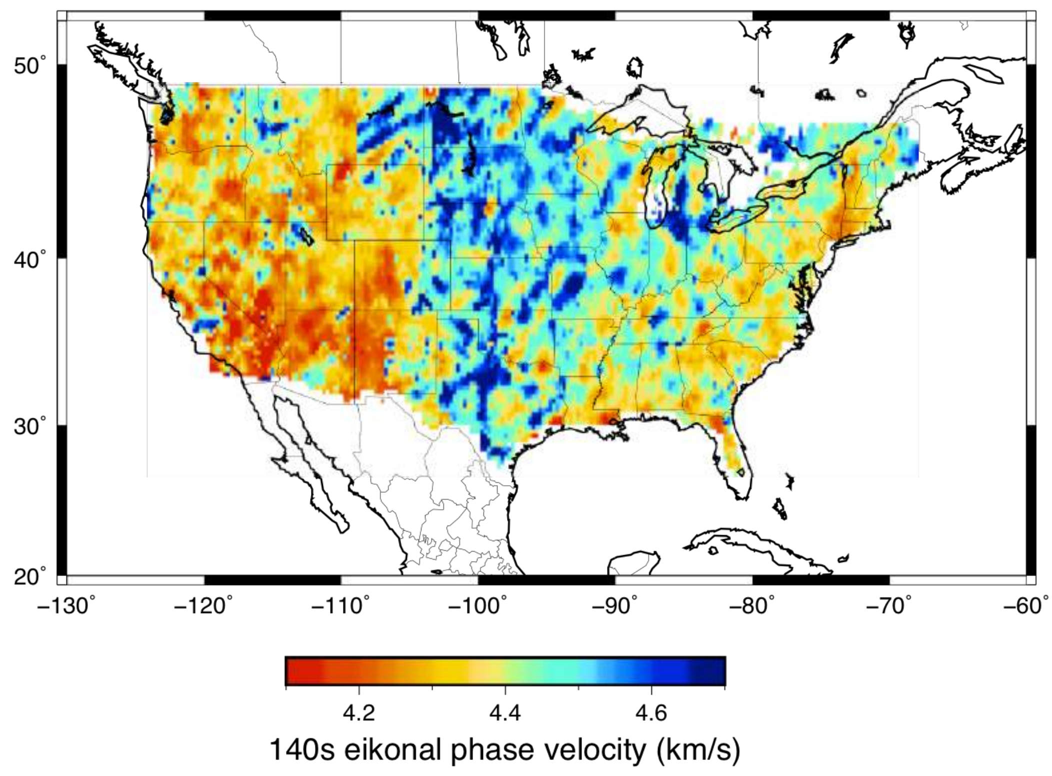

Figure 1. Apparent phase-velocity map for 140s period.

Constraining crustal structure using H-k-Vp stacking

The comprehensive coverage afforded by EarthScope USArray in the lower 48 states provides a unique opportunity to explore crustal variation across a range of tectonic environments and geologic ages. The thickness and average composition of the continental crust are related to its tectonic and geologic history. While crustal thickening or thinning indicate the deformation history, changes in average composition carry information on how crust was formed and reworked through different geologic processes.

The most common method of constraining the crustal structure is to calculate H-k stacks (Zhu and Kinamori 2000), which use arrival times of P-to-s converted seismic waves across the Moho together with waves reverberating within the crust. However, when H-k stacking is applied to regions covered with a thick sediment layer, reverberations mask the Moho P-to-s conversions making interpretation of the crustal structure difficult, if not impossible. Furthermore, H-k stacks are constructed for an assumed average crustal P or S velocity. Therefore, inferences of crustal composition must rely on the ratio of P to S wave velocity alone (Vp/Vs ratio or k), and crustal thickness estimates may be biased. For example, in regions where the assumed Vp is higher than the actual Vp, the crustal thickness will be overestimated and the Vp/Vs ratio will be underestimated.

We overcome both limitations of standard H-k analysis by using complementary data: S-to-p conversions and SsPmp phases. Because sedimentary S-to-p reverberations do not contaminate the direct Moho-related S-to-p conversion, we incorporate S-to-p arrival in our H-k stacks. In addition, the S-p arrival time provides information on P-wave velocity in the crust. We show that doing so is useful in identifying crustal thickness in regions where P-to-s H-k stacks are not sufficient. The large amplitude post-critical S-to-p reflection at the Moho (SsPmp phase) has been used to obtain crustal thickness estimates (see Parker E.H. et al. 2013, Yu et al 2013) in regions where an assumed average Vp is known to be inaccurate. This is because the relative timing of the SsPmp phase depends on Vp but not Vs. We show that we can combine Ps RFs, Sp arrivals and SsPmp waveforms to construct 3-parameter H-k-Vp stacks. These triple stacks allow us to pinpoint Vp and average crustal thickness beneath a station, even in areas with thick sedimentary cover (Figure 1)

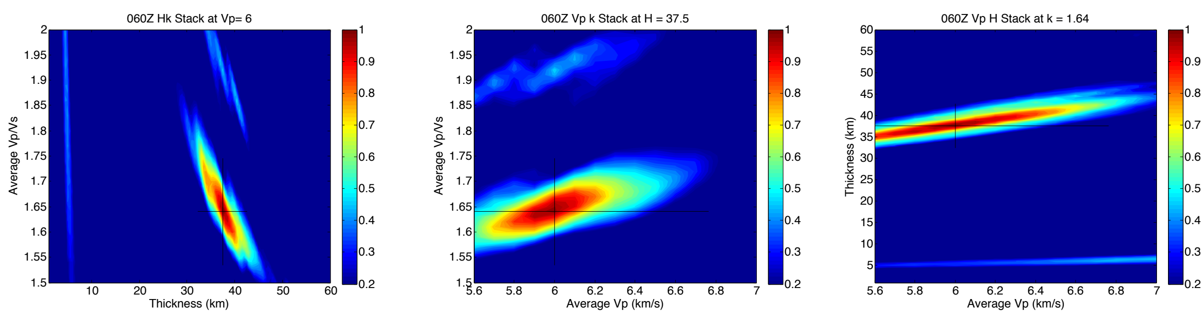

Figure 1- Cross sections through the 3-D H-k-Vp triple stack at the maximum for station 060Z in FL. Station 060Z lies on thick sediment (~4km) where a stacking maximum is not clear from the Ps Hk stacks alone. By calculating the stacks including the Sp and SsPmp phase a clear maximum is found for the H-k-Vp triple stacks at a Vp = 6, H=37.5, and k = 1.64. The black crosshairs represent error evaluated including cross-terms at the maximum.

Bayesian Joint Inversion of Receiver Functions and Surface Wave Velocity across the EarthScope Transportable Array

Chao Gao, Vedran Lekic

When constraining the structure of the Earth's continental lithosphere, multiple seismic observables are often combined due to their complementary sensitivities. The transdimensional Bayesian (TB) approach in seismic inversion allows model parameter uncertainties and trade-offs to be quantified with few assumptions. TB sampling yields an adaptive parameterization that enables simultaneous inversion for multiple types of model parameters (Vp, Vs, density, radial anisotropy), without the need for strong prior information or regularization.

We use a reversible jump Markov chain Monte Carlo (rjMcMC) algorithm to jointly invert surface wave dispersion (SWD) and receiver functions (RFs) beneath the Transportable Array for profiles of shear velocity (Vs), compressional velocity (Vp), and density (ρ). We validate our method on synthetic data. For TB inversion of multi-parameter problems, we propose two schemes of parameterization with one scheme imposing a stronger assumption on model parameters. Several factors including parameter of interest, data sensitivity, and prior information could affect the optimal choice under different circumstances. We then discuss three sources of uncertainty: limitation of data sensitivity, assumed scaling among parameters, choice of parameterizations, including both the number of parameters and attached/unattached parameterizations for multi-parameter problems.

Due to the non-linearity and non-uniqueness of the inverse problem of receiver functions, the convergence of rjMcMC for receiver functions can be time consuming and unstable. To address this issue, we implement a progressive inclusion scheme for the joint inversion of surface wave data and receiver functions. We start the inversion with low-pass filtered receiver function, and progressively include higher frequencies in the receiver function after certain number of iterations. We apply this scheme to the SWD and RFs measured from TA array, and show that the convergence of rjMcMC for joint inversion is significantly improved. Furthermore, the ensemble inversion results at different stages reveal seismic structures with different scales of details. Our results retrieve a low-velocity zone in the lower crust at varies locations; we show that such features could be an artificial effect from the sediment reverberation signals.

Crustal Structure of the Carolina Terrane, Eastern USA

Wenbin Guo, Shuai Zhao, Walter D. Mooney
U.S Geological Survey, Earthquake Science Center, Menlo Park, CA, USA

Rift initiation and evolution is a critically important research topic because of the seismic hazards associated with rifted lithosphere. These hazards can be significant because major population centers and critical facilities are located at rifted continental margins. The NSF-funded GeoPRISMS program has established an initiative to investigate the rifting of the eastern North American margin. One component of this initiative is a pair of onshore/offshore active-source wide-angle seismic profiles in eastern North Carolina and Virginia. The onshore portion of the data were acquired in June 2015 with the assistance of the NSF-funded PASSCAL Instrument Center. Here we report the interpretation of the crustal seismic velocity structure based on one of these onshore seismic profiles. This 230-km-long profile consists of 5 deep-borehole chemical explosions that were recorded by 708 portable Texan seismographs. The shot spacing between the two shots in the west is about 70 km, whereas the shot spacing is 30 km for the 3 shots to the east. The seismograph spacing is 320 m. The data include both P-wave and S-wave arrivals. The upper-crustal crustal refraction Pg/Sg, reflections from the mantle (PmP/SmS) and reflections from a crustal interface (PiP/SiS) are clearly observed on the profile. We have conducted both ray-theory travel time and full-waveform amplitude analysis. We find a pronounced low velocity zone in the upper crust on the western portion of the profile. Waveform analysis indicates that the Moho interface has a complex fine structure. A reliable 2-D crustal seismic velocity model has been obtained from travel time analysis, and this model places important constraints on the evolution of the crust at this rifted margin.

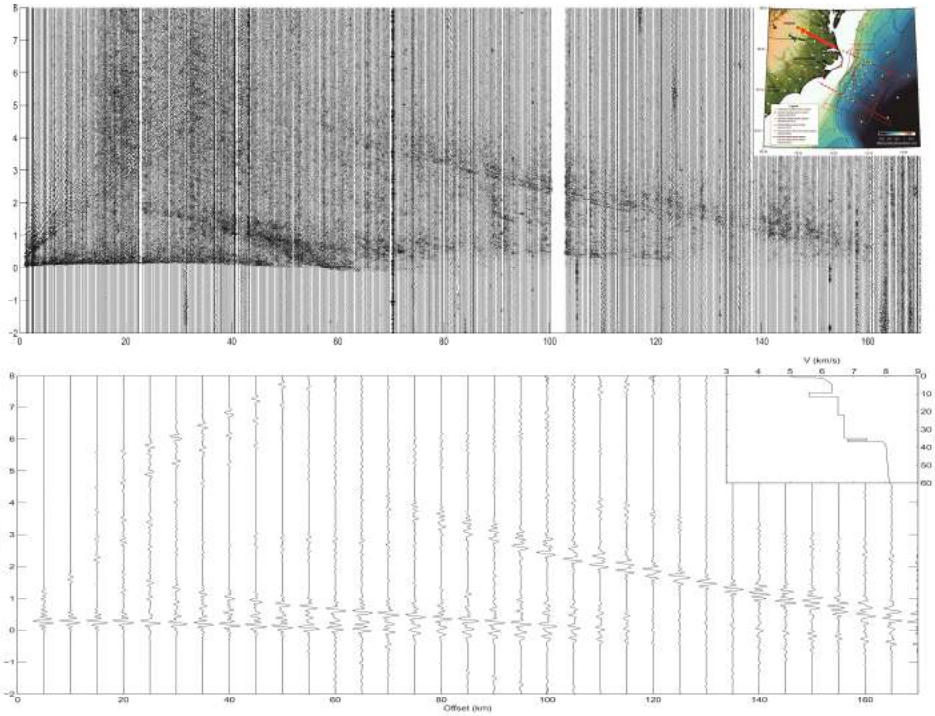

Comparison of seismic recording and Amplitude synthetic

Resolving crustal structure beneath the northern Appalachians using teleseismic receiver function analysis

Cong Li[1*], Haiying Gao[1], Michael L. Williams[1], and Vadim Levin[2]

[1]Department of Geosciences, University of Massachusetts Amherst, Amherst, Massachusetts, USA,[2]Department of Earth and Planetary Sciences, Rutgers University, New Brunswick, New Jersey, USA.

*Corresponding author: Cong Li (conli@geo.umass.edu)

Abstract

Teleseismic P-wave receiver functions are calculated to image the crustal structure in the northern Appalachians. Waveforms of teleseismic events from 1995-2016 are analyzed for a total of over 200 broadband seismic stations. Consistent P-to-S phases converted at the Moho can be clearly observed, showing an increase of the phase arrival time from the passive continental margin to the North American craton. Correspondingly, the crust thickens from 27 km to 52 km northwestward as inferred from the common conversion point stacking. Distribution of the seismically observed Moho demonstrates a complex three-dimensional variation pattern, which is approximately anti-correlated with the surface topography and the Bouguer gravity anomaly and agrees with the northeast-southwest trending terrane boundaries. The crustal thickness varies both across and along the orogenic strike, providing tight constraints on the distribution of the terranes within the lithosphere, and thus significantly improves our understanding of the tectonic history in the northern Appalachians.

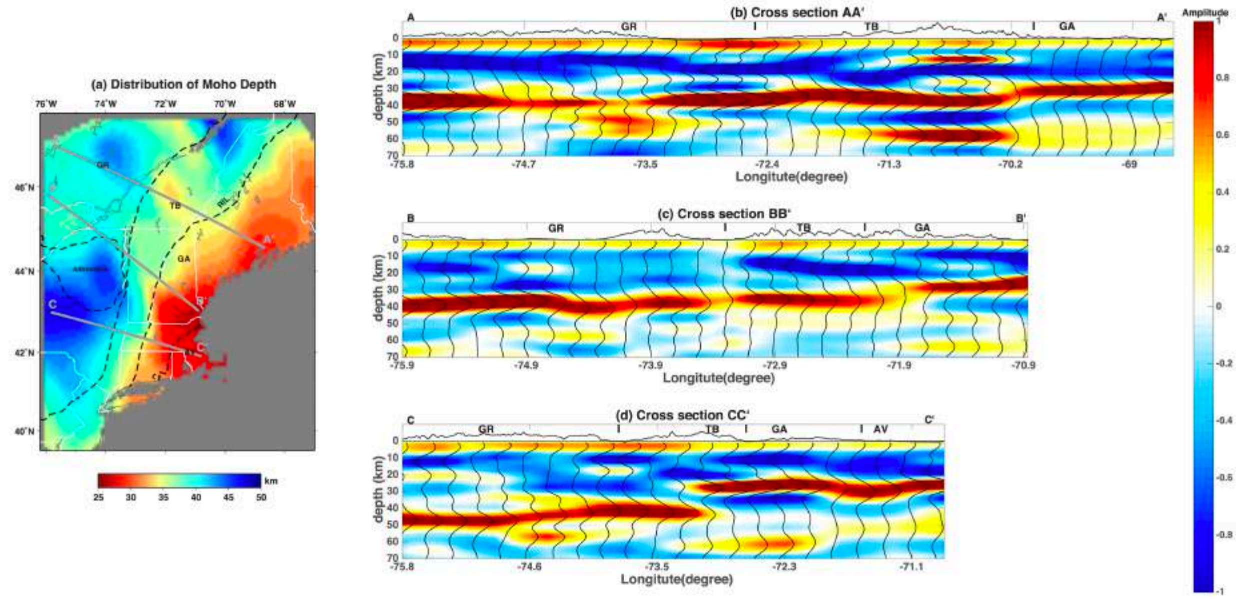

Figure 1. (a) Moho distribution in kilometers extracted from the common conversion point stacking. The white dashed lines mark the terrane boundaries digitized from the United States Geological Survey basement domain map of the conterminous United States and Alaska (http://mrdata.usgs.gov/ds-898/). AA', BB' and CC' are the profile locations in (b)-(d). (b)-(d) Cross sections of the common conversion point stacking to demonstrate the Moho variation from northwest to southeast. Red color denotes the positive amplitude of the binned receiver functions and blue color for the negative amplitude. Each vertical black line represents the average receiver function within each bin. The topographic elevations are shown in the thick black lines above the profiles, separated by the tectonic terranes. AV - Avalonia, GA - Ganderia, TB – Taconic belt, GR - Grenville Province, RIL: Red Indian Line.

Seismic Anisotropy in the Upper Mantle of Eastern North America: Results from Multi-Event Inversion

Yiran Li, Xiaoran Chen, Vadim Levin

The splitting of core-refracted shear phases is a manifestation of seismic anisotropy that may relate to the deformation of upper mantle rocks. Here we collected the observations of core-refracted shear phases from Earthscope FlexArray QMIII, Earthscope Transportable Array, and Canadian and US permanent observatories. The selected sites form a 1300 km long array that crosses the eastern North America from James Bay to the Fundy Basin, allowing the characterization of seismic anisotropy across major tectonic boundaries. Our initial results from Rotation-Correlation method show split shear waves at all sites, with lateral variations of the delay along the array, and directional variation of fast polarization at most sites. Such directional variation of splitting parameters is an expected effect of vertical changes in anisotropic properties.

We assembled a data set of SKS, SKKS and PKS phases from 21 events that occurred between May of 2012 and August of 2015. For sites of our combined array with 10 or more observations we used a multi-event inversion technique to solve for anisotropic structure. We use a bootstrapping procedure to assess the uncertainty of the individual parameters in our models.

For models with a single 100 km thick anisotropic layer with a horizontal fast axis, we find stronger anisotropy in the Appalachian Orogen, with shear-wave anisotropy up to ~6%, equivalent to a splitting delay time of ~1.5 s. The shear-wave anisotropy reduces to ~1.8% in the Superior Province, equivalent to delay times under 0.5 s. There are two changes in the amount of anisotropy required, one near the Appalachian Front, and another near the Grenville Front.

Fast axes of anisotropy are between 65° and 93°, with no obvious link between the value of fast orientation and the location of the site. Also, fast axis orientations within the Superior Province are less tightly constrained, with error bars of up to ±10 degrees.

For sites with larger data sets we also test models with two layers of anisotropy, which do provide better match to data at a few locations.

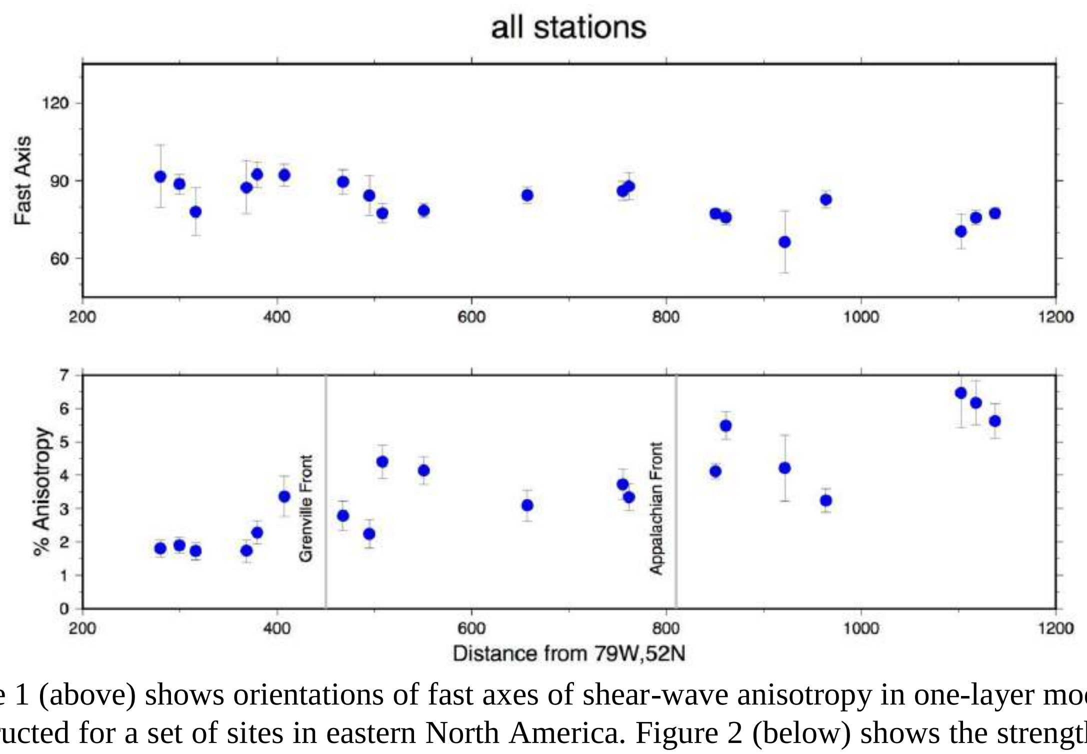

Figure 1 (above) shows orientations of fast axes of shear-wave anisotropy in one-layer models constructed for a set of sites in eastern North America. Figure 2 (below) shows the strength of anisotropy (assuming 100 km thick horizontal layer) for the same sites. The line of the transect goes from 79W,52N to 63W,43N.

Preliminary investigation of crustal and transition zone structure in Texas from P to S receiver functions.

Robert W. Porritt, Juan Benavides, Thorsten W. Becker, and Whitney M. Behr

The passage of USArray has illuminated several key building blocks of the North American continent. Among these, one of the most striking in the upper crust is the Gulf Coastal margin, which has been imaged as a very low velocity anomaly in ambient noise tomography studies. This low velocity anomaly stops abruptly at the Ouachita-Marathon Front (OMF) in central Texas, which marks the transition from low-lands comprised of shelf deposits into the Llano Uplift. The Llano Uplift is a Grenville age dome in central Texas consisting of felsic intrusions, supracrustal deposits, and associated metamorphism overlain by Carboniferous Era marine deposits. Below this crustal structure, the picture is less clear; global tomographic models show this to be near the edge of the Laurentia craton, but it remains unclear if this region can be considered cratonized. Two targeted studies were deployed in Texas along with the Transportable Array to better understand the crust and upper mantle. One, a Flexible Array, Seidcar, densified a square grid in west Texas and southeastern New Mexico to clarify imaging of a lithospheric instability from small-scale convection. The other, X4, is a linear array from the Llano Uplift to the Gulf Coast, which has been used to image the crust and lithosphere with both converted waves and ambient noise derived surface waves. However, these arrays leave a large swath of Texas only sampled by the Transportable Array. This under-sampled region includes much of the Llano Uplift and the transition across the OMF. To explore this region further, we employ high frequency P to S receiver functions for structure within the crust and lithosphere and low frequency P to S receiver functions to investigate the mantle transition zone. From multiple estimates of crustal thickness and bootstrap resampling, we find a clear transition in crustal thickness from ~25 to 35 km south and east of the OMF to nearly 50 km thick crust north and west of the OMF. This thick crust may be the result of errors in the underlying velocity model, but may also suggest a strongly differentiated felsic crust. In the transition zone, we observe relatively flat structures suggesting active structures are confined to the upper mantle. Further results are pending as the USArray, X4, and TexNet data is more thoroughly analyzed.

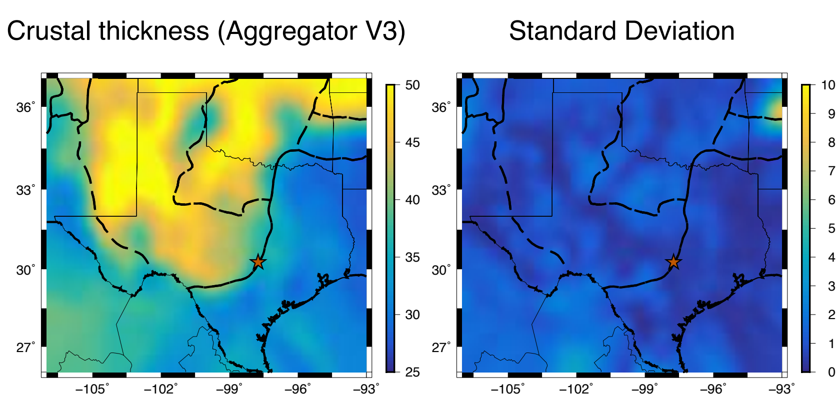

Figure: Crustal thickness (km) and 1 sigma uncertainty (km) from multiple estimates from receiver function data. Solid line is the Ouachita-Marathon Front, dashed lines are other physiographic boundaries, and orange star is Austin, TX.

New insights of the Midcontinent Rift from SPREE

Weisen Shen, Washington University in St Louis

Deep beneath the fertile flat farmland of the midwest, a huge scar gives rise to the most prominent gravity and magnetic anomalies within the old and stable core of the North America continent. The Midcontinent Rift was the location of a short episode of extension between eastern and western North America, and is now filled by large volume of ~ 1.1 Ga old intrusive rocks. Recent deployments of the Earthscope/USArray and the Superior Province Rifting Earthscope Experiment (SPREE) flexible array experiment enable us to perform a comprehensive seismic investigation of the crustal and uppermost mantle structure in the vicinity of the MCR, including the part in the southern Superior craton, and provide a better understanding of MCR geology. Receiver function images show a complex structure near the Moho discontinuity, the boundary between the crust and mantle, perhaps representing a distinct layer of magmatic underplating beneath the rift. Surface wave tomography reveals the spatial distribution of this anomalous crustal underplating structure, extending beneath the Lake Superior. By incorporating these receiver function and surface wave data, a refined seismic model for the MCR area is constructed. The complementarity of these seismic observables assists in obtaining an unbiased shear velocity structure of the crust and mantle. In particular, the joint Bayesian Monte-Carlo inversion finds and a distinct layer with shear wave speed between 4.0 and 4.4 km/sec associated with the Moho beneath the MCR, further indicating crustal underplating associated with the opening of the rift.

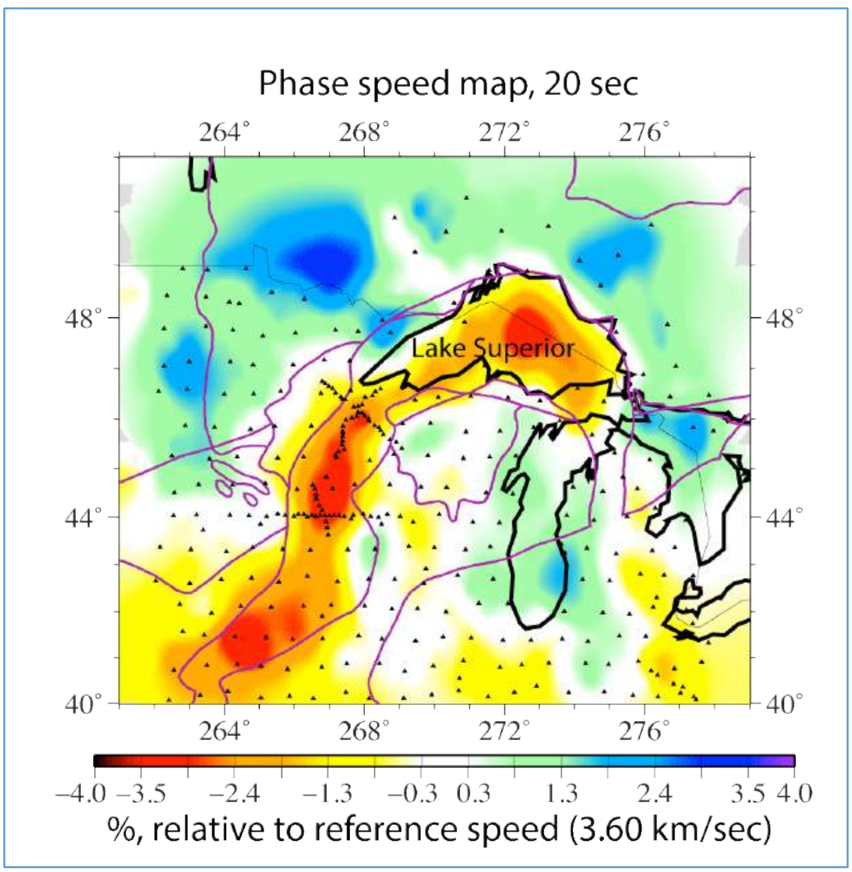

Figure 1. Phase speed map of the 20 sec Rayleigh wave, which is sensitive to the seismic structure at depths between ~ 20 to 35 km. The map reveals that the complex lower crust structure of the MCR extends to the Lake Superior.

3-D shear wave velocity and radial anisotropy models beneath the northwest Gulf Coast of the United States

Yao Yao[1] and Aibing Li[1]

[1]University of Houston

The last major tectonic event in Texas is Mesozoic continental rifting that formed the Gulf of Mexico. The northern Gulf Coast also experienced igneous activity and local uplifts in Late Cretaceous. To investigate geodynamic processes associated with these activities, we have developed 3-D shear wave velocity and radial anisotropy models of Texas from Rayleigh and Love wave phase velocities at periods of 6-167 s, which are computed from ambient noise and earthquake data recorded at the USArray Transportable Array stations.

High Vsv and Vsh anomalies appear in the central and western Texas, the southern edge of the Laurentia craton. The area is slightly anisotropic with 2-3% negative radial anisotropy (Vsv>Vsh) from the middle crust to the shallower upper mantle, indicating that the lithosphere here was not extended by Mesozoic rifting. In contrast, the coastal plain is characterized by significantly low velocity anomalies in the crust, reflecting the influence of thick sediments. Strong positive anisotropy of 10% (Vsh>Vsv) is imaged in the lower crust and shallow upper mantle, which are mainly caused by the horizontal alignment of anisotropic minerals due to lithosphere extension in Mesozoic. The Ouachita belt correlates a narrow high velocity band and negative anisotropy at the depths above 55 km, reflecting lithosphere shortening during the Ouachita orogeny instead of the Mesozoic extension. Our model evidences a fast and strong Ouachita lithosphere that helped to buffer crust thinning from the Mesozoic rifting.

In the mantle beneath 115 km, significantly low and high velocity anomalies of circular shapes appear beneath the Ouachita belt and the coastal plain. The slow anomalies in the central and east Texas correspond to positive radial anisotropy, indicating a weak mantle under shear deformation. However, both the slow anomaly in the southeast and fast anomaly in the northeast are associated with negative radial anisotropy, indicating mantle upwelling and downwelling, respectively. Small-scale mantle convection probably has been operating under the coastal region after the opening of the Gulf of Mexico and is likely responsible for local igneous activity and uplifts.

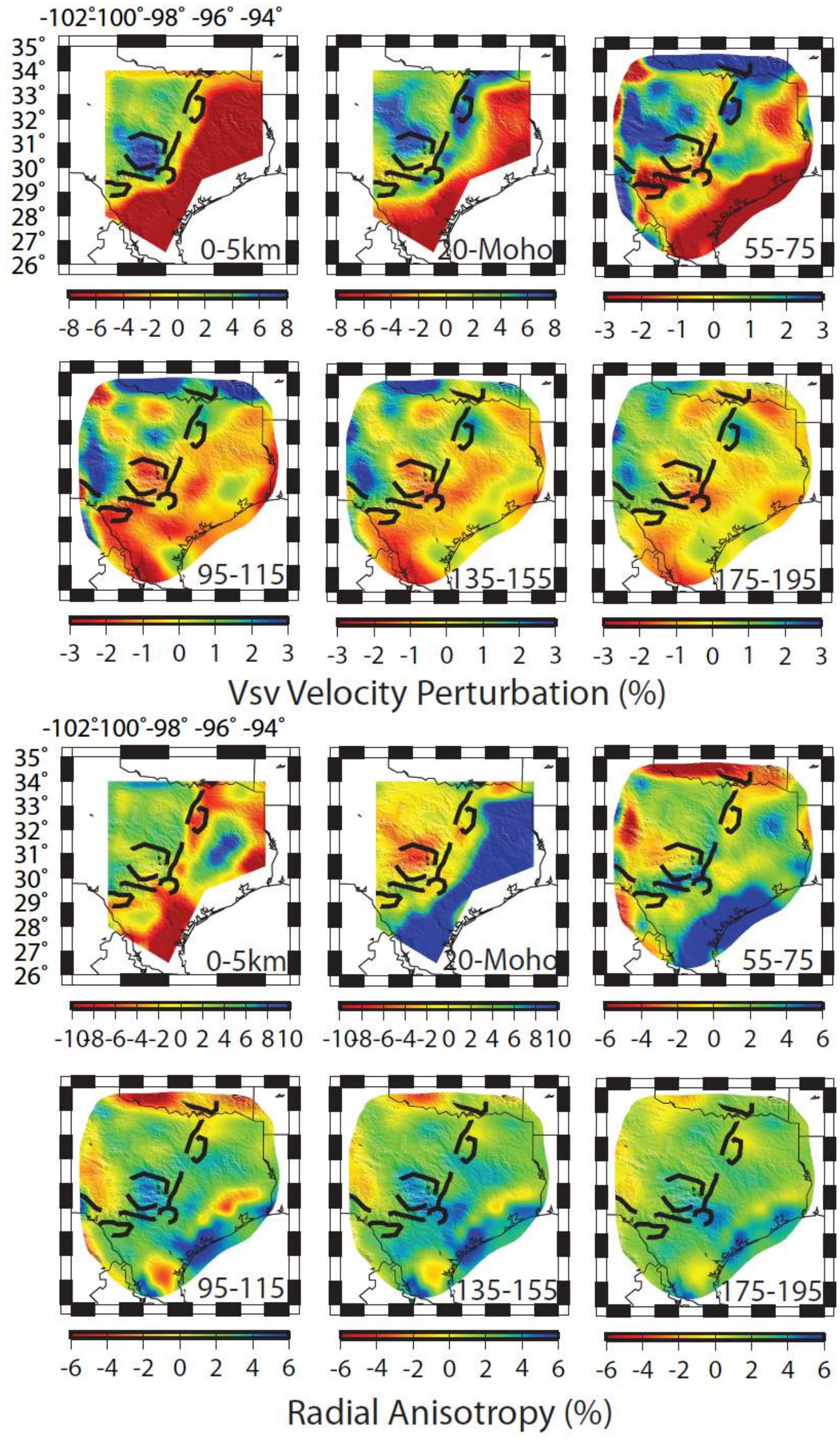

Figure 1. Vsv velocity perturbation and radial anisotropy in the crust and upper mantle. The maps are clipped according to model resolution from ambient noise tomography for the crustal layers and from the two plane-wave method for the mantle layers.

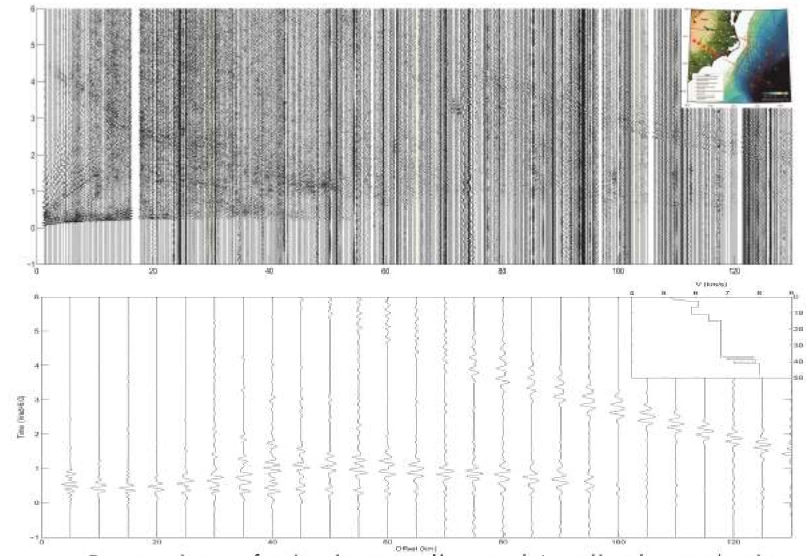
Comparison of seismic recording and Amplitude synthetic

Crustal Structure of Rifted Margin of Eastern North American in North Carolina

Shuai Zhao, Wenbin Guo, Walter D. Mooney
U.S Geological Survey, Earthquake Science Center, Menlo Park, CA, USA

Abstract

Passive continental margins are the boundaries between oceanic and continental regions where neither collisional deformation nor subduction is occurring. Despite their present-day tectonic quiescence, the crustal structure of passive continental margins is diverse and complex because they are formed by the rifting that accompanies the breakup of a supercontinent. The NSF-funded GeoPRISMS Eastern North American Margin (ENAM) Community Seismic Experiment aims to understand the geological evolution of the rifted eastern margin of North America. In 2015, two onshore active-source seismic profiles were recorded in North Carolina. Here we present an analysis of the data from the southern seismic profile. This profile is 216 km long and consists of 6 shots recorded by 708 vertical-component Texan seismographs. The shot spacing is 36 km and seismograph spacing is 320 m. Data quality is excellent and both P-waves and S-waves are visible. There are clear wide-angle reflections from within the crust and from the Moho at a depth of 34-38 km. We present the results of our modeling of the crust using both 1D and 2D seismic velocity inversions, and discuss the implications for the rifting process at the North Carolina continental margin.

Magmatic addition and extension along the Eastern North American Margin (ENAM) from crustal seismic refraction data: Results from the ENAM Community Seismic Experiment

T. Luckie, L. Worthington, M.B. Magnani

Magmatic addition can lead to intraplate crustal growth through plume-generated voluminous underplating of mafic material, particularly during early syn-rift processes. In addition, magmatism facilitates crustal growth and rift development by assisting extensional tectonic forces. Therefore, understanding the relationship between magmatism and rifting may help explain both these processes. In the summer of 2015 the GeoPRISMS Eastern North American Margin (ENAM) Community Seismic Experiment collected two margin-dip active source seismic refraction profiles in eastern North Carolina and southeastern Virginia using five onshore explosive shots on a northern profile and six on a southern profile (see figure). Analysis of these data resulted in 2-D P-wave velocity models of each onshore profile that reveal a crustal thickness between 36-43 km and a high velocity (7.0-7.3 km/s) layer between 5-11 km thick at the base of the crust. We interpret this feature as representing mafic magmatic addition, likely equivalent to the high velocity lower crust layer previously observed offshore at the transition between rifted continental crust and oceanic crust. Additionally, we observe slightly elevated velocities throughout the crust, which we interpret as metamorphic alteration in the mid- and upper-crust in response to magmatic addition from below. This magmatic addition could be related to Jurassic-aged syn-rift magmatism along the ENAM and/or to the voluminous Central Atlantic Magmatic Province (CAMP), and suggests that rift-related ENAM magmatism may be more voluminous than previously thought.

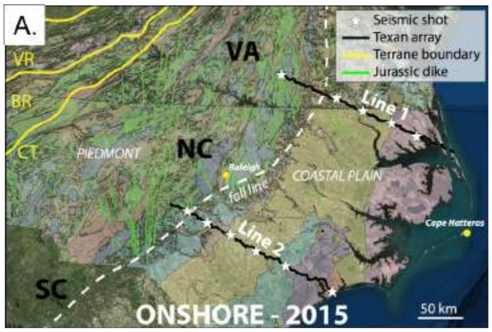

Figure A. ENAM onshore experiment showing station locations (black circles) and explosion locations (white stars) with Jurassic dikes (green lines), physiographic provinces, accreted terranes, and geology (after Fenneman & Johnson, 1946; Brown, 1985). **B.** Line 1 velocity model showing labeled shot points (yellow stars). Chi squares = 1.0l RMS travel time residual = 104 ms. Contour interval is 0.2 km/s. **C.** Line 2 velocity model showing labeled shot points (yellow stars). Chi squares = 1.0l RMS travel time residual = 125 ms. Contour interval is 0.2 km/s.

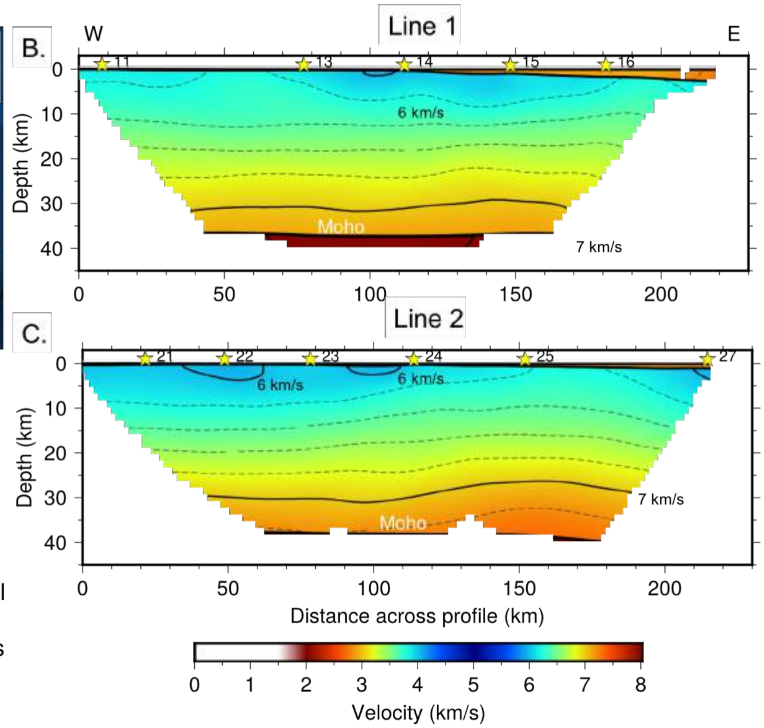

Shallow velocity structure of the Socorro Magma Body from ambient noise tomography using the large-N Sevilleta array, central Rio Grande Rift, New Mexico

Ranasinghe, N.R.; Worthington, L.L.; Schmandt, B.; Jiang, C.X, Finlay, T.; Bilek, S.L.; Aster, R.

The Socorro Magma Body (SMB) is one of the largest recognized active mid-crustal magma intrusions globally. Inflation of the SMB drives surface uplift at rates of up to of few millimeters per year. We examined the upper crustal structure of the northern section of the SMB using ambient noise seismic data collected from the Sevilleta Array to constrain basin structure and identify possible upper crustal heterogeneities caused by fluid or magma migration to shallower depths. The Sevilleta Array comprised 801 vertical-component Nodal seismic stations with 10-Hz seismometers deployed in the Sevilleta National Wildlife Refuge, within the central Rio Grande rift north of Socorro, New Mexico, for a period of 12 days in February 2015. Inter-station ambient noise cross-correlations were computed in all available 20-minute time windows and stacked to obtain estimates of the vertical component Green's function. Clear fundamental mode Rayleigh wave energy is observed from 3 to 6 s period. Beamforming indicates prominent noise sources from the southwest, near Baja California, and the southeast, in the Gulf of Mexico. The frequency-time analysis method was implemented to measure fundamental mode Rayleigh wave phase velocities and the resulting inter-station travel times were inverted to obtain 2-D phase velocity maps.

One-dimensional sensitivity kernels indicate that the Rayleigh wave phase velocity maps are sensitive to a depth interval of ~1 to 8 km depending on the wave period. The maps show (up to 40%) variations in phase velocity within the Sevilleta Array, with the largest variations found for periods of ~5-6 seconds. Holocene to upper Pleistocene, alluvial sediments found in the Socorro Basin consistently show lower phase velocities than the basin-bounding ranges. Two areas of localized low velocities will be the focus of future work. One low velocity zone appears to be co-located with the area of maximum observed uplift related to the SMB. A second low velocity zone surrounds the Paleogene-aged Black Butte Volcano.

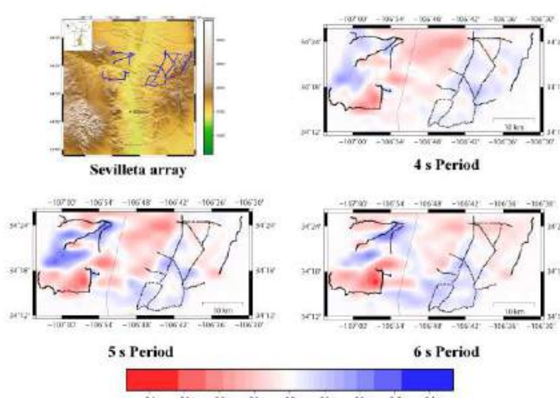

Rayleigh wave phase velocity maps at 4, 5 and 6 s periods

Processing and synthesis of GPS data and other geodetic observations at the Socorro Magma Body, New Mexico

Nicolas George[1], Mousumi Roy[1], and Mark Murray[2]

[1] *University of New Mexico, Albuquerque, NM, USA*
[2] *New Mexico Tech, Socorro, NM, USA*

The Socorro magma body (SMB), an inferred mid-crustal magma body located in the Rio Grande Rift (RGR) in central New Mexico, has been the subject of numerous geophysical studies, both seismic and geodetic. We present new and re-processed data from campaign and continuous GPS stations surrounding the SMB. Our results are presented within a self-consistent local reference frame based on the Earth-centered ITRF08 (which holds north America fixed) and has the RGR extension signal removed, isolating the observed motions to those relating to SMB-induced deformation and local faulting. GPS data collected for the SMB network from 2002 to 2011 and PBO, PBO-RGR, and CORS data are combined using the GAMIT/GLOBK geodetic software suite developed at MIT to realize GPS station positions and velocities within this local reference frame. Our GPS results show an outward radial pattern of horizontal and vertical motions consistent with an inflating magmatic source at depth. These observations are compared with simple analytic models of spherical and penny-shaped crack sources as a first attempt at understanding the nature of deformation above the SMB. Further analysis and comparison with finite element models is anticipated, allowing us to develop a more comprehensive understanding of the actively deforming SMB.

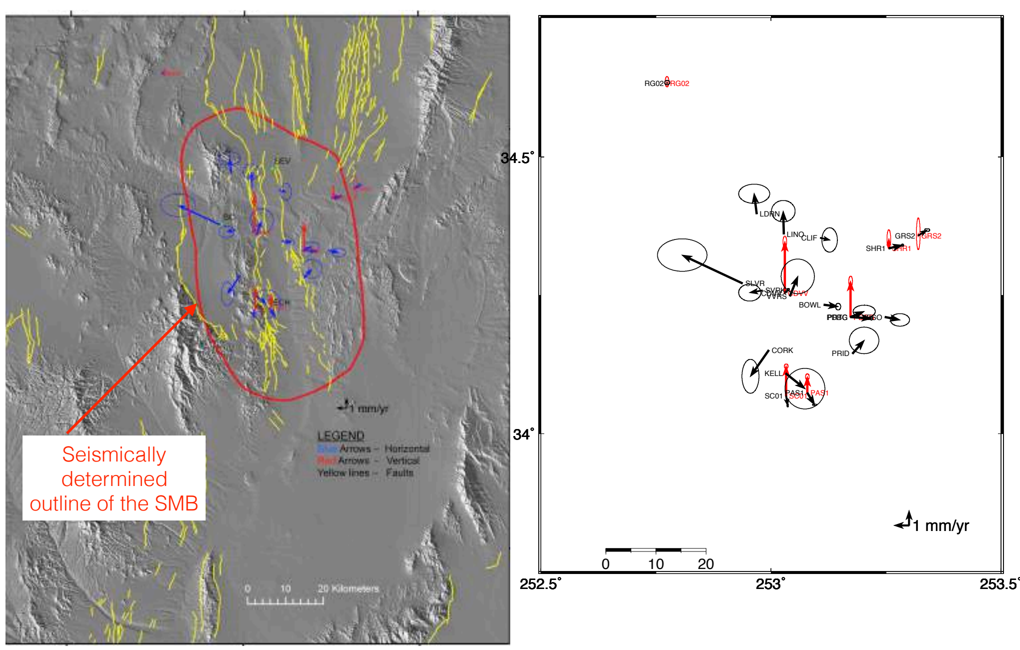

Left: Horizontal (blue) and vertical (red) velocities obtained our SMB GPS sites, with 95% confidence intervals. Continuous sites are labeled, campaign sites are not labeled for clarity. *Right:* Same velocities, without basemap; horizontal velocities are in black.

Poster presentation requested

Sustaining Science through Landowner Relationships

Beth Bartel & James Downing, UNAVCO

Of the more than 1,200 geophysical stations within the EarthScope Plate Boundary Observatory (PBO), approximately 400 are on private land. As with the other components of EarthScope, obtaining permissions to install instruments required relationship-building and permitting. Now, as EarthScope funding sunsets, we are trying to extend the life and legacy of the project by renewing permits for many of these stations. A significant cross-organizational effort at UNAVCO resulted in the first of a series of mailings to a subset of these private landowners and parks hosting PBO stations. The mailing includes a letter; a four-page magazine-style publication called PBO SiteLog that is written for a non-expert audience; and a customized, site-specific one-pager featuring the station's time series and velocity maps, with information on how to understand the plots. Initial feedback from landowners has been highly positive, with the mailing resulting in renewal of multiple permits and savings due to no-cost extensions. We plan to repeat the mailing annually to meet landowner requests for information and to build relationships to ensure network continuity as many permits come up for renewal.

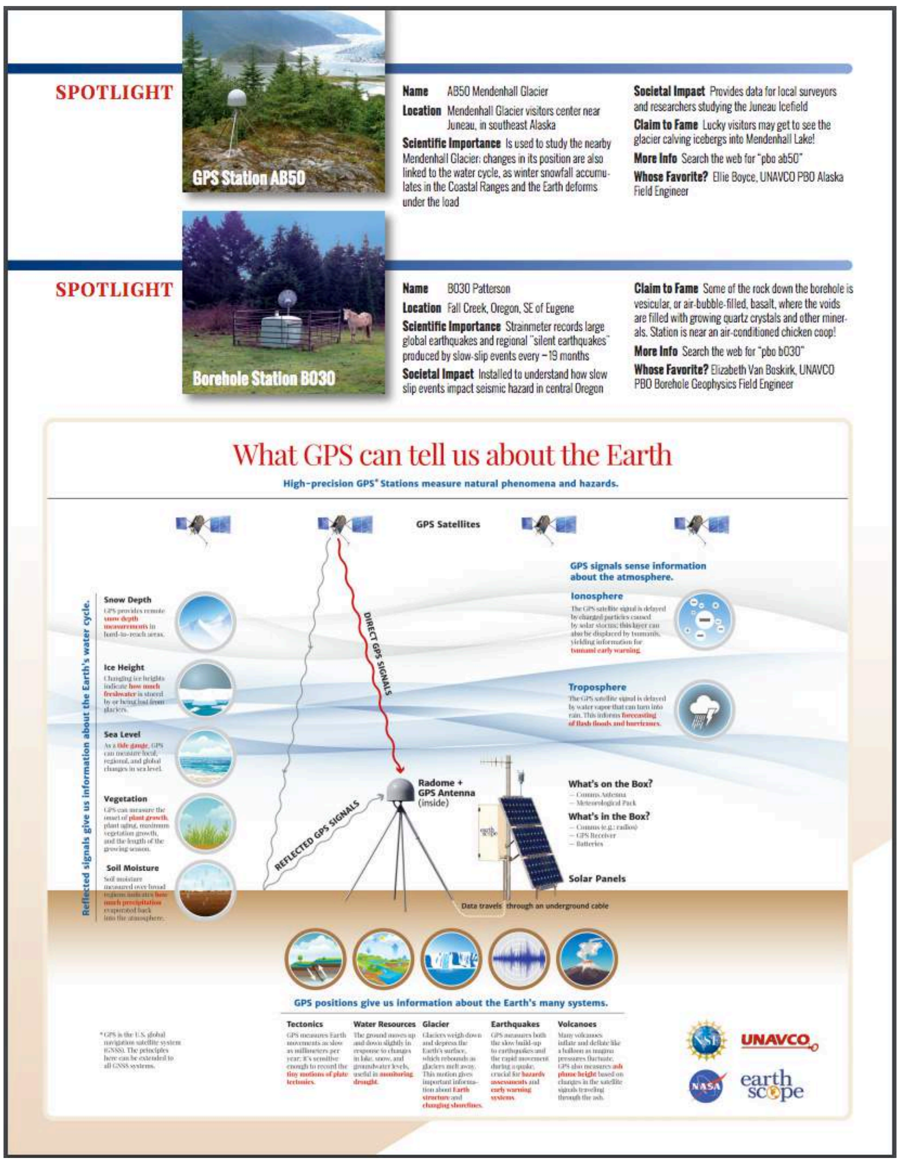
SPOTLIGHT

GPS Station AB50

Name AB50 Mendenhall Glacier
Location Mendenhall Glacier visitors center near Juneau, in southeast Alaska
Scientific Importance Is used to study the nearby Mendenhall Glacier: changes in its position are also linked to the water cycle, as winter snowfall accumulates in the Coastal Ranges and the Earth deforms under the load
Societal Impact Provides data for local surveyors and researchers studying the Juneau Icefield
Claim to Fame Lucky visitors may get to see the glacier calving icebergs into Mendenhall Lake!
More Info Search the web for "pbo ab50"
Whose Favorite? Ellie Boyce, UNAVCO PBO Alaska Field Engineer

SPOTLIGHT

Borehole Station B030

Name B030 Patterson
Location Fall Creek, Oregon, SE of Eugene
Scientific Importance Strainmeter records large global earthquakes and regional "silent earthquakes" produced by slow-slip events every ~19 months
Societal Impact Installed to understand how slow slip events impact seismic hazard in central Oregon
Claim to Fame Some of the rock down the borehole is vesicular, or air-bubble-filled, basalt, where the voids are filled with growing quartz crystals and other minerals. Station is near an air-conditioned chicken coop!
More Info Search the web for "pbo b030"
Whose Favorite? Elizabeth Van Boskirk, UNAVCO PBO Borehole Geophysics Field Engineer

Page 2 of the PBO SiteLog features brief, visual station spotlights and an infographic of the many different uses of GPS/GNSS within the EarthScope Plate Boundary Observatory.

EarthScope Transportable Array Outreach Activities in Alaska and Western Canada

Lea Gardine[1], Maïté Agopian[1], Perle M. Dorr[2], Tammy Bravo[2], John Taber[2], Michael E. West[1], Carl Tape[1], and Robert W. Busby[2]

[1]University of Alaska Fairbanks-Geophysical Institute [2]IRIS Consortium

IRIS and EarthScope are partnering with the Alaska Earthquake Center, part of the University of Alaska Fairbanks Geophysical Institute, to increase awareness of earthquakes in Alaska and western Canada and the benefits of the Transportable Array for people living in this region. We provide an update of ongoing education and outreach activities.

The remoteness and inaccessibility of large portions of Alaska and western Canada requires a multifaceted approached to outreach with a focus at the regional level. Region-specific publications and informational posters have been developed to tie in a sense of place. Meetings and interviews with Alaska Native Elders and tribal councils discussing the seismic history of the regions has led us to a better understanding of how residents view, respond to, and educate themselves about earthquakes.

The creation of Alaska content for IRIS's Active Earth Monitor, which emphasizes the widespread tectonic and seismic features, offers viewers a glimpse into Alaska's complexity and seismic potential. Classroom visits, particularly schools with TA stations nearby, and open invitations for laboratory tours has enriched the learning experience for students not only about seismicity, but the instrumentation and techniques that go into gathering the data. Continued efforts to engage residents at large cultural gatherings and community events have led to increased discussion about EarthScope in both Alaska and Canada. Increased collaborations with the now UAF-hosted EarthScope National Office and UNAVCO have generated more opportunities to disseminate information.

An online, for-credit professional development course for Alaska teachers was offered in Spring 2017 through the University of Alaska Fairbanks. Created in partnership with IRIS Seismographs in Schools, educators learn how to stream, access and interpret seismic data, including data from TA stations, in their classrooms using jAmaSeis, a free software package available from IRIS.

Students at Glacier View Elementary visiting the TA station on the school grounds (M23K).

Education and outreach activities and opportunities in the eastern United States tied to EarthScope and related projects

Maureen D. Long, Department of Geology and Geophysics, Yale University

The eastern United States hosts a large fraction of the country's population and a large number of colleges and universities. Due at least in part to its location on a passive continental margin, however, public awareness of Earth science in general and issues such as earthquake hazards in particular is not particularly high. Data collection efforts associated with EarthScope, GeoPRISMS, and related projects in the region, along with the advent of exciting science results from EarthScope in the eastern U.S., provide a unique opportunity for education and outreach projects geared towards the general public and towards K-16 students and educators. This poster will showcase some of our recent E&O activities in the eastern U.S., including outreach to primarily undergraduate institutions (PUIs), the involvement of high school science teachers in seismology field work in Connecticut, and public talks that highlight EarthScope science results for a general audience. Recent work on the MAGIC seismic deployment in the central Appalachians, done in collaboration with Maggie Benoit at the College of New Jersey, involved a number of PUIs as station hosts and led to opportunities for students and faculty to observe field work. An ongoing seismic deployment in northern Connecticut, the Seismic Experiment for Imaging Structure beneath Connecticut (SEISConn), is closely tied to EarthScope science goals and has provided opportunities for ten high school science teachers to spend one week working on a broadband seismic deployment via the Field Experiences for Science Teachers (FEST) program based in the G&G department at Yale. Several recent talks to general audiences in Connecticut have highlighted the EarthScope project and EarthScope science results from the eastern U.S., and we hope to expand the reach of these public talks in the future.

Left: servicing MAGIC station DENI on the campus of Denison University in Granville, Ohio, with Prof. Erik Klemetti (center) and a group of students. Right: FEST project participants pose next to a completed station of the SEISConn array in East Windsor, CT.

DataBricks: Your own indexed data repository for large, static data collections

Chad Trabant, Tim Ahern, Rick Benson
IRIS Data Management Center

Currently it is possible to request many terabytes of data from the DMC using standard tools. While this is sufficient for most users, some users have need for many tens to hundreds of terabytes of data. The point at which data collection becomes laborious and time consuming for a researcher depends on multiple factors, such as internet capacity, local storage and familiarity with appropriate data request tools. But further, there are limitations with the capacity and data extraction capability at the DMC that is continuously servicing hundreds of concurrent requests from users around the world. In addition to the task of transferring large volumes, the management of a large data set by a researcher or group can be challenging. To address both the transfer limitations to institutions directly, as well as basic data set handling, we have been prototyping the notion of a **DataBrick**. In this concept, the DMC would load a large dataset onto a self-contained, portable storage system and provide the software to run a standard web service for data data access. By running the fdsnws-dataselect web service on a computer connected to the DataBrick, the researcher has their own private data repository that can be accessed with the same tools used to retrieve data from federated FDSN data centers, including the DMC. The DataBrick would also contain a searchable index (database) that identifies what data is included and provides the details needed to efficiently extract subsets.

The DataBrick concept provides the researcher or group with a large degree of flexibility. The raw miniSEED may be accessed directly or through the web service interface. The DataBrick can be used for other storage needs such as data processing. Data may be added to the DataBrick locally and added to the searchable index as desired. The miniSEED indexing scheme and portable fdsnws-dataselect server may be used on any collection of miniSEED data, independent of a DataBrick delivered by the DMC. There are expected to be limitations to this concept. Data selection would likely be limited to predetermined data sets that are static, i.e. not expected to change with time. Furthermore, metadata describing the time series would not be included on the DataBrick as they are easily retrieved from the DMC, ensuring that the latest metadata is used.

A number of questions remain to be resolved before this can be made operational. Primarily: how many users would be interested in a service such as described above? How would the effort be funded? IRIS does not presently have funds to accommodate the generation of unique datasets on DataBricks or for the replication of Bricks containing static data. The funds to accommodate this must be found beyond the traditional IRIS sources of funding and most likely borne by those requesting a DataBrick. We intend to demo as much of the DataBrick prototype concept as possible at the poster. **Your answers to these questions and input on the concept is greatly appreciated.**

(Potential DataBrick, mostly harmless)

PBO Operations in Alaska and Cascadia, Highlighting Collaboration with our Partners

EarthScope's geodetic facility, the UNAVCO-operated Plate Boundary Observatory (PBO) network, operate as a single management unit in Alaska and in the Cascadia region. While still distinct regions with their own challenges and engineering staff, every effort has been made to operate as a single team. The difficulty of logistics and the cost of maintaining large networks is a major concern within PBO as well as with partner agencies both in Cascadia and Alaska. Over the last several years, a concerted effort has been made to work collaboratively with institutions and stakeholders to defray maintenance cost by sharing staff and resources.

UNAVCO currently operates four integrated GPS/seismic stations in collaboration with the Alaska Earthquake Center, eight with the Alaska Volcano Observatory, and ten with the TA. By the end of 2017, PBO and TA plan to install another three integrated and/or co-located geodetic and seismic systems. Two large maintenance pushes in 2016 were shared, the largest being a 5 day-joint operation between PBO, AEC, and TA sharing helicopter and staffing in order to complete maintenance and staging around Cordova, AK. The second, a 10 day helicopter contract was shared between AVO, PBO and TA to complete maintenance work on Unimak Island and up the Alaska Peninsula.

Over the length of the entirety of the PBO project NW staff has developed a close working relationship with the Oregon Department of Transportation (ODOT). Most of the early collaborations have mainly revolved around permitting/siting and communications of PBO stations beneficial to the construction of the network and to the build-out of the Oregon geodetic network. Over the last year, UNAVCO has partnered with ODOT on deployment of the new Septentrio receivers, with ODOT providing 19 of the 32 installed in Oregon and Northern California. In addition to this partnership we have worked with other state DOT's, Federal Agencies, and Commercial users to augment and improve the network in both the Northwest and Alaska.

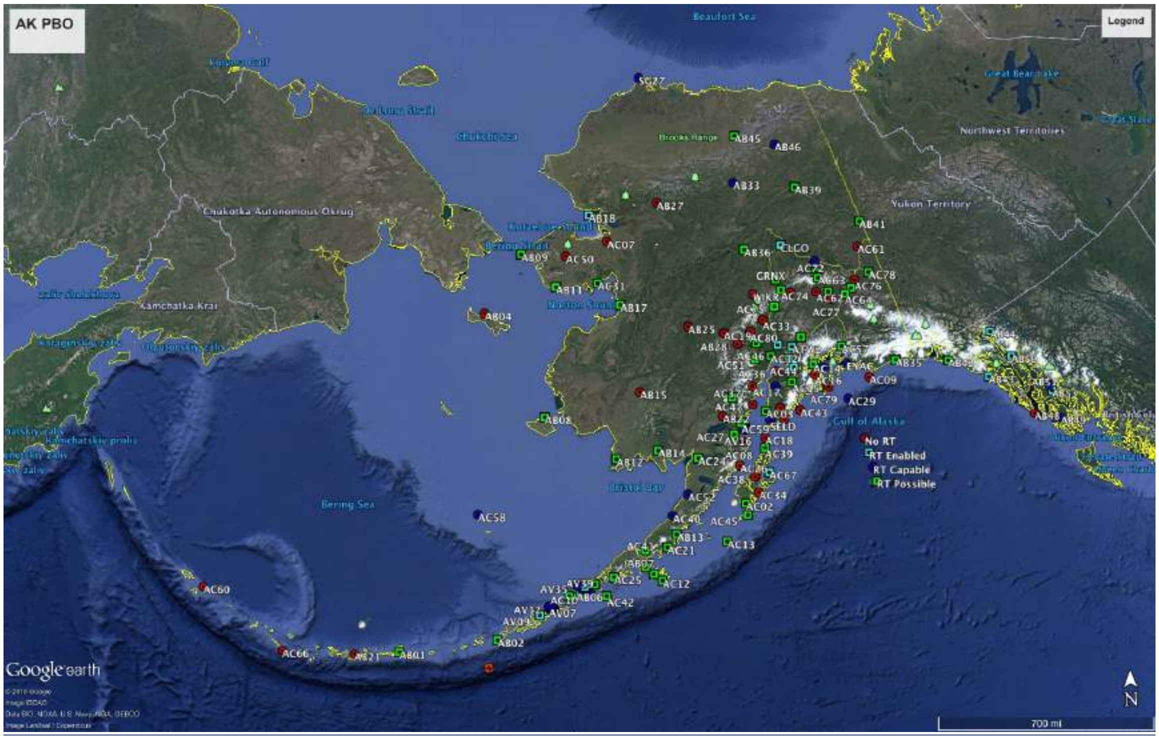
AK PBO
Legend
Beaufort Sea
Chukchi Sea
Bering Sea
Gulf of Alaska
Bristol Bay
Yukon Territory
Northwest Territories
No RT
RT Enabled
RT Capable
RT Possible
700 mi

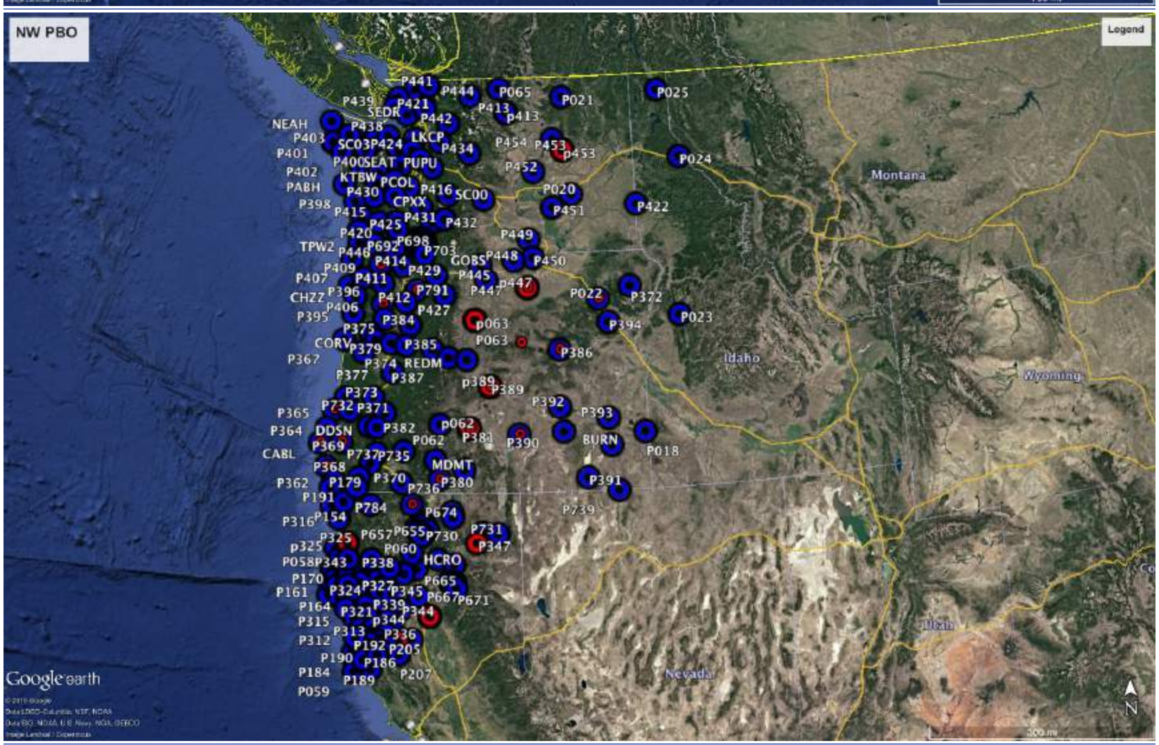
NW PBO
Legend
Montana
Idaho
Wyoming
Nevada
Utah
300 mi

Title: Case studies of anomalous time series signals from GPS stations in the EarthScope Plate Boundary Observatory (PBO)

Authors: people in the PBO ACS, all the field engineers
Christine M. Puskas, UNAVCO
David A. Phillips, UNAVCO
Charles M. Meertens, UNAVCO
Glen Mattioli, UNAVCO
Thomas A. Herring, Massachusetts Institute of Technology
Timothy I. Melbourne, Central Washington University
Mark H. Murray, New Mexico Institute of Mining and Technology
Michael A. Floyd, Massachusetts Institute of Technology
Walter M. Szeliga, Central Washington University
Robert W. King, Massachusetts Institute of Technology
Chris Walls, UNAVCO
Doerte Mann, UNAVCO
Adam Woolace, UNAVCO
Ken Austin, UNAVCO
Ryan Turner, UNAVCO
Ellie Boyce, UNAVCO

Session: Facilities, Operations, and Management

The GAGE GPS Data Analysis Centers and Analysis Center Coordinator analyze data and generate products from more than 2,000 GPS stations in the EarthScope Plate Boundary Observatory (PBO) and other regional networks throughout North America, the Caribbean, and Central America. The resulting time series and station velocities measure tectonic deformation, earthquakes, post-seismic motion, seasonal hydrologic loading and other natural and anthropogenic processes. While most stations deform according to tectonic/volcanic/hydrologic processes and produce data that are of good quality, users analyzing regional subsets of data should be aware of exceptions. These exceptions are local effects that can occur on scales of hours to days to months to years. We present case studies of some of these effects at selected sites. Common site issues that can affect time series include vegetation overgrowth, snow/ice on antennas, equipment damage, and groundwater pumping. Other factors include regional uplift and in some cases subsidence from drought, local loading from reservoirs, landslides/unstable ground, atmospheric changes, and interference in the GPS signal. These issues can cause nonlinearity and/or noise in the time series. While the Analysis Centers track earthquakes, post-seismic deformation, and antenna/radome/receiver changes, many site issues are not documented as part of GPS processing. Individual sites are investigated for unusual activity identified through routine processing, quality analysis, and user or engineer feedback, with short reports posted to the web, on the Geodetic Data Services Technical News Page on Google+. Besides examples of unusual local conditions, we present tools to diagnose and evaluate station data. Users have the option of filtering affected data from time series analysis or using the affected data in their own studies when applicable.


Overview photo of station P656 on the slopes of Mount Shasta, taken by a UNAVCO field engineer during a visit to repair the station after it had gone offline due to heavy snow. Note the damaged solar panel and the broken radome. This station was likely buried under several meters of snow.

Evolution of the California Plate Boundary Observatory GPS-GNSS Network

Christian Walls, Doerte Mann, Ryan Turner, Andre Basset, Shawn Lawrence, Ken Austin, Tim Dittman, Adam Woolace, Summer Miller, Karl Feaux, Glen Mattioli (all at UNAVCO)

The EarthScope Plate Boundary Observatory (PBO) GPS-GNSS network in California, funded by the NSF and operated by UNAVCO, is comprised of 599 permanent GPS and GNSS stations spanning three principal tectonic regimes and is administered by separate management regions (Subduction - Pacific Northwest [91 sites], Extension - East [41 sites], Transform - Southwest [467 sites]). The GPS-only network was initially designed for data file downloads once every 24 hrs primarily for tectonic analysis. This low data volume requirement and circa-2004 cutting edge IP-based cellular/VSat modems provided significant freedom for station placement and enabled science-targeted installation of stations in some of the most remote and geologically interesting areas. Regional high-rate data downloads for GNSS-seismology, airborne LiDAR surveys, meteorological/GNSS/seismic real-time data flow and other demands, however, require significantly increased bandwidth beyond the initial 5-20KB/s transfer rates that were used to design the network.

Since the close of construction in September 2008, various enhancements have been implemented through additional funding by the NSF (ARRA/Cascadia), NOAA, and NASA and in collaboration with stakeholders such as Caltrans, Scripps, and the USGS. Today, only 5 of the original cell modems remain with 337 upgraded cell modems providing 3G/4G/LTE data communications with transfer rates ranging from 80-400 KB/s. Ongoing radio network expansion and upgrades continue to harden communications using primarily the 2.4 GHz and 5.8 Ghz spectrums. 39 VSAT and one manual download site remain (down from 68 VSAT & 12 Manual in 2008). In California, the network capabilities for 1 Hz & 5 Hz downloads or low latency 1 Hz streaming are ~95%, ~90% and ~75% of the stations, respectively, with 422 active 1 Hz streams in California.

A variety of geophysical sensors are co-located with a subset of the stations and include: 21 MEMS accelerometers, 31 strong motion and broadband seismometers, 9 borehole strainmeters and 1 long baseline strainmeter. Vaisala meteorological instruments are located at 53 sites of which 52 stream GPS/Met data. As budget allows, GPS-only receivers are replaced with GNSS receivers and antennas. Today, there are 119 stations in California with GLONASS enabled Trimble NetR9 receivers and 33 full constellation Septentrio PolaRx5 receivers.

Just as the scale and geographical density of the PBO project has opened up new and unexpected avenues for geophysical research across disciplines over the last several years (e.g. atmosphere, meteorology, snow pack, tides, vegetation growth, drought monitoring, etc.), the coming decade under the NGEO banner will undoubtedly present new opportunities as the network continues to be modernized. We are excited to see what our community can do with thousands of additional observations from modern, full-constellation receivers and how California's Earthquake Early Warning, tsunami and flood warning communities can integrate real-time GNSS observations over our vastly improved communications networks.

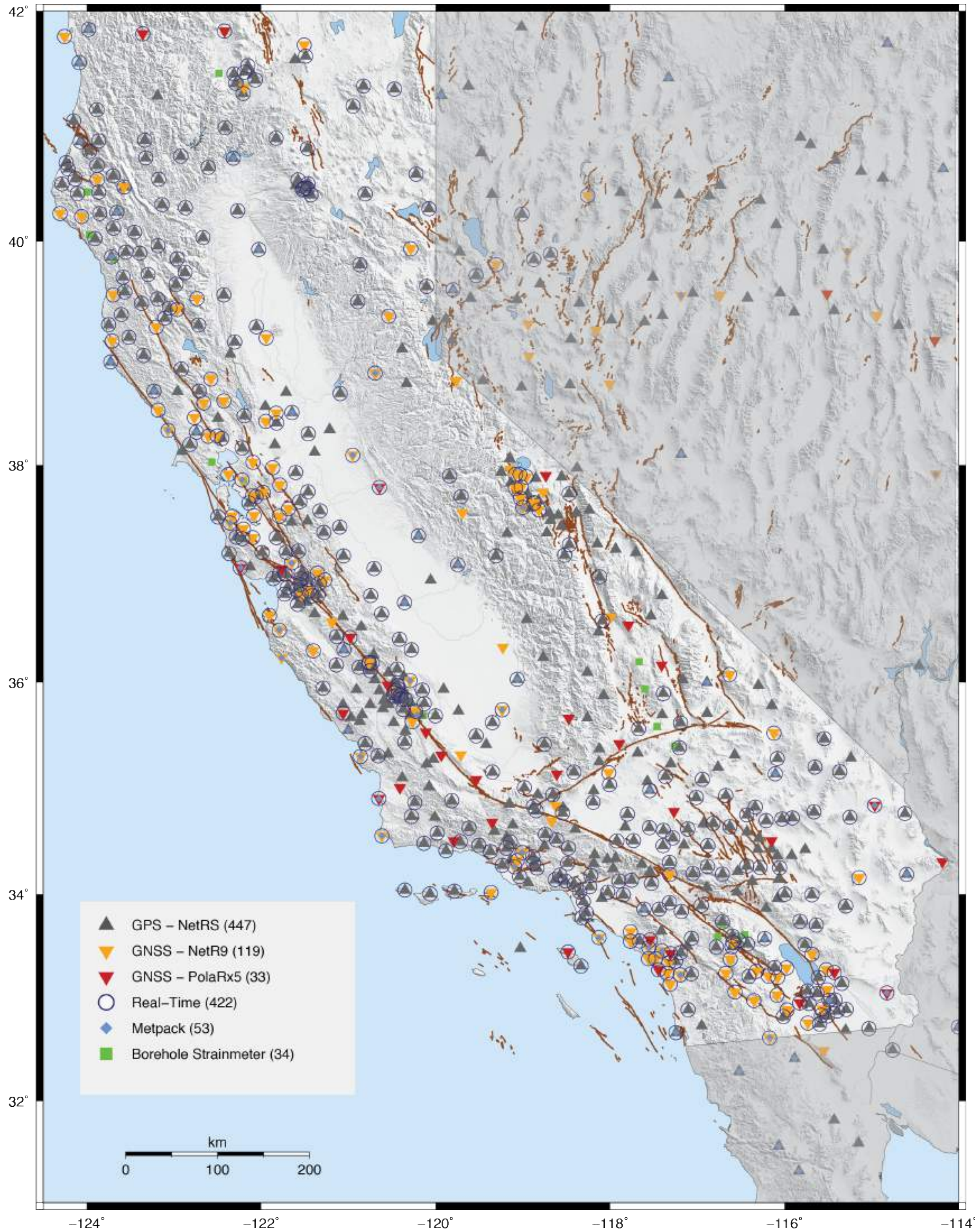

42°
40°
38°
36°
34°
32°
−124°
−122°
−120°
−118°
−116°
−114°
GPS − NetRS (447)
GNSS − NetR9 (119)
GNSS − PolaRx5 (33)
Real−Time (422)
Metpack (53)
Borehole Strainmeter (34)
km
0
100
200

Engineering challenges of operating year-round portable seismic stations at high-latitude

Bruce Beaudoin (1), Paul Carpenter (1), Jason Hebert (1), Dean Childs (1), Kent Anderson (2), and the PASSCAL Team

(1) IRIS PASSCAL, New Mexico Tech, Socorro, NM, United States (bruce@passcal.nmt.edu), (2) Incorporated Research Institutions for Seismology, Washington, DC, United States

Remote portable seismic stations are, in most cases, constrained by logistics and cost. High latitude operations introduce environmental, technical and logistical challenges that require substantially more engineering work to ensure robust, high quality data return. Since 2006, IRIS PASSCAL has been funded by NSF to develop, deploy, and maintain a pool of polar specific seismic stations. Here, we describe our latest advancements to mitigate the challenges of high-latitude, year-round station operation.

The IRIS PASSCAL program has supported high-latitude deployments since the late 1980s. These early deployments were largely controlled source, summer only experiments. In early 2000 PASSCAL users began proposing year-round deployments of broadband stations in some of the harshest environments on the planet. These early year-round deployments were stand-alone (no telemetry) stations largely designed to operate during summer months and then run as long as possible during the winter with hopes the stations would revive come following summer. In 2006 and in collaboration with UNAVCO, we began developing communications, power systems, and enclosures to extend recording to year-round. Since this initial effort, PASSCAL continued refinement to power systems, enclosure design and manufacturability, and real-time data communications. Several sensor and data logger manufacturers have made advances in cold weather performance and delivered newly designed instruments that have furthered our ability to successfully run portable stations at high-latitude with minimal logistics – reducing size and weight of instruments and infrastructure.

All PASSCAL polar engineering work is openly shared through our website:
www.passcal.nmt.edu/content/polar

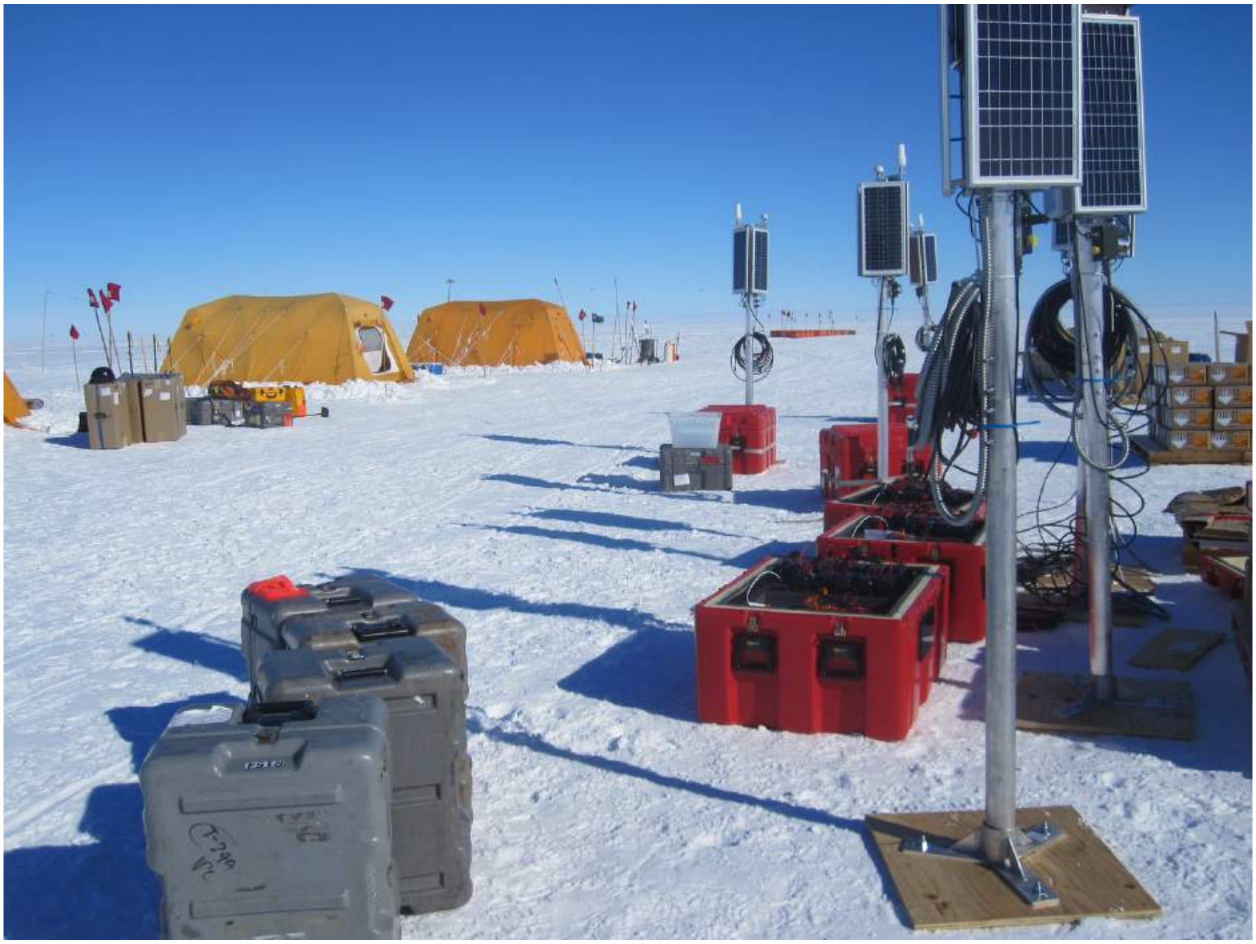

EarthScope Transportable Array: A Remote Observation Platform in Alaska and Canada

R. W. Busby, K. Aderhold, M. Enders, J. Miner, R. M. Bierma, R. Woodward

The EarthScope Transportable Array (TA) program in Alaska and western Canada is primarily operated as a broadband seismic network. The last 78 stations will be installed largely in western Alaska in 2017, with the full network of 270 real-time stations operated until at least 2019. In addition to providing high-quality seismic data, the remote and telemetered TA stations have enabled "piggy-backing" of a multitude of additional sensors. All stations are equipped with a Setra 278 intermediate frequency microbarometer and a NCPA high frequency infrasound microphone. Through partnerships with NASA Arctic-Boreal Vulnerability Experiment (ABoVE), NOAA, and Canadian Hazard Information Service, ~150 stations will have a Vaisala WXT520 meteorological sensor installed at a height of ~3 meters above the ground collecting and transmitting 11 data channels such as wind speed, wind direction, and rain intensity. 14 strong motion sensors have been or will be added to new and existing stations along the subduction zone to the south, complementing the footprint of strong motion sensors already installed in this seismically active zone. Autonomous soil temperature sensors will also accompany ~87 stations, with installation and data servicing provided opportunistically by the TA field crews. Through extensive collaboration, the valuable access and observational capabilities of the ATA have been utilized by numerous science agencies stretching funding dollars even further for the collection of scientific data.

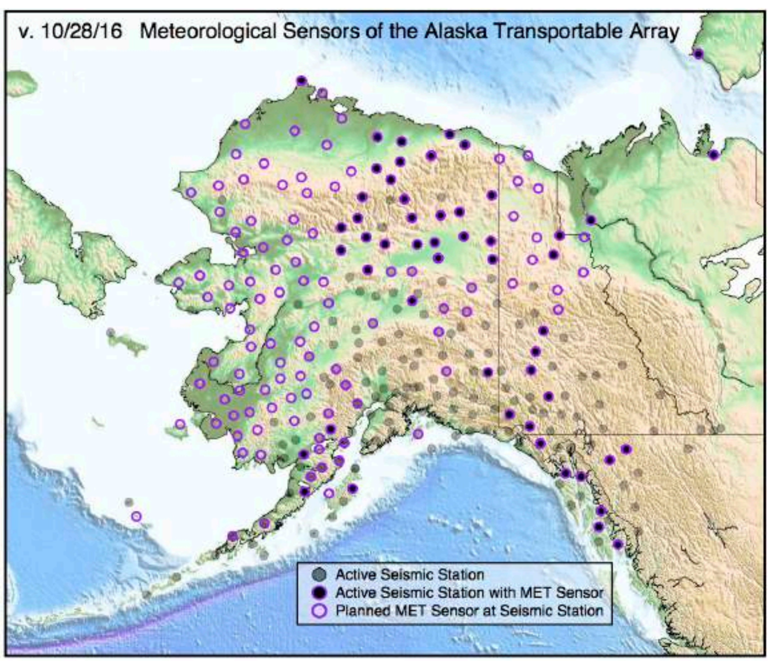

A wireless seismic system for deep earth detection and its test in Xingcheng of Liaoning province, China

Jun Lin

College of Instrumentations & Electrical Engineering, JiLin University, Changchun, China

lin_jun@jlu.edu.cn

Introduction

Seismic exploration has been the most important approach for oil and gas exploration in deep earth. High performance seismic exploration equipment is of great necessity to seismic data acquisition. As the seismic detection gradually extends to cities, rivers lakes, mountains, swamps and other complex terrains, the cable seismographs are difficult to be distributed in the areas above, which drives the demand of large scales of cable-less instruments with flexible features. Therefore, we proposed a scheme of Wireless Seismic System for deep exploration and the proposal was brought in the deep exploration technology and experiment (SinoProbe).

The Wireless Seismic System (Fig. 1) constitutes 10kN electromagnetic controllable VibraSeisvibraseis - PHVS-10000, wide frequency band electrochemical geophone - MECSS3-I, 1Hz coil geophone - CDJ-S1, three component seismic data acquisition system - GEIWSR-II, heterogeneous wireless communication systems, massive data transmission devices and seismic data processing. In order to test and verify the actual performance and application in the field, we carried out two types of experimental research in Xingcheng, Liaoning Province, China. At the beginning, the comparison test experiment of deep reflection between the Wireless Seismic System and Sercel 428XL was conducted. Then, a three-component deep large refraction seismic exploration test with 5 great shots in 200 km was performed. The test results show that the raw seismic data collected by the Wireless Seismic System with high signal-to-noise ratio(SNR) was reliable, and the correspondence of the results were good. The clear information of seismic phases were obtained via the large refraction seismic data in deep earth. Also, the velocity structure of the deep crust was obtained by inversion.

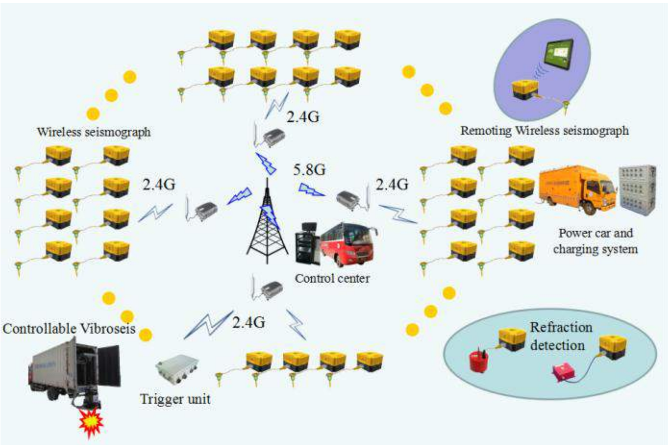

Fig. 1 The Wireless Seismic System

Key techniques

PHVS-10000 constitutes alternator, vibration controller, power amplifier, shock absorber, vehicle carrier and retractable devices, etc. Its maximum output power is 10kN, the frequency range is 1Hz~1500Hz, and the phase control precision is 1°. Through the phased array radar technique and the design of distributed and phase controlled beamforming source, the SNR has been improved.

The sensitive core of MECSS3-I was utilized by stacked micro electrode structure. The substrate of sensitive element is made of silicon, and the silicon wafer is polished. The sensitivity of MECSS3 is 100V/m/s, with the frequency range of 0.05-20Hz. CDJ-S1 is the use of spring spider. It has realized the accurate measurement of three component seismic signal. The sensitivity is 1800mV/cm/s ± 10%, and the frequency range is from 1-100Hz.

The noise level control measures of the seismic acquisition system GEIWSR-II are from three aspects, including the source impedance matching circuit structure design, suppression of external interference, and power supply and ground line decoupling. The noise level of GEIWSR-II is 0.57μV@ (3-200Hz). The united plan of GPS time service and the real time clock (RTC) was adopted, which implements the synchronous sampling in 4000 channels (1000 stations) and the synchronization precision reaches 10μs. GEIWSR-II is integrated with the dual frequency GPS OEM board, so that the data acquisition system is formed with a static relative positioning function with the centimeter level positioning accuracy. GEIWSR-II uses Wi-Fi networks, the satellite communication networks, the mobile communication networks, the wireless self-organized networks in the communication systems, having realized the local and remote quality monitoring in data acquisition.

Results and discussions

By comparing the deep reflection seismic data of single shot, the amplitude in Wireless Seismic System and Sercel 428XL are approximate, which demonstrates that the Wireless Seismic System has cracking preservation to amplitude. What is more，with abundant information in low frequency and high SNR in both of the equipment, the Moho surface can be obtained clearly, which also proves that Wireless Seismic System meet the requirements of deep detection. Continuous and clear reflection seismic layer can be obtained through comparing the results (processing the same parameter).

We can draw the conclusions below by analyzing and inversing the large refractive seismic data: Vertical component seismic records of P wave and y component seismic records of S wave with 5 great shot show the clear Pg, Pm and Sm seismic phases; The inversing results acquired the refractive lines of large channel spacing show the Moho surface flat and the crustal thickness is 32.1-32.7km; Through the inverses, velocity of 5.9 km/s in shallow surface, velocity of 6.57-6.70km/s at the bottom of the crust, we can infer that the crustal structure is acid.

Conclusions

Based on PHVS-10000, we have realized the resources explorations in deep underground space. MECSS3-I at low frequency on the basis of MEMS techniques and CDJ-S1 at 1Hz have been developed. Seismograph has been implemented in a cable free form, with techniques of acquisition in 0.57μV noise level, high precision self-positioning / high precision synchronization acquisition, heterogeneous communication networks used in quality monitoring and massive data transmission.

The results in Xingcheng demonstrates that the wireless seismic system satisfied the requirements of seismic exploration in the deep structure of earth. Moreover, Wireless seismic system has superiority, like widely applicable to a variety of terrain and low manpower and resources consuming, when using in long measuring line and long time acquiring.

Using Machine Learning to Build Seismic Event Catalogs

Increasing data volumes coupled with the need to recover events across a large range of signal-to-noise ratios have helped fuel the dramatic increases in algorithm design for seismic event detection. In spite of this, it has been difficult to leave behind basic amplitude ratio detectors because of their sensitivity, ability to generalize well, computational efficiency and conceptual simplicity. The cost of generalization and sensitivity is high false detection rates when surface noise conditions are unfavorable. Subsequently, optimization for false detection rates instead of minimum magnitudes arises directly from the practical need to reduce manual waveform review to a level manageable for available resources. Here we explore the use of machine learning to build event models at the network level that can be used to review detections, classifying them as events or noise. We use manually reviewed detections from active Transportable Array stations in sedimentary basins in the Central U.S. Using a featureset derived from the weighted averages of the nearest 5 stations, we require the model to find class boundaries between local events, non-local events, surface blasts, and noise. We develop, test and validate the model in the Permian and Denver-Julesburg Basins and are generally able to correctly identify local events and blasts, while non-local and noise labels are generally correct within the top two class likelihoods. We test the portability of the model by evaluating reviewed detections in the Williston Basin, and find that all local events are detected, plus 1 additional event missed by the reviewer. This test suggests that machine learning can play a valuable role in event discrimination and trigger sorting at the network scale and in some cases is capable of outperforming a naive analyst (with no local knowledge about quarry locations or noise characteristics) at event identification.

The EarthScope Magnetotelluric Program: Status, Products, and Science Examples

Authors: Adam Schultz, Andy Frassetto, Bob Woodward

The Incorporated Research Institutions for Seismology operates the National Science Foundation EarthScope Magnetotelluric (MT) Program through a subaward to the National Geoelectromagnetic Facility (NGF) at Oregon State University (OSU). These activities utilize a pool of 29 long-period MT systems, supplemented by an additional ~56 long-period and (ultra)wideband MT instruments also maintained at the NGF. EarthScope MT activities include Backbone (MT-BB), Transportable (MT-TA), and Flexible (MT-FA) Arrays, which respectively provide deep-penetrating “anchor point” views of mid-mantle conductivity and very long-period observations; systematically map mid-crustal to upper mantle resistivity structure on a 70 km station spacing grid that spans the continental USA; and enable targeted, high resolution (including upper crust) surveys by PIs of specific geodynamic and volcanic targets. Six MT-BB stations were removed in 2014 and 2015 after operating successfully for several years. Through 2017, the MT-TA will have covered large portions of the northern and eastern U.S. with two large contiguous footprints. During 2017 and 2018 it will deploy across the Great Plains to connect these two footprints and offer complete 3D MT coverage of well over half the United States. Meanwhile, MT-FA deployments have operated in the Pacific Northwest and Mid-Atlantic.

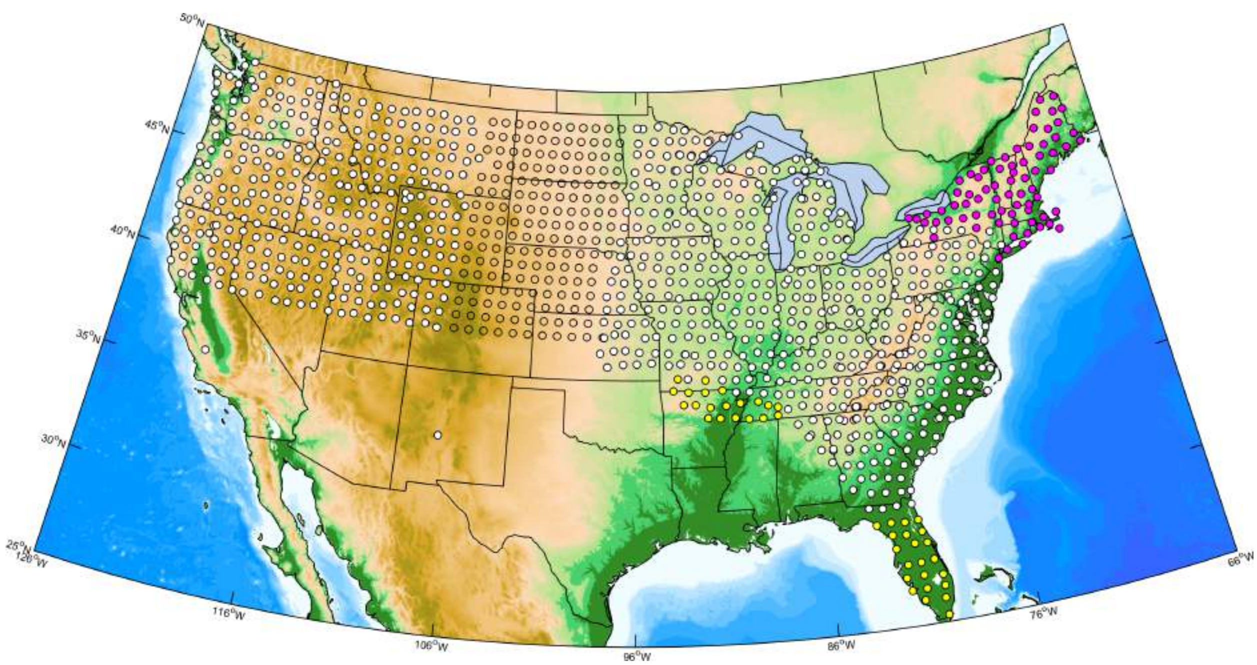

MT-TA as of spring 2017, with existing MT-TA stations (white), MT-TA New England supplement (pink), USGS (yellow), and planned MT-TA sites (open circles).